



Kent Academic Repository

**Drinkwater, A. J. (1980) *The dynamics of trapped monochromic radiation.*
Doctor of Philosophy (PhD) thesis, University of Kent.**

Downloaded from

<https://kar.kent.ac.uk/94317/> The University of Kent's Academic Repository KAR

The version of record is available from

<https://doi.org/10.22024/UniKent/01.02.94317>

This document version

UNSPECIFIED

DOI for this version

Licence for this version

CC BY-NC-ND (Attribution-NonCommercial-NoDerivatives)

Additional information

This thesis has been digitised by EThOS, the British Library digitisation service, for purposes of preservation and dissemination. It was uploaded to KAR on 25 April 2022 in order to hold its content and record within University of Kent systems. It is available Open Access using a Creative Commons Attribution, Non-commercial, No Derivatives (<https://creativecommons.org/licenses/by-nc-nd/4.0/>) licence so that the thesis and its author, can benefit from opportunities for increased readership and citation. This was done in line with University of Kent policies (<https://www.kent.ac.uk/is/strategy/docs/Kent%20Open%20Access%20policy.pdf>). If you ...

Versions of research works

Versions of Record

If this version is the version of record, it is the same as the published version available on the publisher's web site. Cite as the published version.

Author Accepted Manuscripts

If this document is identified as the Author Accepted Manuscript it is the version after peer review but before type setting, copy editing or publisher branding. Cite as Surname, Initial. (Year) 'Title of article'. To be published in *Title of Journal*, Volume and issue numbers [peer-reviewed accepted version]. Available at: DOI or URL (Accessed: date).

Enquiries

If you have questions about this document contact ResearchSupport@kent.ac.uk. Please include the URL of the record in KAR. If you believe that your, or a third party's rights have been compromised through this document please see our [Take Down policy](https://www.kent.ac.uk/guides/kar-the-kent-academic-repository#policies) (available from <https://www.kent.ac.uk/guides/kar-the-kent-academic-repository#policies>).

THE DYNAMICS OF TRAPPED MONOCHROMATIC RADIATION

by

A.J. DRINKWATER

A thesis submitted for the degree of Doctor of Philosophy of the
University of Kent at Canterbury.

Electronics Laboratory,

U.K.C.,

Canterbury,

Kent.

1980

ABSTRACT

This thesis considers a linear system constructed of monochromatic radiation trapped between end reflectors (of negligible mass) which move so that the radiation pressure, measured at the surface of the free reflector, is constant. Kinetically, the system behaves as a rigid measuring rod (which may be compared with the rigid rod suggested by W.H. McCrea) and undergoes Lorentz contraction. If a force is applied to one end while the radiation pressure and binding force maintain equilibrium, then, dynamically, the system behaves as a massive body with equivalent (inertial) rest mass. In contrast to the previous discussion by D.W. Sciama and W. Davidson on the origin of inertial forces, it is suggested that these forces are generated by a local mechanism in the extended system.

A set of three experiments demonstrates some of the properties of such a system. The first is based on an optical Michelson interferometer. One mirror is controlled by a servo unit, for which the error signal is obtained from the interference pattern, so that it tracks the movement of the other mirror and maintains a rigid length between the mirrors. The second experiment is based on a system of two trolleys with microwaves used to measure the radar distance between them. Each trolley has a separate servo control to maintain a constant distance to the other trolley. They form a dynamic system which moves independently of any reference to the laboratory. The third experiment is an electronic analogue demonstrating the time interdependence of the movements of the two ends of the system.

The second part of the thesis takes up the suggestion by R.C. Jennison that Ball Lightning may be structured entirely of electromagnetic fields (and hence be an example of the system analysed above). Then the size of the ball of trapped waves is an indication of the frequency at which some, so far unknown, phenomenon occurs. A description is given of a preliminary experiment to investigate if there is any interaction between an electrostatic field and electromagnetic waves of a specific frequency in the range 0.1-1 G.Hz. No evidence of such an interaction was found within the constraints of this experiment.

DEDICATION

To that dream of my dreamy youth,
Drawn from towers built near my parents
Walking on Thames Embankment.
This Mathematics they set aside then
And watched the ships moving towards far coasts.

CONTENTS

The thesis is in two main parts:

- Part I Chapters 3 to 5 A one dimensional cavity.
 Part II Chapters 6 and 7 Three dimensional structure.

<u>Chapter 1</u> INTRODUCTION	Page No.
1.1 Beginnings.	1
1.2 The Idea.	1
1.3 The objectives of the project.	4
1.4 Chapter contents.	5
<u>Chapter 2</u> A BRIEF REVIEW OF RELEVANT LITERATURE	
2.1 Introduction.	10
2.2 Accurate experiments.	
(a) Accurate experimental determination of length.	12
(b) Accurate experimental determination of the velocity of light.	16
(c) The Caesium clock.	17
2.3 The rigidity of measuring rods.	18
2.4 The nature of inertial mass.	24
(a) Main theories as to the origin of the inertia of mass	25
(b) The controversy over Mach's hypothesis.	31
2.5 Cavity-trapped radiation and closed systems.	33
2.6 Ball lightning.	35
2.7 The work of some previous authors on possible electro- magnetic field structures of fundamental particles.	39
2.8 Experimental investigations for electromagnetic field non-linearities.	42

Chapter 3 THEORETICAL CONSIDERATIONS OF THE PROPERTIES OF
TRAPPED ELECTROMAGNETIC RADIATION FOR INERTIAL
FRAMES IN FREE SPACE

3.1	Introduction.	46
3.2	Kinetics of the Etalon and the Lorentz contraction.	48
3.3	The Etalon as a clock.	56
3.4	The dynamics of the Cavity.	57
3.5	A comparison of the cavity system with the rigid rod described by McCrea.	65
3.6	The relation of the dynamics analysis to the electron.	67
3.7	Conclusion.	69
A3.1	The electromagnetic field patterns in the cavity.	70
A3.2	Radiation pressure.	71

Chapter 4 THREE EXPERIMENTS WHICH DEMONSTRATE REFLECTORS MOVING
ACCORDING TO THE CONDITIONS DESCRIBED IN CHAPTER 3

4.1	Introduction.	72
4.2	The Interferometer experiment.	
	(a) The apparatus.	78
	(b) The Vibrator transducer.	84
	(c) Method of performing the interferometer experiment.	91
	(d) Results of the interferometer experiment.	95
	(e) Conclusion to the interferometer experiment.	97
4.3	The Trolley experiment.	
	(a) The apparatus for the Trolley experiment.	101
	(b) Method of performing the Trolley experiment.	107
	(c) Results of the Trolley experiment.	108
	(d) Conclusion to the Trolley experiment.	111
4.4	The electric analogue experiment.	113
	(a) The apparatus for the analogue experiment.	117

(b) The results of the analogue experiment.	120
(c) Conclusion to the analogue experiment.	121
4.5 Going to the theoretical limit.	121
4.6 Overall conclusion.	123
A4.1 The theory of damped resonant systems.	125
A4.2 The three-term controller.	128
A4.3 Loudspeakers used as transducers.	129
(a)The theory of electrical compensation for the cone resonances.	131
(b)The loudspeaker transducer apparatus.	134
(c)Method of performing the experiment with loudspeakers.	136
(d)Results of the experiments with the loudspeakers.	137
(e)Conclusion to the experiment with the loudspeakers.	139
A4.4 Analysis of a delay in the control loop.	140

Chapter 5 SOME CONSEQUENCES OF THE EXTENDED STRUCTURE OF
THE CAVITY

5.1 Introduction.	142
5.2 A new aspect on the Machian controversy	144
A5.1 The forces generated in the cavity because of a difference in the metric potentials at the two ends.	152

Chapter 6 A PRELIMINARY EXPERIMENT ON THE REFRACTION BY AN
ELECTROSTATIC FIELD OF R.F. AT A FREQUENCY
SUGGESTED BY THE SIZE OF BALL LIGHTNING

Part I Description of the apparatus.

6.1 Introduction.	156
6.2 The experimental technique.	161
6.3 The apparatus.	171
6.4 The Interferometer.	172

6.5	The r.f. Generator.	181
6.6	R.f. power control servo.	184
6.7	R.f. Circuits.	186
6.8	A.f. Circuits.	193
6.9	The switching circuit.	198
6.10	The Van de Graaff generators.	198
6.11	The Perspex shutter.	199
6.12	Positioning of the receiving aerial.	202
6.13	The bandwidth of the aerial.	203
6.14	Method of measuring, approximately, the radio frequency field.	204
6.15	Method of measuring the electrostatic field.	204
	<u>Part II</u> Operation of the equipment and the results obtained.	
6.16	Experiment to simulate the resonance being looked for.	208
6.17	Calibration.	211
6.18	The experimental method.	218
6.19	Results.	226
6.20	Conclusion.	227
A6.1	The Perspex shutter.	234
A6.2	The electrostatic field round the two spheres.	235

Chapter 7 THE STRUCTURE OF BALL LIGHTNING

7.1	Introduction.	243
7.2	A 'quantizing' mechanism.	244
7.3	The implications of the calculations on rigidity and inertia for the lightning ball.	247
7.4	The field intensity required to give measurable non- linear effects.	250

Chapter 8 CONCLUSION

8.1	Main results.	254
8.2	Comments.	257
8.3	Suggestions for future work.	257
A 8.1	Comment on the 'locking in' process.	259
LIST OF REFERENCES		263

* * *

Figures

Each figure precedes the first reference to it in the text. Hence, to find a figure to which reference has been made, turn back the pages until it is reached.

References

Each reference to the work of a previous author gives a number in brackets which refers to its number in the list of references (in alphabetical order) at the end of the thesis. Each reference in the text quotes the name of the author and year of publication.

KEY

The following table describes those symbols which are used repeatedly in the text. Those which are used only occasionally are defined where they occur.

Common to all chapters

\vec{A}	Vector potential of Sciama's induction field.
c	Velocity of light.
E	Energy of the system.
$E_t = E_T$	Total energy of the system.
\vec{E}	Electric field.
G	Gravitational constant.
g_{ik}	Spatial terms of the metric ($i, k = 1, 2, 3$).
$g_{\mu\nu}$	Space-time terms of the metric ($\mu, \nu = 1, 2, 3, 4$).
L	Proper length of the rod or etalon.
m	Mass of body.
m_0	Rest mass of body.
m_1	First mirror.
m_2	Second mirror.
Q	Quality factor of resonance.
q	Charge.
r	Radial distance from object.
S	Laplace operator.
t	Time.
v	Velocity of system past observer.
γ	$= \left[1 - \frac{v^2}{c^2} \right]^{-1/2}$
ϵ_0	Permittivity of space.
λ	Wavelength.
ϕ	Scalar potential of Sciama's induction field.
θ	Phase difference of sinusoidal waves.

ω Angular rate of rotation.

Chapter 2

dl Element of spatial length.

ΔL Change of length of rod caused by force T .

\vec{F}_{grav} Field of gravitational force.

$\vec{F}_{\text{inertial}}$ Field of inertial force.

Chapter 3

E_b Energy in the binding mechanism.

E_w Total energy in the waves.

E_{wr} Wave energy to right of centre.

E_{wl} Wave energy to left of centre.

f_r Pressure of radiation on the right.

f_l Pressure of radiation on the left.

F' External force.

F_b Binding force.

F_w Radiation pressure.

h Planck's constant.

L_1 Length of etalon when ray returns to the first mirror.

t_1 Time for ray to return (m_1 pushed).

t_2 Time for ray to return (m_1 pulled).

T_i Total delay time.

v Velocity of first mirror m_1 during first delay time.

v_2 Velocity of second mirror m_2 .

λ Wavelength of trapped radiation.

τ Proper time per oscillation.

τ_1 Time per oscillation when system is moving at v_2 .

ν Frequency measured and maintained at the reflector.

ν' Frequency reflected off first mirror as it moves at v .

- ν'' Frequency reflected off second mirror moving at V_2 .
- ν_e Frequency of external radiation.

Chapter 4

- C.L.T.F. Closed Loop Transfer Function.
- f Proportion of derivative signal in controller.
- F Coefficient of frictional force.
- g Acceleration due to gravity.
- $G(s)$ Transfer function in Laplace form.
- k Constant of proportionality.
- k_1 Fraction of integrated signal.
- k_2 Fraction of direct signal.
- k_3 Fraction of differentiated signal.
- k' Fraction of signal through the controller.
- $I(t)$ Input signal.
- K Coefficient of the spring. Also a constant of proportion.
- M Mass of moving object.
- $O(t)$ Output signal.
- T_i Time constants.
- T.F. Transfer Function.

Chapter 5

- E_T Total energy.
- ΔF Force required to hold cavity at one end.
- V^i 4-velocity of first mirror.
- ν_1 Frequency of ray leaving one end.
- ν_2 Frequency of ray received at other end.

Chapter 6

- A Amplitude of signal of phase θ to reference.
- C Capacitance of sphere on Van de Graaff.
- f Frequency.
- F.S. Frequency Stepping (mode of operating the equipment).
- h Height of pulse.
- l Distance from centre of sphere.
- N.F.S. No Frequency Stepping (mode of operating the equipment).
- T Time between clock pulses.
- T_f Time constant of filter.
- T_p Time duration of pulse.
- T_{sc} Time to scan the band of frequencies being analysed.
- y_1 A position in the electrostatic field } see Fig 6.27.
- y_2 A position in the electrostatic field }
- λ Wavelength of radio frequency radiation.
- η Characteristic Impedance.

ACKNOWLEDGEMENTS

"Much thanks" to my supervisor, Professor R.C. Jennison, who has both supplied the main theoretical and experimental ideas which formed this thesis and guided me skillfully through the various stages of the course.

Dr. 'Phil' Davies and Dr.D.G. Ashworth have given me steady help over a long time. Phil has been of very real assistance in bringing my thoughts together in a more coherent and presentable fashion (he also indicated the correct approach to the analysis of the movement of the second mirror of the cavity) and Dr. Ashworth has given suggestions for balancing the content of the thesis and supplied references to the works of other authors.

Other members of the teaching staff have given me various items of information and suggestions. In particular, Dr.R.J. Collier gave me an exposition of the calculation of the effect of the Perspex shutter, Dr.M. Oliver put me on the right tracks for calculating the Doppler shift on rays moving through a general metric field, Dr.D. Preece explained the calculation of probabilities in chapter 6, Mr.M. Dent helped with the experiments involving automatic control and Dr.T. Butler helped with comprehending the Ball lightning structure suggested by Edean.

The technical staff have given me assistance as required.

The Science Research Council awarded me a studentship for the three years of the project.

Chapter 1

INTRODUCTION1.1 Beginnings

The project arose out of the thoughts of Professor Jennison after a discussion he had had with McCrea in 1972 on the precise nature of the rod that he (and Hogarth⁽³⁹⁾), 1952, has described, in which the velocity of sound equals that of light. Consideration of an electromagnetic structure for this rod which may be set in motion from rest by a force pushing on one end and the necessity, if the velocity of sound condition is to be fulfilled, that the length of the rod is determined by the electromagnetic wave, led to obtaining the detailed dynamics of the rod, including an effective rest mass. There was also the possibility of combining these results with Jennison's other interest in the rare phenomenon of Ball Lightning. This resulted from a personal experience of Ball Lightning during an airflight and the reviewing of a book by Singer⁽⁸⁹⁾, 1971, on the nature of Ball Lightning. Jennison⁽⁴⁶⁾, 1973, had suggested that Ball Lightning represents a novel electromagnetic configuration which is stable independently of the air.

Some of the work for this thesis has been reported in the paper by Jennison and Drinkwater⁽⁴⁷⁾, 1977, which contains the main ideas and some account of the theory.

1.2 The Idea

Inertial forces occur in common experience quite as frequently as gravitational ones and, because the acceleration can be very great (as in impulsive blows), often involve much greater forces for a given mass. Yet the cause of these forces is unknown, as is any physical explanation

of Newton's three laws of motion. Mach⁽⁶⁵⁾, 1908, and more recent authors following him have attempted to account for inertial forces in terms of the motion of the test body relative to the average rest frame of the Universe.

All masses have some finite extension and it requires a finite time for the effect of a force applied to some part of a body to be transmitted to the whole mass. It is suggested here that the previous failure at a tenable explanation resulted from assuming that one could discuss dynamics in terms of point masses. The explanation required results from the spatial extension of all bodies.

Consider, as an example of a body, an object with extension made of radiation trapped between two perfect reflectors. The interest is in the radiation and the reflectors are assumed to have negligible effect other than confining the radiation. If a force is applied to one end and the distance between the reflectors is maintained a constant number of half wavelengths of the trapped monochromatic radiation, then the object behaves dynamically according to Newton's laws (as described in chapter 3).

It is demonstrated in this thesis that the way in which this object obeys Newton's laws and its properties of inertia can be ascribed to a definite physical mechanism. The variation in radiation pressures and the delay time for the changes of internal conditions, caused by the force, to be distributed through the object gives the following explanations.

Newton's first law (that a body continues in its state of rest or uniform motion unless acted upon by an external force) is accounted for in that the motion of the end reflectors is determined so as to keep an integral number of half wave standing waves between the two ends (equivalent to each end maintaining a constant 'radar distance' to the other). As each end is always referring to a time delayed signal from

the other end, it is in effect always referring to its previous velocity and ensuring that there is no change. These conditions ensure that the object maintains a uniform inertial motion unless acted on by an external force. This inertial motion is not determined directly by any distant masses but by the oscillatory propagation of the internal waves along null geodesics.

Newton's second law (that the acceleration is proportional to the force applied) is accounted for by the increase in velocity (relative to the inertial frame) with which this applied force causes the first reflector to move. It does so for the short time required to distribute the new condition to the whole object and this velocity and delay time give an acceleration. If the force continues to be applied, the step increase in velocity is repeated for a further delay time and the object on average accelerates in proportion to the applied force according to Newton's second law.

Newton's third law (that the forces of action and reaction are equal and opposite) is accounted for in terms of a balance of the radiation pressure of the internally trapped waves by a constant binding force and any further externally applied force.

The basic idea throws some light on the true physical meaning of rigid measuring rods as required at the basis of relativity theory and of the meaning of proper time in terms of the frequency of the radiation trapped between the reflectors.

If the idea is extended by assuming that it describes the actual structure and mechanism of inertia in atomic particles, then the structure of the electron may be related to the gamma radiation required for pair formation.

1.3 The objectives of the project

The system considered consists of monochromatic radiation reflected normally between two perfectly reflecting parallel planes. The component parameters are, the length between the reflectors, the delay time for one complete circulation of the energy, the amplitude (a constant) which is to be maintained in the proper frame of each mirror (hence determining its motion), and the binding force which maintains the correct position of the reflector against the radiation pressure pushing outwards.

The thesis describes the equations for the Special Relativity transformation of length, mass and energy in terms of standing waves and their relativistic transformations and raises questions in the context of a novel approach to the nature of inertia. The motion, dynamics and rest mass of such a system, when a steady force is applied, is described and the analysis gives some account of how inertial and gravitational forces act in the system. The motion of the boundary reflectors being determined by the internal radiation.

A thought-provoking experiment which simulates the theoretical system may be achieved by setting up actual reflectors which are servo controlled so that the effect of friction and the mass of the reflectors is made negligible because of the power supplied by the servo motors. Electromagnetic waves may be reflected off the plates but, as there must always in practice be some loss of energy, a generator of waves at a fixed frequency is required to make up this loss of power. Having set up such a system, it should be possible to demonstrate that it acts as a rigid rod even when accelerated. If the reflectors at both ends of the system are servoed in this way, the system should be independent of reference to the laboratory and move at a constant inertial velocity when no force is applied.

In order to investigate if autonomous, closed, electromagnetic systems which would exactly fulfil the conditions postulated above, exist in nature, an experiment was performed to look for any previously undetected wave-trapping resonances of electromagnetic waves in the space of a strong electrostatic field, that would account for the comparative stability of Ball Lightning.

It should be possible to extend the theory of the essentially one dimensional configuration to a three dimensional structure which would represent some of the properties of Ball Lightning and might, on a different scale of size, be similar to the structure of atomic particles (with the electron as an example).

1.4 Chapter contents

The work is in two main parts. Chapters 3 to 5 deal primarily with the simplified problem of a one dimensional cavity, while in the second part, chapters 6 and 7 investigate a possible structure for Ball Lightning. An overview of each chapter will now be given.

Chapter 2

This chapter is confined entirely to objectively reporting the work of previous authors and putting the contents of the thesis into context.

On the practical side, a brief account is given of the determination of length by optical interferometers, the determination of the velocity of electromagnetic waves by a microwave interferometer and a standard of time. Some description is given from the reports of Ball Lightning. However, this is not an attempt to justify the veracity of these reports which is considered, for example, by Singer⁽⁸⁹⁾, 1971. An account is given of some previous experiments which have been done to investigate any direct interaction between electromagnetic fields.

On the theoretical side, there are three main topics of interest. These are the definition of a rigid rod to measure length, the nature of inertial forces and the structure of Ball Lightning. Solutions to the question of defining rigid rods have evolved as more factors have been added to the original problem; starting with a rod moving inertially and leading through to a rod subject to accelerating forces. The description of the origin of the inertial forces in the cavity described in the thesis suggest that it is a mechanism which is local to the mass. This tends to support the criticisms of the theory that the mechanism of inertial forces arises from motion relative to the distant Universe, summarized next in this chapter. The main attempts to derive stable field structure solutions that represent closed systems and hence are possible particle models, are grouped round two main approaches. The first considers non-linear field equations containing constants whose values can be set to give the required solution. The second considers as the structure a form of rotating wave contained within a confining boundary. The extent to which previous authors have ascribed an internal wave structure to the electron and a brief indication of the various approaches to the basic, unresolved, problem of what holds the extended particle together in its quantum of energy are described.

Chapter 3

A measuring rod is essentially a mechanical object which forms the basis of physical measurement but has to be carefully related to the mathematical definition of length. This chapter considers the system described above when accelerated from one inertial frame to another by the step changes of velocity caused by the continuous application of a steady force at one end. These conditions could be obtained approximately without invalidating the analysis by, for example, having a delay time as long as required (by increasing the length of the cavity) to make the

time of the leading and trailing edges of the step change short compared with the delay time. The kinetic and dynamic equations are obtained, showing that the property of inertia is created when the smoothed average of the fine detail steps in velocity, in response to a steady force, is taken as the acceleration.

If the parameters of frequency for electron pair formation and rest mass energy of the electron are put into the equation, it is shown that the interaction of the cavity with the applied force is in steps corresponding to Quantum theory.

Chapter 4

The reflectors at the ends of the cavity move so as to maintain a constant radar distance between the ends. This property is converted into experimental reality in the experiments described in this chapter.

The Michelson interferometer is often used to measure length. In the first experiment this instrument was used for the reverse process of maintaining a constant length between the reflectors. The position of one of the interferometer mirrors was controlled by a servo whose error signal was derived from the interference pattern. Provided the optical length traversed in each arm is maintained at the same difference, the fringe pattern remains the same despite any tracking movement of both reflectors together.

The second experiment, in which both reflectors were servoed in position so as to maintain a node of the standing microwave on the reflectors, is a true dynamic system which moves independently of any reference to the laboratory and has the properties of rigidity and inertia.

The third experiment showed (by an electronic analogue) the time interdependence of the movements of the ends of the cavity.

Chapter 5

The relation of theories by Sciama and others, presented in chapter 2, to inertial mass as defined by the cavity system, is discussed.

Chapter 6

There have been a number of reports (including Jennison⁽⁴⁵⁾, 1969) of sightings of Ball Lightning about the time of thunderstorms. As reported, these are spherical shaped objects which emit a glow of light and exist long enough to constitute a stabilized system rather than being some transitory explosion. If one takes up the suggestion by Jennison⁽⁴⁶⁾, 1973, then the phenomenon of Ball-type lightning may not be a plasma of ionized air but involve some new self-trapping configuration of waves that could equally well exist in vacuum. The steady movement of the lightning ball according to rare reports of its being observed moving next to the exterior of metal aircraft in flight, suggests that the air passes through it without any dragging of an internal plasma. This, combined with the phenomenon on the atomic scale of electron pair formation from electromagnetic gamma waves, suggests the possibility of a series of exact frequency resonances of free space in which a wave may be self-trapping in a steady electrostatic field.

Then we are dealing here with a mechanism involving a radical and previously unknown physical law. Is some of the radio frequency energy generated in the storm contained in the Ball as self-trapped waves? Could we be dealing here on the scale of several centimeters with the same process that normally occurs at the scale of the size of the electron? Is one literally seeing in a lightning ball a large scale version of an atomic particle?

Unfortunately the rare and apparently random formation of Ball lightning during thunderstorms makes it difficult to perform objective scientific method on the phenomenon. However, the interest generated by the reports which have been collected, combined with the interest of the theoreticians in accounting for the structure of fundamental atomic particles by non-linear fields, leads to performing the experiment described in the second part of this thesis. The magnitude of events

in a thunderstorm cannot be easily set up in a laboratory and here we were looking for only the beginnings of a non-linear effect manifesting itself as refraction of the wave passing through the static field.

The instrumentation was made sensitive by using switching and correlation techniques. However, the experiment was only sensitive to a resonance of narrow bandwidth.

Chapter 7

The experiment of chapter 6 was looking for any interaction between an electromagnetic wave of a specific frequency and an electrostatic field. This chapter discusses the questions raised in this context as to what maintains the size and energy content of the ball, how it becomes luminous and how the field strengths used in the experiment compare with those in Ball Lightning.

If the three dimensional object consists of waves spreading out from the centre and reflected back with perhaps rotation in some way, one may consider two spatially orthogonal elements of such a complete system.

Chapter 2

A BRIEF REVIEW OF RELEVANT LITERATURE

2.1 Introduction

This chapter mentions some of the papers which have been published by authors on topics which are of interest in the remaining chapters. The main papers of reference in each section are summarized under the headings of the author's names.

The first section describes experiments which have accurately determined length and the velocity of light. Length has been measured using optical interferometers (usually based on the He-Ne laser light) and this relates directly to the interferometer experiment described in chapter 4. The method of measuring the velocity of light at microwave frequencies is of interest as it has features comparable with the trolley experiment using microwaves. The most recent experiment to determine the velocity of light uses a multiplicity of inter-locked laser frequencies. A brief note is given on the Caesium clock.

The subject of this thesis has some implications for the description of what is meant by a rigid measuring rod. Born (for reference see Silberstein⁽⁶⁸⁾, 1924) attempted to give a theoretical description of the motion of a rigid body and this set up the form of the debate followed by subsequent authors until McCrea⁽⁶⁷⁾, 1952, postulated his particular type of measuring rod with dynamic properties. However, as this thesis is concerned with rigidity defined from a pattern of standing waves, only a few main points of Born's theory will be briefly indicated here. The dynamics of McCrea's rod, which bears a close relation to the system described in chapter 3, is described next. The

automatic control of the positions of the end reflectors in the experiments of chapter 4 are a further extension to this discussion of an experimentally-described rigid rod.

The theory of chapter 3 investigates the inertial properties of radiation trapped in a cavity which is maintained rigid according to this description. Some of the papers which have discussed the meaning of inertia are introduced and a detailed description is given of Sciama's theory on the physical origins of inertial forces as this theory acts as a central focus to the discussion among other authors.

A summary is given of some of the analyses which have been made of radiation trapped in a cavity.

On very different scales of size, the structure of Ball Lightning (if realizable in a vacuum) investigated in chapter 6, and atomic particles may be similar. A description is given of the rare phenomenon of Ball Lightning and some of the explanations as to how it is formed. A possible phenomenon to account for the structure of Ball Lightning, not contained in classical electromagnetic theory, may be similar to previous theories suggesting an electromagnetic structure of atomic particles. A brief indication is given of some papers presenting ideas which may be applied in this way. They make the hypothesis of extending Maxwell's linear equations of electromagnetism to include non-linear terms and hence account for the formation of closed systems under certain conditions.

A description is given of some experiments done by previous authors to investigate any possible interaction between electromagnetic fields, which may be compared with the experiment described in chapter 6.

2.2 Accurate Experiments

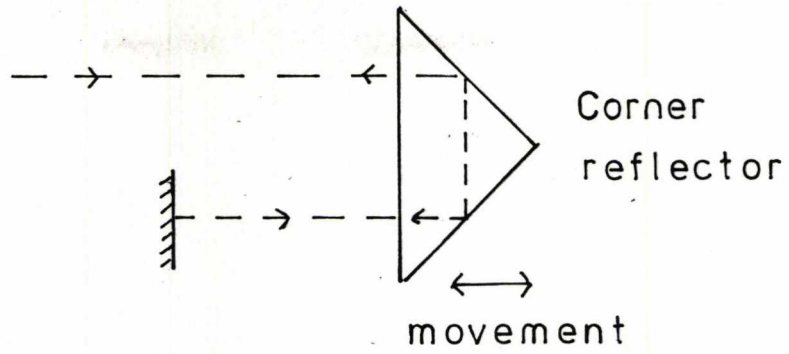
This section describes some of the practical work that has been done on the measurement of length, time and the velocity of light.

2.2(a) Accurate experimental determination of length

The most accurate determinations of length are those which involve the defining unit of length itself. Historically, this unit has been defined as the length of a bar of metal, a wavelength of light in the Cadmium spectrum and, currently, a wavelength of light in the spectrum of Krypton⁸⁶ (Sanders⁽⁷⁹⁾, 1965, comments that line broadening limits the accuracy of this to one part in 10^8). To my knowledge this standard has not been superseded by a Laser light wavelength. However, using the most recent techniques to stabilize the He-Ne laser, it is possible to make measurements to one part in 10^{10} .

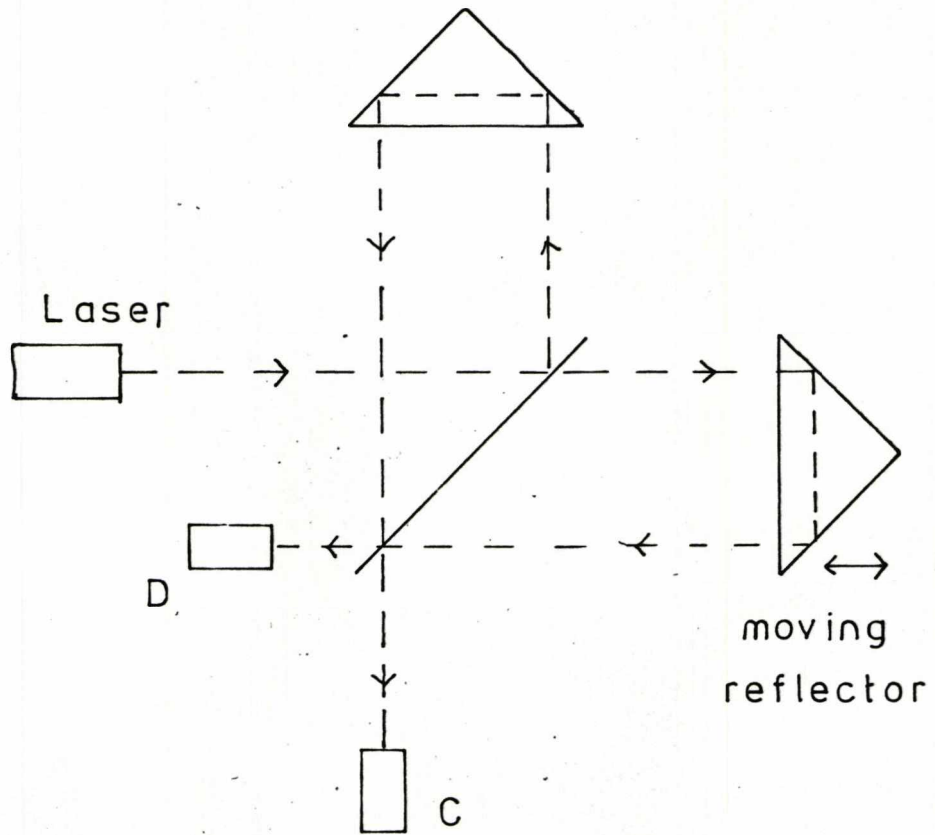
The whole field of accurate length measurement has been revolutionized by the easy availability of laser beams which have a very narrow frequency band. As a result it is trivial to measure movement of the mirror in one arm of a Michelson interferometer, fed from such a laser, to within half a wavelength of the standing waves formed in the optical arm of the interferometer. However, an accuracy to less than this element of length remains considerably less accessible to measurement (for example, it is claimed by Baird⁽⁵⁷⁾, 1967, that displacement can be detected to a thousandth of a fringe). The Fabry-Perot construction of interferometer locates the positions of the interference maxima, for half-wavelength spacings of mirror positions, most accurately.

Most systems use the He-Ne laser (ref. Kaminow⁽⁵²⁾, 1973) with wavelength $0.633\mu\text{m}$. and Doppler broadened by about 1.5 G.Hz. The resonant cavity of the laser is opened walled and can operate in different modes with small frequency separations. There are further practical



Doubling the effect of the movement of the corner reflector on the path length travelled by the ray by returning the ray from a stationary mirror back through the corner reflector.

Fig 2.1



A practical system for measuring linear movements.

signal C



signal D

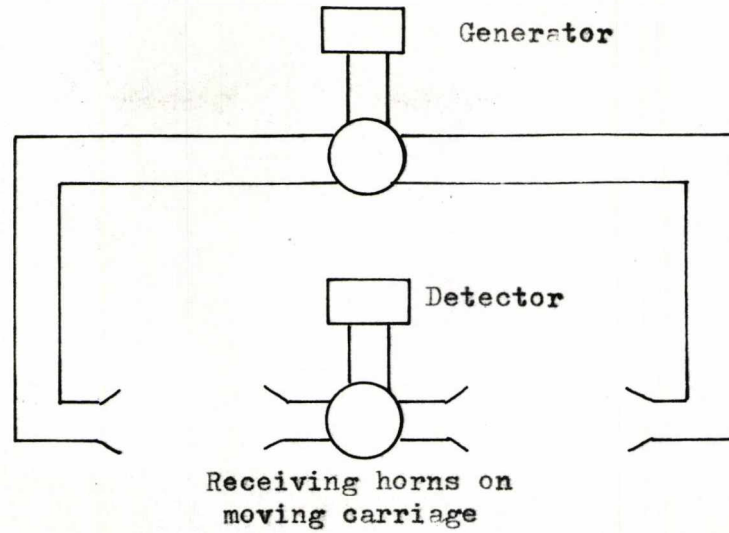


Fig. 2.2

limitations which include the quality of the component optical surfaces, fluctuations in the atmosphere, vibration of components and parasitic light. Some examples of the construction and capability of this type of instrument will now be given.

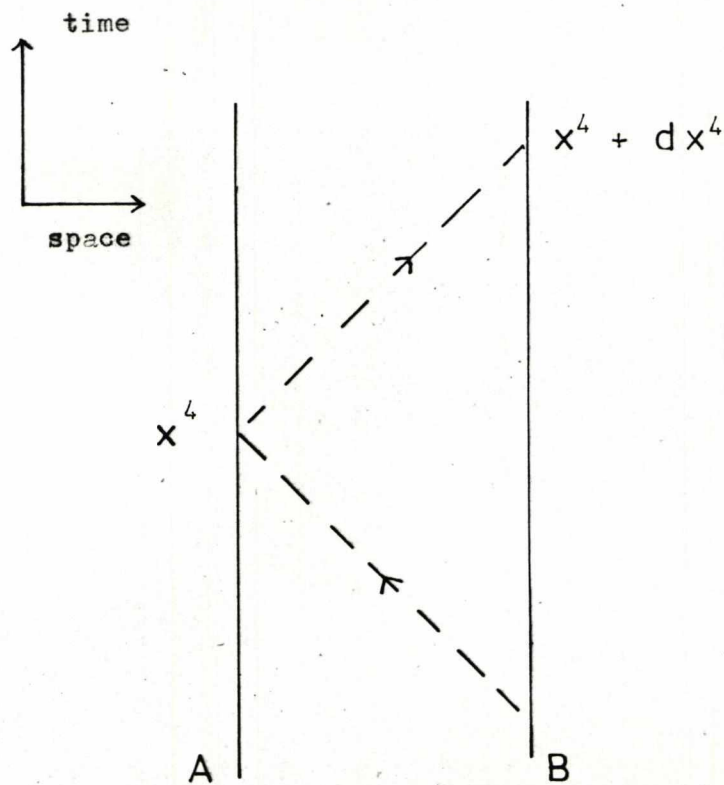
It was reported by Kaminow⁽⁵²⁾, 1973 that the most refined interferometer instruments can measure to better than $0.05\mu\text{m}$. over a distance of 12m. with compensation for atmospheric humidity, pressure and temperature. — Some interferometers use a double path measurement to produce one period for every quarter wavelength of reflector movement (Fig. 2.1).

Fig.2.2 illustrates a simple Laser interferometer developed for use as a length measuring transducer on various types of machine tools, as reported by Schede⁽⁸⁰⁾, 1967. Ranges of 60ins. have been demonstrated and of over 100ins. are reasonable, with air turbulence being the limiting factor. A correction of about $0.6\mu\text{in./in./}^{\circ}\text{F}$ and $0.4\mu\text{in./in./m.m.}$ of barometric pressure, is required. As the moving reflector moves, a sine wave signal is generated in the photo-detector. By electronically counting the cycles of this signal, a record in terms of half wave multiples of the Laser light is obtained. This is $12.46\mu\text{in.}$ per interference fringe. The signal from detector C is out of phase with that from detector D because the beams have travelled slightly different paths. This effect can be used to obtain a sense of direction. To obtain a reliable, narrow band of frequency from the Laser, centred on the frequency emitted from the atoms before Doppler shifts, the resonant feedback cavity formed by the reflecting mirrors at the ends of the Laser has a narrower bandwidth than the Doppler broadened light from the active medium. This cavity resonance is adjusted to the centre of the broadened bandwidth and narrows the bandwidth of the light of the Laser. The length



Microwave measurement of the positions at which the waves from each arm cancel (Froome's experiment).

Fig 2.3



Measuring the very small interval of distance between adjacent particles by sending a radar signal between the particles.

Fig 2.4

of the cavity may be adjusted by a piezoelectric element and the length of the cavity should be kept small to increase the spectral distance between cavity modes. If the pattern has 8×10^4 fringes per in., the frequency response of the detector should reach 160 k.Hz. for a closed loop frequency of 30 Hz. and peak amplitude of 0.02 in. The position transducer was connected as part of an automatic control loop to servo the required position of the machine tool.

An indication of coherence lengths available is given by Berger⁽¹⁰⁾, 1975, of a seismometer based on an interferometer having one arm through an evacuated pipe between two piers a mile apart. It uses a frequency stabilized He-Ne Laser beam and detects movements as small as 3×10^{-6} ins.

2.2(b) Accurate experimental determination of the velocity of light

Froome⁽³²⁾, 1958 measured the velocity of microwaves to an accuracy of $3:10^7$. The basis of the determination consisted of the simultaneous measurement of the free space wavelength, and frequency. He sent 4m.m. wavelength waves through a dividing junction and transmitted the two parts in opposite directions to separate receivers on a trolley (Fig.2.3). The waves were received separately and added. The receivers moved through a number of minima to measure the wavelength (after correcting for diffraction effects). From the frequency and wavelength, the velocity was obtained. This result was corrected for the refractive index of the air. Errors include diffraction of the wave front at the horns and random scattering between transmitter and receiver. The four horn design is symmetrical and had equal power in both waves. It operated in the Fraunhofer diffraction region as the Fresnel mode requires large reflectors to include the half period zone. The position of the minimum was detectable to $1\mu\text{m}$. The distance was measured by end-standard which had

been calibrated against an interferometric measure of length using the spectral line of Cadmium. The greatest single uncertainty arose from the use of the length standards. The microwave frequency was measured (to one part in 10^8) by comparing the klystron output against a high harmonic of a quartz crystal standard and measuring the beat frequency.

Previous determinations of this parameter include that by Essen ⁽²⁸⁾, 1950, using the electrical resonance of a length of cylindrical waveguide closed at both ends. The experiment consisted of measuring the dimensions, resonant frequency and Q of the cavity. The length and frequency were referred to the same type of standards as in the above experiment. It was accurate to one part in 10^6 .

The most recent determinations of the velocity of light, by Blaney et al. ⁽¹²⁾, 1977, uses lasers and frequency locking techniques to obtain an accuracy of one part in 10^9 .

It is of interest that these measurements were all made in the accelerated frame of the rotating earth.

2.2(c) The Caesium Clock

Essen and Parry ⁽²⁹⁾, 1957, described the standard Caesium 133 clock operating on the resonance of Caesium between the hyperfine energy levels of the nuclear and electron spins (at 9193 M.Hz. and accurate to one part in 10^{10}). A uniform magnetic field splits the energy levels into their Zeeman components, and the central component is approximately independent of the amplitude of the splitting field (the accurate value is specified when the field is of a magnitude to split the level a determined amount). The apparatus consists of an oven sending a beam of Caesium atoms through a set of magnetic fields which collimate the spins

and, in a weak uniform field, pass through a cavity into which radio frequency waves are also fed. The radio frequency electromagnetic waves resonate with the atoms when set at the correct frequency (at which frequency it is compared with the secondary quartz crystal clock).

2.3 The Rigidity of Measuring Rods

The problem of defining a rigid rod was first considered, in the context of Special Relativity, by Born and this sets up the form of the debate followed by subsequent authors until McCrea. Although the title of Born's paper was "The theory of rigid electrons in kinematical relativity theory", the analysis was in terms of kinematics until the work of McCrea (who described his system in terms of dynamics). A good summary of the references on this topic is given in the paper by Newburgh⁽⁷¹⁾, 1974.

Born's⁽¹³⁾, 1909, rigidity criterion is a mathematical description in terms of the four dimensional interval between the world lines of the particles comprising the rod. However, Synge⁽⁹²⁾, 1960, has interpreted this in terms of the time elapsed between emitting a ray and its return from the other end of an infinitesimal element of the rod after reflection. For rigidity this time should remain constant. Synge comments that this is the same as testing length by means of an interferometer and emphasises that this one-dimensional definition may not be taken over directly into defining rigidity in a three dimensional body because of problems of integrating.

The radar-type approach has similarities to the geometrodynamical clock of Marzke and Wheeler⁽⁷³⁾, 1964, which measures spatial and temporal intervals between events by reference to the ticking of a clock formed by a light ray reflected back and forth between the parallel world lines

of two mirrors. Time is measured by the number of ticks and distance by assuming the velocity of light and measuring the radar time to cover the distance. This definition of time and distance is independent of the conventional structure of matter.

Landau and Lifshitz⁽⁶⁰⁾, 1951, quote an operational definition of interval as follows: by sending a radar signal between adjacent positions (Fig. 2.4) the time for the return journey in the proper time of B may be obtained. Now, in Special Relativity the spatial distance may be defined between separated events occurring at the same time but in General Relativity the proper time at different positions may vary. Hence the spatial distance calculated assuming a radar type ranging (half the total distance travelled at velocity c) is (ref. also Atwater⁽³⁾, 1974):

$$dl^2 = \left(-g_{ik} + \frac{g_{4i} g_{4k}}{g_{44}} \right) dx^i dx^k \quad \text{E2.1}$$

$$i, k = 1, 2, 3$$

The first term is spatial and the second involves time dilatation. It expresses the relation between the metric of 3-D space and the metric of 4-D space-time.

Problems arise when these definitions for infinitesimal elements are to be extended to finite distances under conditions other than those of flat space-time in inertial frames. In general the metric changes with time and the infinitesimal spatial length, dl , may not be integrated to a macroscopic distance unless the $g_{\mu\nu}$ is independent of time. Ashworth and Jennison⁽²⁾, 1976, have pointed out the essential difference between a mathematical step-by-step integration along the path being

measured and the experimental methods of radar (with extensions to triangulation, parallax and luminosity intensity methods). Ray signal radar employed directly as co-ordinates is described by McVittie⁽⁶⁹⁾, 1945.

Basri⁽⁷⁾, 1965, considers a length-measuring instrument constructed from an interferometer. The ends of such an instrument may be defined as rigid if the instrument always maintains the same fringe pattern. In general this operates over only infinitesimal distances and finite distances can only be measured when co-linearity has been defined by which interferometers can be lined end-to-end. Reichenbach⁽⁷⁸⁾, 1958, defines three particles to be co-linear if they lie along the path of a light signal. However, Basri defines co-linear as the minimum number of interferometers linked together between the end points. Basri suggests that there are two popular ways of measuring spatial distance, by rigid rods and by light signals and clocks. In the absence of a gravitational field the results obtained by these two methods agree but in an arbitrary gravitational field they may not. He lists three authors' approaches to operational methods of determining the interval between two events. Einstein would transform to the local inertial frame and measure the interval using the Minkowski metric. Synge would transform to the specific frame of geodesic motion between the two events so that the proper time can be measured, in this frame, between the geodesic frame passing the two events. Marzke and Wheeler would use the method described above.

Two papers which form a bridge from the above discussion of Born type rigidity to that of McCrea, are those by Evett⁽³⁰⁾, 1963, and Newburgh⁽⁷¹⁾, 1974. Evett considers a rod made up of a series of sections and considers the motion of a sound wave through the rod. Newburgh postulates a standing wave formed along the rod (of proper length L)

by reflection of monochromatic light (of wavelength λ) from the far end to form a resonant cavity. For the observer, K, past whom the rod moves at velocity v , the standing wave must extend over distance d equal to the length of the rod (with Lorentz contraction) plus the distance the rod moves as the wave propagates. Thus:

$$d = L \frac{(1 - v^2/c^2)^{1/2}}{1 - v/c}$$

and

$$\lambda' = \lambda \frac{(1 - v^2/c^2)^{1/2}}{1 - v/c}$$

Hence:

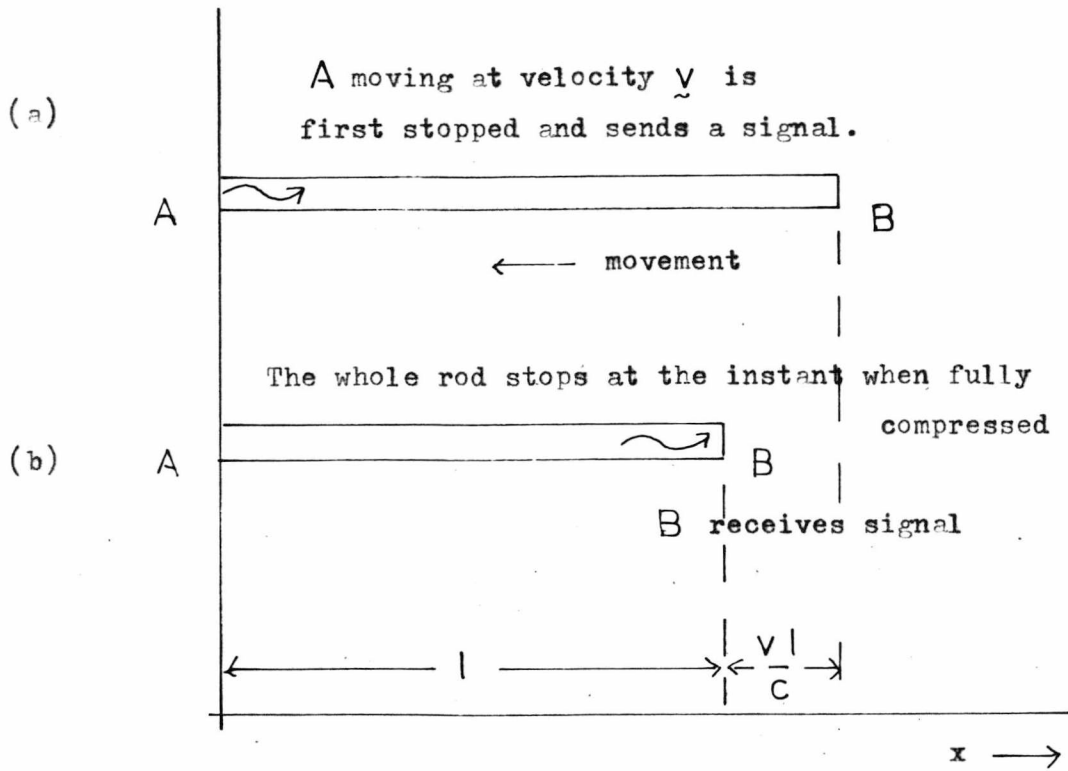
$$\frac{L'}{\lambda'} = \frac{L}{\lambda}$$

E2.2

He concludes that provided the rod undergoes Born rigid motion, the distance along the rod may be determined (for inertial motions) by electromagnetic waves propagating in the K frame. He adds that standing electromagnetic waves appear to be the best method of realising ideal measuring rods with Born type rigidity.

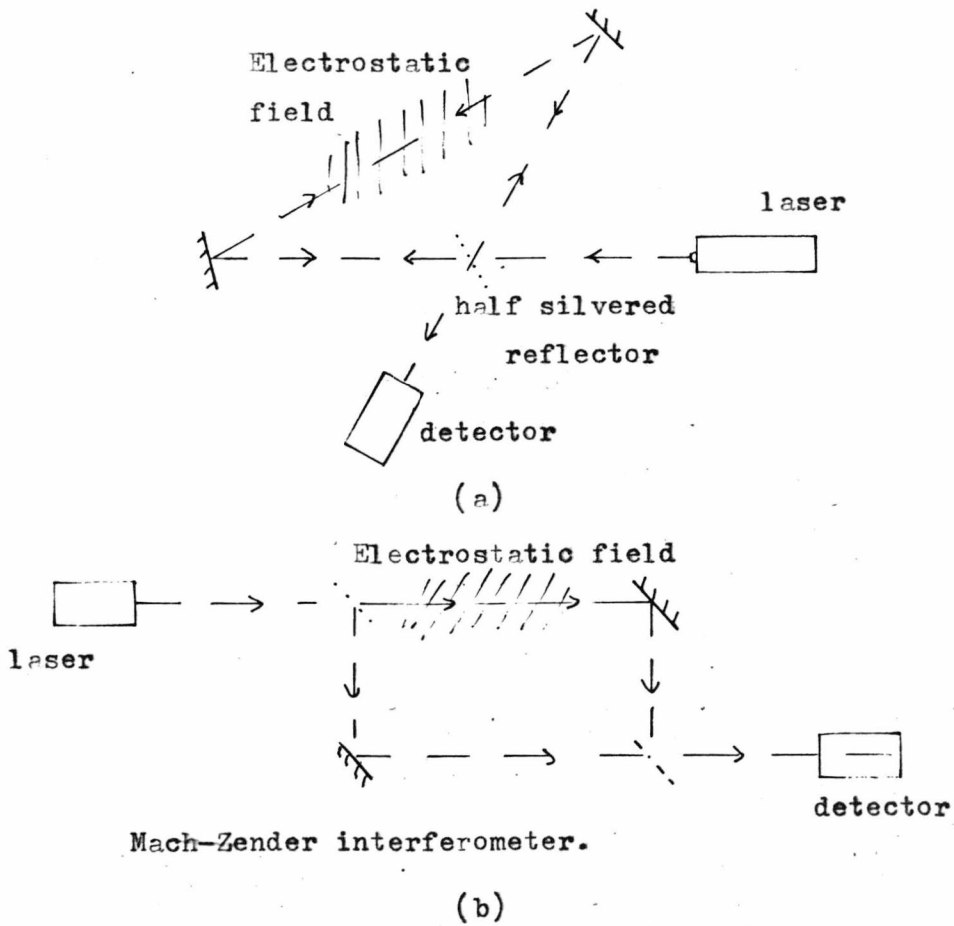
McCrea⁽⁶⁷⁾, 1952

McCrea has reasoned that because the Lorentz contraction occurs



The end A of the moving rod AB is stopped and this event is 'signalled' to the far end.

Fig 2.5



Two forms of interferometer used in Shamir's experiment, (showing the electrostatic field across the beam)

Fig 2.6

in either direction between moving frames, it depends only on the method of measurement rather than a physical change in the rod. Paradoxically, if the moving rod were 'trapped' in some way, the act of stopping it will produce the required contraction if the rod has a certain rigidity. It is now shown that this rod is one along which disturbances are transmitted with velocity c , without dissipating energy. Pushing or pulling such a rod gives different strains which gives significance to the 'drag point'.

McCrea considered a rod with mass density and rigidity such that it transmits disturbances in the mechanical sense of an alternation of kinetic and potential energies of its component particles. If one end is given a change of velocity, there must continue to be some movement in the time taken to transmit the shock wave to the far end. The transmission may be made at a maximum speed of c by electromagnetic waves. For a moving measure of this type stopped at one end with an instantaneous change of velocity, the event is signalled (first 'seen') to the other end at the speed of light. In Fig.2.5, a rod of proper length L moving past at velocity V has a length given by the Lorentz contraction of:

$$L' = L \left(1 - \frac{V^2}{c^2} \right)^{1/2}$$

When one end is instantaneously stopped, the time for the signal to reach the end B is :

$$t = \frac{l}{c}$$

where l is the length when the whole rod is momentarily stationary. In

this time the end B has travelled a distance:

$$v \frac{l}{c} .$$

Thus

$$l = L \left(\frac{1 - v/c}{1 + v/c} \right)^{1/2} . \quad \text{E2.3}$$

At this moment the rod could be trapped in a contracted state. This is also the 'visual' length of the moving rod seen by rays from its ends.

By analogy with compression waves in a rod, the modulus of the above system gives

$$c = \left(\frac{\lambda}{m} \right)^{1/2} , \quad \text{E2.4}$$

where m is the mass per unit length and the modulus λ determines the tension T according to:

$$\lambda = \frac{T}{\Delta L/L} .$$

He proves that the same condition on the modulus gives a perfectly elastic conversion of potential and kinetic energies.

Hogarth and McCrea⁽³⁹⁾, 1952, consider the relativity of the energy in such a system, and calculate the kinetic energy converted to potential energy when one end of a moving rod is stopped.

2.4 The Nature of Inertial Mass

This section starts by indicating how Einstein attempted to embody Mach's principle into a complete theory. The major themes in this

controversial topic include whether Mach's principle is contained in Einstein's General Relativity (Dicke in particular demonstrates that it is not) and, perhaps as a separate issue, whether Mach's principle is valid in some theory alternative to Einstein.

The theory specifically constructed to incorporate Mach's principle is that by Sciama, which is described next. There are also further developments from the original simplified theory.

A more elaborate theory incorporating Mach's principle is that by Brans-Dicke⁽¹⁵⁾, 1961.

2.4(a) Main theories as to the origin of the inertia of mass Einstein

Einstein made two attempts to make his equation fully incorporate Mach's principle.

The introduction of the Cosmological constant so that there would not be a solution for the case of an empty Universe, was challenged by De Sitter and the resulting Einstein-De Sitter Cosmology goes beyond the scope of this thesis.

Einstein⁽²⁴⁾, 1922, considered a weak field solution variation about flat Minkowski space giving a wave-type equation which was solved using retarded potentials to give an expression, in terms of the integral over all space of the matter tensor:

$$\frac{d}{dt} [m(1+\phi)\underline{v}] = \text{grad } \phi m + \frac{\partial \underline{A}}{\partial t} m - m(\underline{v} \wedge \text{curl } \underline{A}) \quad \text{E2.5}$$

where ϕ and \underline{A} are the scalar and vector potentials formed by integrating the delayed effect of all the mass sources and the product of the sources with their velocities for masses which are sufficiently local to

leave the metric at great distance tending to Galilean space-time. This gives the integral effect of matter on a test particle of mass m moving at velocity \vec{v} in the frame in which (\vec{A}, ϕ) has been evaluated. Nightingale⁽⁷²⁾, 1977, has calculated a value for ϕ suggesting that if the known Universe is removed the left hand side in the above equation becomes zero, which agrees with Mach. It was shown by Thirring⁽⁹³⁾, 1918, that the above equation also gives a centrifugal effect as well as the dragging and Coriolis-like effects of the second and third terms in the right hand side. An increase in the inertial mass of the test particle due to the added presence of massive bodies may be attributed, however, to a co-ordinate effect. A critical discussion of this result is given in section 2.4(b).

Sciama

The main attempt to set up a theory alternative to that of Einstein and incorporating Mach's principle, is that by Sciama which has been further modified and developed by Davidson and Brans-Dicke.

An introduction is given in Sciama⁽⁸³⁾, 1957, and more mathematical detail is given in Sciama⁽⁸²⁾, 1953. He postulates a Newtonian type inverse square law field and a further inverse distance induction potential (or radiation field by analogy with electromagnetism). The generation of an inertial force when a body is accelerated is by induction in the four-vector field created by the matter in the Universe. This system is Machian in that 'matter is moving against matter'. A free test particle moves in a gravitational field so that the gravitational field of the local mass is cancelled by the induction field of the Universe as viewed in the proper frame of the test particle. Electromagnetic effects are not included in this simplified form of the theory.

The first component of the field from every body is the inverse

square field from the static scalar potential:

$$\vec{F}_{\text{grav}} = \frac{G m}{r^2} \quad , \quad \text{E2.6}$$

which falls away rapidly with increasing distance. (This component is assumed to be approximately independent of the velocity.) The integral of this field component for all the mass in the Universe gives no net field although there is a uniform, non-zero, potential:

$$\phi = - \int_{\text{Universe}} \frac{G \rho}{r} dv \approx - \frac{GM}{R} \quad , \quad \text{E2.7}$$

where R is the radius of the Universe and M is its mass assumed to be of uniform density ρ .

The second component of the inertial gravitational field is inductive. The Universe generates a 4-potential field as, when a test particle moves with velocity \vec{v} in this ϕ , there is a local and instantaneous formation of a vector potential \vec{A} (as in electromagnetism) where

$$\vec{A} = - \int \frac{G \rho \vec{v}}{c r} dv = \frac{\phi}{c} \vec{v} \quad . \quad \text{E2.8}$$

(The Hubble law distribution of radial velocities gives, because of symmetry, zero net vector potential). Again by analogy with electromagnetism, the vector potential gives a field having a negative sign:

$$\vec{F}_{\text{inertial}} = - \frac{\phi}{c^2} \frac{\partial \vec{v}}{\partial t} \quad \text{E2.9}$$

It may be observed that this field is proportional to the potential ϕ (rather than the gradient of the potential ϕ) which means that its

amplitude, as for ϕ itself, decreases inversely with distance. The case of centrifugal forces in a rotating frame is also considered here. An important property of this field is that, although all bodies generate ϕ according to E2.7, it is primarily determined by the large quantities of matter at great distances because of the inverse distance law. Local masses have negligible effect on the inertial force.

A test particle moving near a mass m , moves so that in its own frame the sum of the inverse square law field $F_{\sim \text{grav}}$ and the inverse distance field $F_{\sim \text{inertial}}$, cancel to zero. Hence

$$-\frac{Gm}{r^2} - \frac{\phi}{c^2} \frac{d^2 y}{dt^2} = 0$$

$$\text{Acceleration} = -\frac{c^2}{r^2 \phi} m G, \quad \text{E2.10}$$

which gives a value for the gravitational constant of:

$$1 = -\frac{c^2}{\phi} \cdot \quad \text{E2.11}$$

Thus in a sense G is not constant but depends on the masses of the Universe according to E2.7, giving:

$$G \approx \frac{c^2 R}{M} \quad \text{E2.12}$$

The form of this equation may also be derived, by simple dimensional argument, from the basic dimensions of the Universe. Dicke⁽¹⁷⁾, 1964, has remarked that in order for this equation to remain valid, it is as if the Universe were a giant servosystem, continually adjusting particle masses to the value appropriate to the above equation as a feedback

condition.

Equation E2.9 considered only the analogue of the 'electric' field generated by the 4-potential. In general there may also be a 'magnetic' field:

$$\vec{F}'_{\text{inertial}} = \text{curl } \vec{A} \quad \text{E2.13}$$

This acts on a particle, moving with velocity \vec{v} past the main body, to give

$$\text{Coriolis acceleration} = \vec{v} \wedge \vec{F}'_{\text{inertial}} \quad \text{E2.14}$$

Thus Sciama, used a four-vector potential with which he was able to obtain the main properties of inertia. However, to derive Newton type laws for all possible motions requires that inertial forces should be derived from a tensor potential. Ten potentials are required to specify the stress-energy-momentum of the sources of the gravitational field and ten are required to give the effect on light rays (Sciama⁽⁸⁴⁾, 1969) which is twice that for a scalar potential.

Lynden-Bell⁽⁶⁴⁾, 1967, criticised Sciama's simplified theory for not including electromagnetism. Light cones in 4-space are both the limiting surfaces onto which very fast particles tend and the invariant structure of space-time. To be consistent, the light cones must be twisted in precisely the same way as the limit at great velocity of particle paths, so the twisting should be attributed to the same cause. Inertia and the local space-time frame must be determined by the same cause.

Davidson⁽²⁰⁾, 1957, equated Sciama's 4-vector potential with certain complete components of the metric tensor. These components are transformable to any frame.

$$A_i = -c^2 g_{4i} \quad \phi = \frac{c^2}{2} g_{44} \quad \text{E2.15}$$

Sciama's equation for the combined effects of the inertial fields is:

$$\text{Acceleration} = -\text{grad } \phi - \frac{1}{c} \left[\frac{\partial \underline{A}}{\partial t} - \underline{v} \wedge \text{curl } \underline{A} \right] \quad \text{E2.16}$$

which Davidson writes (strictly l.h.s. involves $g_{ii} v^i$, but $g_{ii} \approx 1$) as

$$\frac{dv^i}{dt} = -\frac{c^2}{2} \frac{\partial g_{44}}{\partial x^i} - \frac{\partial}{\partial t} (-g_{4i} c) + c v^k \left(\frac{\partial g_{4i}}{\partial x^k} - \frac{\partial g_{4k}}{\partial x^i} \right) \quad \text{E2.17}$$

$$v^k \equiv \text{particle velocity} \left(\frac{v}{c} \ll 1 \right) \quad i, k = 1, 2, 3$$

However, this equation may also be obtained from the spatial equations of the geodesic equations of General Relativity for the approximation of small velocities and deviations from Galilean conditions. Hence it has been demonstrated that the acceleration of a test particle by the field postulated by Davidson (and Sciama) is (approximately) the same as for a particle following a geodesic of General Relativity. The former, however, accounts for the complete value of the components of the metric tensor rather than only the variations about their value at great distance from matter. In the frame in which the Universe is stationary the component g_{44} is obtained by an integral over all matter by Sciama's approach. Then by general transformation the metric is determined in any other frame and hence A_i and ϕ are determined in any other frame.

The Integration of Gravitational Effects

The integral, rather than differential, form of Einstein's field

equation was considered briefly by Einstein⁽²⁴⁾, 1922, (and E2.5 above) by obtaining by approximation an equation of the 4-D form of Poisson's equation and re-writing it in integral form. To avoid the approximations made by Davidson (following Einstein) in accounting for the integral effect of all matter received at some position, the integral form of the field equation has to be considered in detail. Lynden-Bell⁽⁶⁴⁾, 1967, has specified the main problems as being how to integrate effects from ~~components of the energy-momentum tensor of matter at different metric potentials and how to account for the non-linear properties of gravitational effects in the summation.~~

2.4(b) The controversy over Mach's hypothesis

The main papers are by Dicke who is primarily concerned with proving that Mach's principle is not fully contained in Einstein's theory, Wheeler who is primarily concerned with boundary conditions, and McCrea who is primarily concerned with local versus Cosmic origins of inertia.

Dicke⁽¹⁷⁾⁽²²⁾⁽¹⁾, 1964, has pointed out that the metric derived from Einstein's field equations is partially dependent on the total mass in the Universe and is not fully dependent on it. According to this description, space has physical structure and properties despite its mass-energy content. In particular he makes the following objections to Einstein's approach in the context of Mach's principle.

Einstein's equation has solutions for a Universe which is almost empty (apart from the masses of the test equipment), having structure and boundary conditions little related to the trivial amount of mass present. For example, a laboratory inside a small hollow shell of mass M and radius R rotating at ω , inside such a Universe would be influenced by the Lens-Thirring effect dragging the inertial co-ordinate

frame by an amount $\frac{GM\omega}{Rc^2}$, but the full inertial properties do not depend on the mass of the shell. Again, Taub has found a solution of this equation for an empty Universe containing space-time curved by gravitational radiation. There are flat space-time solutions for both an empty Universe and the space within a massive hollow shell (although this latter is the nearest to incorporating Mach as the shell will give a small proportion of Machian effects).

Einstein's differential equation requires boundary conditions and these are usually supplied by reverting to Newtonian equations as a first approximation when the fields have become weak.

Mach's principle requires that G is (at least potentially) a variable depending on the total distribution of matter. Local masses should have some small (but unmeasurable) effect on the inertia of test particles.

It has been suggested that Mach's principle cannot be obtained in General Relativity because the energy-momentum tensor for matter presupposes already metrical magnitudes. This point is explained by McVittie⁽⁶⁹⁾, 1954.

Wheeler⁽¹⁷⁾, 1964, makes the following objections. Einstein's equations are non-linear, and it is wrong in principle to superpose the effects from different sources. For a general space-time metric the distance is not well defined and yet is required for the inverse-distance property. The retardation of potential from sufficiently distant matter may go back to some undefined initial condition. The necessity for initial conditions has been taken up by Graves⁽³⁶⁾, 1971, and Ohanian⁽⁷³⁾, 1976.

McCrea⁽⁶⁸⁾, 1971, has suggested that Mach's principle is founded on an illusion. By looking at a distant object one is looking in a fixed

direction, if distant objects are defined as those so far away that the angle they subtend does not vary appreciably even if they move near the speed of light. By watching such a remote object, one is picking out a succession of parallel null lines. The remote object sets up the null-cone structure observed in the locality of the observers world-line. This suggests that a mechanical system such as a Foucault pendulum explores or detects the local null cone structure. Thus looking at distant objects or watching Foucault pendulum are just alternative ways of exploring the local null-cone structure. The remote masses need not determine the local structure.

Klein⁽⁷⁵⁾, 1962, suggests there is hardly any direct meaning of Mach's principle in General Relativity. Present knowledge suggests regarding the Cosmos as a weak zero point energy excitation of the vacuum state comparable with Newton's absolute space (c.f. Sciama⁽⁸⁵⁾, 1978).

2.5 Cavity-Trapped Radiation and Closed Systems

This thesis is specifically concerned with trapped monochromatic radiation. However, the subject arose out of the work of authors on black body radiation and the thermodynamics of cavities for which Schmid⁽⁹¹⁾, 1970, is a summary containing the following points. Einstein (1907) emphasised that whether or not the energy and momentum of a system are the components of a four vector depends on whether or not the stress energy of the container is included. Hasenohrl⁽³⁷⁾, 1905, attempted to improve Abraham's model of the electron by considering the radiation pressures on the boundary containing the electron. He indicated that the second laws of thermodynamics (that entropy does not decrease) requires a Lorentz type contraction, and obtained an expression for the effective mass of the trapped radiation. Lenard⁽⁶³⁾, 1936, analysed a cavity system in which the whole container moves off instantaneously when pushed and so he does not consider the energy interchanges with the Binding mechanism.

Also he considered a multiplicity of frequencies so there is no locking of the system according to wavelength but only by the radiation pressures when there has been one circulation of the energy. He summarized previous work by considering radiation along one direction for a cavity containing energy E pushed by force \bar{F} against its increase of internal radiation pressure, at velocity δv for time δt :

$$\bar{F} = \frac{E}{c^2} \frac{\delta v}{\delta t} \quad \text{E2.18}$$

Pauli⁽⁷⁴⁾, 1921, in a section on the relative motion of a black body cavity of radiation, observes that the radiation pressure on the walls is an invariant.

Birtwhistle⁽¹¹⁾, 1927, obtains the result (to first order in v/c) that when a spherical enclosure of perfectly reflecting walls has the walls moved in or out, the Doppler shift of the frequency of the internally reflected waves in any direction is such as to change the wavelength in the same ratio as the cavity size (thus standing waves may be maintained within perfectly reflecting walls when moved to a different separation).

Krause⁽⁵⁹⁾, 1975, notes some suggestions by G. W. Leibniz as to how considerations of cavity radiation may be extended to considering fundamental atomic particles as modes of oscillation in resonant elementary volumes of space. Inertial forces experienced when such an element is accelerated are due to differences of radiation pressure on the reflecting surfaces. After being accelerated, such a cavity of radiation has an additional wave, certain parameters of which should contain a measure of the momentum absorbed and relate to the De Broglie wave.

Newburgh and Dewan⁽⁹¹⁾, 1970, considered (in the context of thermodynamics) the kinetic and dynamic aspects of the Lorentz contraction for a

spring binding two rockets and clarified the role of the potential energy changes of the binding mechanism. The authors call a 'pure' acceleration one of Lorentz contraction which leaves the internal state unchanged. The subsequent discussion report mentions using an electrostatic field for the binding energy and travelling waves to determine the separation. Also the distinction between the total system including the container, and the part-system of the confined radiation, is made. This point was considered in detail by Landsberg and Johns⁽⁶¹⁾, 1967, who derived in a very simplified fashion (considering the trapped energy as particles with momentum) the equations for the moving system:

$$E = \gamma \left(E_o + \xi \left(\frac{v}{c} \right)^2 p V_o \right) \quad \text{E2.19}$$

$$\underline{P} = \frac{v}{c^2} \gamma \left(E_o + \xi p V_o \right) , \quad \gamma = \left(1 - \frac{v^2}{c^2} \right)^{-1/2}$$

where $\xi = 0$ for a system including the container and $\xi = 1$ for a confined part-system. E_o , p and V_o are the energy, pressure and volume in the rest frame of the container. v is the velocity with which the system is moving past. E and \underline{P} are the energy and momentum of the system.

2.6 Ball Lightning

This section describes the conditions during a thunderstorm (which is the environment in which Ball Lightning_g may be formed). It then describes Ball Lightning_g itself. Only a mention of the main references will be given here because the interest of this thesis is only in the existence size and possible electromagnetic structure of this phenomenon.

Malan⁽⁶⁶⁾, 1963, and Encyclopedia Britannica⁽²⁶⁾ describe the formation of thunderclouds and distinguish between tropical convection of air off

the warm ground and temperate climates where a warm air front is pushed up and over a cold front. Fork lightning consists of a leader stroke taking a negative charge down from the cloud with emission of h.f. electromagnetic waves and, when a full conducting plasma has been formed, a return stroke emitting lower frequency waves. The cloud is at about 10^8 - 10^9 Volts and the base of the thundercloud is about 2km and the top of the cloud about 12km above ground. The lightning stroke is preceded by a leader with stepped motion, whose tip gives a highly convergent electrostatic field (much more intense than the average over the space below the cloud) of the order of 30-60kV/cm for propagation of the leader. The flash discharges about 20 coulombs and an energy of about 10^{10} Joules. Estimates of ionisation in the plasma give about 4×10^{18} electrons/c.c.

Kosarev⁽⁵⁸⁾, 1969, reported measuring radio frequency radiation from thunderclouds at 800 M.Hz. and 1300 M.Hz. and possibly another maximum at higher frequencies. The h.f. was emitted with the stepped, dart, leader stroke. An explanation of the h.f. radiation as being from intra-cloud streamers based on current variations is still problematic.

A survey of Ball Lightning reports has been made by Singer⁽⁸⁹⁾, 1971 and Rayle⁽⁷⁷⁾, 1966, conducted a questionnaire to which he received 112 positive replies. Different shapes reported include hollow, oval, torus and some report a halo. Most observations are 1-5sec. duration but cases up to one and even 15 minutes are recorded. Singer's report on the sizes of the ball is reproduced in Fig.6.1 and Rayle's report indicates an average diameter of about 14 in.

The absence of any heat radiating has been especially noted in the surveys but if the ball becomes attached to a conductor (including humans) it is burnt. Most estimates of the energy trapped in the ball seem so large as to suggest that it is not true Ball Lightning which is being

described. Thus Rayle quotes 10^6 joules as the average energy content. The energy content has been indicated by the water-tub report of Morris⁽⁷⁰⁾, 1936, as 10^7 joules and Balyberdin⁽⁵⁾, 1965, estimates 4×10^9 joules released in the final explosion. However, the Smethwick report of Wooding⁽⁹⁶⁾, 1976, of a Ball 10 cm. diameter with halo, suggested the damage caused corresponded to 2×10^3 joules total Ball energy.

In frequent reports the Ball travels in passageways and through orifices (those travelling near the ground appear guided by possible electrical conductors). Rotation of the Ball is commonly reported.

Individual reports on Ball Lightning include the following. Jennison⁽⁴⁵⁾, 1969, reported a personal observation of a Ball within a flying metal aircraft. It was about 22 cm. diameter and appeared to be guided by the walls of the craft. In a postscript, Jennison⁽⁴⁶⁾, 1973, suggests no steady strong magnetic field was associated with his observation, and that a further aircraft report suggests that the Ball is independent of airflow past it. He suggests the formation of a phase-locked loop of electromagnetic radiation at a specific frequency in the intense fields of the lightning storm (which may be analogous to electron-positron formation by 1.1 MeV gamma rays).

Mention will now be made of the work of two authors who have considered possible structures for Ball Lightning involving the trapping of electromagnetic waves.

Kapitza⁽⁵⁴⁾, 1955

Kapitza proposed a plasma mechanism resonant to impinging electromagnetic waves and postulating the existence of an intense, external electromagnetic radiation to supply a continuous energy input (and hence account for the comparatively long life-time of the Ball). He suggests

that waves reflected off a conducting earth surface form standing wave antinodes which tend to stabilise the height of the Ball (these waves may also be formed in waveguide-like openings). This theory was extended by investigating the confinement of charged particles by a polarized standing electromagnetic wave where particles are drawn into the electric nodes.

Kaptiza⁽⁵⁵⁾, 1970, has attempted to reproduce Ball Lightning-type conditions in the laboratory. He conducted a series of experiments on a gas trapped in a spherical metal cavity that was resonant for high power microwaves, of wavelength about 19 cms. being continuously supplied from a magnetron. The results were in two main sections. At higher pressures (about 2.9 atmospheres) and with more microwave power supplied (of the order of 100 k.watts), a filament of discharge was formed of about the length of a half wavelength of the radiation. This filament tended to float upwards in the cavity unless stabilized by rotating the gas about the central horizontal axis of the container. The filament was stable with reflection of internal electrons off the double layer formed at the boundary with the cooler gas (this was most easily performed with helium gas but air could be used as the gas). At lower pressures (below one atmosphere) and lower power supply of the microwave, a diffuse, oval shaped glow (which might represent Ball Lightning) tended to be formed in the region of maximum electric field.

Endean

Endean⁽²⁷⁾, 1976, suggests that positive and negative space charges may on occasion be formed by the leader stroke of fork lightning as it approaches the ground drawing charge of opposite polarity from the ground in such a way that they are out of alignment and form a rotating vortex

of air separated into different charged regions which forms a rotating dipole field in a cylindrical cavity with an ionised sheath separating it from the atmosphere. The return path for the current in the walls of the cavity is the displacement current. In this mechanism for Ball Lightning, the extremity of the field from the dipole rotates with a phase velocity greater than c and gives an outward radiation pressure on the ionised sheath separating the internal cavity from the atmosphere. For a stable configuration he obtains for the rotating dipole field a relation between the magnetic and electric fields which ensures a balance of the internal radiation pushing outwards and the atmospheric pressure pushing inwards.

2.7 The Work of some Previous Authors on Possible Electromagnetic Field Structures of Fundamental Atomic Particles

The possible similarity between the structure of Ball Lightning and stable atomic particles is only mentioned in passing in this thesis, and this section will be kept very brief.

Theories on atomic particles may be classed into those which consider point or diffuse particles and those which consider the structure of extended particles. In the present context both approaches raise problems in that point particles constitute singularities and infinities of the fields while extended particles raise questions of rigidity across the extended region and a coercive force acting over an extended space. Here we shall be concerned primarily with those aspects of the second class of theory which throw light on a possible trapped wave extended structure based on an electromagnetic wave configuration or a small non-linear modification of Maxwell's equations.

One approach to the problem has been to account for the extended

structure (and, in some cases, source of electric field) of atomic particles by non-linear fields forming the particle). For example, non-linear electromagnetic fields were postulated by Born and Infeld⁽¹⁴⁾, 1934, (following an unsuccessful attempt by Mie (q.v. Sen⁽⁸⁶⁾, 1968)). By analogy with the relativistic form of the expression for kinetic energy compared with the Newtonian expression, they extended the Lagrangian for the electromagnetic field to give an upper limit to the electrostatic field (say, at the centre of the electron) and obtained modified Maxwell equations in terms of a maximum field strength (analogous to a limiting velocity). These authors quote the value of this physical constant as 10^{16} e.s.u. of electric field. The field equations have the form of Maxwell's equations for a polarizable medium for which the dielectric constant and magnetic susceptibility are special functions of the field components.

Following this theory there has been a range of work developing a more accurate account of relativistic (e.g. Dirac⁽²³⁾, 1951), and quantum (e.g. Schiff⁽⁸¹⁾, 1962) properties. A non-linear field equation for electromagnetism causes both self-interaction of the wave so that it appears to be in a medium of different refractive index and wave-wave interaction in which one field may act to refract the other wave.

Another approach to the problem has been in terms of an internal wave structure of the particle and what binds such an extended structure together (the waves should circulate in the proper frame of the particle to give the effects considered in chapters 3 and 4).

Japolski⁽⁴⁰⁾, 1935, made an extensive study of rotating electromagnetic waves. He postulates a wave whose motion may be described as corkscrew. This shape of wave may either be said to propagate along the

line of axis or rotate about the line of axis without change of shape. Using Maxwell's differential equations he obtains a solution of the field pattern. He divides the circularly polarized wave into plane polarized components and makes an analogy between the rotating electric field and the magnetic field of a polyphase induction motor. Using multiple frequencies he obtains a wave packet which he relates to De Broglie wave requirements. This analysis has been criticised by Podolsky⁽⁷⁶⁾, 1936, on the grounds that the Maxwell equations are linear and therefore cannot give rise to interactions (or self-interactions) of the 'whirl' wave packets envisaged by Japolsky. Later Japolski⁽⁴¹⁾, 1936, refers to interactions between fields due to interactions between displacement currents in the medium.

Thompson⁽⁹⁴⁾, 1939, considers the waves constituting the electron as spiralling in a helix and equates these with the waves calculated by Japolski. The size of this electron varies with its velocity becoming large at low velocities. This wave spiralling around the direction of motion in a helical motion, viewed in the frame of the electron, would be a wave rotating about the centre which is equivalent to two waves in space and time quadrature.

Jennison⁽⁴⁸⁾, 1978, has suggested that modes of electromagnetic standing waves in a cavity may represent a simplified form of the three-dimensional spinning wave configuration which may represent an atomic particle.

Gerharz⁽³³⁾, 1976, postulates a strong local curving of space (c.f. Wheeler's 'geons') causing a collision process between γ and ν rays in counter rotation about the electron circumference.

The binding mechanism has been a perennial problem since Abraham

assumed a mechanical stress on a spherical electron structure (c.f. Yadava⁽⁹⁷⁾, 1976, for a brief list of authors on this topic). The cohesion pressure introduced by Poincare (1906) which enveloped the electron at rest like a membrane under confining tension is not unlike the 'quark bag' structure suggested recently for the nucleus (Hasenfratz and Kuti⁽³⁸⁾, 1978).

2.8 Experimental Investigations for Electromagnetic Field Non-Linearities

One of the consequences of a non-linear property of electromagnetic waves is that there should be self-interaction of the wave. The experimental result of this is that the waves should travel slightly more slowly depending on frequency (dispersion). Some physicists describe this in terms of the photon having an appreciable rest mass.

Goldhaber and Nieto⁽³⁵⁾, 1976, in the context of the Proca equation tabulated the results of a number of exact investigations on Coulomb and Gauss laws for electrostatic and magnetic fields (the inverse square law is normally assumed to apply for Coulomb). The most accurate was the measurement of Jupiter's magnetic field by a spacecraft which indicated no measurable field non-linearity corresponding to the photon rest mass being less than 10^{-48} gm.

Bass and Schrodinger⁽⁸⁾, 1955, refer to De Broglie's estimate from the lack of colour phenomenon in distant eclipsing binary stars (lack of dispersion) that there was no wave self-interaction corresponding to the photon rest mass not exceeding 10^{-44} gm.

Clark and Watson⁽¹⁸⁾, 1929, investigated if there is any change of wavelength of a plane polarized wave as it moves into a static electric field parallel to its E vector. They used a diffraction grating to

measure (any change of) wavelength and applied a steady field of 80 k.V./cm. The image on the photographic plate would have detected a change of wavelength $\Delta\lambda = \lambda \times 3 \times 10^{-5}$. Thus there was no greater change in refractive index produced by the transverse electric field than 1.3×10^{-7} per e.s.u.

Kennedy and Thorndike⁽⁵⁶⁾, 1931, compared the frequency of a spectral line from a mercury discharge lamp at zero potential with that of the electrostatic potential of 50 k.V., the observing apparatus being at zero potential. To avoid Stark effects the source was screened. The light was detected in a Michelson interferometer and a type of synchronous detection was used by repeatedly photographing the pattern with the e.h.t. alternately on and off. The change in frequency was less than three parts in 10^{14} per volt (the experimental error).

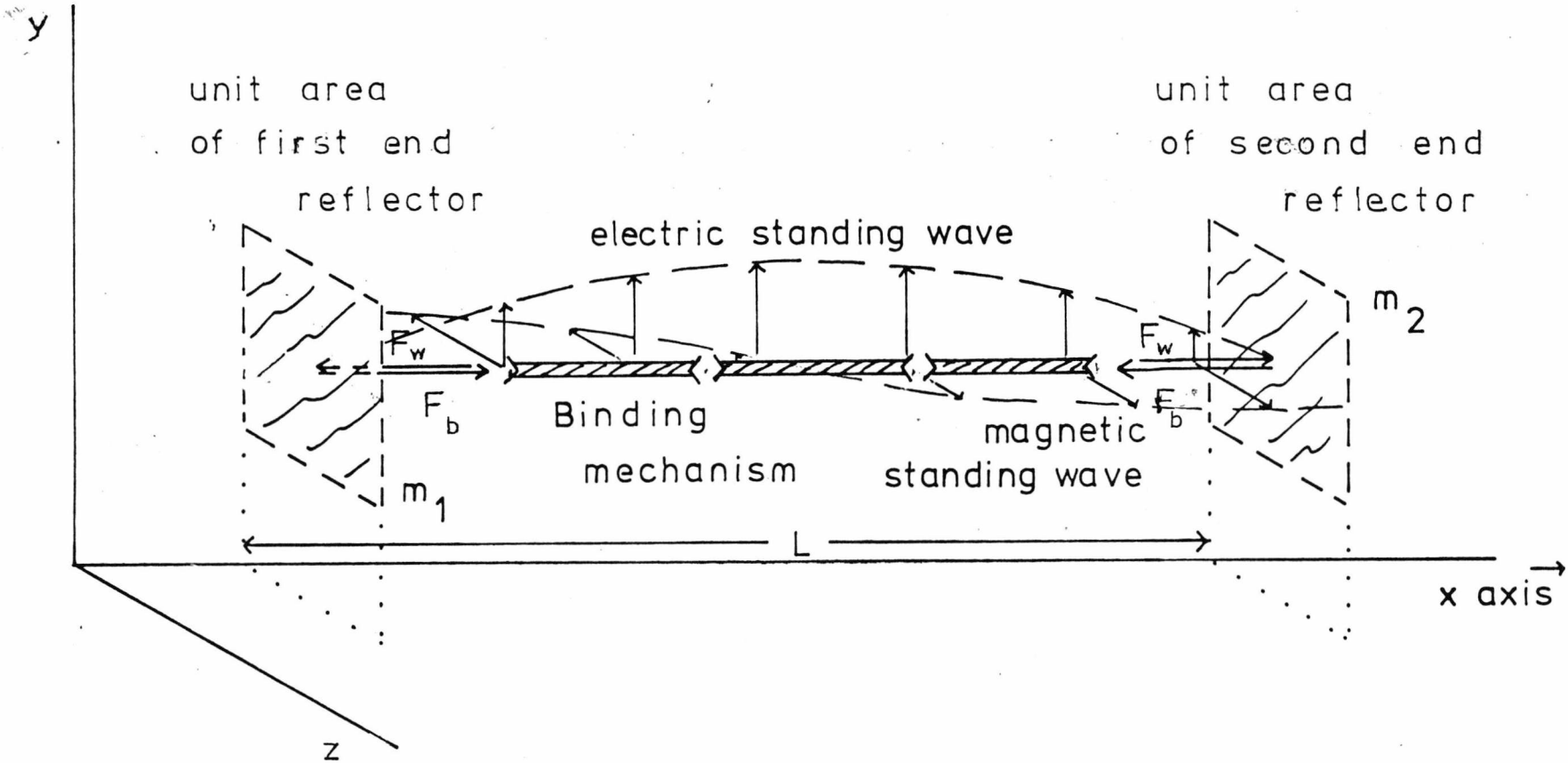
Jones⁽⁵⁰⁾, 1961, performed an elaborate experiment to determine any deflection in a beam of light due to a wedge shaped (prism) magnetic field. Synchronous detection was used. There was no change in refractive index to one part in 10^{12} due to a field of 8×10^3 oersted (6×10^5 amp m⁻¹). The author comments that this method would not have detected a split or symmetrical scatter by the magnetic field.

Banwell and Farr⁽⁶⁾, 1940, report an experiment using a Michelson interferometer to detect the effect of a magnetic field on the velocity of light. The result indicated a possible increase in the velocity of 34 (×19) cm./sec. in a field of 2×10^4 oersted (1.6×10^6 amp m⁻¹) but the authors expressed doubt about the result.

Shamir⁽⁸⁷⁾, 1970, passed the beams of an interferometer (using a laser) in opposite directions through an electrostatic field (Fig.2.6(a)) over a distance of 60 cm. and in a second experiment with the field in only one beam (Fig.2.6(b)). He showed the change in refractive index was

such as to cause a change of velocity of less than $\Delta C < C \times 7 \times 10^{-10}$ for an electrostatic field of 7×10^5 V/m.

There are some further authors on this subject listed by Kane and Basavaraju⁽⁵³⁾, 1967.



The system of internal waves trapped by end reflectors.

Fig. 3.1

Chapter 3

THEORETICAL CONSIDERATIONS OF THE PROPERTIES OF TRAPPED
ELECTROMAGNETIC RADIATION FOR INERTIAL FRAMES IN
FREE SPACE

3.1 Introduction

This chapter derives in detailed theory the movement of the particular system described below when a steady force is applied to one of its reflectors. The force causes it to move from its initial state of rest in the laboratory (assumed to be an inertial frame). The chapter is entirely restricted to the conditions of Special Relativity for movement from one inertial frame to another. The analysis shows how a series of step increases in velocity constitutes an acceleration of the system regulated by the (stepping) time for the disturbance caused by the force to distribute throughout the system. The derivations of the physical operation of the change of length and frequency of the internal radiation, as the system is moved from one inertial frame to another, as described herein, are original work of this author based on the system set up by Jennison in the papers of Jennison and Drinkwater⁽⁴⁷⁾, 1977, and Jennison⁽⁴⁸⁾, 1978. A discussion compares this system with those of previous authors, set up to define rigid measuring rods. The final section indicates how Jennison has related this approach to the physical properties of the electron.

The undisturbed system consists, in its proper frame, of monochromatic waves of equal amplitudes moving in opposite directions and forming a standing wave (Fig. 3.1). To close the system it is assumed that perfect reflectors of negligible mass are placed at two of the nodes of the electric field to recirculate the energy. However, the movement of the free reflectors is determined by the wave. A binding

force balances the radiation pressure and the amplitude (and frequency) observed on the reflector remains constant. An external force applied to one of the reflectors over-rides the above condition on frequency by pushing against the increase in radiation pressure of the internal waves.

It is shown that the distance between the reflectors and the frequency of the internal radiation, in the final inertial state, compared with that in the initial inertial (laboratory) frame agree with the equations of transformation of length and time given by Special Relativity. The parameters of length and time are referred to measurements made with apparatus that could, at least in imagination, be constructed around electromagnetic waves. This suggests that length and time in a moving frame should be established by similar principles. It is also shown that the trapped waves behave as an inertial mass.

The calculations are performed as follows. The kinematic equations for the movements of each end of the system, when the first end is given a steady change of velocity, is analysed first. This is done by repeated application of the Einstein⁽²⁵⁾, 1905, equation for transformation of frequency of a light ray (as seen by an observer moving at another velocity) to the wave reflected off each mirror. It is then required that the frequency, ν , observed on the mirror is constant and this then determines the motion of the mirror.

The change of frequency of a clock, based on the repeated returns of a ray to the first reflector as its timing mechanism, is calculated for the same change of conditions of the system, using a space-time diagram.

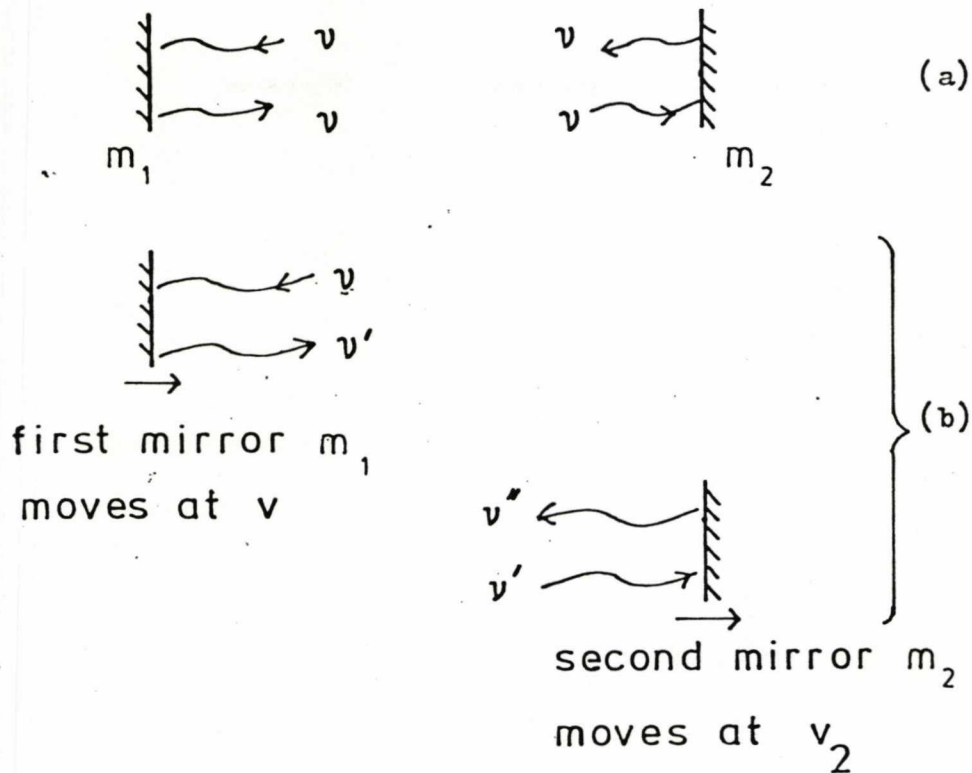
The analysis of the dynamics of the system is performed by considering the extra force when the system is pushed at one of the nodes of its internal standing wave. The calculation is based on the method of considering the condition as seen by an observer moving with the reflector as it is pushed into the radiation. In this frame the

usual laws of reflection of the waves describe the physical condition. An equation is obtained relating the total trapped energy (which is required in the final equation for the equivalent mass) to the conditions at the first reflector. A second equation equates the forces for equilibrium at the first reflector. These equations are then solved to express the externally applied force in terms of the total energy of the system and the average acceleration (calculated in the previous section on kinematics).

3.2 Kinetics of the Etalon and the Lorentz contraction

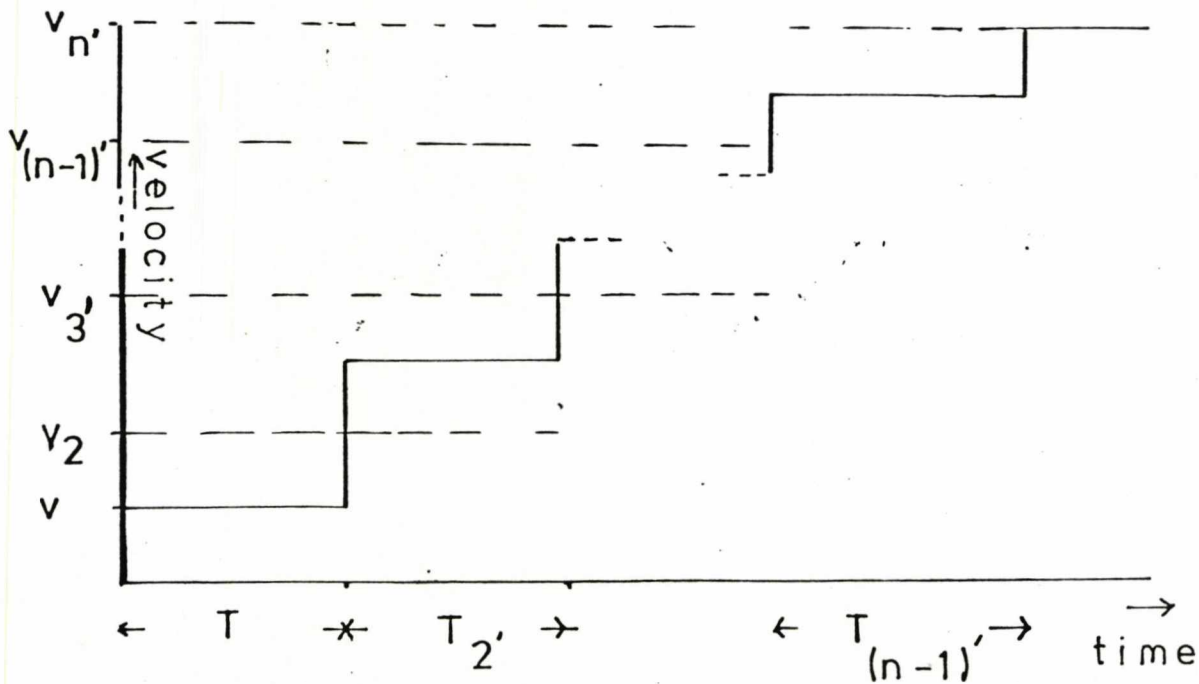
This section obtains equations for the movements of the reflectors at the ends of the system when it is pushed, at one end, from one inertial frame to another. It demonstrates that the system 'lock's into' a new stable state of motion after each complete circulation of the wavefront caused by the external disturbance. If one reflector is changed to a different velocity, the frequency of the monochromatic wave reflected off it will change and therefore the second reflector has to change to a suitable velocity if the waves are to continue to appear at the same frequency, ν , to an observer on this mirror. The reflectors only reverse the direction of the travelling wave at the node of the standing wave and it is the waves and their nodes which determine the motion. Because the forces at the reflectors must always balance, there must be a binding force to balance the radiation pressure and these binding forces are constant. To keep the radiation pressure in equilibrium with this constant binding force as observed on each reflector, the amplitude of the wave as seen by this observer must remain constant (apart from the condition when an external force on the reflector enters into the equilibrium equation). The equations of Einstein⁽²⁵⁾, 1905, show that amplitude and frequency transform according to the same function of velocity. Hence the condition requiring constant amplitude of the wave

Etalon stationary in lab frame



Frequency conditions at the two ends of the etalon (seen from the laboratory), (a) Before and (b) After the external force is applied.

Fig 3.2



The stepped motion of the first end of the etalon, showing velocity changes.

Fig 3.3

for an observer on the mirror is the same as requiring constant frequency.

The conditions may be thought of as maintaining a constant length, after accelerating from one inertial frame to another, by a type of radar ranging of each mirror to the other with a delay time for the ranging signal to make the return journey. The distance is kept a constant number of half wavelengths by the condition that the wave returning to the mirror is π out of phase with that leaving it.

Fig. 3.2(a) shows the frequency, ν , of the monochromatic travelling wave circulating between the reflectors when the system of Fig. 3.1 is stationary and in equilibrium in the laboratory frame. Fig. 3.2(b) shows the first mirror, M_1 , when a step increase of velocity, V , moves it into the radiation of frequency ν . By a double application of the relativistic equation of Einstein⁽²⁵⁾, 1905, the reflected wave has frequency:

$$\nu' = \nu \frac{1 + V/c}{1 - V/c} . \quad \text{E3.1}$$

This travels to the second mirror which then moves at velocity V_2 (as shown in the lower part of Fig. 3.2(b)) so as to maintain the above condition that frequency ν is seen in its own frame. As a result, the wave seen on the moving mirror M_2 has frequency:

$$\nu' \left[\frac{1 - V_2/c}{1 + V_2/c} \right]^{1/2} = \nu . \quad \text{E3.2}$$

This gives an equation relating V_2 and V .

$$\nu \left[\frac{1 + V/c}{1 - V/c} \right] \left[\frac{1 - V_2/c}{1 + V_2/c} \right]^{1/2} = \nu \quad \text{E3.3}$$

From which:

$$V_2 = \frac{2v}{1 + \left[\frac{v}{c}\right]^2} \quad \text{E3.4}$$

This is the equation for the relativistic addition of the velocity v to the velocity V . It may be re-written in the form:

$$\left[1 - \left[\frac{V_2}{c}\right]^2\right]^{1/2} = \frac{1 - v^2/c^2}{1 + v^2/c^2} \quad \text{E3.5}$$

It has now to be confirmed that if the mirror M_2 moves with this velocity V_2 , it gives a frequency of the ray returning to M_1 which allows M_1 to have the correct coasting velocity V_2 if the external disturbance is removed at this instant and the mirror M_1 moves so as to maintain the frequency ν in its own frame. The frequency of the wave reflected off M_2 is:

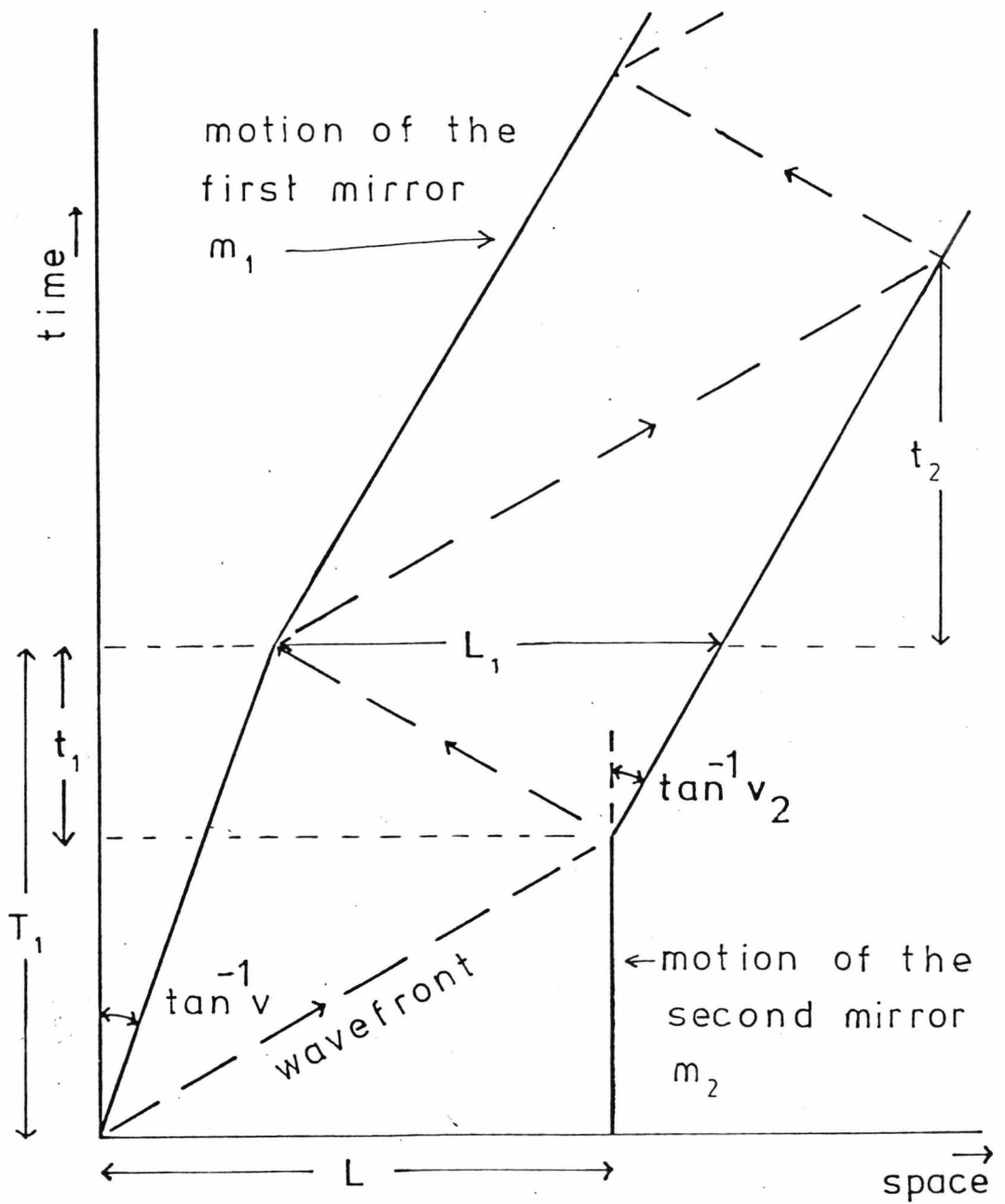
$$\nu'' = \nu' \left[\frac{1 - v_2/c}{1 + v_2/c} \right] \quad \text{E3.6}$$

When this ray returns to M_1 , M_1 should coast at velocity V_2 (as the external force has now been removed) and see a frequency:

$$\nu'' \left[\frac{1 + v_2/c}{1 - v_2/c} \right]^{1/2} = \nu \quad \text{E3.7}$$

from equations E3.6, E3.1 and E3.3. This is the condition that is required for the mirror M_1 to continue to coast at velocity V_2 .

If M_1 continues to move at velocity V_2 , the frequency of the waves reflected off it as seen in the laboratory frame, is:



The motion of each end reflector, as seen from the laboratory frame, when the first end is pushed (showing the timings of each event).

Fig 3.4

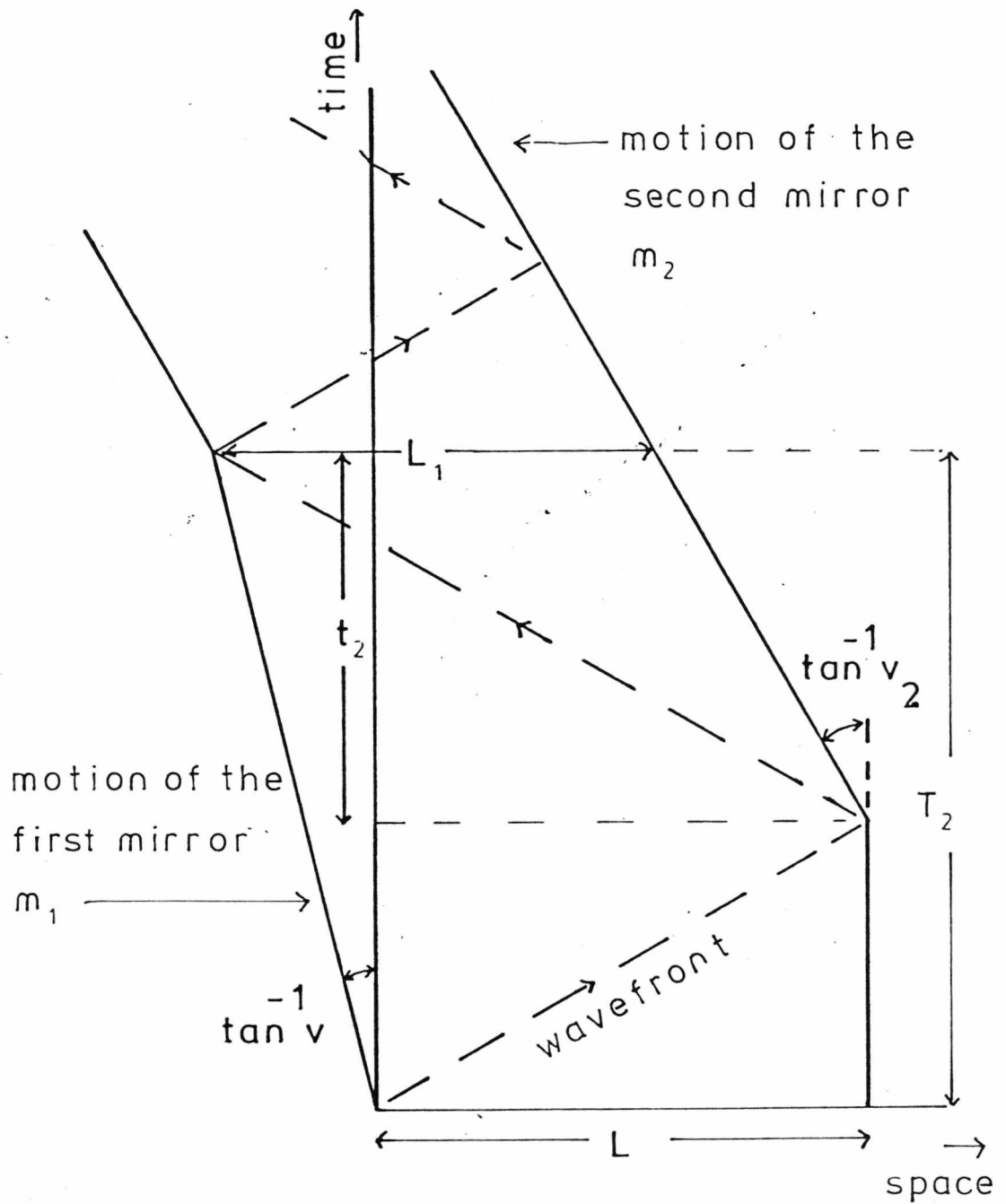
$$\nu \left[\frac{1 + v_2/c}{1 - v_2/c} \right]^{1/2} = \left[\frac{1 + v/c}{1 - v/c} \right] \nu .$$

This is the same frequency as was reflected off m_1 during the previous period (equation E3.1) and hence the wave path is closed without any further discontinuities circulating between the mirrors.

If the force continues to be applied after the system has been established in the second inertial frame, the same process will be repeated in the new inertial frame where the final velocity when established in this frame moving at v_2 , is given by the relativistic addition of velocities. Thus, if the force continues to be applied, a series of steps of velocity is built up, which becomes progressively smaller (in the laboratory frame), as indicated in Fig. 3.3 for the first mirror. The final coasting velocity, v_n , after n steps is derived from the coasting velocity of the step before, v_{n-1} , as:

$$v_n = \frac{v_2 + v_{n-1}}{1 + \frac{v_2 v_{n-1}}{c^2}} . \quad \text{E3.8}$$

The change in length (observed from the laboratory) between the mirrors, when the system is moved from the laboratory frame to lock into the inertial frame moving at velocity v_2 , will now be calculated. Consider the time interval from when both mirrors are stationary to when one mirror moves with constant velocity and the wavefront due to this change of velocity has returned to the first mirror (Fig. 3.4). The system starts with length L and the first mirror, starting to move at velocity v , sends a ray to reach m_2 in time L/c . If this ray returns in time t_1 , the mirrors m_1 and m_2 moving at velocities



The motion of each end reflector, as seen from the laboratory frame, when the first end is pulled (showing the timings of each event).

Fig. 3.5

v and v_2 , have moved distances such that:

$$L - v \left(t_1 + \frac{L}{c} \right) = c t_1$$

$$t_1 = \frac{1 - v/c}{1 + v/c} \frac{L}{c} \quad . \quad \text{E3.9}$$

In the case that M_1 is pulled rather than pushed (Fig. 3.5), the corresponding time for the ray to return to M_1 is given by:

$$t_2 = \frac{1 + v/c}{1 - v/c} \frac{L}{c} \quad . \quad \text{E3.10}$$

The total delay time, T , is:

$$T_i = \frac{L}{c} + t_i \quad . \quad \text{E3.11}$$

For the case of the mirror being pushed, in the laboratory frame, the distance between the mirrors, at the instant when the ray returns to the first mirror, is (from equations E3.4 and E3.5):

$$L_1 = L \left[1 - \frac{v}{c} \left(1 + \frac{1 - v/c}{1 + v/c} \right) + \frac{v_2}{c} \left(\frac{1 - v/c}{1 + v/c} \right) \right]$$

$$= L \left[\frac{1 - \frac{v^2}{c^2}}{1 + \frac{v_2^2}{c^2}} \right]$$

$$= L \left(1 - \left[\frac{v_2}{c} \right]^2 \right)^{1/2} \quad . \quad \text{E3.12}$$

This is the same as the Lorentz contraction, seen from the laboratory frame, at the moment of return of the ray.

A calculation similar to that above but based on Fig. 3.5 shows that the etalon still has a Lorentz contraction if the first mirror is pulled instead of pushed.

If the external force were removed part-way through the delay time, T , then the energy added in this part-cycle should be re-radiated out of the system to maintain the binding condition. Thus the change of state from one inertial frame to another is performed in a type of 'quantized' step which has to be completed for the system to lock into the next state.

3.3 The Etalon as a clock

It is shown in this section that the repeated return of a particular wavefront of the circulating wave to a mirror of the system may be taken as the ticks of a proper clock of the system. The time for each tick, T , when the system is stationary in the laboratory frame is related to the time for each tick, T_1 , when the system is established in the frame moving at velocity V_2 , according to the equation of Special Relativity for time dilatation. The system also has the property that a full definition is given of how the clock may be accelerated from one inertial frame to another.

In both Fig. 3.4 and Fig. 3.5 the final speed of the system is V_2 , although in opposite directions, and L_1 is the same for both diagrams. Thus the time t_2 in Fig. 3.4 is the same as the time t_2 in Fig. 3.5. Hence from equations E3.9 and E3.10, the time (observed in the laboratory frame) for one complete circulation of a wavefront for the system moving at velocity V_2 is:

$$\tau_1 = t_1 + t_2 = \left[\frac{1 + V_1^2/c^2}{1 - V_2^2/c^2} \right] \frac{2L}{c} \quad .$$

But the time for one complete circulation in the original laboratory frame was:

$$\tau = \frac{2L}{c} .$$

Thus the ratio of these times (in terms of V_2 from equation E3.5) is:

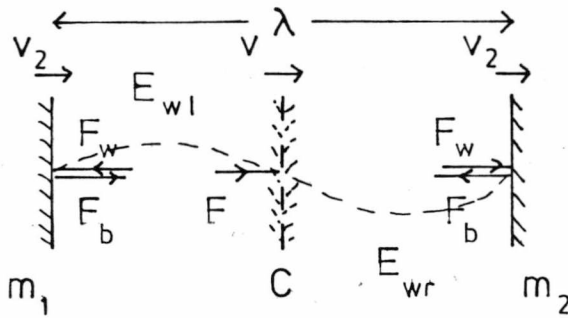
$$\frac{\tau_1}{\tau} = \left[1 - \left[\frac{V_2}{c} \right]^2 \right]^{-1/2} . \quad \text{E3.13}$$

This equation is the same as the equation of Special Relativity for the dilatation of time.

3.4 The dynamics of the Cavity

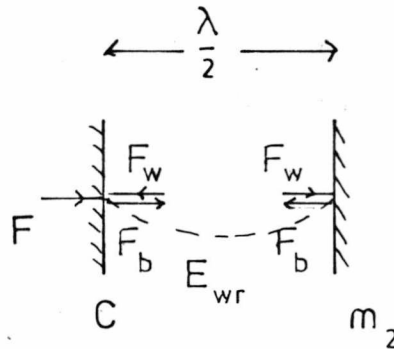
The mirrors of the system considered in section 3.2 have radiation pressure on them. This is shown in detail in Fig. 3.1 where the system is aligned along the x axis and the plane wave radiation moves in both directions along this axis. Because a full three dimensional system is now being considered, rather than just rays between end reflectors, the system will be referred to as a cavity. The analysis of this section considers unit cross-sectional area of the cavity and reflectors although, to make edge effects negligible, this unit area may be considered as part of an extended cavity. Because unit area is considered, the force on this area is numerically equal to the pressure. In Fig. 3.1, the radiation pressure per unit area on each mirror is indicated by F_w .

In the stationary system in equilibrium in the laboratory frame, the pressure of the internal radiation must be balanced by some binding mechanism. An example of this binding mechanism is given below. However the exact detail is not required but only that it supplies a constant force at each end to balance the radiation pressure in the proper frame of the system (indicated by F_b in Fig. 3.1).



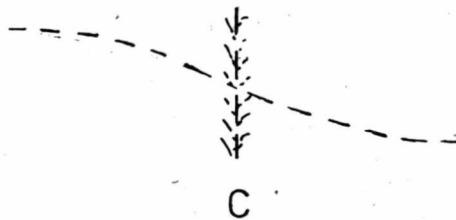
A balanced cavity system being pushed by it's central node (showing the forces on the end reflectors).

Fig 3.6



An unbalanced cavity system being pushed by one end (as in the case of the etalon of section 3.2).

Fig 3.7



A single-noded system for which the conditions at it's ends form anti-nodes.

Fig 3.8

The energy associated with the binding mechanism will now be calculated for the particular example of having opposite electric charges on each end reflector so that the attraction between the charges acts as a binding force. Fig. 3.6 indicates the parameters of the system which are required for this calculation. The case has been taken of the mirrors being separated by one wavelength, λ , of the internal radiation. The electrostatic field between the mirrors holds the system in equilibrium against the pressure of a monochromatic electromagnetic standing wave of wavelength λ . Then, neglecting edge effects, the energy in this binding system will be that to pull the plates apart from when in contact to distance λ . Assuming the field lines between the plates remain parallel as this is done, the force, F_b , remains constant and the energy, E_b , stored in the binding mechanism is:

$$E_b = F_b \times \lambda \quad \cdot \quad \text{E3.14}$$

However, the force, F_w , from the radiation pressure (the waves are totally reflected) is equal to twice the incident energy density. If the total wave energy is E_w , then:

$$F_w = \frac{E_w}{\lambda} \quad \cdot \quad \text{E3.15}$$

Hence, as the force from the binding mechanism balances the force from the radiation pressure when the system is stationary in the laboratory frame:

$$E_b = E_w \quad \cdot \quad \text{E3.16}$$

In terms of the total energy, E_t , this gives:

$$E_t = 2 E_w \quad \cdot \quad \text{E3.17}$$

The dynamics of the system will now be analysed by considering what happens when the system, initially at rest in the laboratory frame, is pushed by one of its reflectors. There are different ways of setting up the problem. For example, the analysis in the paper by Jennison and Drinkwater⁽⁴⁷⁾, 1977, considers pushing the end M_1 , similar to the case in section 3.2. The paper by Jennison⁽⁴⁸⁾, 1978, mentions different possible wave configurations and pushing the system from a reflector at a node of the standing wave, at the centre of the system. The first case to be considered here is a linear system pushed by a reflector at its central node, C , indicated in Fig. 3.6. This has the advantage of being a balanced system and is effectively two etalons of section 3.2 attached end-to-end so that the binding forces at C cancel each other. However, it has the disadvantage that the time for one complete circuit of the radiation after the moment when the force has been applied is different for the two sides. Thus 'locking into' the next state is a two stage process with the second stage taking a small fraction of the total time, for small values of v/c .

Considering the system of Fig. 3.6 at rest in the laboratory frame with the wave energy, E_w , divided equally between each side of the reflector C . The total wave energy is the sum of that to the right of C , E_{wr} , and that to the left, E_{wl} , so that:

$$E_w = E_{wr} + E_{wl} = 2 E_{wr} = 2 E_{wl} \quad \cdot \quad E3.18$$

If the reflector C is set moving at velocity v towards the right, the forces experienced in the frame of an observer moving with the reflector are given as follows.

Because M_2 has not moved, the conditions on the right of the mirror C appear to the moving observer as a train of waves moving towards him (part of this train is being reflected off M_2) of energy

E'_{wr} (The relativistic transform of the energy E_{wr} according to the equation of Einstein ⁽²⁵⁾, 1905, for a light complex) and length λ' (the Doppler transform of λ). This gives an energy density received by the moving observer of:

$$\begin{aligned} \frac{E'_{wr}}{\lambda'} &= \left[E_{wr} \frac{1 + v/c}{\left[1 - v^2/c^2\right]^{1/2}} \right] \left[\frac{1}{\lambda} \left[\frac{1 + v/c}{1 - v/c} \right]^{1/2} \right] \\ &= \frac{E_{wr}}{\lambda} \frac{1 + v/c}{1 - v/c} \end{aligned} \quad \text{E3.19}$$

As the radiation is fully reflected, the radiation pressure is twice the normally incident energy density. As unit cross sectional area is being considered, the pressure is equal to the force. Hence the force on C generated by the radiation moving in on the right is:

$$f'_r = \frac{2 E_{wr}}{\lambda} \frac{1 + v/c}{1 - v/c} \quad \text{E3.20}$$

A similar calculation for the radiation moving in from the left gives a force on C , measured by the moving observer, of:

$$f'_l = \frac{2 E_{wl}}{\lambda} \frac{1 - v/c}{1 + v/c} \quad \text{E3.21}$$

There is also the externally applied force, F' , pushing from the left. These three forces are in equilibrium at the surface of C . This gives an equation of equilibrium, for the observer on the moving mirror, of:

$$F' = f'_r - f'_l \quad \text{E3.22}$$

Putting in the values from equations E3.20 and E3.21, and using

equations E3.18 and E3.17 to obtain an expression in terms of the total energy, gives:

$$F' = \frac{E_t}{\lambda} \frac{2 v/c}{1 - v^2/c^2} = \frac{E'_t}{\lambda} \frac{2 v/c}{\left[1 - v^2/c^2\right]^{1/2}} \quad \text{E3.23}$$

As shown in section 3.2, after a delay time (which is different for the cavities on each side of C) the system will lock into the next state at a new velocity v_2 . The time for this will now be taken as the average of the times for each side as given by equations E3.11 (there being a second order term for the transformation to the moving frame). As this is only an approximation, the calculation is now made to first order in v/c . The average time is approximately:

$$T'_{av} = \frac{T'_1 + T'_2}{2} \approx \frac{\lambda}{c} \quad \text{E3.24}$$

The velocity gained when it locks into a new state after this delay time corresponds to an average acceleration:

$$a' = \frac{v_2}{T'_{av}} \approx \frac{2vc}{\lambda} \quad \text{E3.25}$$

from equation E3.4, to first order in v/c .

Taking equation E3.23 to first order in v/c , the force, F' , may be expressed in terms of the acceleration (given by E3.25) as:

$$F' = \frac{E'_t}{c^2} a' \quad \text{E3.26}$$

This equation is Newton's law in which E'_t/c^2 represents the inertial mass.

The calculation may be made to greater accuracy, as briefly indicated below, but the system considered is unbalanced. Fig. 3.7 shows a system which is equivalent to just the right hand side of Fig. 3.6 by itself, so that some of the previous equations remain valid.

Because the system is not balanced by internal waves on both sides of the motive reflector, consideration must be made of the binding force, F_b , at the reflector C. When the system is stationary in the laboratory frame, the binding force equals the force from the radiation pressure and hence is equal to:

$$F_b = \frac{2 E_{wr}}{\lambda} \quad . \quad \text{E3.27}$$

When the mirror C is pushed by an external force, F' , so that it moves at velocity v , the binding force remains the same and hence the equilibrium of forces as measured on the moving reflector is:

$$F' = f'_r - F'_b \quad . \quad \text{E3.28}$$

From equations E3.27 and E3.20 ($F' = F$ if F' parallel to v):

$$F' = \frac{E_T}{\lambda} \frac{2 v/c}{1 - v/c} = F \quad \text{E3.29}$$

where E_T is the total energy of this system and is twice the energy of the waves (see also appendix A8.1).

For this system the delay time, T_1 , may be calculated accurately at the single instant when the system locks into its next stable state. Applying equations E3.11 and E3.9 for the case of an etalon of length $\lambda/2$, the time according to the observer in the laboratory frame, is:

$$T_1 = \frac{\lambda}{c} \frac{1}{\left[1 + v/c\right]} \quad . \quad \text{E3.30}$$

Hence the equation E3.29 for the force may be written in terms of the delay time, T_1 , of equation E3.30 and the change of velocity from rest to V_2 , observed in the laboratory frame, as given by equations E3.4 and E3.5:

$$F T_1 = \frac{E_T}{c^2} \frac{V_2}{\left[1 - \frac{V_2^2}{c^2}\right]^{1/2}} \quad \text{E3.31}$$

This analysis should be considered with care in regard to the frame in which the acceleration is measured (a force, however, remains the same value in different, relatively moving, co-ordinate frames when the relative velocity is in the same direction as the force). The analysis above has been made for a constant force which, viewed from the laboratory frame, causes a change of velocity from zero to V_2 in time T_1 . If this is compared with equation (1-28) in the book by French⁽³¹⁾, 1968, for exactly similar conditions, they are seen to be of the same form. The equation (1-28) in French's book is now quoted verbatim as:

$$F t = m v = \frac{m_0 v}{\left[1 - \frac{v^2}{c^2}\right]^{1/2}}, \quad \text{E3.32}$$

for a force F acting on a body for a time t . The acceleration measured in this frame is not constant (as the effective mass is varying with velocity). The term E_T/c^2 in equation E3.31 may be equated with the rest mass of the body according to equation E3.32.

The analysis might have been made in terms of the frame moving with the accelerating system and in this frame the acceleration is constant for a constant applied force. The approach to the analysis of acceleration is discussed by French⁽³¹⁾, 1968.

3.5 A comparison of the cavity system with the rigid rod described by McCrea.

Because the end mirrors of the cavity move so that, to an observer on the mirror, an exact number of half wave standing waves is maintained between them while the frequency is maintained the same, in the final steady state of the system it always has the same proper length. Hence, in inertial frames, it is rigid. However, this system also defines what happens in the process of accelerating and this may be compared with McCrea's consideration of the problem.

McCrea⁽⁶⁷⁾, 1952, and Hogarth⁽³⁹⁾, 1952, (described in section 2.3) is almost entirely concerned with the conditions of his rod between the times when the first end of the rod is stopped until the other end has first (momentarily) stopped. What happens after this is not fully discussed. The analysis of the previous sections (3.2 to 3.4) has considered giving one reflector of the cavity system a steady increase in velocity. However, the reverse process of stopping one end when the rod is initially moving at v , will follow a similar type of analysis. This means that, because the velocity of an impulse in McCrea's rod is the 'velocity of light', the reaction to stopping one end of either McCrea's rod or that of the system of this chapter is at first the same. That is, a 'signal' is sent at the speed of light to the other end which continues to move in its previous motion until it receives this signal. At the instant at which this signal reaches the other end the rod has momentarily a length given by $E2.3$ (the analysis being similar for the system considered in this chapter). McCrea calculates for this instant the perfect conversion of the initial kinetic energy to stress energy in the rod. The cavity system is also lossless and undergoes a similar operation.

The subsequent motion is defined for the cavity. When the radiation

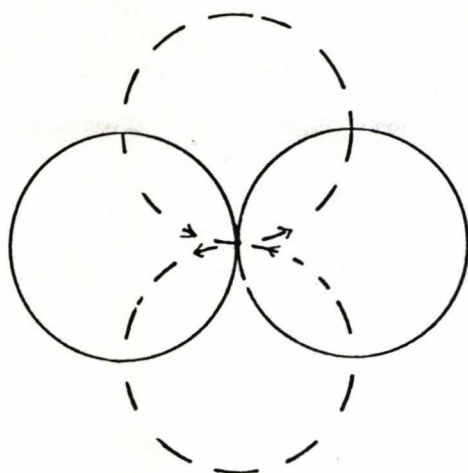
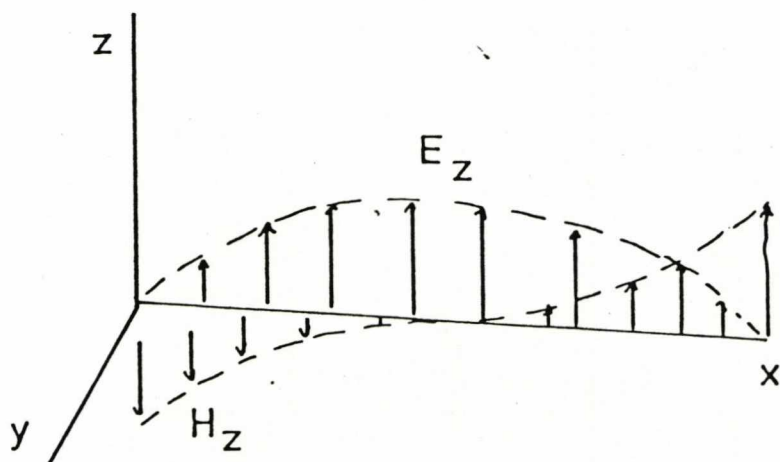
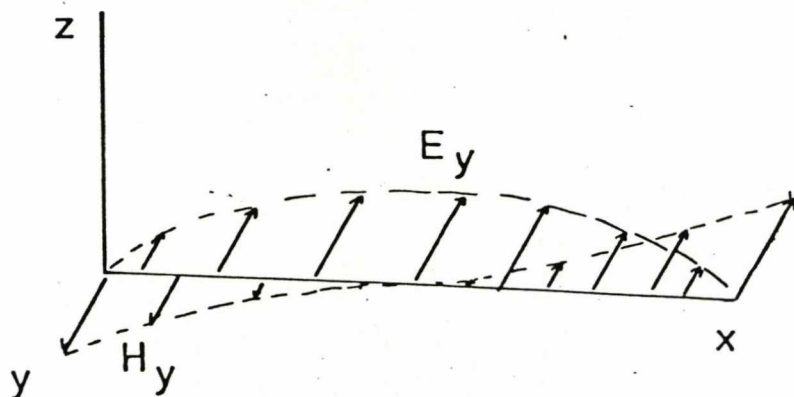


Diagram from Jennison ⁽⁴⁸⁾, 1978, showing (dotted line) the waves of the system following a closed path to each side of the central node and (full line) a similar system forming the binding mechanism.

Fig 3.9



The electric and magnetic fields for a standing wave formed from circularly polarized waves. The second diagram is the time quadrature of the first.

Fig A3.1

completes one circuit, the first end locks into the next state and, if the constraining force is removed at this instant, the cavity moves at velocity V away from the object that had been holding it. That is, the cavity performs a bounce off the constraining object.

3.6 The relation of the dynamics analysis to the electron

This section presents the analysis made by Jennison⁽⁴⁸⁾, 1978, relating the stepping action, caused by the delay time for the internal waves to perform each circulation, to the quantum conditions for the electron atomic particle. It is not known exactly how the electron may be formed by internally trapped waves. Section 2.7 of chapter 2 discusses this. Appendix A3.1 gives some detail of the field configurations for a linear system. It is suggested for the following analysis that the electron may be represented by the double-sided, balanced, system of section 3.4 and that in the physical phenomenon of pair formation there may be some novel mechanism which forms the single noded linear system of Fig. 3.8 into a self-closing system of some configuration like that of Fig. 3.9, which represents the rotation of the linear system.

If the node of such a two-sided, balanced, system (for example, mirror C in Fig. 3.6) is pushed by a force generated by external radiation of frequency ν_e being reflected normally off it, the external force pulsates at $2\nu_e$ (see Appendix A3.2). The external frequency should balance the difference in frequency of the two internal waves Doppler shifted from the original frequency ν , in the proper frame of the moving node. It is shown by Jennison⁽⁴⁸⁾, 1978, that the velocity of the node is related to the frequency of the impinging radiation according to:

$$\nu_e = \nu \frac{\nu/c}{\left[1 - \frac{v^2}{c^2}\right]^{1/2}} \quad \text{E3.33}$$

This may be used to calculate the momentum gained, in the time for one return journey of the internal radiation, by associating a rest mass, m_0 , with the system and calculating (from E3.4 and E3.5):

$$m v_2 = \frac{m_0}{\left[1 - \frac{v^2}{c^2}\right]^{1/2}} \frac{2v}{1 + \frac{v^2}{c^2}}$$

$$= \frac{2 m_0 v}{1 - \frac{v^2}{c^2}} \quad \text{E3.34}$$

When this is combined with equation E3.33 to eliminate v :

$$\text{Momentum gained} = \left[\frac{2 m_0 c^2}{v} \right] \frac{v_e}{c \left[1 - \frac{v^2}{c^2}\right]^{1/2}} \quad \text{E3.35}$$

The gaining of this amount of momentum corresponds to the system locking into the next stable state and is a type of quantized taking on of momentum with the quantity in brackets being a proper constant of the system. To an accuracy of first order in $\frac{v}{c}$, it is of the form
Momentum = constant \times frequency.

This may be applied to find the value of the proper constant in the case of an atomic particle such as the electron. In pair production the energy of the gamma ray is :

$$h \nu = 2 m_0 c^2, \quad \text{E3.36}$$

where h is Planck's constant and m_0 is the rest mass of each particle of the pair. If it is now assumed that this frequency is the frequency of an internally trapped wave which constitutes the particle then:

$$\nu = 2 \nu_{\text{Compton}}, \quad \text{E3.37}$$

and the proper constant in equation E3.35 is:

$$\left[\frac{2 m_0 c^2}{\nu} \right] = h \quad \cdot \quad \text{E3.38}$$

This suggests that the internal structure of the particle contains in some way the frequency of the gamma ray from which it was formed.

3.7 Conclusion

The analysis in one dimension of the cavity dynamics may now be regarded in the overall view. It seems feasible to loosely think of extending the container of energy to three dimensions. A complex of energy is trapped in a container whose dimensions are controlled by the wavelength of the trapped monochromatic waves and there is a balance of the forces at the boundary containing the energy. This container of energy contracts in size, according to an observer who does not move, when it starts to move. The holding forces containing the energy may remain of the same magnitude when (kinetic) energy is added to the system because the container in its own frame of reference still has the same radiation pressure.

Appendix to chapter 3

A3.1 The electromagnetic field patterns in the cavity

To give a steady radiation pressure on the mirrors, it is assumed that the waves are circularly polarized. If the waves in the stationary cavity form a half wavelength standing wave, then the two plane polarized components of the two waves travelling in opposite directions are:

Moving forward-

$$k = \frac{2\pi}{\lambda} = \frac{\pi}{L}$$

$$\hat{E}_y \sin(\omega t - kx)$$

$$\hat{H}_z \sin(\omega t - kx)$$

$$E_z \cos(\omega t - kx)$$

$$-H_y \cos(\omega t - kx)$$

Moving back-

$$-\hat{E}_y \sin(\omega t + kx)$$

$$\hat{H}_z \sin(\omega t + kx)$$

$$-\hat{E}_z \cos(\omega t + kx)$$

$$-\hat{H}_y \cos(\omega t + kx)$$

Where the electric field is reversed on reflection at $x=0$.

These forward and back waves combine to give a standing wave:

$$\tilde{E} = 2 (\hat{E}_y \cos \omega t - \hat{E}_z \sin \omega t) \sin kx$$

$$\tilde{H} = 2 (\hat{H}_z \sin \omega t - \hat{H}_y \cos \omega t) \cos kx$$

Which is a pattern of electric and magnetic fields rotating about the X axis without change of shape. Fig. 3.1 indicates the standing

wave formed by a plane polarized wave, Fig. A3.1 indicates the wave formed by circularly polarized waves.

Over the length of the cavity, at the moment when $\omega t = \pi$:

$$\text{Total linear momentum} = 0$$

$$\begin{aligned} \text{Total electromagnetic energy} &:= \frac{1}{2} \int_0^L \left(\hat{E}_z^2 \sin^2 \frac{\pi x}{L} + \hat{H}_z^2 \cos^2 \frac{\pi x}{L} \right) dx \\ &= \frac{L}{4} (\hat{E}^2 + \hat{H}^2) \end{aligned}$$

$$\text{Total electromagnetic angular momentum} = \frac{L}{c\pi} (\text{Energy})$$

according to Dicke and Whittke⁽²¹⁾, 1960.

A3.2 Radiation pressure

As an indication of the order of magnitude involved, the radiation pressure, for example, caused by reflection of a wave of 3×10^3 watts/sq.m. normally off a mirror has an incident energy density of 10^{-5} Joules/m³. This gives a radiation pressure of 2×10^{-5} Newton/m², which is of the order of magnitude of one milligramme weight per square metre.

For a plane polarized wave, the radiation pressure fluctuates as the square of the amplitude of the incident wave. This may be written as:

$$\text{Pressure} \propto A^2 \sin^2 \omega t = \frac{A^2}{2} (1 - \cos 2\omega t)$$

which is a sinusoidal oscillation at twice the original frequency.

Chapter 4

THREE EXPERIMENTS WHICH DEMONSTRATE REFLECTORS MOVING ACCORDING
TO THE CONDITIONS DESCRIBED IN CHAPTER 3

4.1 Introduction

The work described in this chapter is entirely experimental. It has the purpose of showing, with simple apparatus, how reflectors driven by servo-controlled motors may be made to follow conditions similar to those of the reflectors in the system analysed in chapter 3. The first two experiments use monochromatic electromagnetic waves which form standing waves on reflection. By having a detector to sample the interference pattern formed by the waves, the servo control positioned the reflector so as to maintain a constant optical distance between the reflectors. Thus, although in practice the reflectors must have appreciable mass, the amplifiers and transducers positioning the reflectors cause the reflectors to move according to the signals from the trapped waves. This is as if the movement were caused by the waves themselves. These experiments have been reported briefly by Jennison and Drinkwater⁽⁴⁷⁾, 1977.

The first experiment is based on a Michelson interferometer powered by a He-Ne laser beam. The mirrors of the interferometer were positioned by transducers. One mirror was positioned by a closed loop servo control with a three term controller in the circuit processing the signal from photo detectors of the interference pattern. The second mirror could be positioned by an external test signal. Thus the servo control maintained the position of the first mirror so that there was a constant number of waves difference between the lengths of each arm of the interferometer. In this experiment it is not the conditions at the mirror which are sampled

but the interference pattern formed according to the comparative distances of the two mirrors from the beam splitting prism. The object of this experiment is to illustrate how a type of rigid measuring rod is formed according to the interferometric measure of length. When one end is accelerated, the other automatically follows. This should have implications in the description of a relativistically rigid rod.

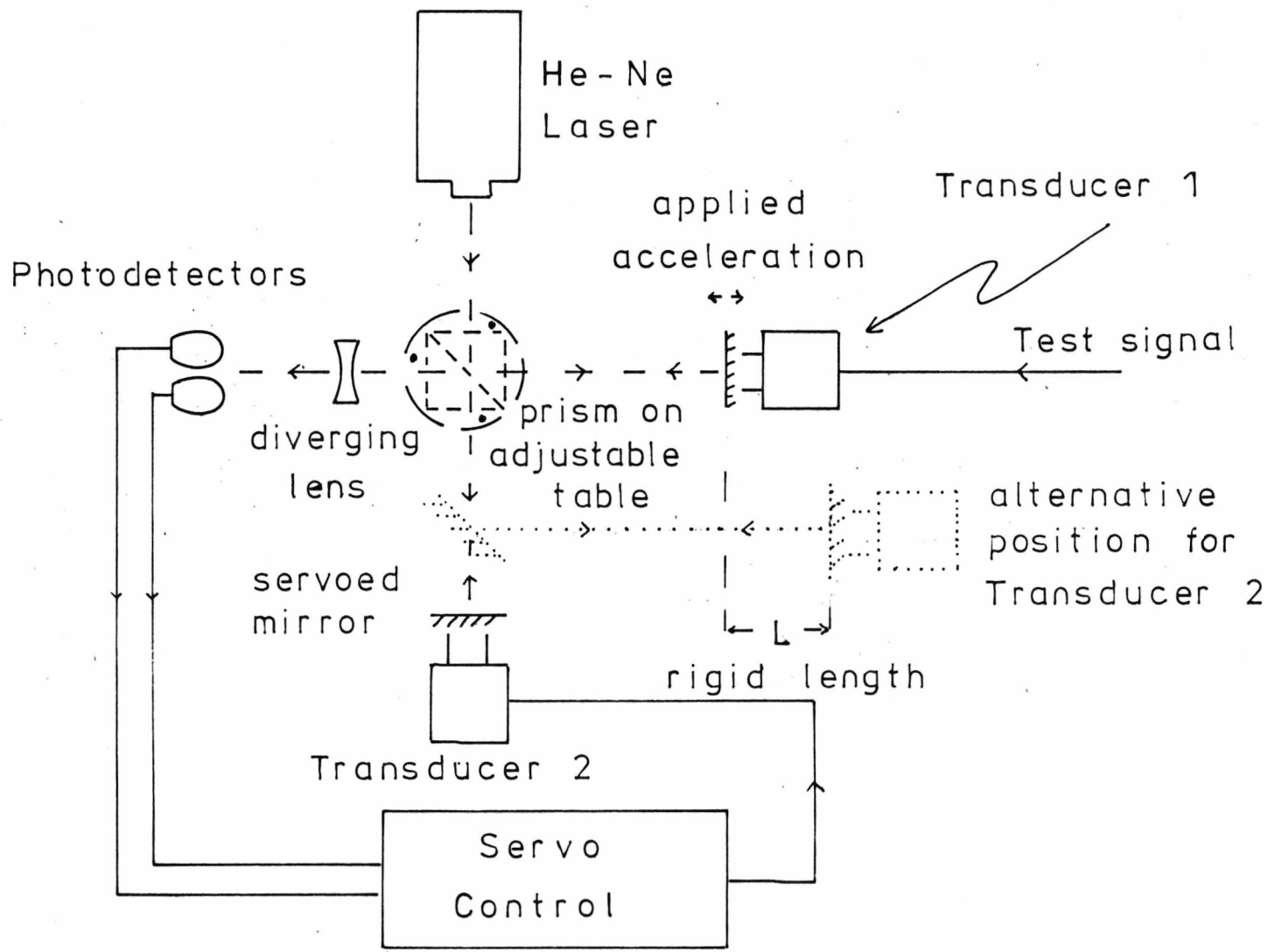
The second experiment consisted of two trolleys on a pair of rails. The first trolley carried an X-band Gunn diode microwave generator and transmitted the waves from a horn to the second trolley which had a concave reflector, (perturbed at audio frequency about its mean position to give a direction-detecting mechanism for the control signal), to trap the waves. There were current loop aeri-als on the surface of the reflector and in the horn of the transmitter, which sampled the interference pattern for each trolley to give control signals (after phase sensitive detection) to the motors driving each trolley. Thus each trolley was independently servo-controlled to maintain a maximum of the magnetic field anti-node of the standing wave at the position of its current loop aerial detector. Hence the system should maintain a distance corresponding to a constant number of half wave standing waves between the trolleys without any reference to the laboratory by making mutual continuous wave radar-type measurements continuously and independently from each end. This condition should be maintained even if either end trolley is pushed or both are free to move together.

The third experiment arose out of the difficulty in obtaining the effect caused by the delay time for the propagation of signals between the end reflectors. Because any mechanical system will have too low a frequency response compared with the time for electromagnetic waves to traverse the apparatus, an analogue computer circuit, with time scaling, of the delays was set up. This apparatus should demonstrate the general

property of a lossless, distributed, system in which time is taken to propagate the effects of a displacement to the far end and back again.

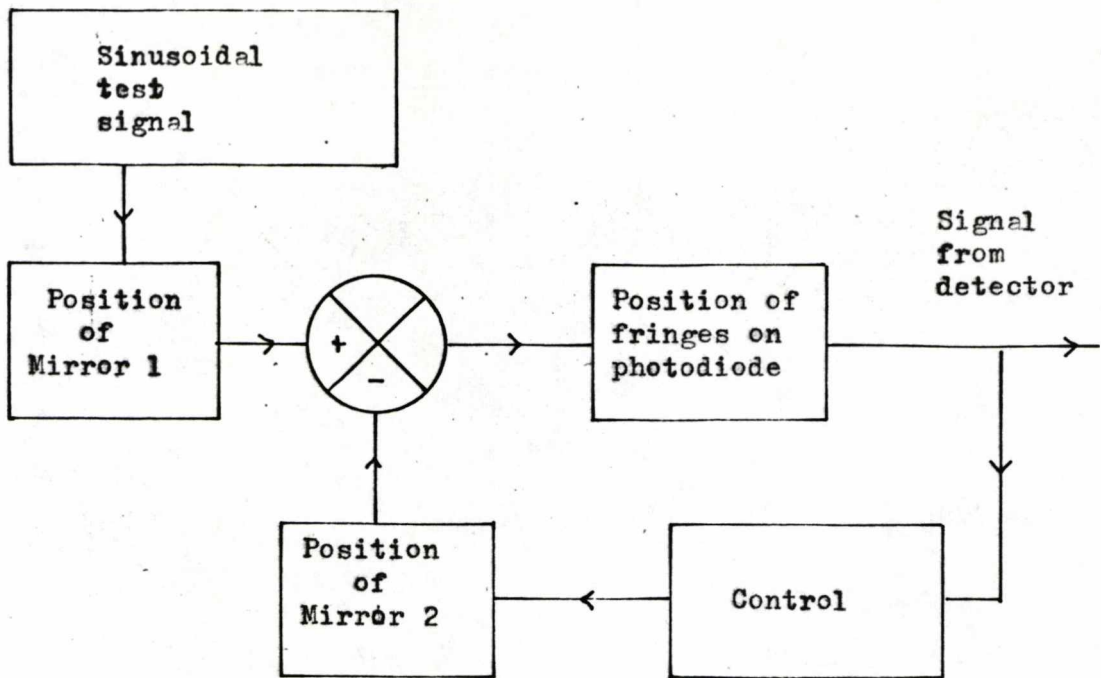
The main property demonstrated by these experiments is that of a self-regulating system which has reference only to its internal radiation. The condition on the reflectors in the theory of chapter 3 is that they are perfectly reflecting so that the same radiation is continually circulating, and that the frequency and amplitude of the wave onto the reflectors remains the same except when an external force is applied to the reflector. The main limitations to a practical realization of these conditions are as follows. The reflectors are not perfect and there is always some loss of radiation from the cavity, which has to be made up by a generator (in this case, of a fixed frequency from a laser or Gunn diode). Although the trolleys of the second experiment do make the detection at the reflectors, it is not the frequency or radiation pressure which are measured directly but the nodes of the interference patterns. This generates an error signal depending on the difference between the distance between the reflectors and an integral number of half wavelengths.

The contents of this chapter are arranged as follows. Section 4.2 describes the apparatus, setting up a control loop round components having a certain open loop frequency response, and the results for the interferometer experiment (a preliminary experiment on a type of transducer to position the mirror using a loudspeaker system is described in appendix A4.3). Section 4.3 describes the apparatus for the trolley experiment and the operation of the closed loop control for each trolley. The results are then given. Section 4.4 describes the construction of the delay units for the analogue experiment and the setting up and results for this experiment. Section 4.5 considers how the feedback control on the reflectors may be taken to a theoretical limit to simulate the ideal, massless, reflectors described in chapter 3.



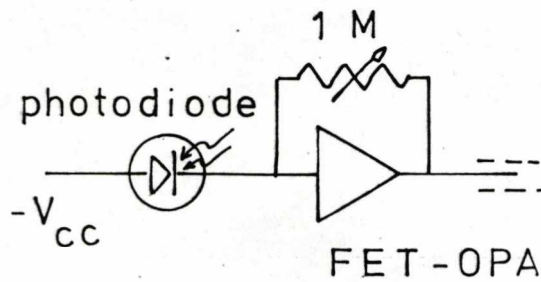
Apparatus for the interferometer experiment, showing the servo control loop positioning the second mirror.

Fig 4.1



Block diagram of the closed loop control system

Fig 4.2



The photodiode detector circuit

Fig 4.3

4.2 The Interferometer experiment

4.2(a) The apparatus.

This section describes the apparatus and a diagram of the complete system is shown in Fig. 4.1. The experiment was based on a Michelson interferometer (Photo 1). One mirror was positioned by the test signal. The position of the other was controlled by a servo unit, consisting of a comparator, three-term controller and power amplifier, for which the error signal was obtained from the interference pattern, as in Fig. 4.2.

A 1 m.watt, He-Ne Rofin, C.W. Radiation Inc., Laser (Model S102) of central frequency 6328 \AA , visible red, was used to supply the interferometer light beam. Because of the narrow bandwidth of light from a laser ($\delta\lambda = 10^{-4} \lambda$) the coherence distance for the beam was far greater than the length of the apparatus. The main problem was to adjust the positions of the transducers and the beam splitting prism on an adjustable table to give an angle between the interfering beams which gave a pattern of suitable spacing.

To reduce the effect of ambient mechanical vibrations, the beam splitting glass block and mirrors were mounted separately on an acoustic filter made of concrete blocks (paving flagstones) interlayered with thick, firm, but pliant packing material. It was found that to reduce vibrations over the whole frequency range, all supports must be secure and the lengths of iron rods kept short. The interlayer material absorbing vibrational energy should be sufficiently rigid not to allow swaying at low frequencies. Wooden supports tend to absorb vibrations without allowing swaying. The focussing and detecting units were mounted on an optical bench as vibrations in this section have comparatively little effect. To give an interference pattern of size suitable for detection, an adjustable diverging lens was inserted in the beam.

A beam-splitting prism was used as a 'half silvered mirror' to

The comparator and variable gain amplifier, showing the switch to open or close the control loop.

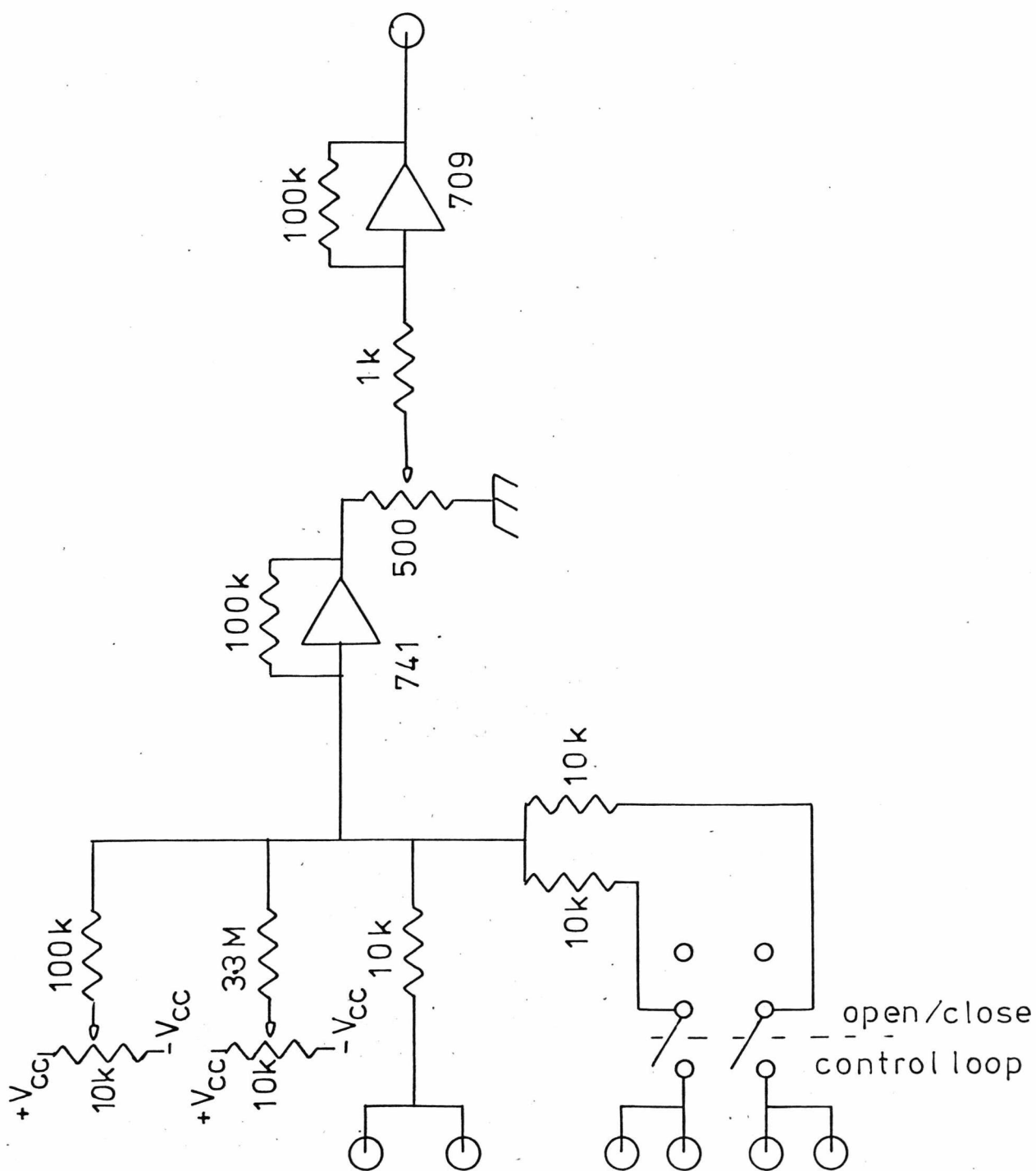


Fig. 4.4

divide the beam. It consisted of two 45° glass prisms stuck together along their hypotenuse surfaces so that the beam was split at this thin film. The beam entered and left the prism normal to the surface but, even so, there were multiple reflections off these surfaces.

The two photocells and preamplifiers (Radiospares FET-OPA) were mounted on adjustable optical bench supports so that they could be readily positioned at a half fringe width distance apart on the interference pattern. This gave a differential signal measure of the fringe position which was sensitive to fringe movement but insensitive to changes in the ambient light in the room. The photodiodes (Radiospares) were arranged to set on either side of a fringe minimum, when the servo control circuit was operating, so that, if the interference pattern started to move, the light on one increased and on the other decreased. Each circuit consisted of a photodiode and amplifier circuit as in Fig. 4.3 in which a small, light dependent, leakage current from a reverse biased diode is fed into an operational amplifier with feedback adjusted to give a signal of the order of volts as the fringe moved. The other photodiode with reversed polarity was connected to the positive supply volts so that its amplifier output was in opposite phase to the first circuit. These signals of opposite phase were fed into a summing amplifier at the comparator input. Thus the summed result measured the change in light between the two diodes but not the same change on both of them. The resulting signal went through the comparator and three-term controller to the transducer positioning the mirror. Hence the position of the mirror was controlled by the phase difference between the two beams forming the interference pattern.

The comparator of Fig. 4.4 has a switch to open or close the overall control loop. The input is compared with the bias on the potentiometers, or an external signal can be added into the summing

Circuit diagram of the three-term controller, showing the direct, integrated and differentiated signal paths.

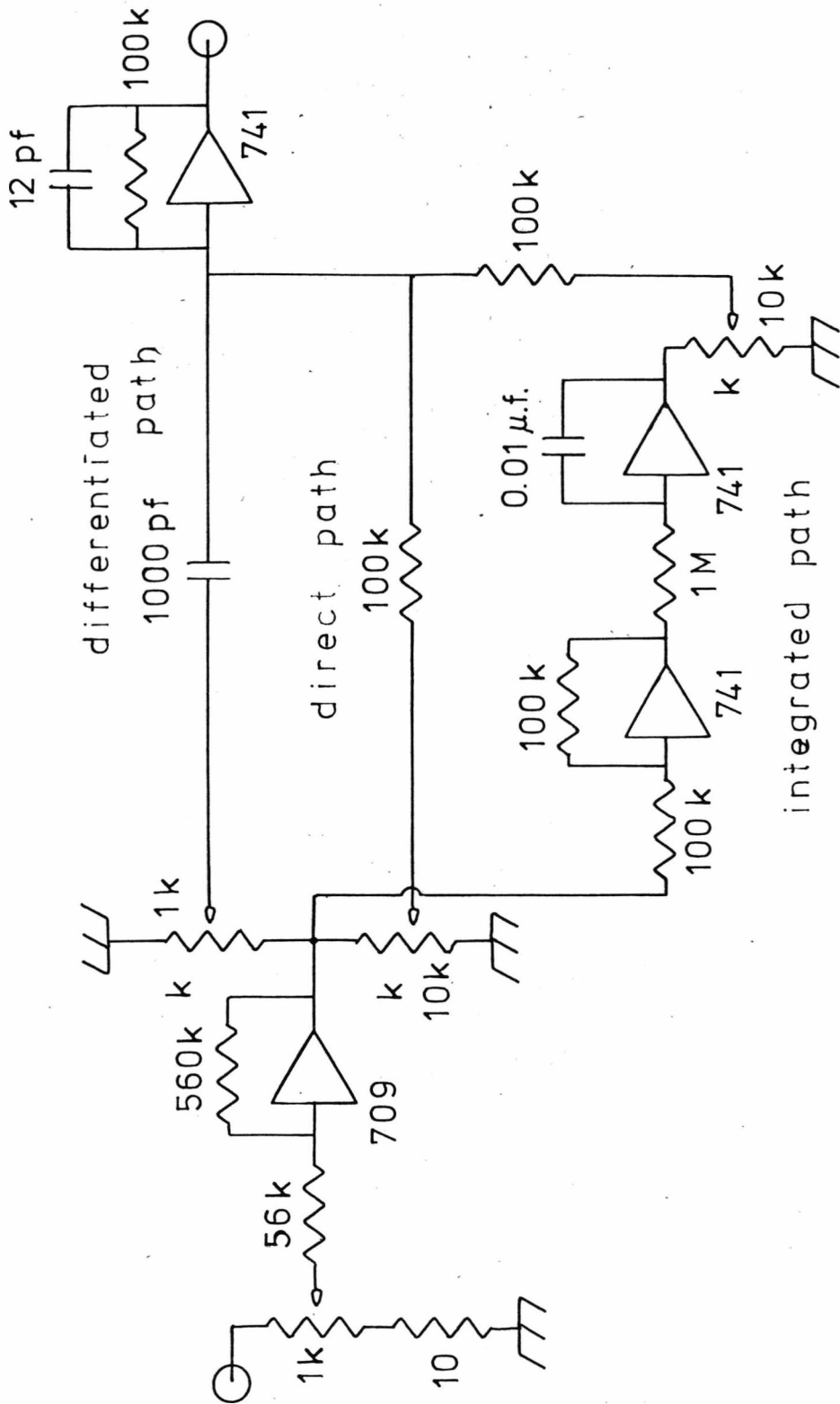
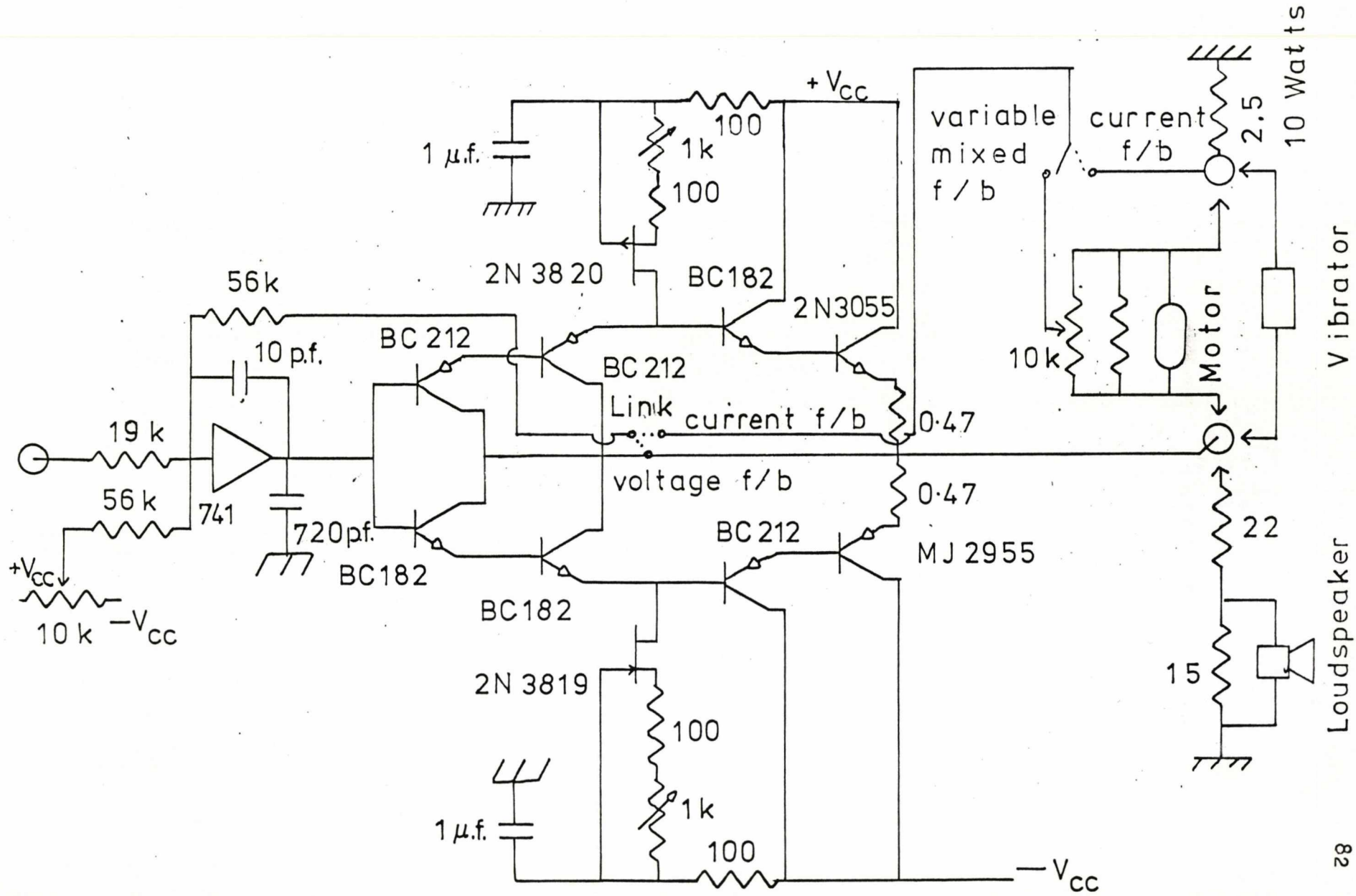


Fig 4.5

Fig. 4.6

The power amplifier for driving the transducer or trolley .



junction. There is a variable gain control.

The circuit of the three-term controller is given in Fig. 4.5. It combines variable proportions of derivative and direct signal in the output summing amplifier and also a variable amount of the signal integrated by the circuit in the lower part of the diagram. There is a potentiometer at the input to control the overall gain. The theory of the three-term controller is described in appendix A.2.

The power amplifier circuit is described in Fig. 4.6. There is either current feedback from the voltage generated across the 2.5 ohm resistor in series with the load, or voltage feedback from the amplifier input. A biasing potentiometer feeds current to the summing junction to allow adjustment for any off-set further back in the circuits. The FET transistors supply a constant bias current to the power transistors which could be adjusted to minimise cross-over distortion.

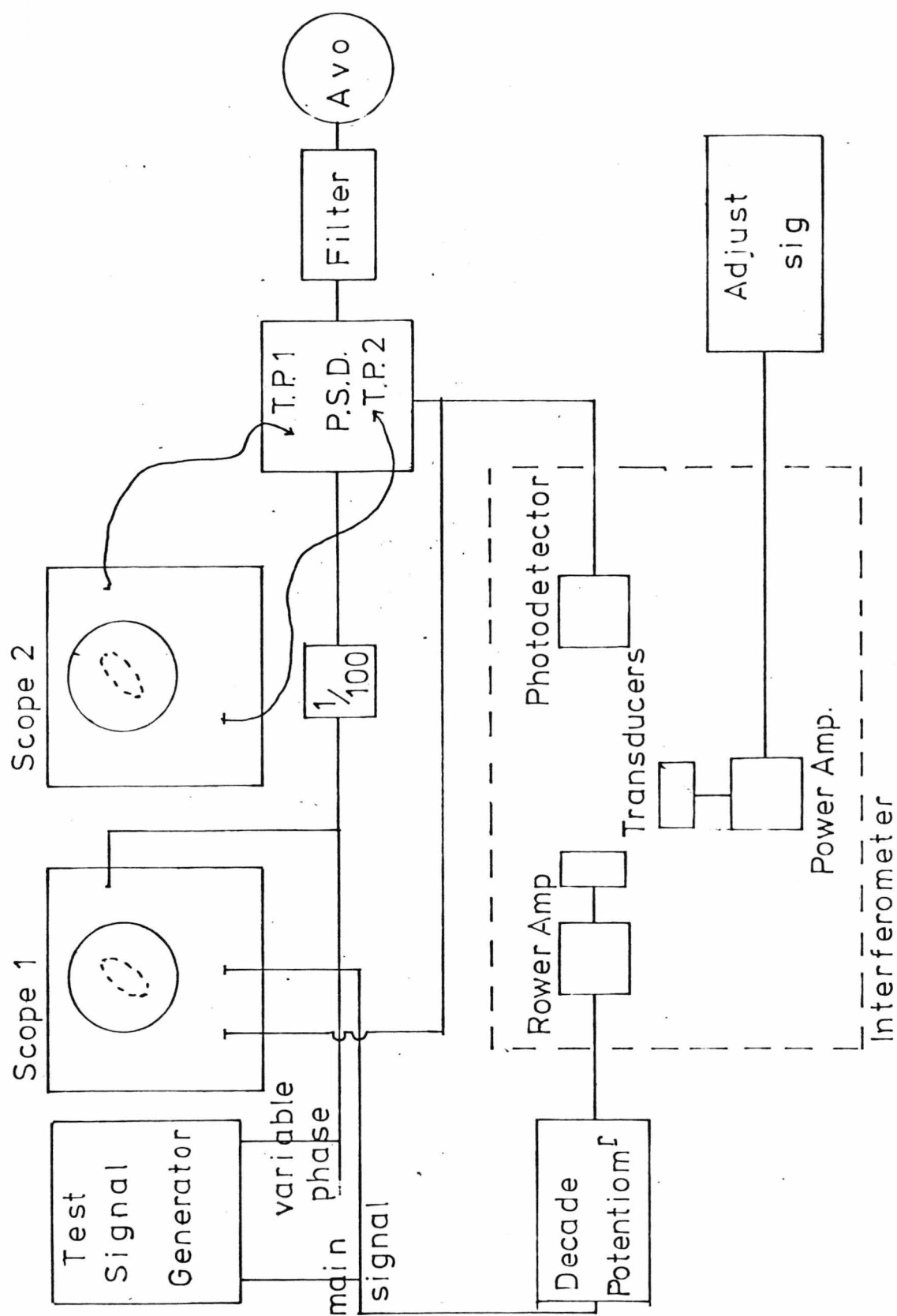
The first transducers used in the experiment to position the mirrors were two Radiospares 15 ohm, 10 watt Wide Range Speakers with the inner cone removed and a small mirror (made from a silvered microscope slide cover glass) fixed to the centre. The final version of the experiment used Vibrator transducers as described below. Each 15 ohm speaker was driven by the power amplifiers with a 15 ohm resistor connected in parallel with the speaker and 22 ohms in series with it and voltage feedback on the amplifier as shown in Fig. 4.6. The resistor in parallel tended to damp resonances in the cone. The speakers were attached to building bricks which increased the inertia of the fixed components of the speakers and reduced the effects of reactive forces when the coils moved. This size of speaker was used to allow a large (0.25 inch) swing in position while maintaining a good frequency response. As well as the fundamental resonance at about 60 Hz., there were resonances due to 'break up' of the surface of the vibrating cone in the range 1-10 k. Hz. The effect of microphonous pick-up of vibrations in the air leading

to possible acoustic resonances in the room did not seem to occur because surrounding the speaker with padding and placing a heavy block with a window in front of the speaker, did not change these resonances. As an experiment, the entire cone of the speaker was cut away and the coil and former supported by two rubber bands at right angles, fixed to the metal frame of the speaker. This gave a much less rigid support but there were still resonances in the range of interest. A different 'horn type' speaker was tried but still gave resonances in this range (and had less movement). Also an 8 inch speaker was mounted in a 12 inch length of drainpipe packed with wool and blocked at the far end with foam rubber. This did reduce the 2.6 k.Hz. resonance but increased the pick-up of vibrations in the air. Vibrations were not transmitted between the loudspeaker supports as was shown by acoustically isolating the speaker by standing it on foam rubber. Hence the only way of dealing with these resonances was to compensate for them electronically. Some preliminary experiments using the loudspeaker transducer and notch filters to compensate for the worst resonances of the cone are described in appendix A4.3.

In the final version of the experiment, the mirrors were driven by Vibrator units (ling Dynamic, 200 series Vibration Testing system) which were set with Plaster of Paris in 8 inch concrete blocks. These did not require the notch filters. Using these more powerful transducers, the light mirrors could be replaced with heavy glass corner reflector prisms (made by AGA-SWEDEN) which always return the beam along the direction of incidence and are useful for beams travelling over large distances. However, the flat mirrors were used for this experiment.

4.2(b) The Vibrator transducers.

Because the response of the control loop is dominated by the transducer in terms of its amplitude and phase response as an element



The complete interferometer system and units for measuring its open loop amplitude and phase response, using the Phase Sensitive Detector as a correlator.

Fig 4.7

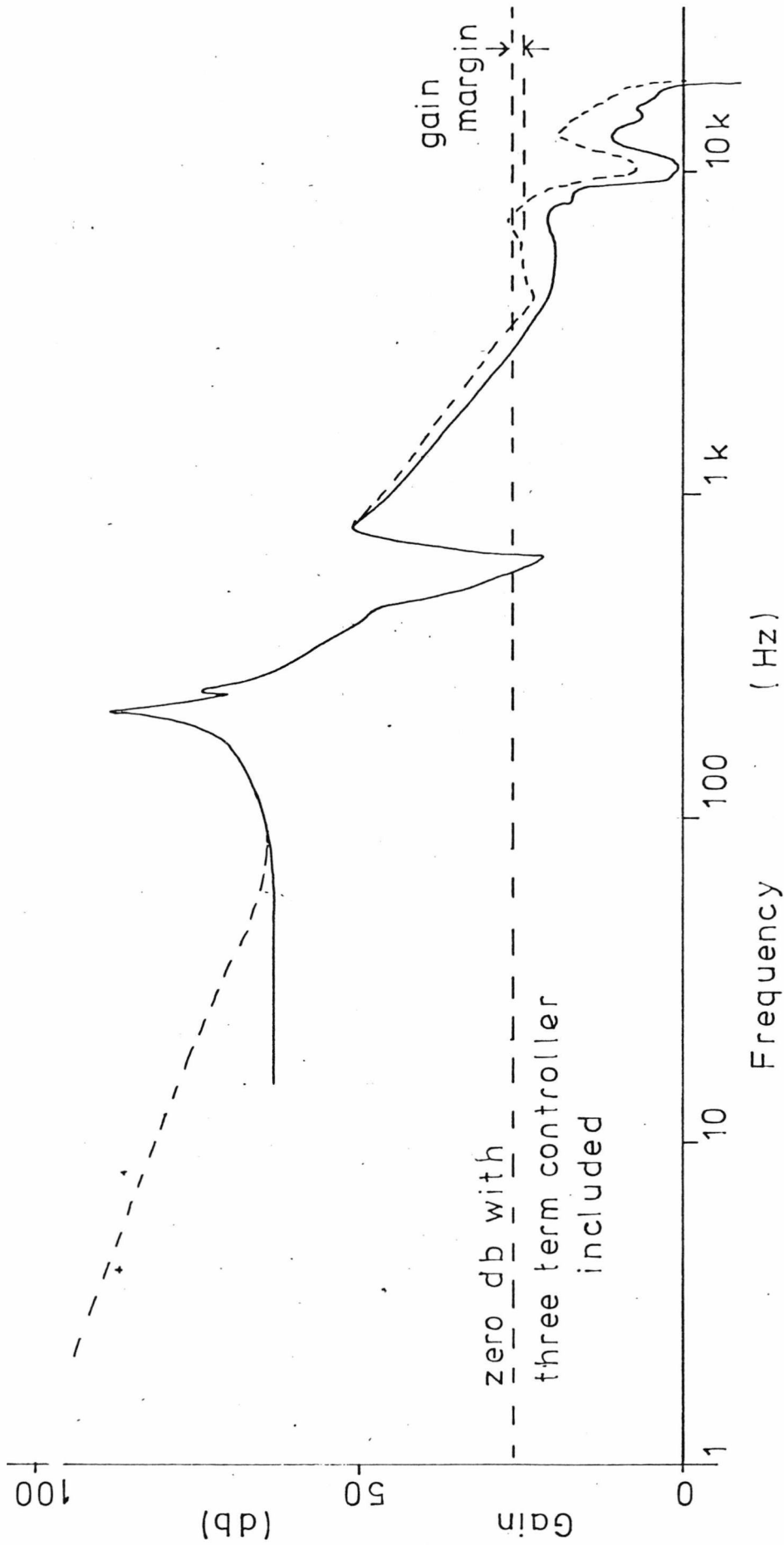
of the system, this section gives a detailed description of the transducer open loop response. The transducers are compact and enclosed compared with the loudspeakers so that there was far less problem of microphony. They require more power than the loudspeakers and were connected directly to the outputs of the amplifiers of Fig. 4.6 with 2.5 ohm resistors in series to enable current feedback to be used round the amplifiers. According to the manufacturer's specification, current feedback gives a more even variation of amplitude with change of frequency. The coil has 1.5 ohm d.c. resistance and operates up to 2.5 amp. r.m.s. without forced cooling. It gives a maximum displacement swing of 0.5 cm. The extra load added by the small mirror was less than the effective armature weight of 20 gm.

A survey of the open loop response was made with greater accuracy than had been made for the loudspeaker. Because there was a random fluctuation of the interference pattern due to mechanical vibrations, quite large compared with the signal for one fringe width over some frequencies, it was necessary to use a correlation technique. For this purpose the phase sensitive detector described in section 4.3 was used, with the constant amplitude signal from the function generator used as the reference signal. The phase of the reference signal was adjusted so that it was always in phase with the system output and $\theta = 0^\circ$.

$$\text{Output of p.s.d.} = A B \cos \theta = A B \quad \text{E4.1}$$

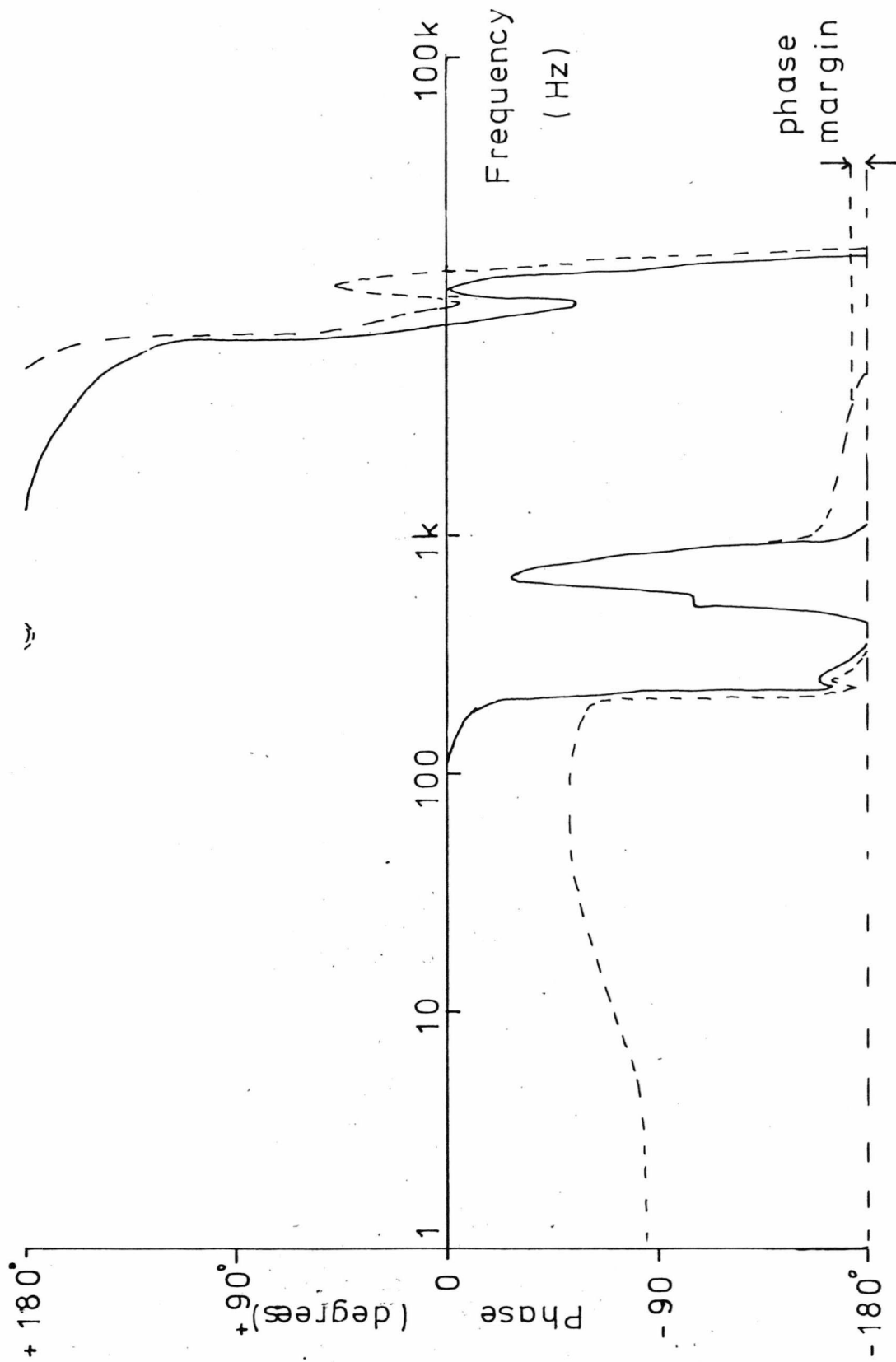
As A was constant, the output was a measure of B .

The apparatus of Fig. 4.7 was arranged so that an adjustable signal from the generator was fed through the amplifier to the transducer. The output from the photodetectors was monitored on the oscilloscope by Lissajous figure to compare its phase with the test signal from the function generator. This test signal was of adjustable phase with respect to the main signal. The output also went to a p.s.d. whose output was



Bode plot of the amplitude response of the open loop system
 (full line) - Without three-term controller

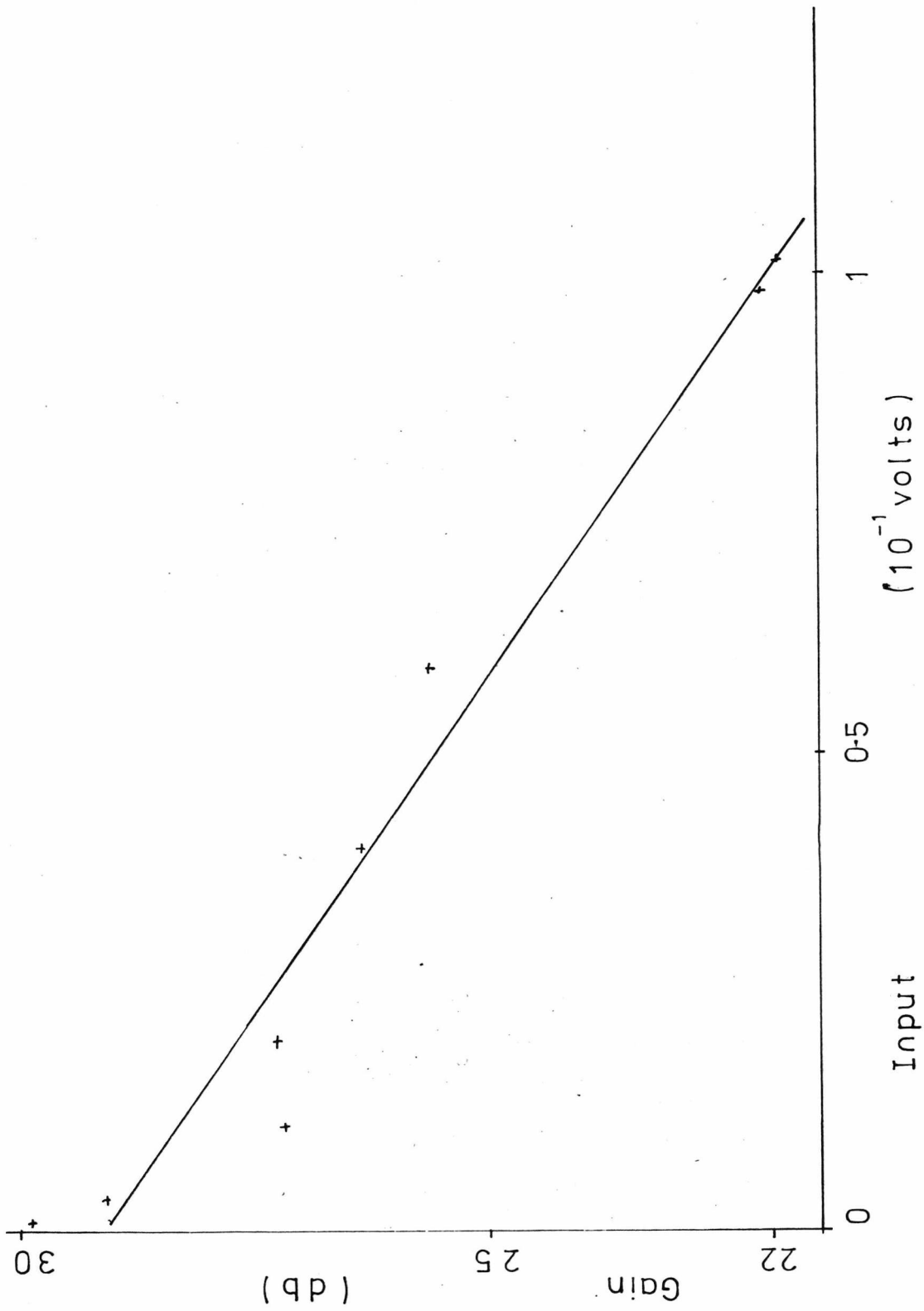
Fig 4.8



Bode plot of the phase response of the open loop system including Vibrator transducer. (full line) - Without three-term controller.

(dashed line) - With three term controller.

Fig 4.9



Graph showing the non-linearity of the system as the open loop gain varies with the amplitude of the input signal.

Fig 4.10

a measure of the correlated, averaged, signal as read on the Avometer. The phase of the signals in the p.s.d. was also monitored (by Lissajous figure) on a second oscilloscope so that the phase difference could be set to zero before measuring the amplitude (to account for any phase shift in the p.s.d.). There was an adjustable current signal to the second transducer so that the light path distance could be adjusted to bring the interference pattern back to the same mode as used in the control condition (bright or dark band between the phototransistor detectors).

The measurements were performed over a range of frequencies from 40 Hz. to 20 k.Hz. by adjusting the input signal to give a suitable output signal and the second mirror to position the interference bands. The phase of the test signal was adjusted to give a zero phase line on the Lissajous figure, and recorded. Then the phase was adjusted to give zero phase line on the oscilloscope 2 so that the true amplitude of the output was obtained from the phase sensitive detector and recorded.

The system was calibrated by replacing the interferometer by a direct link. This calibration indicated that the phase sensitive detector required special calibration below 40 Hz. and was not used in this range.

The resulting amplitude response, between the input to the power amplifier and the output from the photodetectors, is presented in Fig. 4.8 (the full line being the result before the three-term controller was added). The phase response, measured at the same time, is presented (by the full line) in Fig. 4.9.

The linearity of the system was measured at 4, 8 and 13 k.Hz. by varying the amplitude of the input oscillation and measuring the gain. The result of the measurement at 4 k.Hz. is plotted in Fig. 4.10 and indicates a non-linearity causing a variation of more than 6 db. over the different size of input amplitude. At 8 and 13 k.Hz. the variation

was more random. This non-linearity of the transducer may account for the discrepancy between the manufacturer's specification of a sprung mass resonance at 50-60 Hz. and the fundamental resonance indicated in Fig. 4.8 and Fig. 4.9 at 210 Hz. for very small amplitudes. The linear theory of appendix A4.1 relates the resonant frequency to the coefficient for the spring of force per unit displacement, K , and its inertial mass, M . Equation EA4.2 indicates that if the effective K is 16 times less for larger amplitudes than for the small amplitudes of less than a half wavelength of the light used, then the resonance frequency would be 4 times smaller. This is in the ratio of the results for small and large amplitudes.

If the Vibrator is represented, for small amplitudes of movement, by linear equations, the results given in Fig. 4.8 indicate that there is a fundamental sprung mass resonance at 210 Hz. of width 80 Hz. and putting these parameters in the linear equation EA 4.1 of appendix A 4.1 gives a basic transfer function for the Vibrator of:

$$T.F.(s) = \frac{k/M}{s^2 + 500s + (1320)^2} \quad \text{EA.2}$$

This being given in the form of the Laplace transform where S is a complex variable and the result of operating in the frequency domain is obtained by setting $S = j\omega$.

4.2(c) Method of performing the interferometer experiment.

This section describes how the apparatus was operated when the servo control on the one mirror was running with its control loop closed. The performance of the system was investigated by modulating the position of the first mirror from a sinusoidal test signal so that the second, controlled, mirror should follow its motion. The measurements described

here are of the amplitude and phase response of the open loop system, whose response is dominated by the transducer and three-term controller, from which it can be shown how the system is stable when the loop is closed.

The purpose of the three-term controller may be described, in terms of the complete open loop response, as being to reduce the effect of phase lag in the transducer (when the phase lag becomes 180° , the closed loop will be unstable if the open loop gain is more than unity at this frequency) at higher frequencies, by the differential term of the controller, and to increase the gain (and hence reduce the error signal) at lower frequencies, by the integral term. The gain of the controller should be as large as possible (to give a full sweep of the transducer for a small value of the error signal) within the constraint of having stable phase and gain margins on the Bode plot of the open loop response. Whereas the open loop response has an amplitude maximum near the natural frequency of the system, the closed loop response has a maximum approximately where the open loop response most closely approaches the gain = -1, phase = -180° point.

The controls on the complete circuit of the servo loop were set up as follows. Because the operation of the integrator in the three-term controller depends on stable conditions round the control loop (otherwise it integrates the error signal to saturate the amplifier), the integrator term was at first set to zero. The gain and d.c. bias on the comparator were adjusted to suitable positions. The direct and differential terms of the three-term controller were increased so that the fringes of the interference pattern became locked. The first mirror was then oscillated by the test signal over a small amplitude of displacement at low frequency and the gain and differential terms given further adjustment so that the servoed mirror followed the first mirror.

At this stage the integral term was increased and then the amplitude of the test signal could be increased to give a much greater swing in the oscillations of the two mirrors. The gains of the controller were increased as far as possible, however the noise in the photodetector units limits the signal which can be detected from the interferometer. The maximum signal which may be generated at the photodetector, due to movement of the mirrors causing the fringe pattern to make the maximum change in light, is caused by a relative movement between the mirrors of half a wavelength of the light. After amplification, this signal controls the position of the servoed mirror over approximately 10^4 wavelengths. However, the noise in the photodetectors is amplified by the same factor and if it gives an output displacement of more than a half wavelength, there is jumping of fringes.

When the adjustments had been made, it was found possible to modulate the position of the first mirror by a test signal and the servo control would cause the second mirror to track the movement of the first without jumping a fringe of the interference pattern. If the first mirror was moved at a higher frequency, the frequency response of the control loop could cope with only a smaller amplitude before the tracking was lost. The accuracy of this tracking depended on the accuracy of setting the optics of the interferometer and the gains of the three controller terms.

To measure the frequency response of the three-term controller when it had been correctly adjusted, with the loop closed a small amplitude sinusoidal signal was applied to the first transducer and the amplitude and phase of the resulting signal into and out of the controller, both with and without the integrator term, were measured over a range of frequencies by a method similar to that described above for the transducer. Hence the frequency response of the integrator was measured while in the control loop.

With the integrator term set to zero, the frequency and phase response of the controller were measured directly on the controller on its own.

Thus the amplitude and phase responses of the controller had been measured over both the low frequencies where the integrator has an effect, and the high frequencies where the differentiator has gain. The dotted lines in Fig. 4.8 and Fig. 4.9 show the combined result of the addition of this response to the uncompensated response (full line). These results are discussed in the conclusion to this experiment.

As a further check on the system, a frequency measurement was made as follows. At low frequencies the integrator of the controller should reduce the error signal at the detector for a given amplitude of driving the test signal mirror. The error signal on the photodetector was measured at 1 Hz. with the loop closed having no integrator term and again with the integrator term. The error signal, as measured, was reduced by -39 db. Then the response of the controller was measured. Without the integrator it had a gain of $k_2 = 2.3 \times 10^{-2}$. The integration was measured by putting a step function into the integrator and measuring the ramp. Then:

$$\text{Controller term } k_1 = \frac{O}{I} \frac{1}{T} = 9.8 \text{ sec}^{-1} \quad \text{E4.3}$$

where O is the output after time T ,
and I is the amplitude of the step input.

The differentiator has negligible effect at this low frequency and so the effective transfer function is:

$$\text{T.F.}(s) = \frac{k_1}{s} + k_2 = \frac{9.76}{s} + 2.3 \times 10^{-2} \quad \text{E4.4}$$

Hence the sinusoidal response at $\omega = 2\pi$, obtained by setting $s = j\omega$, gives at this frequency:

$$\text{Amplitude gain} = \frac{9.79}{2\pi} \cdot$$

Comparing this with the controller having no integrator (gain = 2.3×10^{-2}), the increase in gain is 37 db. Within the experimental error, the reduction in size of the signal error by -39 db is accounted for by the increase in open loop gain at 1 Hz. of 37 db.

4.2(d) Results of the interferometer experiment.

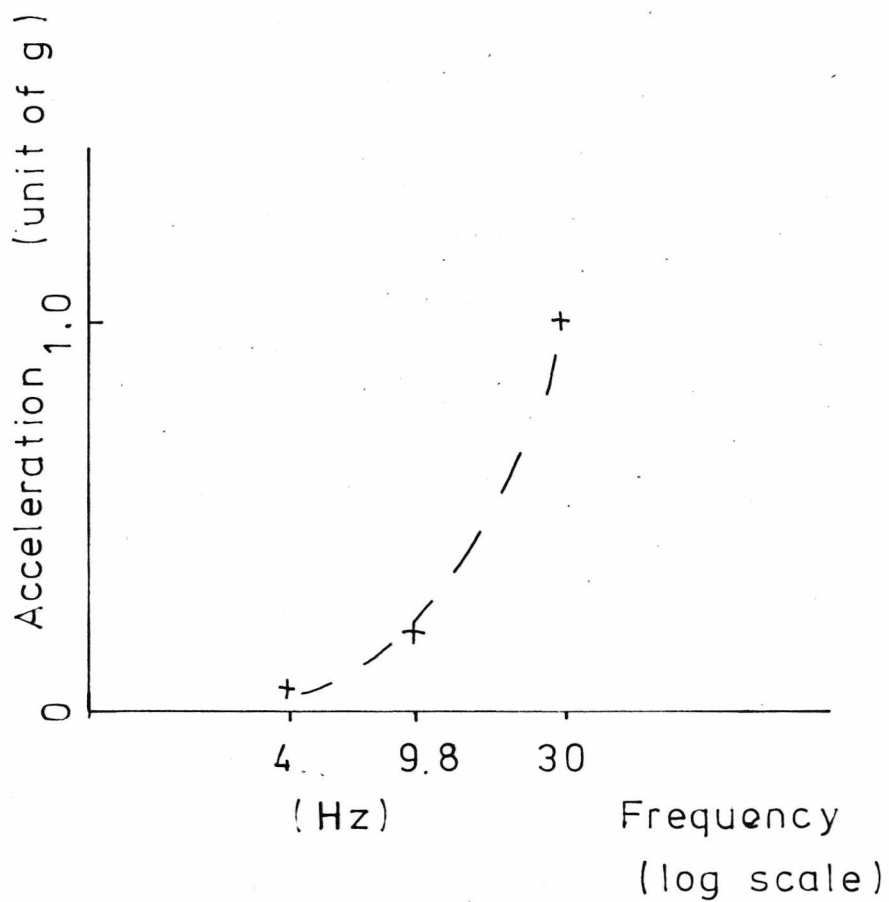
As indicated in Fig. 4.2, the position of the fringes is effectively a comparator of the relative positions of the two mirrors and hence a measure of the rigidity of the system considered as a measuring rod. For the apparatus of Fig. 4.1 to represent this rod, the second transducer might be positioned alongside the first with a passive mirror turning the beam through a right angle as indicated by a dotted section in Fig. 4.1. The control system had limited gain and hence the system is not perfectly rigid but gives a displacement of the fringes when one end is accelerated. The rigidity was estimated by driving the first mirror with what was assumed to be a sinusoidal motion of $A \sin \omega t$, where A could be measured on a scale placed next to the moving mirror, giving:

$$\text{Acceleration} = -A \omega^2 \sin \omega t . \quad \text{E4.5}$$

For a number of spot frequencies, the amplitude of the test signal was increased until the system lost control. The amplitude (A) of the transducer displacement at this setting was:

Frequency	Amplitude (A)	
Hz.	m.m.	
4	1.8	
9.8	0.9	E4.6
30	0.5	

It is assumed that for this condition the error signal on the position



The maximum accelerations which could be obtained without loss of control by the feedback circuit controlling the second mirror.

Fig 4.11

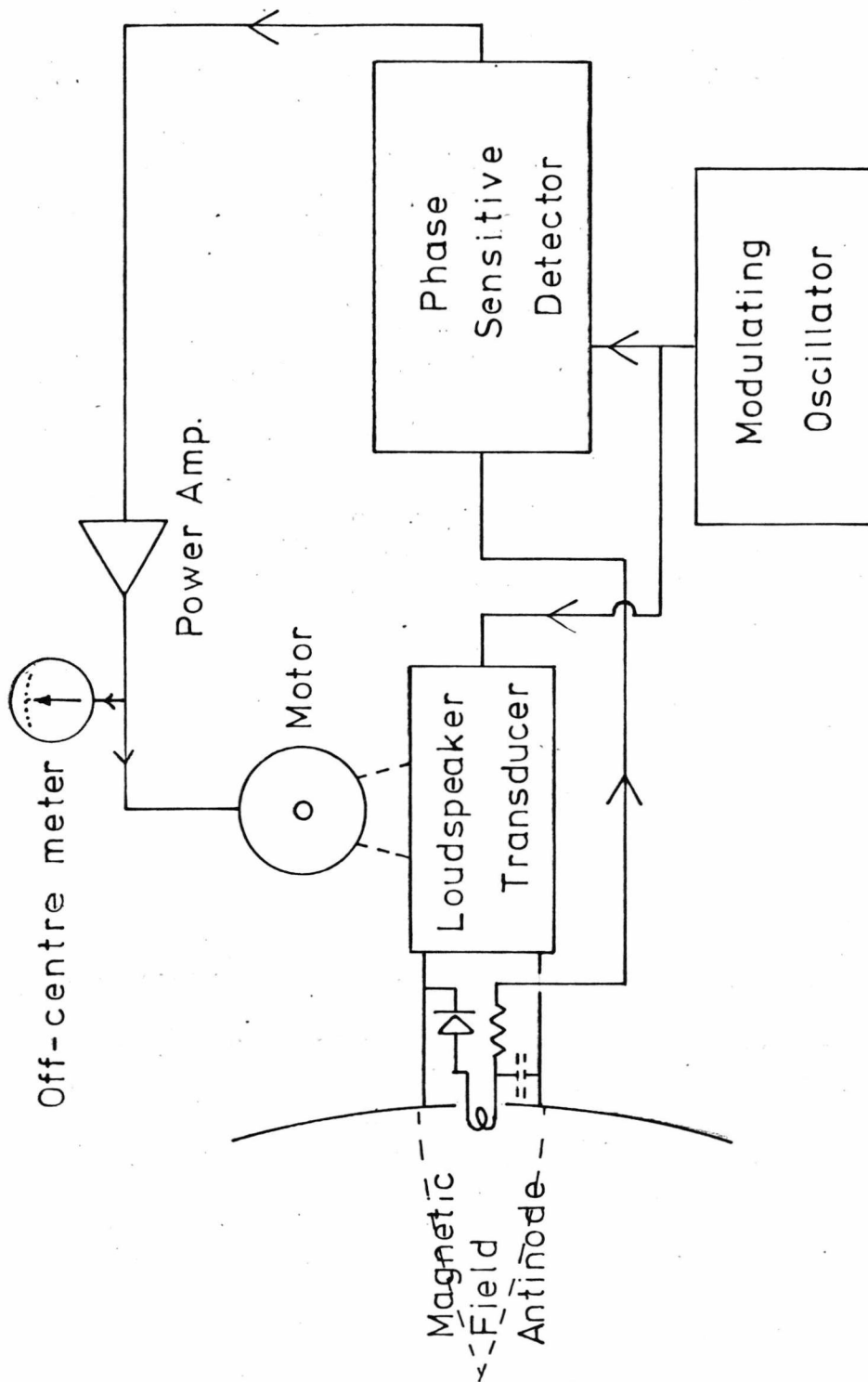
of the fringe is the distance of a half fringe width so that it just starts jumping fringes. The graph of Fig. 4.11 indicates the maximum acceleration against frequency calculated by equation E4.5 (for an error signal of one half fringe width). Thus, considering the distance between the mirrors as a rigid rod, at 9.8 Hz. a strain of about 3×10^{-5} cm. was caused by accelerating one end at 0.2 g.

4.2(e) Conclusion to the interferometer experiment.

At the high frequency end of the range it may be noted that, without the controller, the phase changes to -180° by 1.1 k.Hz. (Fig. 4.9) and hence the gain reduced by more than 45 db on that shown by the full line on Fig. 4.8 would be required to give a stable gain margin. Due to non-linearities these are approximate results and the effect of the main resonance at 210 Hz. (Fig. 4.8) bringing the phase rapidly towards -180° at 400 Hz. did not in fact reach -180° under control conditions as indicated by the final stable system. With the controller (adding gain -26 db.), the phase changes to -180° by 5 k.Hz. giving a gain margin of 2 db. and phase margin of 7° at 3.3 k.Hz.

At the low frequency end of the range the integrator has considerable effect. A relative movement between the mirrors of a half wavelength of the light causes maximum change of fringe position. This maximum error signal causes a tracking movement of the servoed mirror by a distance equal to the gain of the control loop times $\lambda/2$. Thus, taking typical values of gain for the complete control loop from Fig. 4.8:

<u>f</u> <u>Hz.</u>	<u>gain</u> <u>db.</u>	<u>gain $\times \lambda/2$</u> <u>cm.</u>	
1	73	1.7	E4.7
10	55	0.22	
80	37	0.03	



Block diagram of the trolley servo control loop, positioning the trolley according to the signal from the detected magnetic field antinode (similar for the other trolley with transmitting horn).

Fig. 4.12

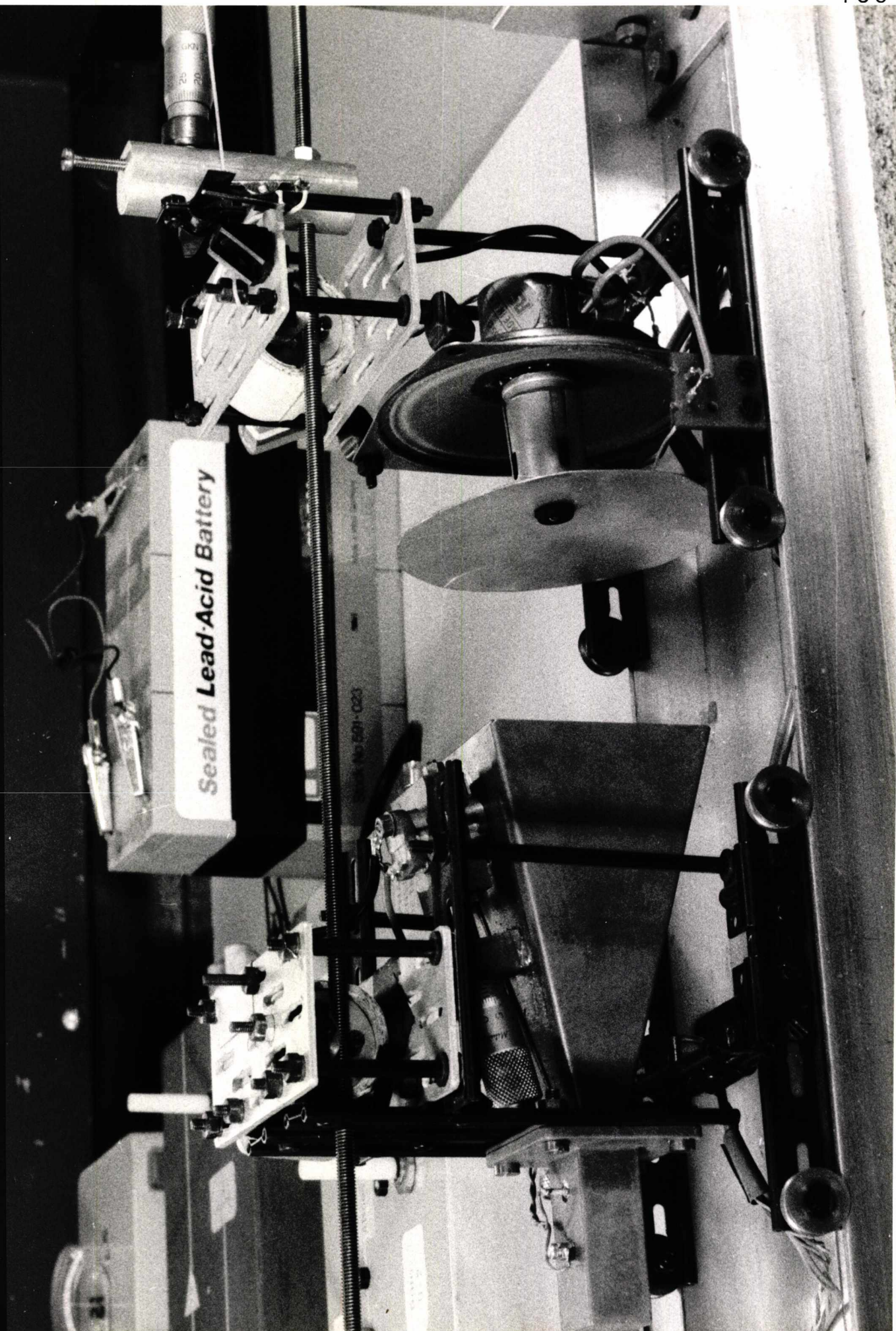


Photo 2

The final column indicates the maximum swing of the mirrors by the test signal before the servo loses control due to having only a maximum signal into the controller of one fringe. In practice, it was about half these values (c.f. Table E4.6).

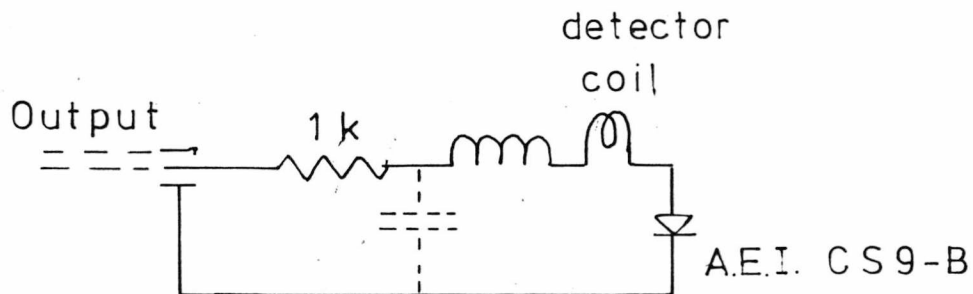
4.3 The Trolley experiment.

The purpose of this second experiment is to extend the idea of a rigid interval being maintained by control from waves travelling between reflectors, to a system in which both reflectors may move at any velocity relative to the laboratory while being controlled by the waves. In this experiment the fields of the standing waves are detected at the reflectors (corresponding to the positions of the mechanism determining the motions of the reflectors in the analysis of chapter 3) and this signal goes round a control loop to drive the motor positioning the trolley. Each trolley and its control loop were entirely independent except for the waves between them and the complete loop of the automatic control for one of the trolleys is shown in Fig. 4.12. Because the time for the microwaves to traverse the gap of about 10 cm. between the trolleys is 0.03μ . sec. which is so short compared with the response time of the apparatus, the stepping motion between the two ends (described for the system in chapter 3), caused by the delay time for information to cross between the reflectors, was not demonstrated.

4.3(a) The apparatus for the Trolley experiment.

The apparatus is based on a system of two trolleys, built by M.A. Jennison, with F.A.C. construction kit (Fig. 4.13 & Photo 2). They run on rails set 10 cm. apart and are 13 cm. high. Towards the top of each trolley is a 3 cm., 6 V. d.c. reversible motor (Swiss made, Escap SR 601.A12, 3.72 and used by Feedback Co. as motor for SA 135, Part No. 2565-221) with a small cog on its output shaft that engages in a length





The detector circuit of the microwave magnetic field.

Fig 4.14

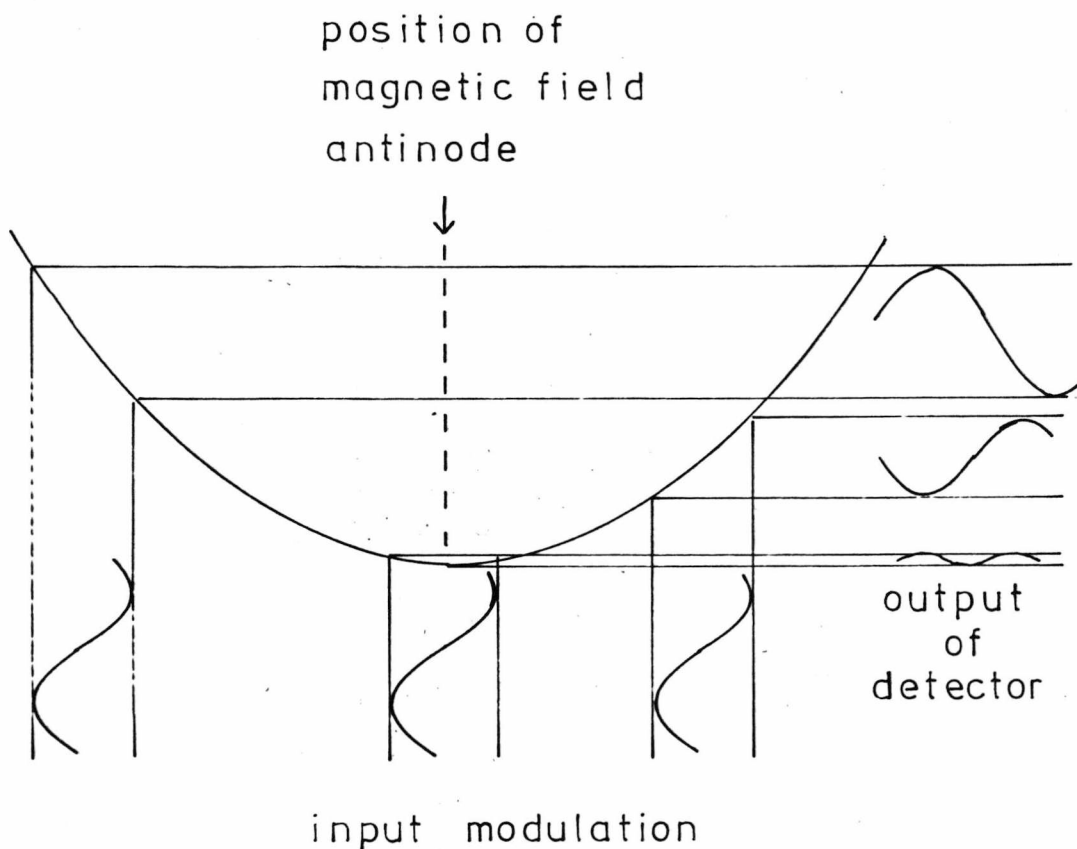


Diagram of the 'characteristic' of the trolley system, showing the change of phase of the output, caused by the modulation of the reflector, as the trolley moves through the required position (where the frequency is doubled).

Fig 4.16

of 2 BA studding running along the top centre of the rails. This motor has a 4 μ .f. capacitor across its terminals to reduce interference feeding back to the amplifiers. There is an idler pulley on the trolley above the studding to hold the studding onto the cog.

The first trolley carries a 4.5 cm. length of waveguide with a short at its outer end 3 cm. from a Gunn diode (Mullard CL 8630) mounted across the guide. This generator of 10.7 G.Hz. microwaves is bolted to a horn which flares out to 5.5 cm. square aperture. The electric field in the guide is orientated vertically. A probe of two turns of diameter 0.5 cm. of wire, with its axis horizontal across the aperture, can be positioned inside the length of the top edge of the horn by a micrometer. The loop connects to a detector diode AEI CS9-B as in Fig. 4.14 and the output went by screened cable to the phase sensitive detector.

The second trolley carries a 35 ohm Radiospares 3" speaker on the centre of the cone of which was stuck a metal cap and socket (from a valve cover) carrying a 3 inch diameter, slightly concave reflector to trap the microwaves, and in the centre of which was a rubber grommet supporting a similar two turns of detector coil behind which was the detector circuit.

A point contact of sprung metal (clock spring) was attached to the top of the second trolley and a micrometer mounted on the fixed studding enabled small movements of the trolley to be measured by adjusting the micrometer until it just made electrical contact with the spring. There was a free pulley over one end of the chassis rails to enable a cord fixed to the second trolley to go over the pulley and hang down to weights. There were flying lead cables to the moving trolleys.

The two trolleys facing each other were each automatically driven by the motors controlled from the detectors of the standing wave between the trolleys. The 3 cm. waves were generated by a Gunn diode, a device

in which the oscillations occur in the bulk of the material rather than at a narrow junction (Baden Fuller⁽⁴⁾, 1969). The frequency range of the radiation is determined by the dimensions of the specimen and a fine control is given by the resonant cavity in which the diode operates (there being feedback from the microwave field to the device) reducing harmonics. The device was run from a 7.5 volt d.c. supply as this gives the greatest frequency stability. The output power is about 10 m.watt. The frequency of the waves was determined by the resonance of the shorted waveguide behind the diode and to a small extent by the total cavity formed by the horn and reflector on the other trolley. Depending on exactly at what angle the waves were reflected from the other trolley, it would resonate in different ways and there was some instability due to switching between resonances. This problem was partly solved later by isolating the generator from the rest of the system by a partly absorbing padding attenuator (of resistance paper) in the guide between the diode generator and the horn.

The loop aerial on each trolley couples in to the magnetic field of the microwaves, detecting a signal which goes to a phase sensitive detector. Instead of taking the error in position directly, one of the mirrors was perturbed at audio frequency about the required position and the phase change of the signal generated by the magnetic field as it moved through the antinode, was used to servo to the required position. The audio frequency perturbation was obtained by driving the loudspeaker an excursion of the order of 100 microns. The two detectors operate in slightly different ways. That on the trolley with the microwave generator finds the standing wave antinode between the emitted wave and that reflected back from the second trolley. The detector on the other trolley is always at an antinode because it is in the plane of the reflecting surface where the electric field is maintained zero. It looks

Circuit diagram of the Phase Sensitive Detector, showing the four diode ring detector circuit and output smoothing.

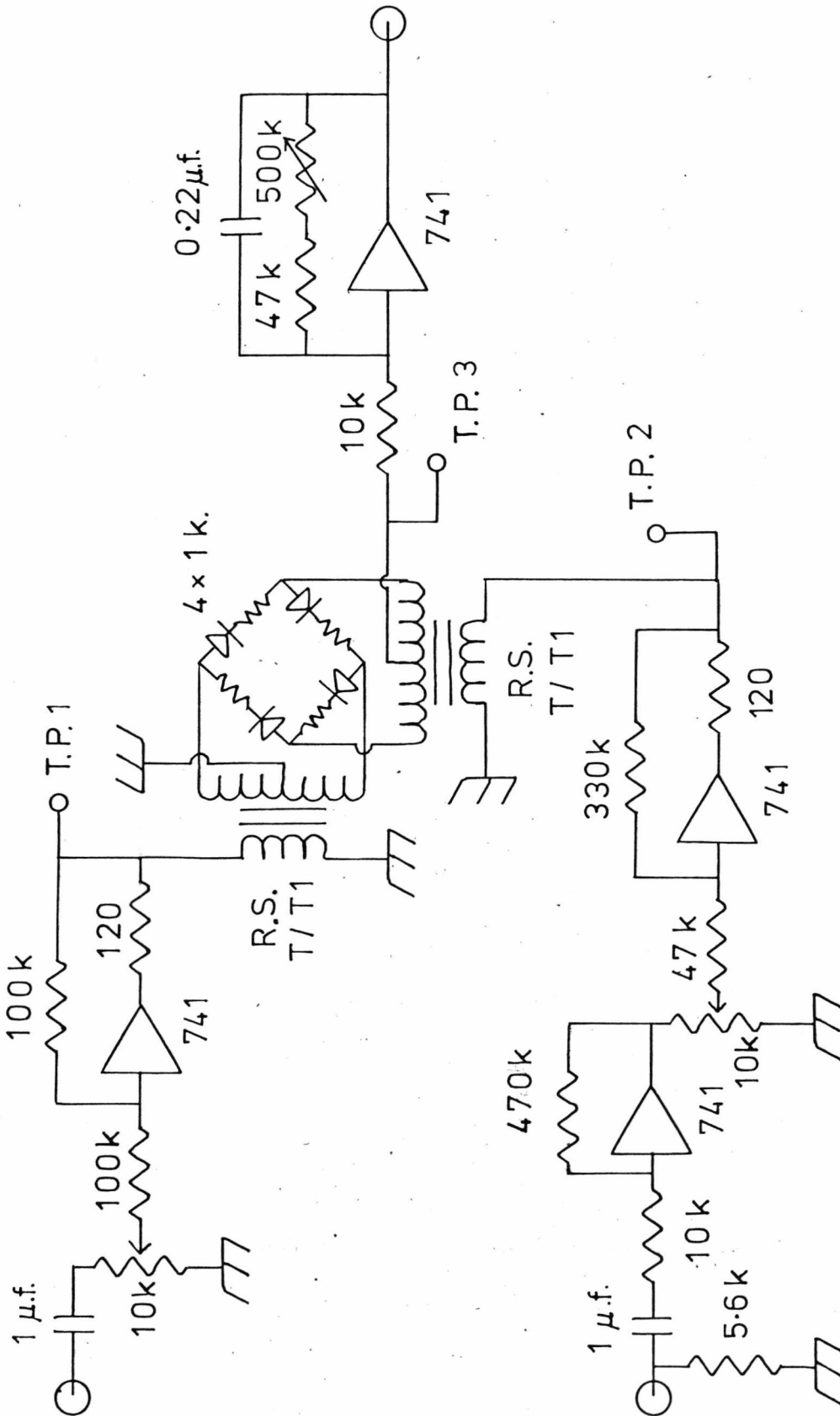


Fig. 4.15

for the condition of resonance of the complete system of multiple reflections indicated by a build-up of the amplitude of the standing wave.

The signal from the microwave detector circuit (Fig. 4.14) went to the input of the amplifier with gain 47 on the circuit of the phase sensitive detector shown in Fig. 4.15. The signal which goes to the loudspeaker also went to the other input of the phase sensitive detectors. The diode ring detector effectively forms the scalar product of these two signals of the same frequency but different phase. It is followed by an integrator to smooth the fully rectified signal. The phase sensitive detector performs two functions. For waves of a single frequency it gives an output according to the equation:

$$\text{Output} = A B \cos \theta \quad \text{E4.8}$$

where A and B are the amplitudes of the two signals and θ is the phase angle between them. For a signal mixed with noise it acts as a correlator and improves the signal/noise ratio. The phase sensitive detector generates an error signal from the phase difference between the signals from the detector and the reference signal (Fig. 4.12). The loudspeaker transducer had a resonance at 74 Hz. so the required phase could be set by driving the loudspeaker modulation at this frequency and moving to either side of the resonance to give the required phase in the loudspeaker oscillation. The phase of the detected signal sweeps rapidly from positive to negative as the trolley moves through its correct position, giving a tight detection of its position but when the output has swung to full voltage in either direction, the amplifier is saturated and there is no further control.

The signal from the phase sensitive detector, which was a measure of the error in position of the trolley, was fed directly to the power amplifier circuit shown in Fig. 4.6 (but with current feedback) which

drove the motor, thus completing the control loop. Each driver amplifier was powered by a separate pair of Radiospares accumulators (RS No. 591-023). This ensured that there was no electrical effect of one circuit on the other and also that surges of current were available from the supply when required. It was found later that, by having a 10 k. potentiometer between the voltage and current feedback points on the power amplifier circuit, it was possible to tap off a variable type of feedback. Some of this feedback came from the back e.m.f. generated by the motor and on going back through the amplifier caused it to effectively damp the movement of the trolley.

4.3(b) Method of performing the Trolley experiment.

The loudspeaker modulation vibrates the detector about the magnetic field antinode such that on one side of the node the variation of output is in opposite phase to that when it is on the other side (Fig. 4.16). Although there is only a small variation of the amplitude of the standing wave about the antinode, this null-searching technique gives a rapid change of the phase of the output signal as the trolley moves through the correct position. The detector gives a measure of the power signal at the aerial, with polarity depending on the polarity of the diode, and all phase information about the microwave and standing wave is lost, leaving only information on the amplitude of the standing wave as the modulation moves the detector across the field.

The complete adjustment for each control loop was as follows. With opposite motor unpowered, adjust the gain of both inputs to the phase sensitive detector to give a smooth, balanced, variation of error signal (monitored on the oscilloscope). Then the overall gain was varied until the mechanical friction was just sufficient to give a non-oscillatory system. Then the Gunn diode source of microwaves was switched off and the d.c. bias set to give zero output with zero input.

When this had been done for both control loops, they were both connected in working order and the position of the loop detector on the micrometer on the trolley adjusted so that, when in a static condition, both outputs were zero (i.e. both trolleys were controlled to maintain the same, rather than different, distances). A final check was made with the Gunn diode off, that both circuits gave zero output.

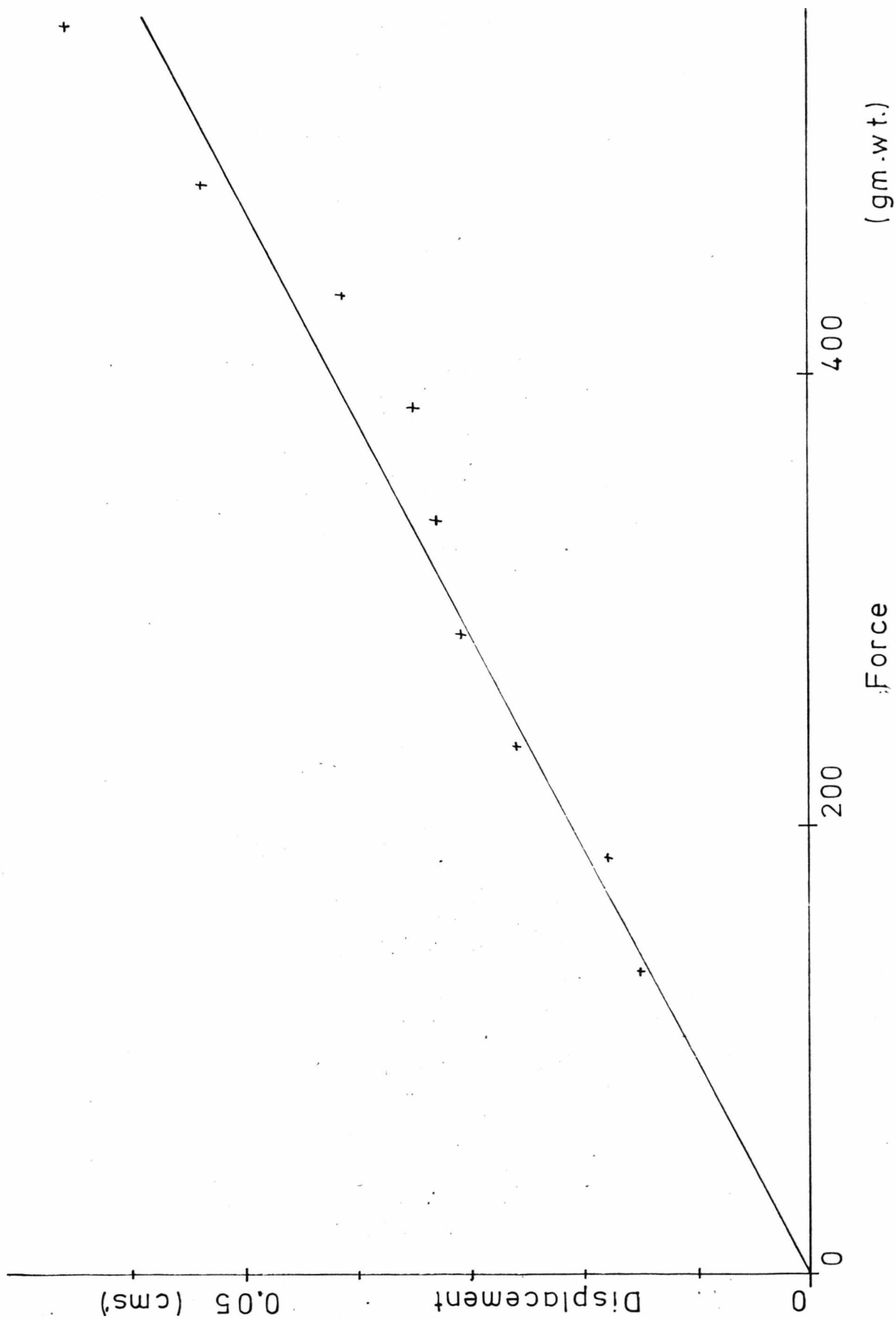
The resulting system would maintain the distance between the trolleys however either trolley was separately moved provided it was not moved faster than the frequency response of the control could respond. While the external force was applied, the outputs of both control loops swung over to drive the trolleys in the appropriate direction. However, when one trolley moved generating an error signal, the gains of both loops should be adjusted so that this error gives much the same driving force to each trolley. If this is not so, it was found that the resistance to being pushed of the trolley in the higher gain circuit was greater (or much greater).

As the operation of each control system in this case was determined mainly by the driving of the trolleys, which was somewhat random due to stiction and the multipole construction of the motors, they were non-linear compared with the transducers of the previous experiment and linear frequency compensation was not added to the electronics.

In order to simulate the delay time of the system considered in chapter 3, consideration was given to introducing an artificial delay in the control circuit. The reason why this was not implemented is discussed in appendix A4.4.

4.3(c) Results of the Trolley experiment.

The parameters required for equation EA4.4, which describes the trolley in terms of its transfer function, were measured for one of the trolleys and found to be:



Graph of change of length between trolleys versus force pushing one trolley (the other trolley being fixed).

Fig 4.17

$$\text{Mass} = M = 1.36 \text{ k.gm.} \quad \text{E4.9}$$

$$\text{Friction coefficient} = F = 50 (\pm 15) \text{ gm.wt. sec/cm.}$$

The value of F was vague, varying with velocity and position along the track. Inserting these values into equation E4.4 for the open loop function for the trolley gives:

$$\frac{F}{M} = \frac{50 \times 981}{1360} = 36 \text{ sec}^{-1} \quad \text{E4.10}$$

By inspection, the Bode plot of the frequency response of a system, described by equation E4.4 with this value of parameter, has a break frequency at $6 (\pm 3)$ Hz. The form of equation E4.4 suggests that there is a pole at the origin giving -6 db/octave up to this break frequency above which it should be -12 db/octave.

The (open loop) frequency response of the trolley driven by the power amplifier was measured roughly and found to be:

$$\begin{aligned} & -6 \text{ db/octave from } 0.5 \text{ Hz. to } 1 \text{ Hz.} \\ & -12 \text{ db/octave from } 2 \text{ Hz. to } 4 \text{ Hz.} \end{aligned} \quad \text{E4.11}$$

Thus there appears to be slightly more frictional force when the motor is being driven than when being pushed without electric power. This may be due to feedback of the back e.m.f. generated by the motor, through the power amplifier.

With the power disconnected from one trolley, a displacing force was applied to the other (by weights hanging from a cord over the pulley). Fig. 4.17 plots the displacement of the trolley caused by a series of increasing forces. This is an indication of the rigidity of the etalon. The graph is approximately a straight line so that Hooke's law is obeyed with modulus, for a total length of 7 cm. between the current probes:

$$\text{Modulus } \lambda = \frac{\text{Force}}{\text{Strain}} = 63 \text{ k.gm. wt.} \quad \text{E4.12}$$

The system had a breaking force of about 2 k.g.m. wt. (this depended on how accurately the controls had been set up).

If a block of Perspex was placed between the trolleys, they moved so as to set the same optical distance modified by the refractive index of the Perspex. It was also possible to control the movement of the complete system by moving the Perspex.

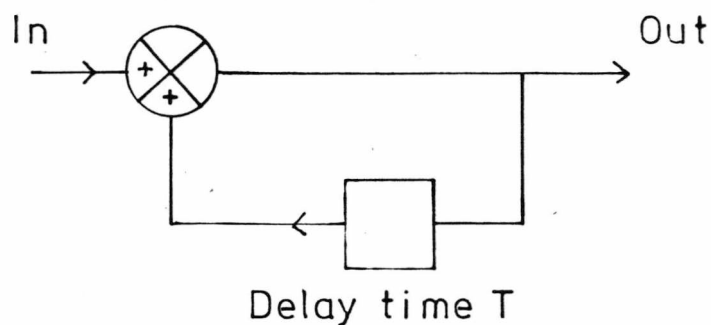
If either trolley was pushed slowly, the other followed and, if the controls were well adjusted, would continue to move when the external force was removed (thus demonstrating conservation of momentum).

4.3(d) Conclusion to the Trolley experiment.

The apparatus demonstrated motion independent of the laboratory and the result of E4.12 demonstrates a type of rigid system which may be compared with McCrea⁽³⁹⁾, 1952, and his theory of a rigid rod described in chapter 2.

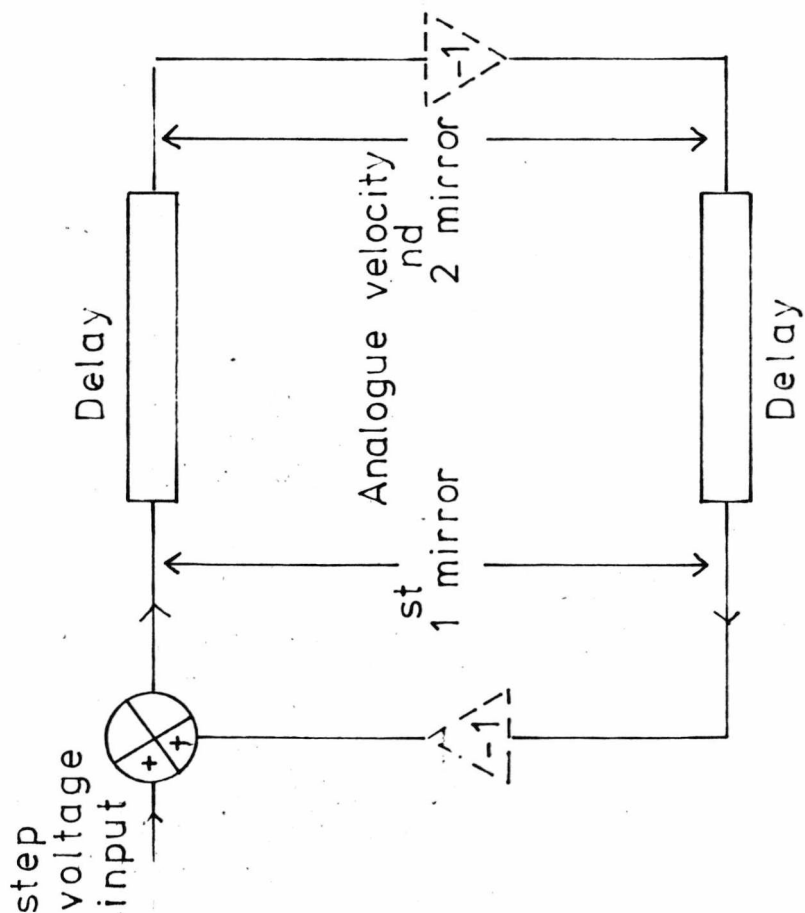
The following comments are made on the equipment. The phase sensitive detector, as well as operating on the phase difference between the signals at its inputs, also operated on the amplitude of the detected signal. To be strictly phase sensitive, the signal from the detector would have had to be further amplified and clipped to give it a constant amplitude.

As the motor on each trolley turned, it generated spikes of noise voltage. Attempts were made to reduce the spikes getting into the amplifier. This included a good earth wire between the trolley chassis and the detector amplifier case, 4 μ .f. capacitors across the motor terminals and a 0.5 μ .f. capacitor across the output of the microwave detector circuit. It was suggested that there should be an emitter follower type buffer stage between the control amplifier output and the motor (that is, the power transistor stage in Fig. 4.6 should be outside the feedback loop of the power amplifier circuit).



Basic positive feedback circuit with delay unit.

Fig 4.18



Analogue of the delay time for the waves to traverse the etalon in each direction. The voltage differences correspond to velocities in the etalon system.

Fig 4.19

The optimum condition for positioning a system such as the trolley is when the system is critically damped. Equation E4.5 shows that the closed loop system behaves like a damped oscillatory system with inertia, damping and a 'spring' holding it about the required position. The only damping in the trolley system was the friction in the traction drive (which tended to vary along the track) and an electronic derivative term was likely to be of limited use because the signal in the control circuit contained too much noise and was non-linear (although the back e.m.f. generated by the motor could be fed back into the power amplifier). A suggestion for future improvement would be a bar between the tracks on which friction pads, attached to each trolley, would clamp and give more (and more even) friction damping than that measured in E4.9 above.

4.4 The electric analogue experiment

The purpose of this experiment is to demonstrate (non-relativistically) the effects of the time delay for radiation to cross the cavity. As this could not be done in real time, an analogue at reduced speed was made to send electric analogue signals along a delay unit (built round a tape recorder and play-back) and back on a second unit. This was fed back into the input as positive feedback with unity gain as shown in Fig. 4.18.

Because of the doubling effect, the velocity of the reflector moving according to the conditions described in chapter 3, is double that of the original change (to first order in v/c). Hence the exact analogue is that of Fig. 4.19, where the inverter gives a difference signal which is doubled. Likewise the inverter at the summing end gives a signal which is the original step combined with a doubling of the signal returning on the second delay unit. As double inversion may be removed so far as the electronics is concerned, the inverters were omitted. However this means when reading the experimental graphs, that

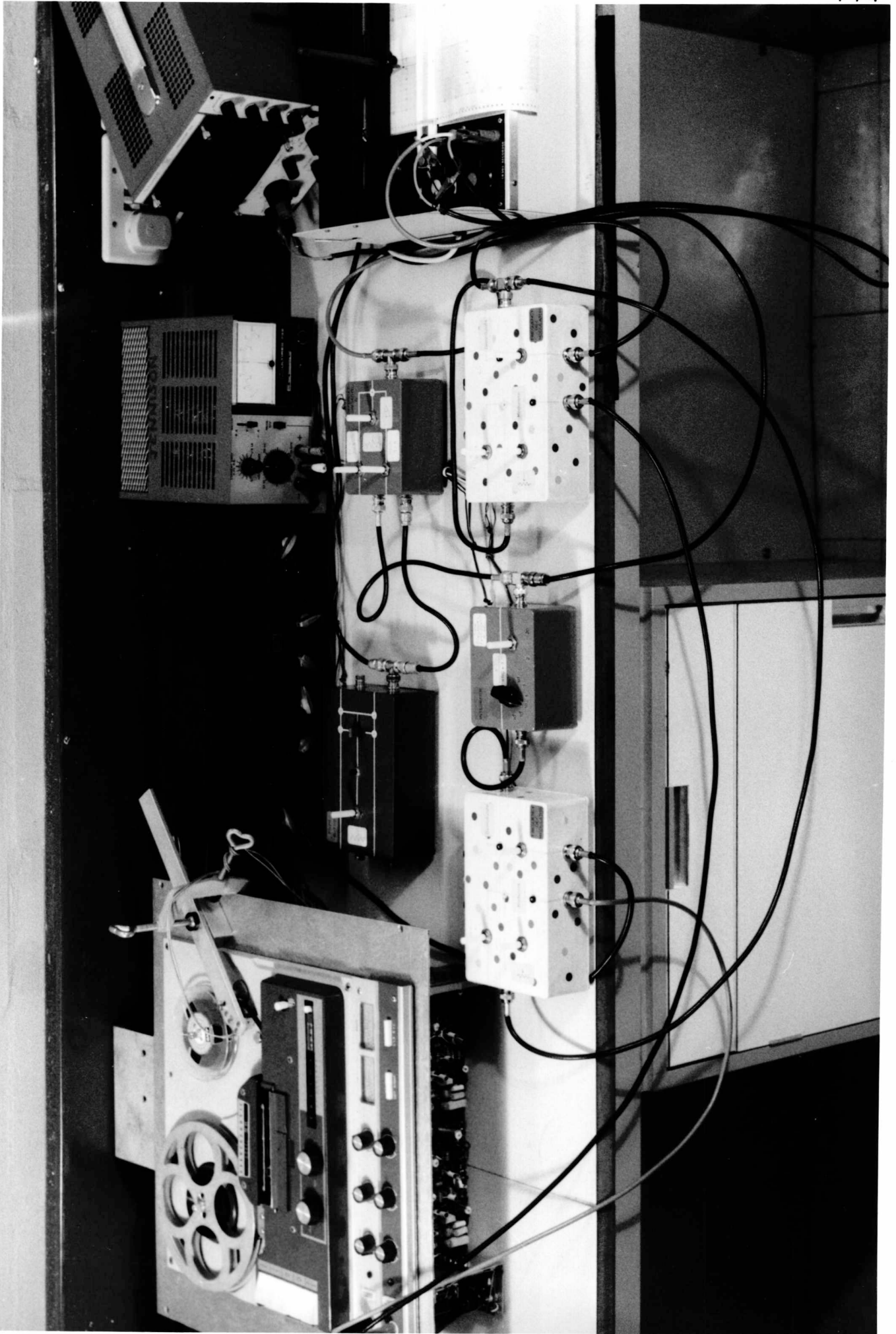


Photo 3

Circuit for frequency modulation decoder, showing the pulse shaping circuits (including amplitude clipping by diodes) and integrating circuit.

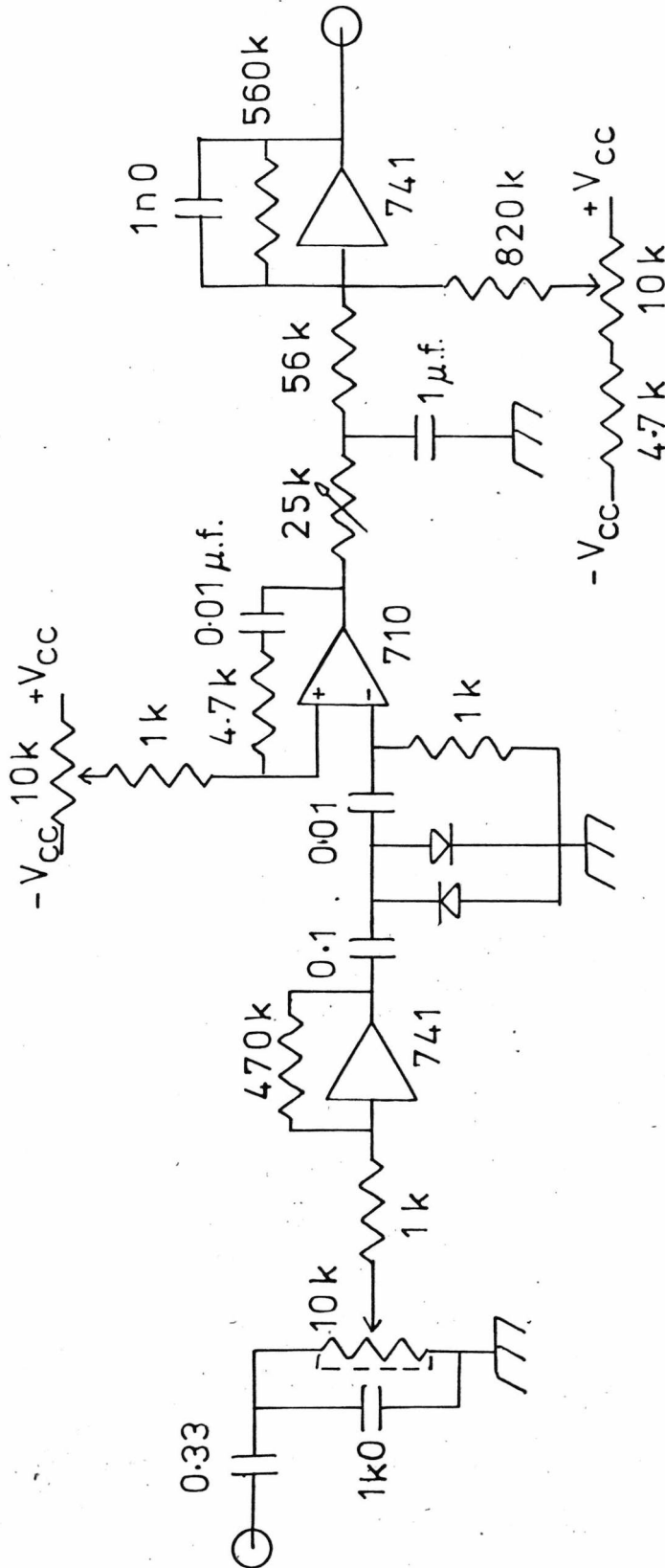


Fig. 4.20

Circuit for frequency modulation coder, showing the voltage controlled oscillator circuit.

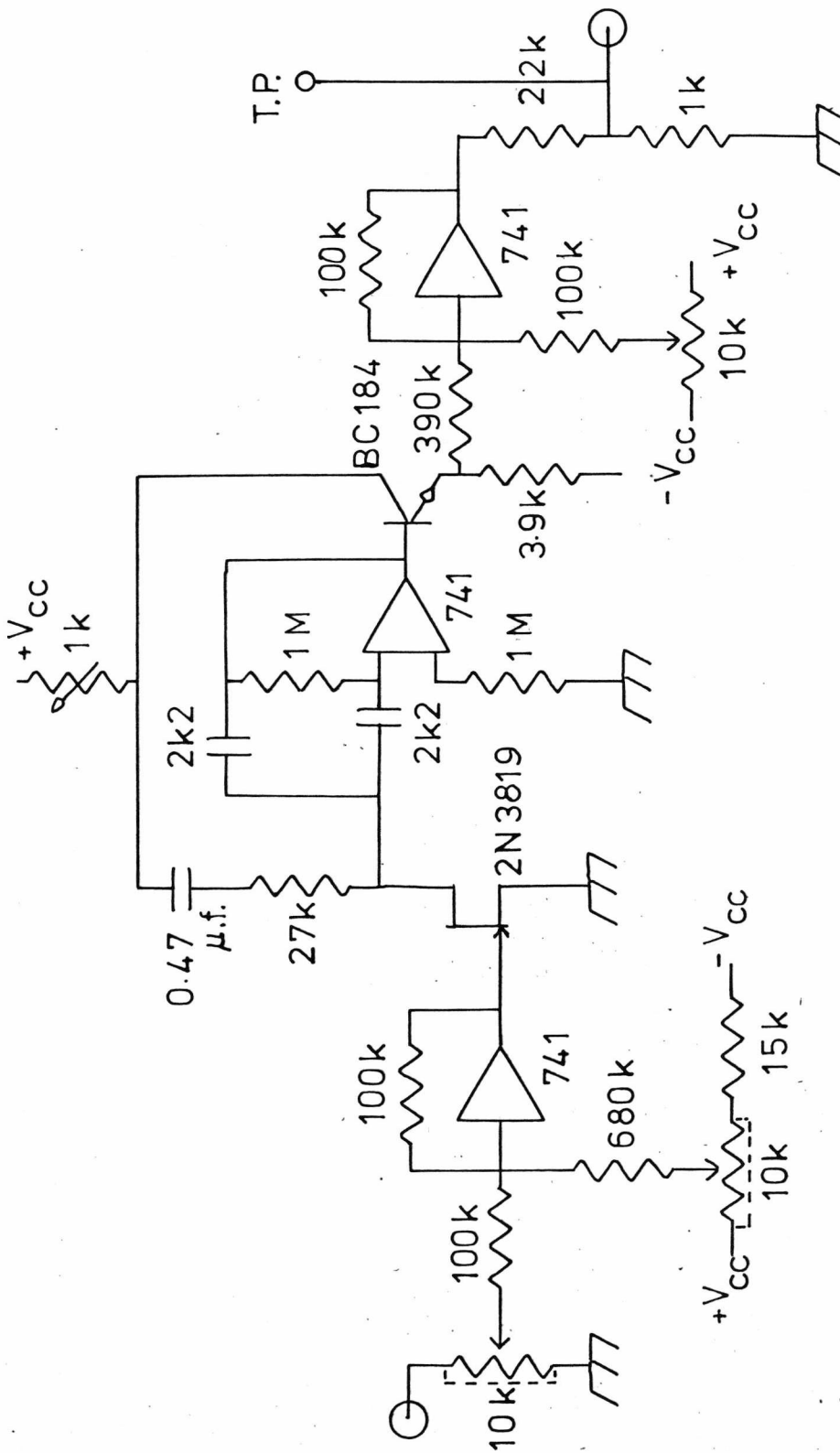


Fig. 4.21

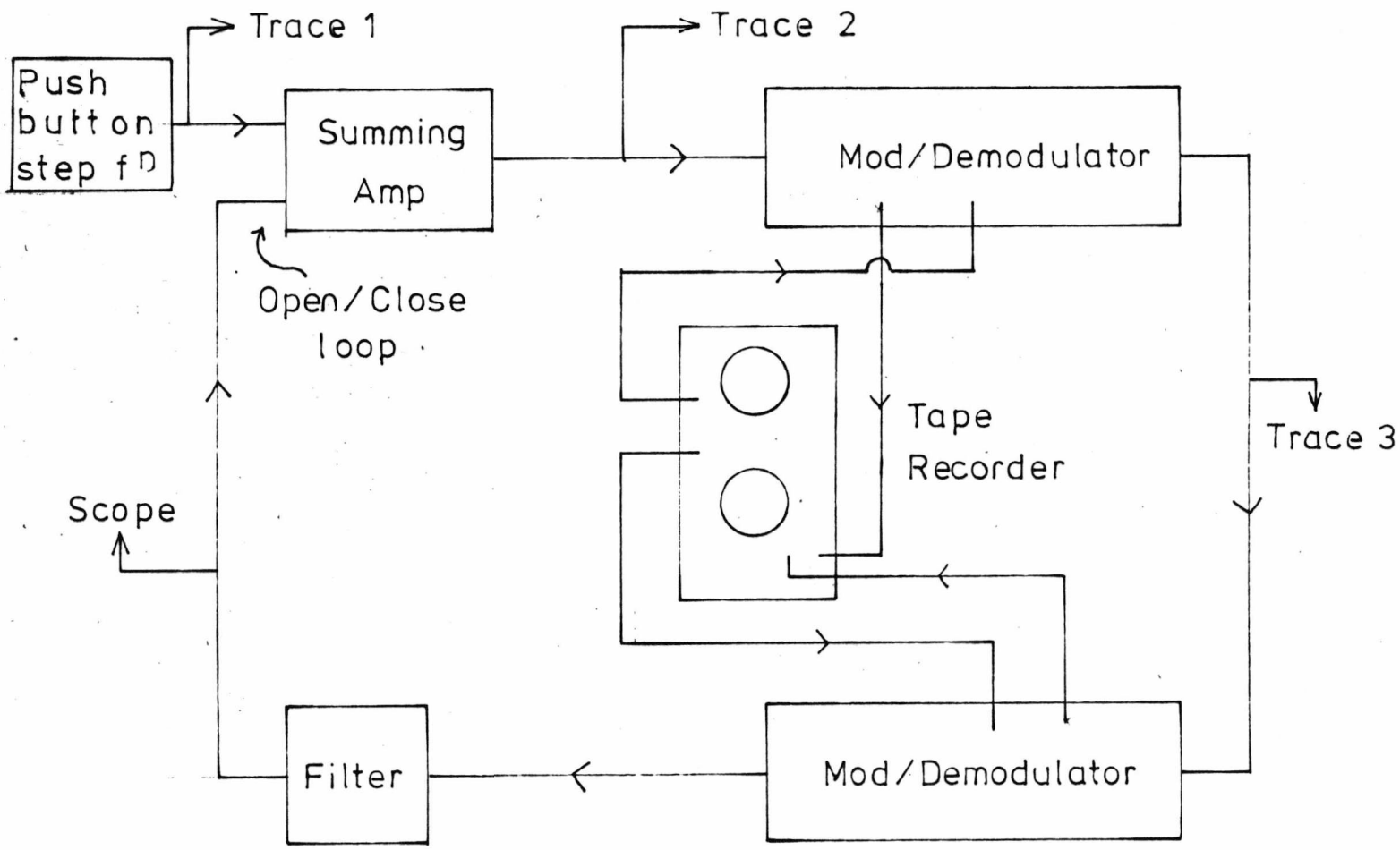
trace 2 for the reflector velocity (Fig. 4.23) should be:

$$\begin{array}{l} \text{Analogue of 1}^{\text{st}} \\ \text{reflector velocity} \end{array} = \left(\text{Trace 2} - \frac{1}{2} \text{Trace 1} \right) . \quad \text{E4.13}$$

As the gain of the recording of trace 1 already reduces it by about a half, this function should be subtracted from trace 2.

4.4(a) The apparatus for the analogue experiment.(Photo 3).

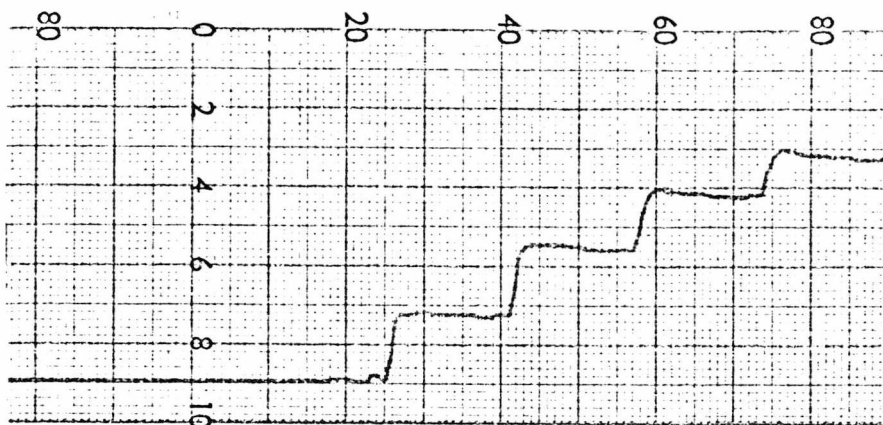
The two delay units were made as follows. A two channel stereo Tape Recorder (Truvox Stereophonic Model PD104) was modified by mounting a two channel playback head in an adjustable yoke positioned just before the wind-on $\frac{1}{4}$ inch tape reel. A Teflon bobbin was added on the far side of the head to guide the tape over the gaps in the head. This arrangement was used to give two delay units. The tape was run at $7\frac{1}{2}$ i.p.s. in Recording mode and there was a distance of 6.25 inch along the tape between record and playback heads. The signals from the playback head went to a dual amplifier (Stern's Tudor). The output of this amplifier went to the demodulator (Fig. 4.20) and was adjusted to a suitable amplitude. It was clipped and triggered a monostable which supplied a stream of pulses of fixed width. This stream was smoothed to give the final output. In order to be able to delay signals of frequency down to d.c., this system of first recording a frequency modulated signal to represent the original signal was used. The amplitude-to-frequency conversion was performed by the circuit of Fig. 4.21. In this circuit, the signal goes through a biasing amplifier to an FET transistor whose resistance is modulated by the signal. This transistor formed the resistance component of the feedback in the oscillator circuit so that the frequency of oscillation was controlled by its resistance. The frequency was modulated by about 2:1 about 7 k.Hz. The delay unit operated from d.c. to 30 Hz. when the tape was running at $7\frac{1}{2}$ i.p.s. and gave a delay of 0.8 sec.



Block diagram of the analogue system, showing the points at which the chart recorder channels were connected to give the traces.

Fig. 4.22

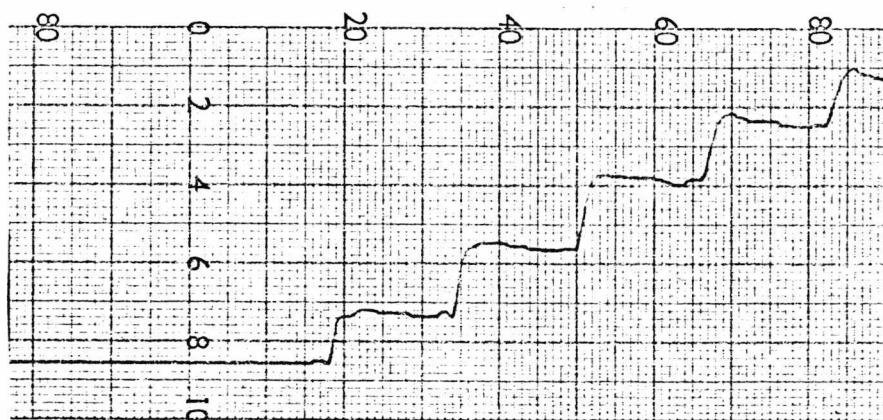
Trace 3



Output from the first delay unit.

1 cm/sec

Trace 2



Input to the first delay unit.

Trace 1

Step perturbation to the
summing
amplifier.

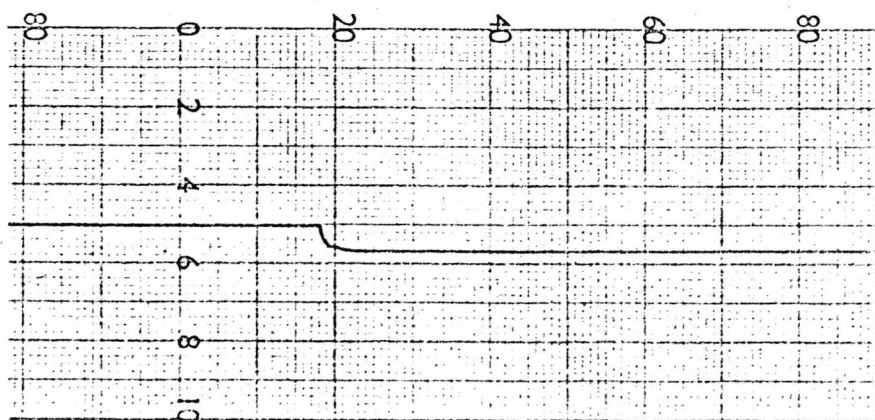


Fig 4.23

The units were arranged as in Fig. 4.22 so that the signal from the summing amplifier (analogue of the velocity of the first reflector) went through a delay unit (analogue of the delay time along the etalon) the output of which was the analogue of the velocity of the second reflector. This signal returned through the second delay unit. There was an extra filter with time constant 50 m.sec. to remove high frequency noise introduced into the system by imperfections in the delay units. The signal returned to the summing amplifier where the loop was completed.

At a second input to the summing amplifier a step signal could be added from a unit with a push button which added an adjustable step of voltage when required.

The chart recorder recorded the signals simulating the two reflector velocities and also the signal from the push button unit.

4.4(b) The results of the analogue experiment.

The experiment was run and the system would run (on open loop in the first case) and settle down with both outputs steady. The gain was reduced until with a closed loop and adding a step input, a slightly decreasing series of steps were obtained (it was found that the gain had to be somewhat less than unity as measured on the open loop. However, the converters were not quite linear and there was ambiguity of gain). The measurements were made by starting the tape recorder, monitoring the open loop output and adjusting the bias to give zero output with zero input. The chart recorder was started and the loop closed. The push button signal was added.

The charts shown in Fig. 4.23 were obtained with gain such that steps of almost steady size (perhaps slightly increasing) were obtained. The signals corresponding to these traces are indicated by corresponding labels in Fig. 4.22 of the circuit diagram.

4.4(c) Conclusion to the analogue experiment.

This experiment has demonstrated the effect of the delay time, for the signals to cross between the reflectors, by using a time scaling in which the 0.03μ . sec., required for the electromagnetic waves to move between the trolleys of the previous experiment, is represented by 0.8 secs in the tape recorder. This is a time scaling of $1 : 3 \times 10^7$.

The results of Fig 4.23 show the stepping motion of the first reflector and this may be compared directly (apart from the second order relativistic term in v/c) with the graph of Fig. 3.3 obtained in theory. Remembering equation E4.13, the analogue of the first step in reflector velocity is half that of subsequent steps.

The timing of the motions of each end reflector was considered in Fig. 3.4 of chapter 3. For small velocities t_1 is approximately equal to $T_1 - t_1$, and this corresponds to the steps in trace 3 of Fig. 4.23 which are mid way between those of trace 2.

4.5 Going to the theoretical limit

If the mass of the reflectors in the experiment were reduced, then the control should be improved so that in the limit there would be no error (Also, no energy would be expended in moving a massless reflector and there would be no energy of the reflector to be dissipated by frictional damping). Then, in equation EA4.5 describing the closed loop transfer function for the reflector, when M , f and F are zero, the transfer function becomes unity if the gain in the feedback loop is unity. This means that the reflector would perfectly follow the motion indicated by the control signal.

When the mass tends to zero, the conditions approach those assumed in the theory of chapter 3 and the movement of the reflector may be determined by the radiation pressure (no additional enhancement

of the conditions by the controller amplifier now being required). Then, if the reflector is held by the binding force against the radiation pressure until an external force is applied, it moves the reflector until the increase in radiation pressure balances the external force. From chapter 3 it follows, to first order in v/c , that the increase in radiation pressure is proportional to the velocity (equation E3.23).

Thus:

$$\text{Increase in radiation pressure} = A \dot{x} \quad \text{E4.14}$$

where A is some constant.

If the external pressure applied is a step function of amplitude p :

$$p = M \ddot{x} + A \dot{x}$$

In Laplace:
$$\frac{p}{s} = M s^2 x(s) + A s x(s)$$

Solving for $x(s)$ and transforming back:

$$x(t) = \frac{p}{A} t - \frac{p M}{A^2} (1 - e^{-A/M t})$$

When $M \rightarrow 0$ this becomes:

$$x(t) = \frac{p}{A} t \quad \dot{x}(t) = \frac{p}{A} \quad \text{E4.15}$$

Hence, for zero mass, the velocity immediately changes to that value at which the radiation pressure balances the applied force.

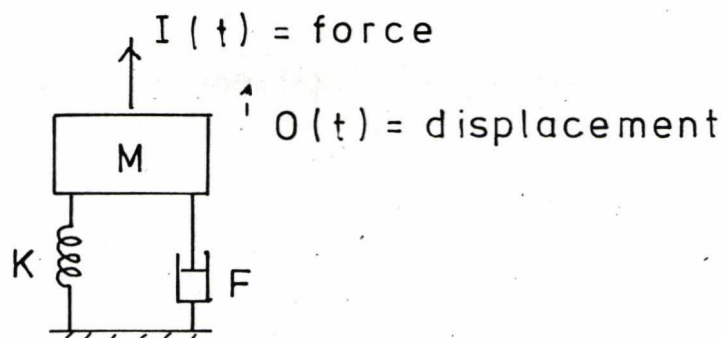
This is a velocity control whereas the previous controls have been of position.

4.6 Overall conclusion

It has been shown that it is possible with comparatively simple apparatus to control the position of reflectors to within a very small fraction of the wavelength of He-Ne laser light and X-band microwaves. However, the closed loop frequency responses of the resulting systems were not remarkably good.

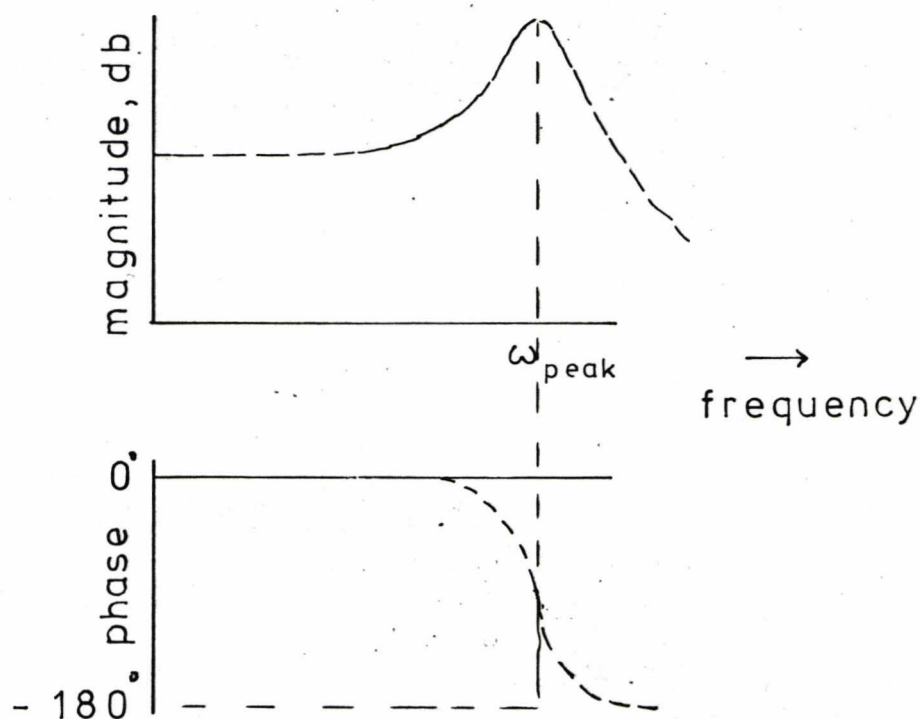
The experiments have demonstrated that a system with the properties of rigidity can be set up by trapped monochromatic waves whose standing wave nodes determine the positions of the confining boundaries, when stationary or when the whole system is moving. The trolley experiment demonstrated inertial-like properties of requiring a force to set the system in motion and of continuing in that motion when the force was removed. The experiments have demonstrated that servo controlled systems can effectively reduce the effect of the masses of the reflectors themselves and make them behave as if maintaining a condition determined by the low power waves reflected between them. The effect of the delay time for the waves to traverse the system was not demonstrated in the mechanical system but was demonstrated in an electrical analogue. The experiments have demonstrated the required principles (apart from the effects of the delay time in the mechanical system) and little more would be gained by a future extension of these experiments.

Another version of the trolley experiment was built, as a third year undergraduate project, at Exeter University in the Winter of 1978-79. The phase sensitive detector and power amplifier circuits were copied almost exactly. The trolleys were larger, driven by Meccano motors and had the complete control unit on each trolley with only the power supply from the laboratory fed to them by sliding contacts on rails. When this author visited them, one control unit was working but it appeared that this type of motor has too much backlash and the circuits had been removed from the trolleys and connected by flying leads.

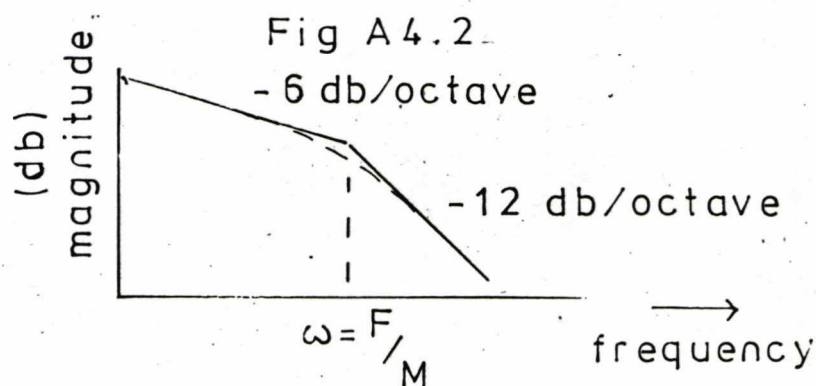


A simple damped resonant mechanical system.

Fig A4.1



Frequency response of the resonant system.



Amplitude response of the trolley, from the break frequency asymptotes.

Fig A4.3

Appendix to chapter 4

A4.1 The theory of damped resonant systems

The loudspeaker and Vibrator transducers may be represented as, basically, having inertial mass, M , a restoring force with constant of proportionality K force per unit displacement and a frictional force with constant of proportionality F force per unit velocity. These systems may be represented by the standard transfer function equation for the system of Fig. A4.1:

$$\frac{O(s)}{I(s)} = \frac{k}{Ms^2 + Fs + K} \quad \text{EA.1}$$

A system with this transfer function has a frequency and phase response as indicated in Fig. A4.2. The maximum amplitude at the peak of the resonance occurs at a frequency:

$$\omega_{\text{peak}} = \left[1 - \frac{F^2}{4MK} \right]^{1/2} \left[\frac{K}{M} \right]^{1/2} \approx \left[\frac{K}{M} \right]^{1/2} \quad \text{EA.2}$$

The peak has a 3 db. bandwidth given by:

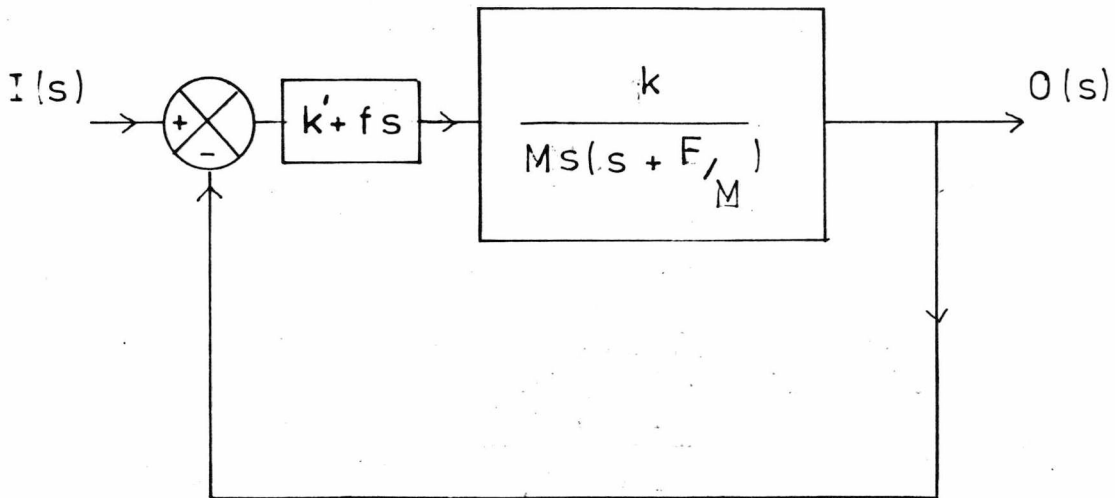
$$\Delta\omega \approx \frac{F}{M} \quad \text{EA.3}$$

In the case of the trolleys there is no restoring force and the transfer function for a trolley is:

$$\frac{O(s)}{I(s)} = \frac{k}{Ms(s + F/M)} \quad \text{EA.4}$$

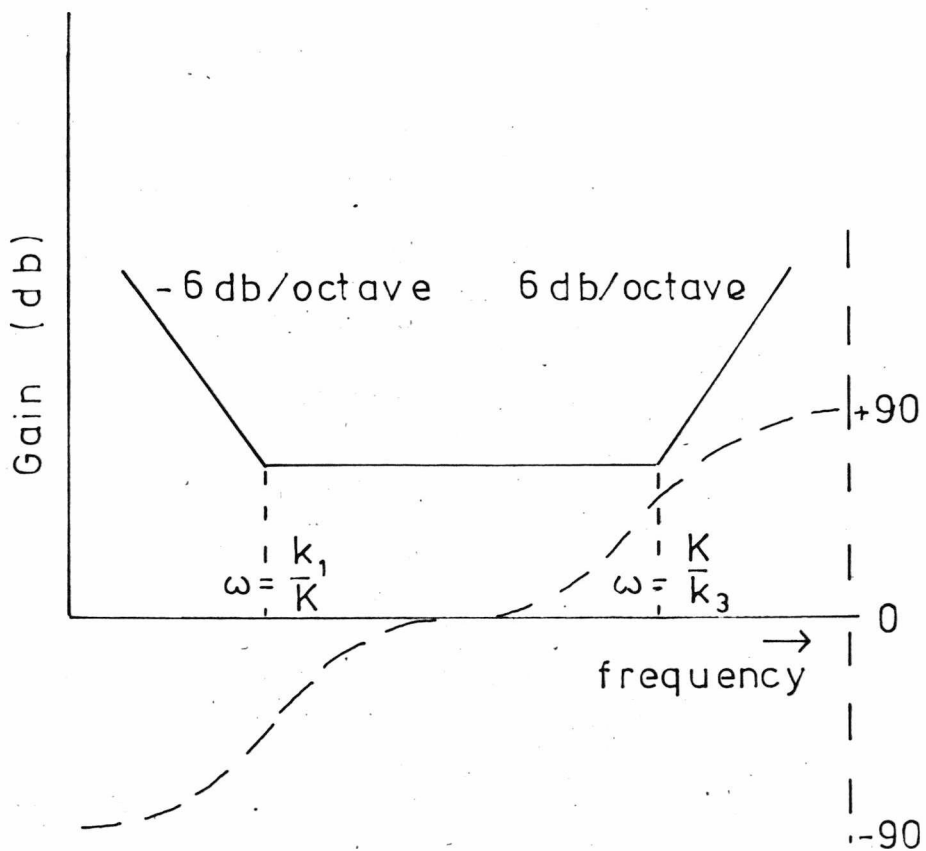
The frequency response of a system with this transfer function is indicated in Fig. A4.3.

It has been assumed, in representing the transducers by the above functions, that the force in the transducer is proportional to the



Direct and derivative signal control on the trolley gives a system like that of a damped resonant mechanical system.

Fig A 4.4



The frequency response in amplitude and phase of a three-term controller.

Fig A 4.5

current and that the devices are current driven. Because of back e.m.f. this will be only approximately correct.

Closed loop servo control.

In general the relation of the closed loop response to the open loop response is complicated. The closed loop response (with unity feedback) resulting from a known open loop response may be obtained by plotting the open loop response on a Hall chart (or Nichol's chart if the gain is in db.) and the grid of M lines (constant amplitude ratio) and N lines (constant phase shift) enable the gain and phase of the closed loop response to be plotted. However, if it is only required to know that the closed loop system will be stable, the Nyquist stability criterion on the open loop response may be used. In the straightforward case this means that the open loop gain should be less than one at the frequency when the phase lag has become 180° . The system of interferometer and three-term controller in the first experiment was analysed in this way.

The trolley system of the second experiment is sufficiently simple to be able to usefully analyse the closed loop transfer function as follows. If the system described by the equation EA4.4 is controlled in a loop with direct signal of proportion k' and derivative signal of proportion f , it is represented by Fig. A4.4. This has a closed loop transfer function:

$$\frac{O(s)}{I(s)} = \frac{k(k' + fs)}{Ms^2 + (F + fk)s + kk'}. \quad \text{EA4.5}$$

This is an equation of the same form as EA4.1. It indicates that derivative feedback is comparable with adding frictional force and position feedback is comparable with a constraining spring. The step

function response of such a system is critically damped when:

$$(F + fk)^2 = 4k'kM. \quad \text{EA4.6}$$

This is the condition which should be set up in the control loop for each trolley. As an f term was not used, the correct value of k' was fixed by the values of F and M .

A4.2 The three-term controller

The output of this control unit is the sum of adjustable amounts of direct, differentiated and integrated terms of the input signal. It has an overall transfer function:

$$\frac{O(s)}{I(s)} = A(k_1/s + k_2 + k_3s). \quad \text{EA 4.7}$$

This may be re-written:

$$\frac{K(1 + T_1s)(1 + T_2s)}{T_1s} = K\left(1 + \frac{T_2}{T_1}\right)\left(1 + \frac{T_1T_2}{T_1+T_2}s + \frac{1}{T_1+T_2}\left(\frac{1}{s}\right)\right) \quad \text{EA 4.8}$$

From which the frequency response amplitude asymptotes and phase may be plotted, as in Fig. A4.5. In this diagram:

$$K = \frac{1}{2} \left(k_2 + (k_2^2 - 4k_1k_3)^{1/2} \right). \quad \text{EA 4.9}$$

Hence the break frequencies are determined by k_1 and k_3 , and the mid-frequency gain by k_2 .

The purpose of the derivative term is to ensure that the open loop phase response, as the frequency is increased, never changes by 180° before the gain drops below unity. This term first tends to cancel the effects of time delays in the system and then increases the damping for high frequency signals.

The integrating term is needed to reduce steady state errors.

This may be thought of as giving infinite gain in infinite time. If the open loop transfer function has a pole at the origin (the integrator of the three-term controller), it may be represented as:

$$A(s) = \frac{N(s)}{s D(s)} \quad \text{EA 4.10}$$

Then applying the final value theorem to obtain the output, to a unit step function input to the closed loop system, after sufficient time:

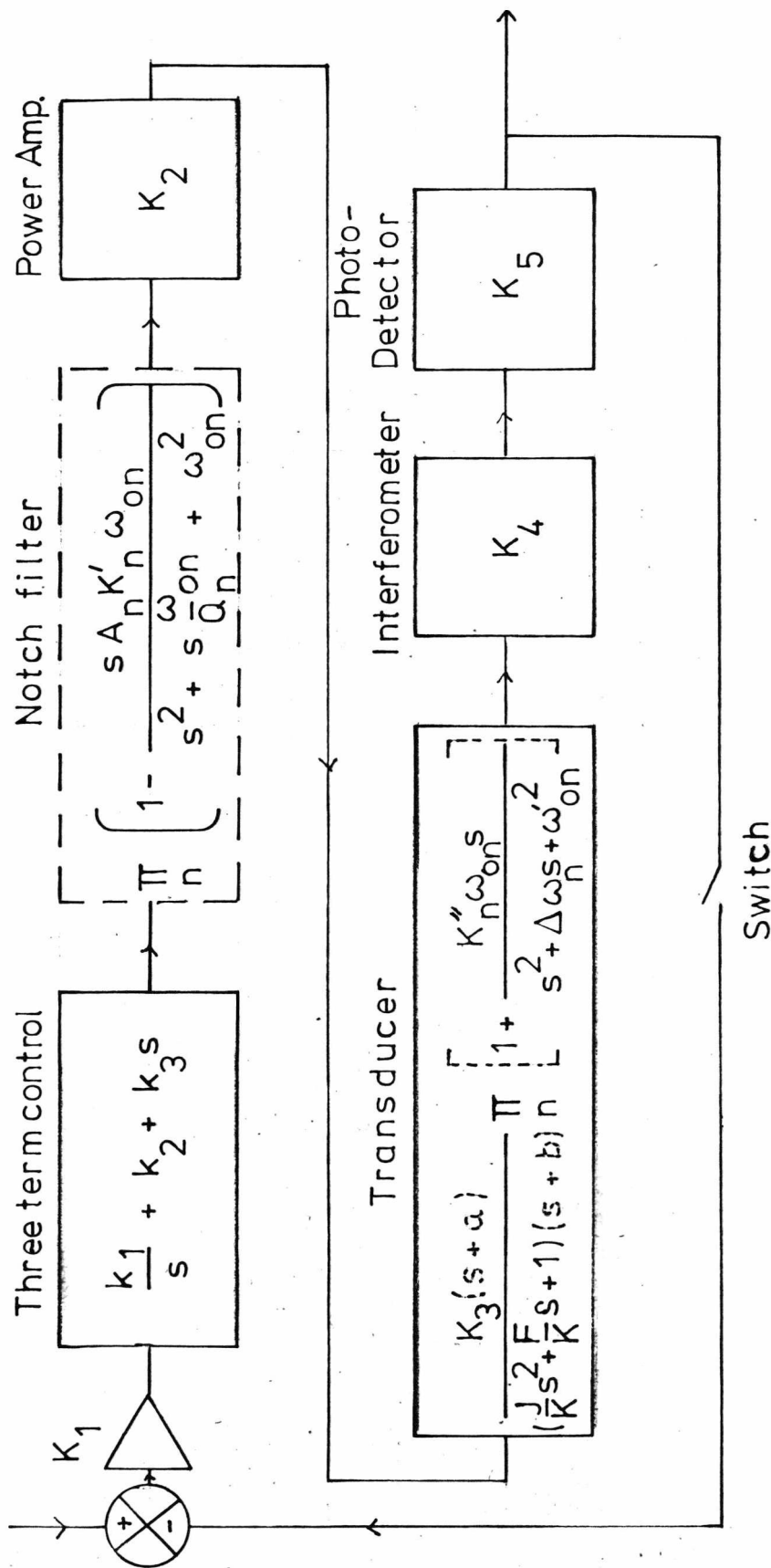
$$\lim_{s \rightarrow 0} s \left(\frac{1}{s} \frac{N(s)}{s D(s) + N(s)} \right) \rightarrow 1 \quad \text{EA 4.11}$$

This indicates that, after sufficient time, the output becomes equal to the input and the error becomes zero.

A4.3 Loudspeakers used as transducers

Initially the mirrors of the interferometer experiment were positioned by transducers made from loudspeakers. These transducers had mechanical resonances in the cones in the range 1-10 k.Hz. in addition to the main low frequency resonance. This section describes how two of these additional resonances were compensated for electronically to give a stable closed loop control. The final version of the experiment replaced these transducers with Vibrators.

As a unit of the control loop, the transfer function of the loudspeaker transducer is determined by the main natural resonance of its mass and the elasticity of the supporting cone, and a number of minor resonances in the cone itself. The subject of good loudspeakers (Beranek ⁽⁹⁾, 1954) will not be considered here. In general, the cone of a speaker will move as a whole up to about 500 Hz. Above some such frequency the cone vibrates in separate zones separated by nodal regions.



The control loop when using the loudspeaker transducer, showing in dotted line the functions not present for the Vibrator transducer.

Fig A4.6

The amplitude of vibration in the outer cone is relatively small and the effective mass of the vibrating cone is reduced. As the cone forms different nodal patterns at different frequencies, there are a number of resonances.

The complete control loop is described in Fig. A 4.6 which indicates in dashed lines those functions which occurred in the first experiment using the loudspeakers having additional resonances, but were not in the final experiment using the Vibrator transducers. The anti-resonances of the Notch filter compensate the two largest of the minor resonances in the loudspeaker transducer. The switch enabled the loop to be broken so that the open loop transfer function between the input to the comparator and the output from the photodetectors could be measured.

A 4.3(a) The theory of the electrical compensation for the cone resonances.

The two largest of the minor resonances in the cone gave peaks in the amplitude response and these were compensated by an electrical filter whose response dipped at those frequencies where the transducer response peaked. A bandpass-type resonance with asymptotic roll-off of ± 6 db/octave on either side of resonance has a transfer function:

$$G(s) = \frac{K s \omega_0}{s^2 + \Delta\omega s + \omega_0^2} \quad \text{EA 4.12}$$

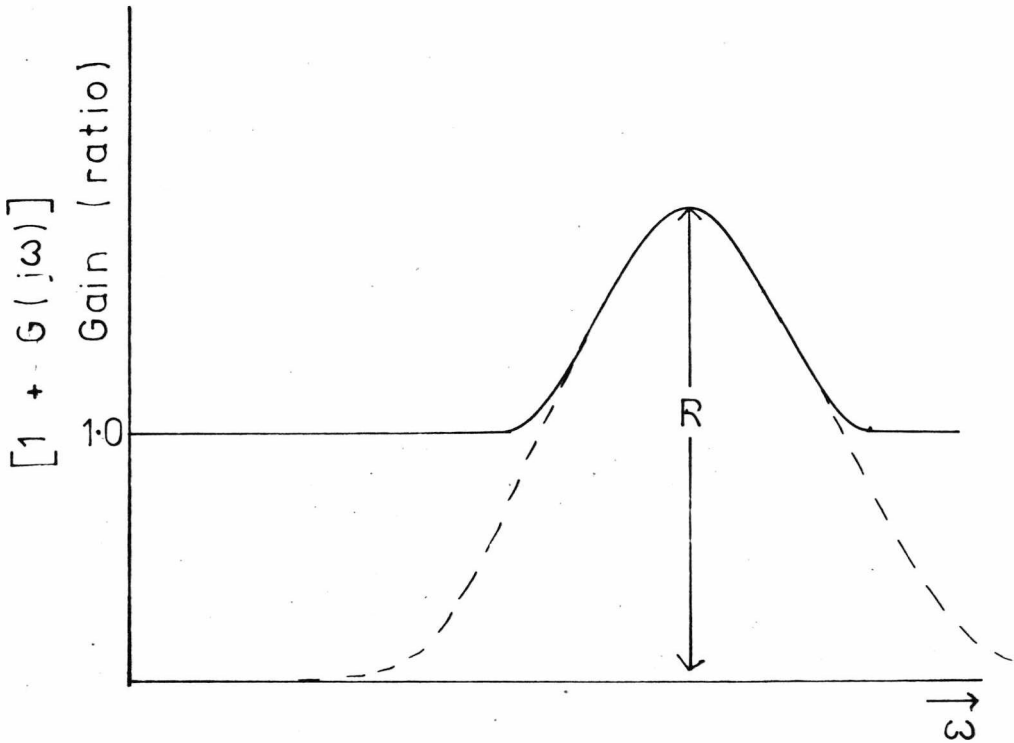
where

ω_0 is the undamped central resonant frequency

$\Delta\omega$ is the bandwidth of the resonance to the 3 db points

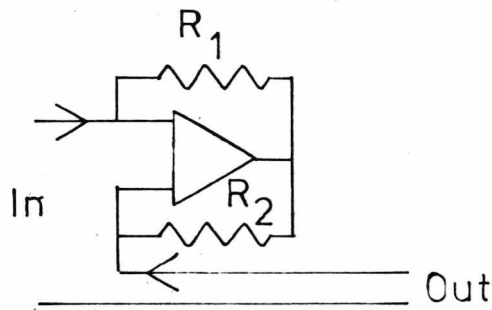
and

$$\frac{\omega_0}{\Delta\omega} = Q .$$



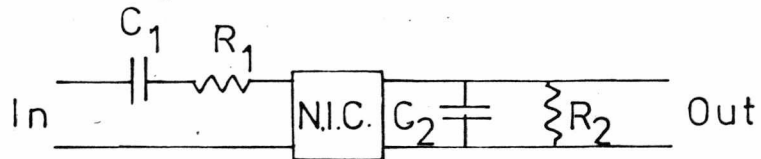
Showing how the minor resonance effects only a limited range of frequencies.

Fig A 4.7



The Negative Impedance Converter.

Fig A 4.8



A resonant circuit for the Notch filter.

Fig. A 4.9

For the loudspeaker transducer, each minor resonance was considered as an addition to the fundamental characteristic of the transducer. Thus the minor resonance mechanism was represented by a transfer function such that away from its resonance it has nearly unity amplitude. The total transfer function was represented as the product of the transfer function without the minor resonances (fundamental transfer function) and the transfer function for the minor resonance, giving:

$$\text{Total T.F.} = (1 + G(s)) (\text{fundamental T.F.}) .$$

The amplitude plot of $(1 + G(j\omega))$ is indicated in Fig. A 4.7. When $\omega = \omega_0$, the amplitude has increased to:

$$1 + G(j\omega_0) = 1 + KQ = R$$

and
$$K = \frac{\Delta\omega}{\omega_0} (R - 1) . \quad \text{EA 4.13}$$

The compensation was achieved by an electrical filter whose response dipped as the transducer resonance peaked:

$$\text{Filter T.F.} = (1 - G'(s))$$

If K, ω_0 and Q describe the mechanical resonance and K', ω'_0 and Q' describe the notch filter, then:

$$\text{Combined T.F.} = \left[\frac{s^2 + s(\frac{\omega'_0}{Q'} - K'\omega'_0) + \omega'^2_0}{s^2 + s\frac{\omega'_0}{Q'} + \omega'^2_0} \right] \left[\frac{s^2 + s(\frac{\omega_0}{Q} + K\omega_0) + \omega^2_0}{s^2 + s\frac{\omega_0}{Q} + \omega^2_0} \right] \quad \text{EA 4.14}$$

This combined function is unity if:

$$\left. \begin{aligned} \omega'_0 &= \omega_0 \\ K' &= K \\ \Delta\omega' &= \Delta\omega + K\omega_0 \end{aligned} \right\} \quad \text{EA 4.15}$$

As the uncompensated frequency response of the loudspeaker has minor resonances, each resonance determines a value of ω_0 (strictly $\omega_0(1 - \frac{1}{4}Q^2)^{\frac{1}{2}}$), $\Delta\omega$ and R . From equation EA 4.13 the value of K is determined. These parameters in turn determine the values of ω'_0 , $\Delta\omega'$ and K' in the electrical filter, according to equations EA 4.15. Therefore it should be possible to build a circuit with this form of transfer function and adjust its parameters to give the required compensation.

A 4.3(b) The loudspeaker transducer apparatus.

The $6\frac{1}{2}$ inch (Radiospares 163-TC) loudspeaker cones could be moved smoothly over a distance of about $\frac{1}{4}$ inch by varying the current. The experiment was operated successfully using these transducers although it was susceptible to vibrations in the air being picked up on the cone. If the elastic forces in the cone could have been increased, more energy would have been required to displace the transducer and the energy of ambient vibrations would have had less effect.

A double notch filter circuit was built to compensate the two largest minor resonances in the loudspeaker. The circuit employs Negative Impedance Converter circuits (Burr-Brown Co. ⁽¹⁶⁾, 1966) which gave sufficient stability and a good range of Q . The principle of the Negative Impedance circuit is that the input and output voltages are the same. There are two feedback paths (Fig. A 4.8) which balance to give currents in the ratio:

$$I_1 R_1 = I_2 R_2$$

It effectively reverses the direction of the current and has a gain of K , depending on the ratio of R_1 to R_2 . The circuit of Fig. A 4.9 has a transfer function:

Circuit diagram of the double notch filters, showing in dotted boxes the Negative Impedance Converter circuits which form part of each resonant circuit.

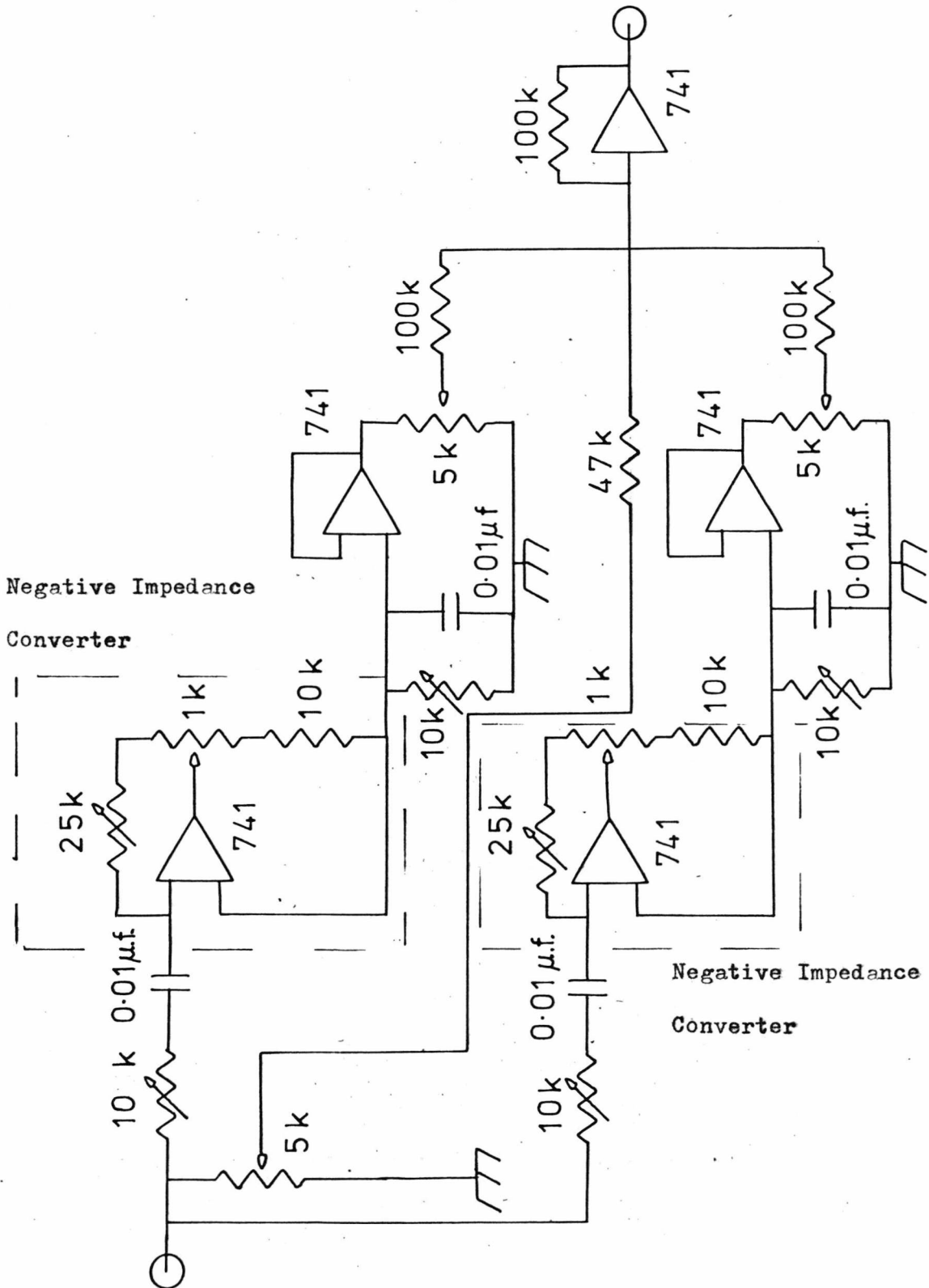


Fig. A4.10

$$T.F.(s) = \frac{-Ks \left[\frac{1}{C_2 R_1} \right]}{s^2 + s \left[\frac{1}{R_1 C_1} + \frac{1}{R_2 C_2} - \frac{K}{R_1 C_2} \right] + \frac{1}{R_1 C_1 R_2 C_2}} \quad \text{EA 4.16}$$

which is of the form of equation EA 4.12 (with inversion) if $R_1 = R_2$ and $C_1 = C_2$. This circuit has the advantage that Q may be changed without changing the resonant frequency.

The double notch filter circuit was built as in Fig. A 4.10. It generates a function $1 - G'(s)$ for each notch frequency by subtracting, at the output amplifier, the resonant signal of equation EA 4.16 from a steady fraction of the original signal. Each notch filter has two (10 k.) potentiometers to be set to the same value and give the required ω_0 . The 25 k. potentiometer sets the value of Q and the 5 k. potentiometer sets the nett gain.

A 4.3(c) Method of performing the experiment with loudspeakers.

Despite the ambient noise of mechanical vibrations disturbing the open loop system, it was possible to roughly measure the amplitude frequency response without using the correlator system that was employed in the main experiment. (except for low frequencies where the ambient vibrations were of too large an amplitude).

In practice, the open loop response of the loudspeaker was measured with the filter in circuit and the potentiometers of the notch filters adjusted until the amplitudes of the two largest minor resonances had been minimised. This could not be done perfectly but the two largest resonances were reduced to about 10% of the uncompensated amplitude and this improved the overall control operation of the system.

When the adjustments for the compensation for the two minor resonances had been made in the open loop system, the control loop was

closed and the terms of the three term controller were adjusted to reduce the error signal to a minimum when a test signal modulation was applied to the first mirror.

A 4.3(d) Results of the experiments with the loudspeakers.

The frequency response of the combined power amplifier and loudspeaker transducer (without any notch filter or controller) was measured up to 10 k.Hz. (this preliminary experiment was less accurate than the main experiment). The output signal was taken from the photodetector (only one of them being monitored for this measurement).

The results were:

100-600 Hz. was -15 db/octave (say, -18 db/octave)

600-2000 Hz. was -10 db/octave (say, -12 db/octave)

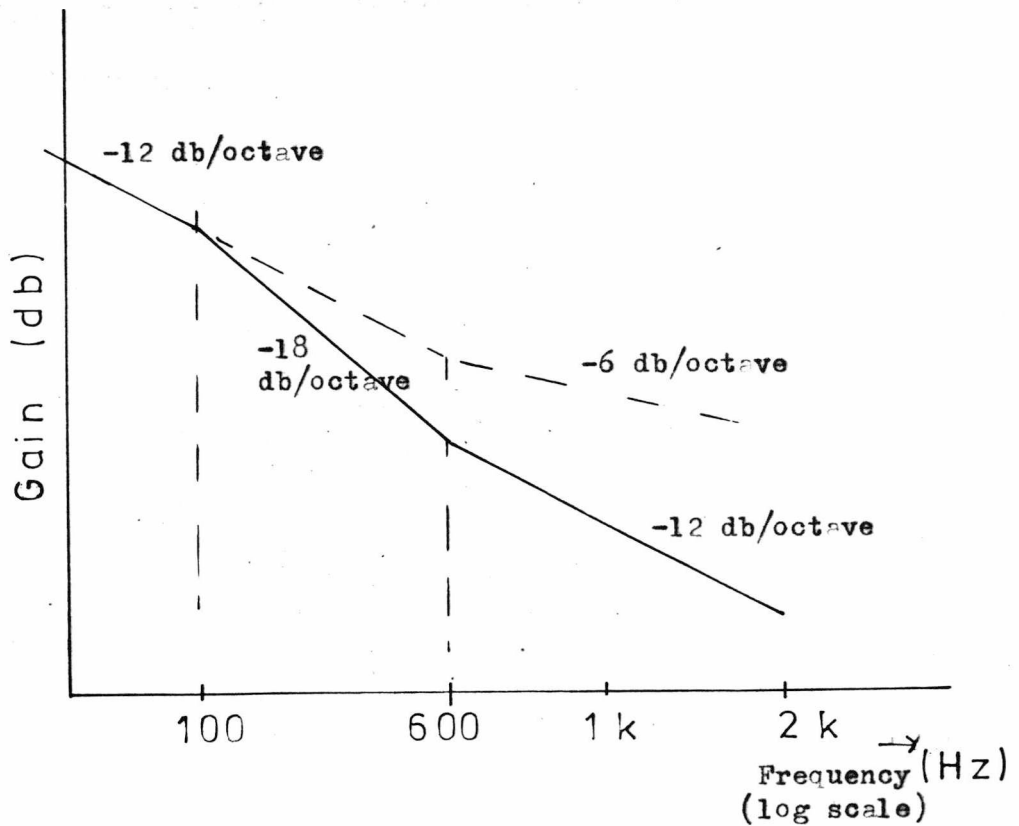
2-10 k.Hz. vague.

EA 4.17

The two largest minor resonances at 2.6 k.Hz. and 4.1 k.Hz.

When the notch filter circuit and three term controller were included in the circuit and adjusted as described above, the closed loop system operated correctly so that the second mirror automatically tracked the movement of the first mirror when the first mirror was perturbed by a test signal.

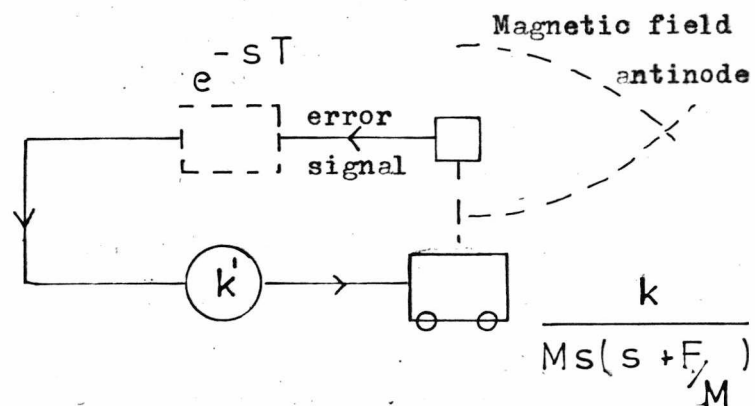
The closed loop was opened and the amplitude frequency response of the open loop, with the notch filters and three term controller (without the integrator term) operating in the same conditions as for the closed loop, was measured. The result indicated that the effect of the differential term of the three term controller was to give a slope of -10 db/octave from 150 Hz. upwards, adding about 10 db to the gain in the range above 500 Hz.



Break frequency asymptotes for the open loop amplitude response of the loudspeaker transducer. Full line- Without controller

Dashed line- With controller

Fig A 4.11



A simplified closed loop control of the trolley including an artificial electronic delay.

A 4.12

A 4.3(e) Conclusion to the experiment with the loudspeakers.

The notch filters compensated for the effects of the two worse minor resonances in the cone but this type of transducer was susceptible to vibrations in the air being picked up on the loudspeaker cone.

The improvement in stability caused by the differentiator term of the three term controller is now considered. Only the frequency range from 100 Hz. to 2 k.Hz. will be considered as the extra term only has an effect above about 100 Hz. In this limited frequency range the fundamental resonance of the loudspeaker may be approximated by a double pole near the origin. Then the results of the open loop (uncompensated) measurements indicated in Fig. A 4.11 (full line) suggest a transfer function of:

$$T. F. (s) = \frac{A (s + 3700)}{s^2 (s + 630)} \quad \text{EA 4.18}$$

Assuming from the experimental data a pole with break frequency at 100 Hz.

Now the Routh stability criterion (Langill⁽⁶²⁾, 1965) applies to the denominator polynomial of the closed loop transfer function and states that for stability there should be no alternations of signs of the Routh coefficients. For the open loop transfer function:

$$T. F. (s) = \frac{A (s + a)}{s^2 (s + b)} \quad , \quad \text{EA 4.19}$$

the closed loop Routh coefficients are:

$$1 \quad , \quad b \quad , \quad \frac{A(b - a)}{b} \quad , \quad aA$$

All these will only be positive if $b > a$. Applying this condition to equation EA 4.18 it gives an unstable closed loop and therefore the differential term of the three term controller is adding a zero to the

transfer function which tends to cancel the pole at about 100 Hz. in the function of equation EA 4.18 (shown in a dotted line in Fig. A 4.11). Then at some frequency above 600 Hz. there will be another break frequency giving a pole such that this $b' > a$. Within the large experimental errors, the zero of the controller at about 150 Hz. cancelled the pole assumed to be at about 100 Hz. of the Transducer (the above calculation indicates that, as there was stability, the zero must have occurred at a lower frequency than the pole).

A 4.4 Analysis of a delay in the control loop

Consideration was given to introducing an artificial delay which might give a stepping type of motion between the trolleys. If this delay is placed in the control loop as shown in Fig. A 4.12, then the transfer function of the delay for time T is:

$$e^{-sT}$$

Hence the transfer function when the loop is closed with controller fraction k' of the signal is:

Without the delay unit, from equation EA 4.5 (when $f = 0$):

$$\text{C.L.T.F.}(s) = \frac{kk'}{Ms^2 + Fs + kk'} \quad \text{EA 4.20}$$

With the delay unit, using EA 4.4 for the trolley:

$$\text{C.L.T.F.}(s) = \frac{kk'e^{-sT}}{Ms^2 + Fs + k'ke^{-sT}} \quad \text{EA 4.21}$$

However, the required function is a delay combined with the control of equation EA 4.20, which would be:

$$\text{C.L.T.F.}(s) = \frac{kk'e^{-sT}}{Ms^2 + Fs + kk'} \quad \text{EA 4.22}$$

As EA 4.21 cannot be put in the form EA 4.22, this is not a valid method of simulating the delay.

Chapter 5

SOME CONSEQUENCES OF THE EXTENDED STRUCTURE OF THE CAVITY5.1 Introduction

The cavity has been shown to have properties of inertial mass. This chapter discusses this in the context of the work of previous authors (described in section 2.4 of chapter 2) on the problem of the origin of inertial forces when a body is accelerated and the attempts which have been made to account for these forces in terms of induction from the total of the masses of the Universe. The main new idea in the system with inertial mass described in chapters 3 and 4 is that the cavity is not a point particle but is both extended between its end reflectors and has radiation propagating back and forth within it. Section 5.2 suggests that these properties account for a local mechanism for the formation of inertial forces in such a system.

Newton assumed an 'absolute' space with respect to which forces are caused by acceleration and rotation. In this context one might consider velocities as being between clearly defined objects (for example, the relative velocities of massive bodies) but acceleration as being 'absolute' (for example, the centrifugal acceleration arising from forces which give the sun an oblate shape). Attempts to rationalize this 'absolute' acceleration as being relative to something started with Berkeley and Mach. The controversy over Mach's hypothesis (described in section 2.4(b) of chapter 2) has been debated at increasing levels of detail, from Berkeley and Mach's initial linking, in some way, of inertial forces to acceleration with respect to the fixed stars, to attempts to obtain integral solutions of Einstein's equation. The following section points out the importance to this debate of analysing the structure of

the masses in which inertial forces are generated.

Part of the reason for this subject becoming controversial was that the problem, or terms used in the debate, were insufficiently clearly described. For example, Mach was unaware that gravitational potentials from distant stars have to be delayed potentials. Also, some theories have not included electromagnetism. Or again, when Sciama equates dynamic motions with relative kinematic motions of the Universe, he omits to include the process of accelerating (from, say, an inertial frame to one in rotation) the Cosmos which some examples of this require.

Section 5.2 considers first the component stages of the sequence to accelerate the cavity, as described in chapter 3, in the context of explaining inertial effects in terms of local interactions.

Chapter 3 has considered in detail the actions at the end reflectors of the cavity while assuming the wave propagation between the reflectors does little other than act as a delay line. The second part of section 5.2 makes some comments on what may happen to the rays as they pass between the reflectors (of the double noded cavity) due to gravitational and inertial-type fields. These comments are based on the key equation (in the version obtained by Einstein, it is equation E2.5 of chapter 2) which has been derived by several authors in different versions of the same form and in particular by Davidson (equation E2.17 of chapter 2), in terms of the metric potentials of General Relativity, for the integral effect of a number of masses moving past a test particle (this problem is basic to the Machian question of the effect of all masses in the Universe on a test particle). Section 5.2 suggests how the forces generated according to this equation may be physically formed as the radiation moves along ray paths within the cavity. Thus the inertial forces in the cavity derive from changes in the amplitude (or, equivalently, the frequency) of the wave as observed at each end of the cavity.

Appendix A 5.1 gives an (approximate) quantitative analysis (for the case of a double-noded cavity) of these effects of the metric field on the rays in the cavity when it is held stationary in the frame in which the Sciama field is evaluated.

5.2 A new aspect on the Machian controversy

It is to be expected that not only the cavity but also atomic particles have some extension. The work of Born and authors following him (described in section 2.3 of chapter 2) had in mind the extension of the electron particle and they derive a system, like that of the cavity, which has the physically maximum possible rigidity. When an extended system is pushed by a force acting on a limited part of it then the maximum rate at which this effect can be communicated to the rest of the body is at the speed of light. The accelerating of the cavity by a force acting on the reflector, for example, is a compound process involving the transmission of effects by the internal radiation.

One may distinguish two stages in the sequence of operations for accelerating the mechanism described in chapter 3. The initial movement of the first reflector of the cavity on which the force is applied is not that of a massive entity but is governed entirely by equations for the movements of radiation. The second stage is the delayed 'locking' into the next inertial condition to generate the next step of velocity (c.f. Fig. 3.3 of chapter 3). This is a local operation resulting in a nett acceleration. Further, equation E3.31 of chapter 3 describes what is happening during the time of the first of these stages. This equation, in terms of $F T_1$, which has the dimensions of momentum, is:

$$F T_1 = \left[\frac{E_T}{C^2} \left[1 - \frac{v_2^2}{C^2} \right]^{-1/2} \right] v_2 \quad E5.1$$

This equation has the same form as that (rearranged) of Sciama (c.f. equation E2.9 of chapter 2) for the inertial force generated by moving in the vector potential field and giving an inductive effect. This equation is:

$$\partial_t \underline{F}_{\text{inertial}} = \left[- \frac{m \phi}{c^2} \right] \partial \underline{v} \quad \text{E5.2}$$

These equations show how a similar resultant effect is obtained from essentially different approaches. Equation E5.1 describes an electromagnetic mechanism resulting from the forces from fields trapped locally within the cavity. Equation E5.2 describes a mechanism resulting from the forces due to a field extending from all distant matter to the test particle. An extension to having these two different approaches may be obtained by considering that the inertial forces are generated locally inside the cavity when it is pushed and the rays crossing the space inside the cavity depend upon the local null geodesics of this space. Hence one may summarize the sequence of physical interactions:

1. Matter and the initial and boundary conditions set up the geometry of space;
2. The metric determines the null geodesics throughout the Universe;
3. The cavity is a mechanism for detecting the local null geodesics;
4. The waves internal to the cavity create additional force on the end as its velocity is increased;
5. To accelerate such a cavity, an external force has to balance the internally generated, inertial, reactive, force.

The rest of this section will consider how the (local) movement of the rays in the extended cavity, observed in the rest frame of the cavity (or one end of it), may be accounted for in terms of an inertial-gravitational field and give rise to gravitational and inertial forces (which for the particular case of rotation, are centrifugal and

Coriolis forces) acting in the cavity.

Theories of the origin of inertial forces, up to and including Sciama's ⁽⁸²⁾, 1953, initial theory, do not specify what happens in their account of inertial forces on ray paths. However, Davidson ⁽²⁰⁾, 1957, equates the components of the inertial field with components of the space-time metric (from which the effect on ray paths may be derived) and McCrea ⁽⁶⁸⁾, 1971, has suggested that inertial forces generated in a rotating mass are derived from a detection of the local null geodesics. It is then of only secondary importance that the rays by which the far Universe is observed reach the mass along these same null geodesics.

The Maxwell-type ponderomotive equation of the scalar-vector field investigated in the work of authors described in section 2.4(a) of chapter 2, for each component (c.f. Equation E2.16 of chapter 2) is:

$$\text{Acceleration of free particle} = \frac{dv_i}{dt} = \underbrace{-\frac{\partial \phi}{\partial x^i}}_{\text{Centrifugal term}} - \underbrace{\frac{\partial A_i}{c \partial t}}_{\substack{\text{Linear motion} \\ \text{acceleration term}}} - \underbrace{\frac{v^k}{c} \left(\frac{\partial A_i}{\partial x^k} - \frac{\partial A_k}{\partial x^i} \right)}_{\substack{\text{Coriolis} \\ \text{term}} - \text{circular motion}} \quad \text{E5.3}$$

$i, k = 1, 2, 3$

where ϕ and \underline{A} are the scalar and vector potentials formed by integrating the delayed effect of all the mass sources and the products of the sources with their velocities. v^k is the velocity of the mass in which the forces described by this equation are being generated, with respect to the frame in which the scalar-vector field potentials have been evaluated.

In this equation, the first term on the right hand side, being the gradient of the scalar component of the potential field, is compounded from two physical effects. Heavy local masses generating a permanent gravitational field give a gradient to the scalar potential. Secondly,

if the frame in which the (\underline{A}, ϕ) field has been determined is such that different parts of it are moving at different velocities, with respect to the frame in which the average of the distant masses is stationary, at the time of evaluating the potential from the integral, then there is a gradient of the ϕ field due to this inertial term. (This results from the velocity for the transformation of the components of the four vector (as in the inertial frame) being different at different positions, as expounded by Sciama⁽⁸²⁾, 1953). An important example of this is the case of rotating co-ordinates, when this term accounts for centrifugal acceleration.

The second term on the right hand side is a function of \underline{A} which by definition is itself a function of the apparent velocity of the distant masses. If the frame in which the \underline{A}, ϕ field is evaluated is such that the whole frame has a (uniform) acceleration with respect to the distant masses, then the apparent velocity of the distant masses is varying and this term contributes an inductive effect (for example, generating the inertial force when a mass is given a linear acceleration). Notice that in the case of rotation, because of the symmetry of the Universe about the rotating observer, there is no variation with time of the \underline{A} field.

The third term is a type of addition of the effects of one movement onto another movement. It involves a velocity \underline{v} within the frame which is already moving in a non-inertial fashion. Under conditions similar to those for the spatial derivative of the scalar field, ϕ , as described above for the first term, the spatial derivative of the vector field, \underline{A} , (in the form of its curl) may be non-zero when the velocities of the distant Universe, seen from different positions in the frame being considered, vary with position such that there is a rotation term of this field. For the case of rotation, $\text{curl } \underline{A}$ is a vector parallel to

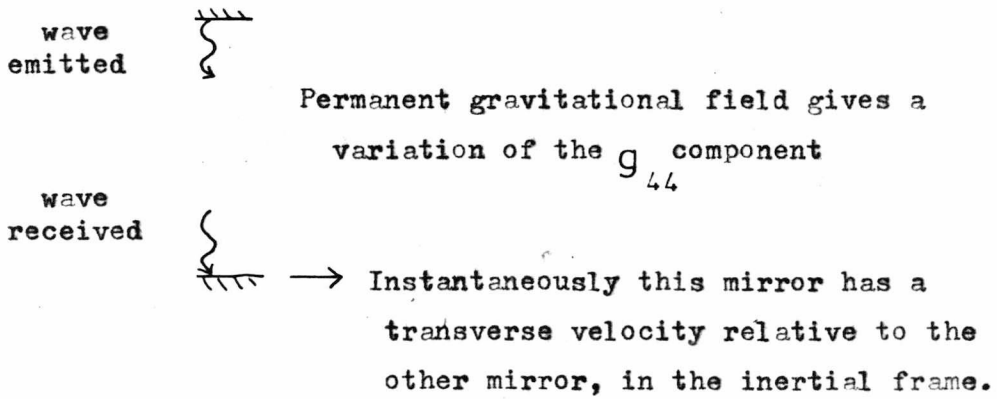
the axis of rotation. This term then gives the Coriolis acceleration which is perpendicular to the curl \tilde{A} vector and the velocity \tilde{v} . Sciama⁽⁸²⁾, 1953, attributes the curving of light ray paths in a rotating frame to this term.

Equation E5.3 has been written (approximately) by Davidson⁽²⁰⁾, 1957, with $\frac{c^2}{2}g_{44}$ in place of the scalar ϕ and $-c^2g_{4i}$ in place of the vector \tilde{A} , where g_{44} and g_{4i} are the components of the total metric tensor in the frame in which the previous \tilde{A}, ϕ field was evaluated. For example (from Atwater⁽³⁾, 1974.) the components of the metric in a frame with acceleration Q with respect to the distant Universe (there being no local gravitating masses) are (approximately, for small $\frac{at}{c}$)

$$\begin{aligned} A_1 &\equiv -c^2g_{41} = act && \text{assumed to be:} \\ A_2 &\equiv -c^2g_{42} = 0 \\ A_3 &\equiv -c^2g_{43} = 0 \\ \phi &\equiv \frac{c^2}{2}g_{44} = \frac{1}{2} \left[c^2 - a^2t^2 \right] \end{aligned} \tag{E5.4}$$

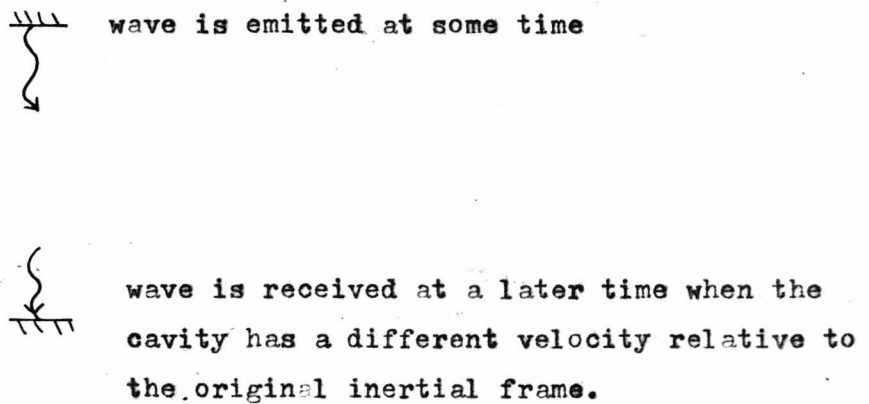
and if these values are inserted in equation E5.3, there is an acceleration, of a free particle in this frame, of Q (as is to be expected). This is an example of conditions of small variation from the Lorentz metric. The metric in the frame of the cavity, which is in general linearly accelerating and rotating in the inertial frame, has small fractional variations of its main diagonal elements and may have large fractional changes of its off-diagonal elements.

An indication of how this metric guides the rays crossing from one end of the cavity to the other, in the frame of the cavity with both ends of the cavity stationary in this frame, will now be given. The g_{44} term (which has been related to ϕ and hence the first term in equation E5.3 for the motion of particles) changing along the path of



Instantaneous movement of the cavity in the inertial frame, showing the change of frequency due to the permanent gravitational field and to the rotation giving different velocities to the two ends (measured in the inertial frame).

Fig 5.1(a)



Rays in an accelerating frame of reference.

Fig 5.1(b)



Rays in a rotating co-ordinate frame.

Fig 5.1(c)

the ray as it crosses the cavity, gives an apparent change of frequency as received by the second end. This change may be caused, for example, by its moving to a different potential in a permanent gravitational field and/or by the observer having an instantaneous transverse velocity to the emitter, in the inertial frame, whose clock runs at a different rate (e.g. in rotation). Both these physical operations are represented by the same term in the effect on the ray as seen in the frame in which \tilde{A}, ϕ is evaluated (Indeed, in free orbit motion about a massive body these two effects cancel in the frame of the cavity). For the reflector mechanism described in chapter 3, this change of frequency (and amplitude) gives an extra force which is balanced by an external holding force to keep the cavity in this frame. Fig. 5.1(a) attempts to represent this; although, as explained above, the two effects are indistinguishable in the frame of the cavity. Appendix A 5.1 gives an analysis of the force generated in the cavity by this term, thus linking both the permanent gravitational field force and the inertial centrifugal force (in the case of rotation) in the cavity held in this frame, to this mechanism as the ray crosses the cavity. It accounts for the first term in the right hand side of equation E5.3 and gives a physical justification for Davidson's relating ϕ to the g_{44} term of the metric.

The effect of the time variation of g_{4i} (which has been related to \tilde{A} and hence, for the time derivative, to the second term in equation E5.3 for the motion of particles) is to give a (type of Doppler) shift in the wavelength. As in the case above, there is a change between the frequency at the emitter and receiver but in this case it is due to a change of the metric (over the whole frame perhaps) in the time taken for the ray to cross the cavity. With respect to the distant Universe there is a change in velocity, in the direction of the ray, in the time taken for the ray to cross, due to the acceleration. The magnitude of the shift depends on the product of the rate of change and the time for

the ray to cross the cavity. The frequency shift is in the opposite sense for a ray travelling in the opposite direction. Fig. 5.1(b) represents this effect of the time variation of g_{4i} and the analysis of appendix A 5.1, for the effect of a frequency shift on the balance of forces at the second reflector of the cavity, applies here as well as to the previous section. This accounts for the second term in the right hand side of equation E5.3 and shows how the g_{4i} component of the metric may be linked by a physical process to the inertial force when the cavity is linearly accelerated.

A curved path of motion of the frame of the cavity with respect to the inertial frame, gives metric components g_{4i} which vary with position and may have a non-zero curl function for the field. For example, the approximate metric for rotating co-ordinates quoted by Davidson⁽²⁰⁾, 1957, has:

$$g_{4i} = -\frac{\omega}{c} y, \frac{\omega}{c} x, 0 \quad . \quad \text{E5.5}$$

For a frame moving with a further velocity \underline{v} in this field there is a change of metric with time because the velocity carries the new frame to different positions on the original frame. This variation with time gives an effect analogous to that considered for the time variation of g_{4i} above. Hence there is an additional frequency shift as the rays cross the cavity (the length of the cavity being orthogonal to the velocity \underline{v}). Furthermore, although there is some debate as to what is the exact metric in a rotating frame, it has been shown (for example, by Ashworth and Jennison⁽²⁾, 1976) that the ray paths become curved in opposite directions for rays travelling in opposite directions, as shown in Fig. 5.1(c).

A 5.1 The forces generated in the cavity because of a difference in metric potentials at the two ends

If the metric is not changing with time and a ray of frequency ν_1 at a position of metric potential g_{44} moves to a position of metric potential g'_{44} , the frequency ν_2 observed at the second position will be given by (Atwater⁽³⁾, 1974):

$$\frac{\nu_2}{\nu_1} = \left[\frac{g_{44}}{g'_{44}} \right]^{1/2} \quad \text{EA 5.1}$$

If the metric is changing with time (a description of the effect of the $\partial g_{4i}/\partial x^4$ term requires this) the calculation is not so direct and the method, using a number of mathematical techniques, is described by Synge⁽⁹²⁾, 1960. It is not in general possible to give a direct explicit equation for the ratio of frequencies in terms of the change of metric in the time for the ray to cross the cavity because an integration of the effect on the ray, following a null geodesic path, has to be performed. The details will not be given here, as mathematical rather than physical principles are used, but an indication of what is involved in Synge's method is as follows. He considers a ray moving from the emitter to receiver (here, the ends of the cavity have no spatial coordinate velocity) and obtains an expression for the frequency shift in terms of the four-velocity difference between the emitter when the ray leaves and the receiver when the ray arrives. Being a four-vector it includes the effects of both the spatial and time components. To evaluate this change in four-velocity it is necessary to integrate the equation describing the parallel transport of the velocity four-vector along the path of the ray. This equation describing the parallel transport is in terms of the metric field.

Consider the double noded cavity being held in this frame in which the metric has been evaluated and held by its second mirror (m_2). The radiation from the first mirror (m_1) will reach m_2 and appear with a frequency shift given by one of the methods above. Because m_2 does not move, the ray will return to reach m_1 with the original frequency. Although there is no actual movement, the first mirror appears at m_2 (because of the frequency shift) to be moving with velocity ΔV given by equation E3.2:

$$\frac{v_2}{v_1} = \left[\frac{1 + \frac{\Delta V}{c}}{1 - \frac{\Delta V}{c}} \right]^{1/2} \equiv \psi \text{ (say)}$$

$$\frac{\Delta V}{c} = \frac{\psi^2 - 1}{\psi^2 + 1} \quad \text{EA 5.2}$$

The force required to hold this end of the cavity against the increase in radiation pressure is now calculated as if ΔV of additional velocity were being given to this end of the cavity. Thus from equation E3.29 of chapter 3:

$$\begin{aligned} \Delta F &= \frac{\frac{\Delta V}{c}}{1 - \frac{\Delta V}{c}} \frac{E_T}{L} \\ &= \frac{1}{2} \left[\left[\frac{v_2}{v_1} \right]^2 - 1 \right] \frac{E_T}{L} \end{aligned} \quad \text{EA 5.3}$$

where L is the (approximate) distance between the ends of the cavity.

An example of the application of this equation is when the cavity is held stationary in the frame of a massive body. The length of the cavity is held vertically in the field so that the potentials at its ends may be written in terms of the standard expression for the Schwartzchild solution about a single mass M (ref. Atwater⁽³⁾, 1974):

$$\frac{g_{44}}{g'_{44}} = \frac{1 - \frac{2MG}{c^2 r_1}}{1 - \frac{2MG}{c^2 r_2}}$$

EA 5.4

where g_{44} is the potential at radial position r_1 and g'_{44} is the potential at radial position r_2 . G is the gravitational constant. From equation EA 5.1, when equation EA 5.4 is inserted in expression EA 5.3 it gives (approximately for $r_1 - r_2 = L \ll r_1$) a force:

$$\Delta F \approx \frac{\frac{2MG}{c^2} \left[\frac{1}{r_2} - \frac{1}{r_1} \right]}{1 - \frac{2MG}{c^2 r_2}} \frac{E_T}{2L}$$

$$\approx \frac{MG}{r^2} \left[\frac{E_T}{c^2} \right],$$

EA 5.5

or Force = (gravitational acceleration) x Mass.

This result is comparable with that obtained by Jennison⁽⁴⁹⁾, 1979, for the single noded system.

A second example is that of the inertial force generated when the cavity has the metric of E5.4, which is changing with time. For this particularly simple (approximate) metric, the equations for the parallel transport of the velocity vector along the path of the ray (i.e. in the direction of the x^1 -axis) are:

$$\frac{dV^1}{d\mu} + a D V^4 = 0 \quad \frac{dV^2}{d\mu} = \frac{dV^3}{d\mu} = \frac{dV^4}{d\mu} = 0$$

EA 5.6

where D is the constant of integrating the fourth equation. Having obtained the equations for the null geodesic of the ray moving in the direction of the x^1 axis, one may obtain the change in the four-velocity in time T on transporting it along this geodesic:

$$\Delta V^1 = -a T$$

EA 5.7

Using Synge's equation and the property of the ray that Energy = $c \times$ Momentum, the fractional change in frequency is:

$$\frac{\Delta \nu}{\nu_1} = \frac{a T}{c}$$

or
$$\left[\frac{\nu_2}{\nu_1} \right]^2 - 1 \approx \frac{2aT}{c} \quad \text{EA 5.8}$$

Substituting in equation EA 5.3 and using $T \approx \frac{L}{c}$ gives:

$$\Delta F \approx \left[\frac{E_T}{c^2} \right] a \quad \text{EA 5.9}$$

or Inertial force = Mass \times a .

where a is the linear acceleration of the cavity with respect to the inertial frame.

Chapter 6

A PRELIMINARY EXPERIMENT ON THE REFRACTION BY AN ELECTROSTATIC
FIELD OF R.F. AT A FREQUENCY SUGGESTED BY THE SIZE OF
BALL LIGHTNING

Part I - DESCRIPTION OF THE APPARATUS6.1 Introduction

The experiments of chapter 4 and the theory of chapter 3 have shown that electromagnetic waves trapped under certain conditions give rise to properties of rigidity and inertial mass. As usually understood, waves have to be reflected off a conducting material or, possibly, be internally reflected in a refracting medium. It would be of interest, however, to find a system of trapped electromagnetic waves which involved a mechanism that did not already have massive reflectors, but moved so that the radiation pressure on the reflectors was constant (so that a fixed number of half-wave standing waves was maintained between them). The balancing of the radiation pressure caused by the waves on reflection requires a definite binding force and this would have to be obtained in some way. A possible example of a system of this type is the phenomenon of Ball lightning. Although this has the disadvantage that its rarity makes it effectively inaccessible to direct experiment, it may represent a case of electromagnetic waves trapped without any additional material agent.

The relevance of Ball lightning to the considerations made in the first part of this thesis has already been partly explained in section 1.4 of chapter 1 and is further discussed in chapter 7. The main reasons for

doing this experiment in an attempt to detect an effect which would account for the phenomenon of Ball lightning (described in section 2.6 of chapter 2) are as follows. Jennison ⁽⁴⁶⁾, 1973, has suggested that Ball lightning is an entirely electromagnetic structure which is stabilized in a closed system independently of the air. The size of the ball could be determined by the wavelength of the waves trapped within it (similar to the length between the reflectors in the experiment of chapter 4) but there would have to be some property of space (in the presence of an electrostatic field) which caused the waves of this wavelength to be trapped. The following experiment assumes that this property causes some refraction of the waves even at low energy densities. The emission of visible light is discussed in chapter 7.

The assumption of self-trapping by the fields to account for Ball lightning is quite radical but no previous explanation (some of which are indicated in section 2.6) has been fully acceptable. The essence of the mechanism suggested here is that it occurs for waves at a very specific frequency in an electrostatic field. It is the properties of the electromagnetic waves at this frequency which are being investigated in the following experiment.

The spatial extension of the lightning ball shows how a binding mechanism must be present about its circumference. Despite its size, the stepped movement of the ball (following the analysis of chapter 3) would be in such small steps as not to be apparent to the observers in the reports that have been made of Ball lightning events.

To account for the stability of Ball lightning (according to a number of reports, of 1-5 sec. duration (ref. Singer ⁽⁸⁹⁾, 1971)) and its average size, it is assumed that there is some mechanism operating around the enclosed energy. Without advocating a precise system, the energy may be stored in an electromagnetic standing wave across the ball (c.f. Golde ⁽³⁴⁾, 1977, p.422). The suggestion is made here that the,

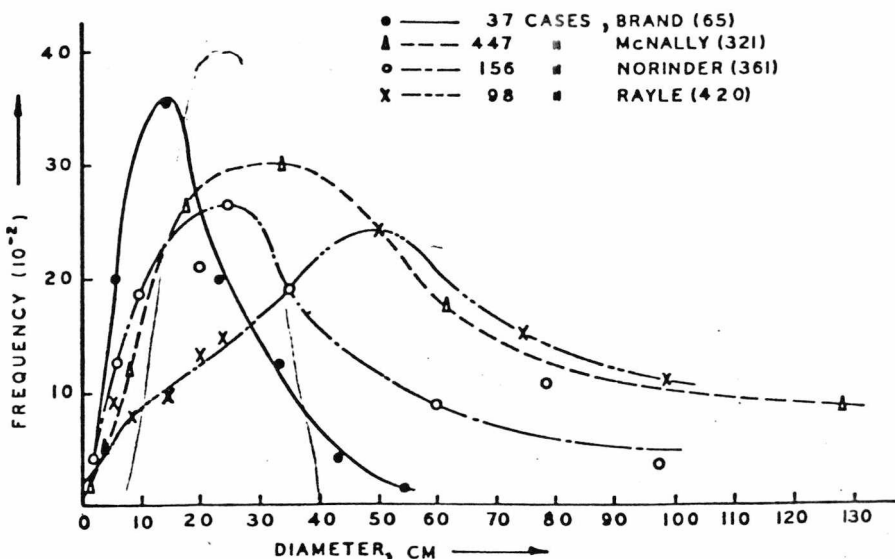
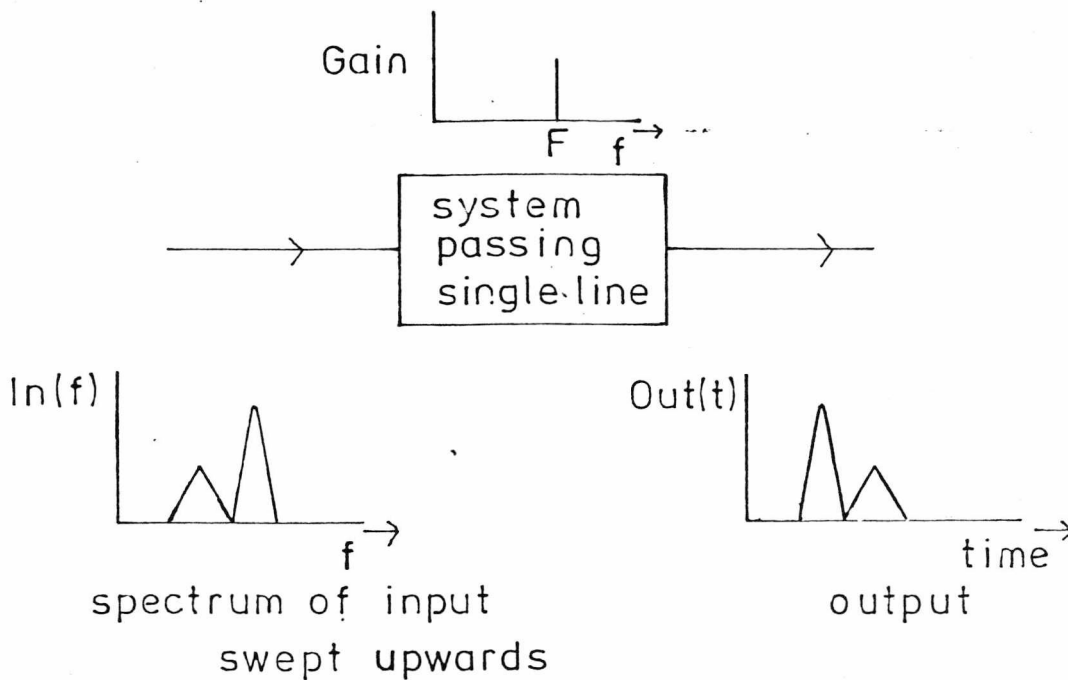


Fig. 19. Distribution of ball lightning diameters.

p.66 of "The Nature of Ball Lightning"
by S. Singer (Plenum 1971).

The results of surveys of Ball lightning diameters.

Fig 6.1



The result of convolving the system response with the spectrum of the input signal.

Fig 6.2

otherwise untrapped, waves are caught in some form of resonance which occurs in a strong electrostatic field (thunderstorm fields are described in section 2.6). Thus at a specific frequency the vacuum itself becomes resonant to electromagnetic waves under certain conditions of electrostatic field. Although such a suggestion is quite radical, it has a parallel at much higher frequencies in the formation of electron-positron pairs in the presence of an atom's electrostatic field.

The frequency at which the interaction between electromagnetic and electrostatic fields occurs is unknown and so a scan had to be made over the likely range of frequencies. The result of analysing collections of reports by four different investigators of the size of the sphere of the lightning ball is presented in Fig.6.1 from Singer⁽⁸⁹⁾, 1971. This suggests that Ball lightning, most probably, has a diameter of 15-33 cm. If this is formed by a half-wave standing wave, the indication is that the phenomenon occurs at a frequency in the range 1000-450 M.Hz. (assuming the refractive index is approximately unity).

The following experiment does not attempt to replicate the energies and energy densities occurring during a thunderstorm, but to look for the beginnings of a refractive effect which under more extreme conditions would become a full resonance. The electrostatic field was arranged to cover a volume of dimensions comparable with the size of Ball lightning, and of strength greater than about 300 k.V./m.

A major limiting factor in the result is that the convolution of the frequency spectrum of the r.f. signal used, with the frequency spectrum of the effect being looked for, gives a very narrow response line and only a very approximate estimate can be made of its frequency. The scan is likely to pass through the spectral line in a small fraction of a second.

Some of the main results of a number of previous experiments by other authors which have some relevance to the investigation for non-

linear electromagnetic fields are described in section 2.8 of chapter 2. They may be compared with the experiment of chapter 6, however, the experiment of chapter 6 differs in that it is investigating a possible resonance within a range of frequencies.

Part I of this chapter describes the instrumentation used for constructing a system that would be sensitive to only effects caused by a strong electrostatic field (using a system of alternating rapidly between the interferometer under test and a reference interferometer with no electrostatic field), frequency stepping in small steps to pick out the narrow resonance band being looked for, and correlating. Each part of the wideband (half octave) equipment is described under separate headings which include the interferometer, Van de Graaff electrostatic field generator, Perspex shutter for calibration, radio frequency circuits to generate the signal and switch it between interferometers, audio frequency circuits to correlate the detected signal with the switching and stepping control signals, and method of field estimation.

Part II first describes a run on the equipment using a simulation of the effect being looked for. It gives a description of the results of calibrating the equipment at each run using the oscillating Perspex shutter. The method of performing the experiment is described and the results for each run are given in section 6.19.

The experiment described in this chapter transmitted electromagnetic waves with wavelength varied over the range 30 to 70 cm. (half wavelength 5.9 to 13 inch) through an electrostatic field (of the order 10 k.V./cm.) and looked for an effect with a frequency band small compared with the bandwidth of the generator. The sensitivity of the instrumentation was improved by comparing the signals from the interferometer with those from a duplicate interferometer with no electrostatic field, and using correlation and small (0.2 to 4.5 M.Hz. in 500 to 900 M.Hz.) stepping

frequency techniques. The experiment was performed over three half octave bands of 450-600, 550-800 and 600-960 M.Hz. and these sweeps of frequency necessitated wideband apparatus. The frequency was scanned at about 5 k.Hz./sec. which, for the time constants of the instruments, would have allowed the detection of a resonance of the order of 0.4 k.Hz. bandwidth.

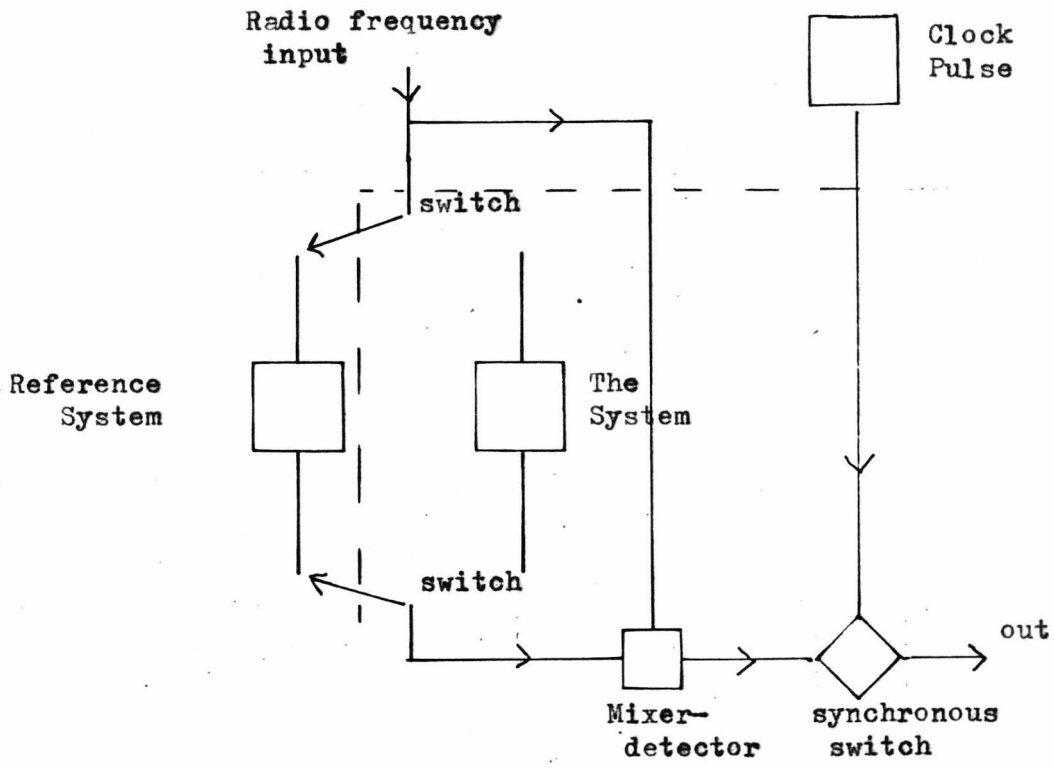
This experiment is reported as 'preliminary' because it is not known what configuration the waves may follow in the ball and hence the limited range of frequencies investigated cover only some of the possibilities. Also the electrostatic field required may be different from that used in the experiment.

6.2 The Experimental Technique

As it was required to detect an effect at one frequency over a range of frequencies, caused by the electrostatic field, the instrumentation was devised to cancel all changes due to other effects than those two being sought. The discrimination of a frequency effect (and discrimination against other effects) was obtained by stepping the frequency and detecting any change due to just this step. Also, all other effects in the system were cancelled by having two similar interferometers and balancing one against the other, the only difference being the electrostatic field and hence picking out just this one cause as being detected in the output.

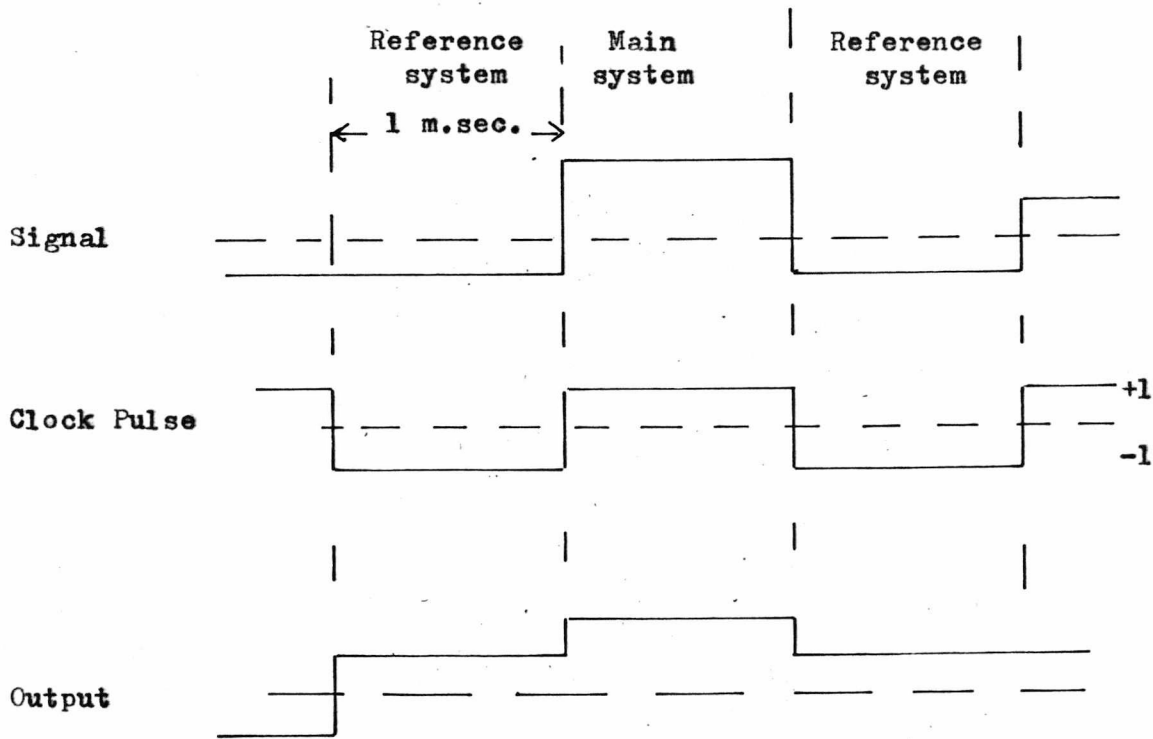
The build-up of the complete detection system will now be considered in a series of instrumentation stages where the next stage contains the previous one.

The frequency response depends on both the space in the electrostatic field and the transmitting and receiving aërials and their



A simplified system diagram of the switching between interferometers.

Fig 6.3



Correlating the result of switching between systems.

Fig 6.4

associated r.f. electronics which have some frequency characteristics. If this system had zero response except at the narrow band of frequencies at which the phenomenon occurs, Fig. 6.2 indicates the output which is the convolution of the input signal spectrum as it is swept across the band, with the line spectrum of the system (as the sweep was made upwards in frequency, the output is in reverse time sequence to the usual convolution equation).

$$\text{Out}(t) = \int_{Kt}^{\infty} \text{In}(f - Kt) \delta(f - F) df \quad \text{E6.1}$$

Where:

K is the rate of scanning in frequency change per unit time.

δ is the delta function.

Because this system has in fact considerable variation with frequency, the next instrumentation loop compared, at each frequency, the system response with a reference system (Fig. 6.3). If the systems were identical there would be no change in output (Fig. 6.4). Because when multiplied by the Clock pulse the reference output is made to cancel the system output, the smoothed output is zero if both systems give the same response. This output more closely approximates the condition postulated above as the reference system should only differ from the system at the frequency at which the r.f. interacts with the electrostatic field (there being no electrostatic field in the reference system). Multiplying by the clock pulse rectifies the alternated signal.

This technique means that the system is being analysed only half of every Clock pulse interval. Effectively, the result that would be obtained by a continuous analysis is multiplied by a square wave of zero and unity. If the response of the system is a pulse (for example that of Fig. 6.28), then depending on its duration compared

The effect on the response of sampling the signal.

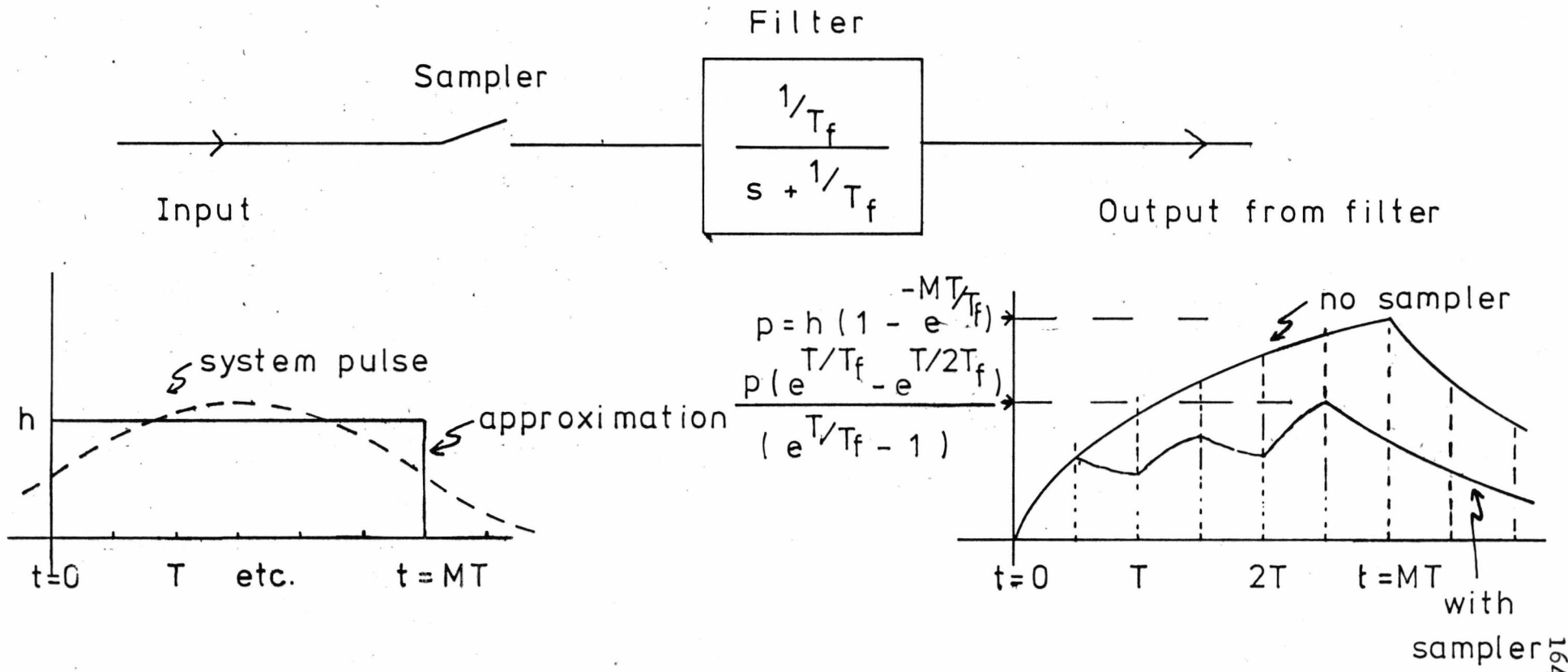


Fig 6.5

with the Clock pulse time, the following conditions may be considered:

i. System pulse time less than the clock time.

The pulse may fall in part or whole outside the time of the Clock pulse being on. Thus in part or whole it may be missed.

If it falls in the on half Clock cycle, and proceeds to the integrating filter, it is an impulse compared with the time constant of the filter. The response of the filter to an impulse of area hT_p , where h is the pulse height and T_p is its duration, is:

$$\text{Output}(t) = \frac{hT_p}{T_f} e^{-t/T_f} \quad \text{E6.2}$$

Where T_f is the time constant of the filter.

ii. System pulse time long compared with clock time.

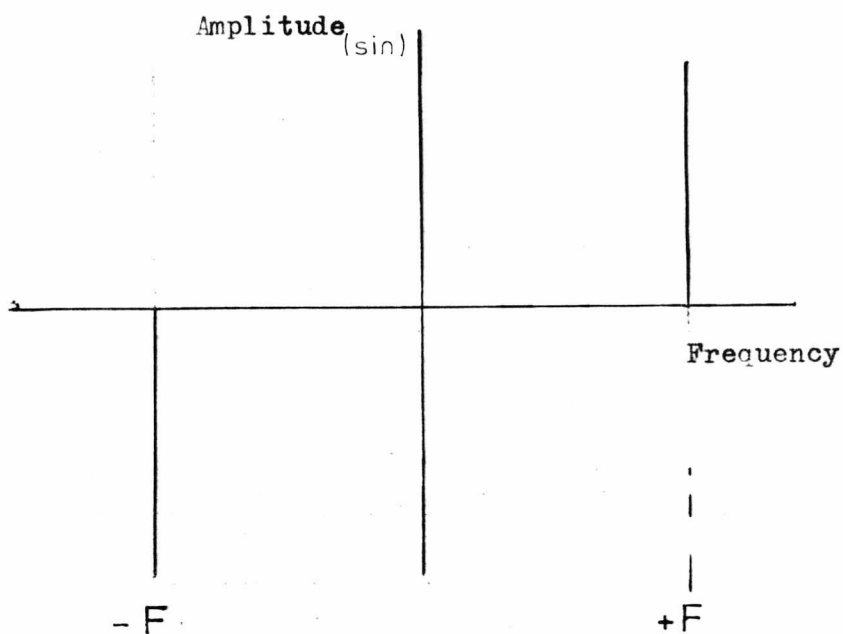
Consider the system pulse approximated by a rectangular pulse extending over M clock pulses (and synchronous with them). This may be analysed as the addition of two step functions (Fig. 6.5) each of which generates a sampled data with finite pulse width (Jury, 1958)⁽⁵¹⁾ response:

$$\text{Output}(s) = \frac{1 - e^{-sT/2}}{1 - e^{-sT}} \frac{h/T_f}{s(s + 1/T_f)} \quad \text{E6.3}$$

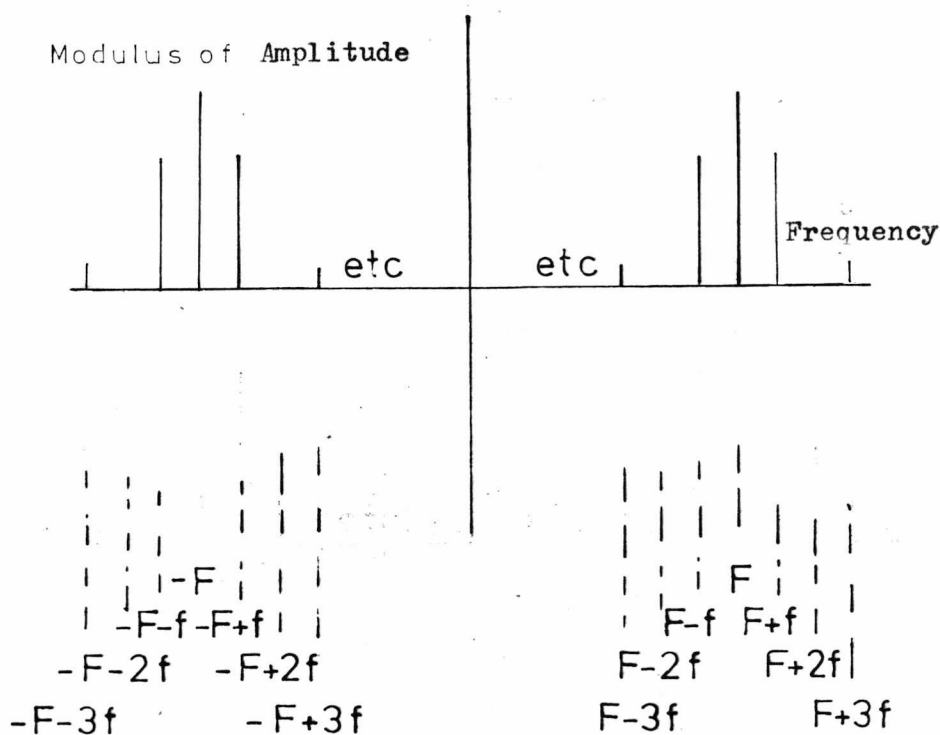
Where T is the time for the Clock pulse repetition. The inverse transform of E6.3 is now combined with that for a second step delayed by time MT ($\Gamma(-b)$ is a time delay b , shift, function such that $\Gamma(-b)f(t)$ is $f(t-b)$ for $(t-b) > 0$) to give:

$$\text{Out}(t) = [1 - \Gamma(-\frac{T}{2})] h \left(n - \frac{1}{(e^{T/T_f} - 1)} (e^{-(m-1)T/T_f} - e^{-t/T_f}) \right) \quad t < MT$$

$$= \frac{h (e^{T/T_f} - e^{T/2T_f}) (1 - e^{-MT/T_f}) e^{-[t - (M - \frac{1}{2})T]/T_f}}{(e^{T/T_f} - 1)} \quad t > (M - \frac{1}{2})T$$



a) The single frequency component of the unmodulated wave.

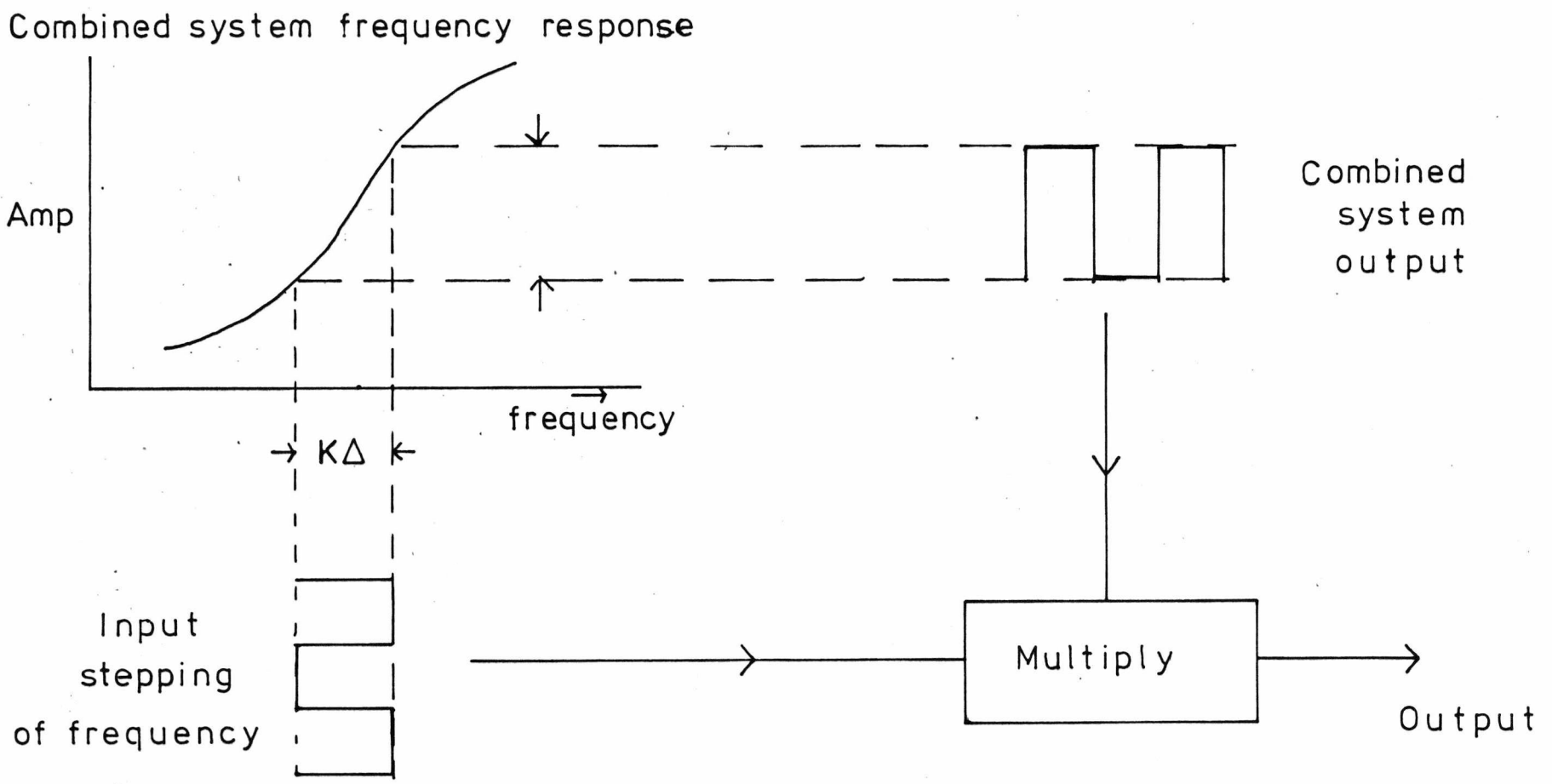


b) Each harmonic of the modulating square wave introduces an upper and lower line, displaced in frequency from the unmodulated frequency by its own frequency.

Fig. 6.6

Fig 6.7

The effect on the amplitude of the output of stepping the frequency.



Where:

E6.4

$t = (n-1)T + mT$. n is the number of the sampling period after $t = 0$ and m is the fraction of the final clock pulse being completed. Fig. 6.5 indicates the form of this result (Jury⁽⁵¹⁾, 1958).

An additional effect of amplitude modulating the r.f. by the square wave, is to multiply it by a set of harmonic components of amplitudes $\frac{2}{n\pi}$, and frequencies $n f$ where f is the frequency of the clock pulse. Each harmonic produces a spectral line displaced from the original c.w. frequency F by its frequency (Fig. 6.6), and of amplitude given in the equation:

$$A \left[\sin(2\pi F)t \right] \left[\frac{1}{2} + \sum_n \frac{2}{n\pi} \sin(2\pi n f)t \right] \quad \text{E6.5}$$

$$n = 1, 2, 3 \text{ etc}$$

$$= \frac{A}{2} \sin(2\pi F)t + \sum_n \frac{A}{n\pi} (\cos(F-nf)2\pi t - \cos(F+nf)2\pi t)$$

In the experiment, this gives only a very small broadening of the spectral line from the r.f. generator.

In order to detect only an effect varying rapidly with frequency, a further loop of instrumentation was added round the above system which stepped the frequency rapidly back and forth. The resulting signal was multiplied by the square pulse stepping the frequency (derived by dividing down the clock pulse) to give the same effect as in the previous loop described by Fig. 6.4. The loop is summarized in Fig. 6.7, where the multiplier output is a measure of the amplitude of the combined system output because the amplitude of the other input and relative phase are constant. The generator frequency was scanned while being stepped and the resulting output may be considered in two regions.

- i. The bandwidth of the pulse being looked for is less than the step in frequency.

The frequency stepping effectively scans the whole of the pulse band in its upper switch and gives an output the same as a single frequency scan. Then it scans the pulse band in its lower switch and the output, being multiplied by the switching pulse of opposite polarity, is an inverted amplitude of the previous scan (Fig. 6.29). Thus there is a characteristic double pulse on the output under these conditions (Jennison⁽⁴⁴⁾, 1966).

- ii. The change of response with frequency is slow compared with the step in frequency.

From E6.1, the output at time t and $t + \Delta$, where Δ is the time the scan takes to change frequency by the amount the stepping changes the frequency, are known and the difference is:

$$\begin{aligned} \left[\text{Out}(t) - \text{Out}(t - \Delta) \right] &= \text{Out}(s) (1 - e^{-s\Delta}) \\ \text{transform} & \\ &= \text{Out}(s) (1 - (1 - s\Delta \dots)) \end{aligned}$$

$$\frac{1}{\Delta} (\text{Output change}(s)) \approx s \text{Out}(s) \quad \text{E6.6}$$

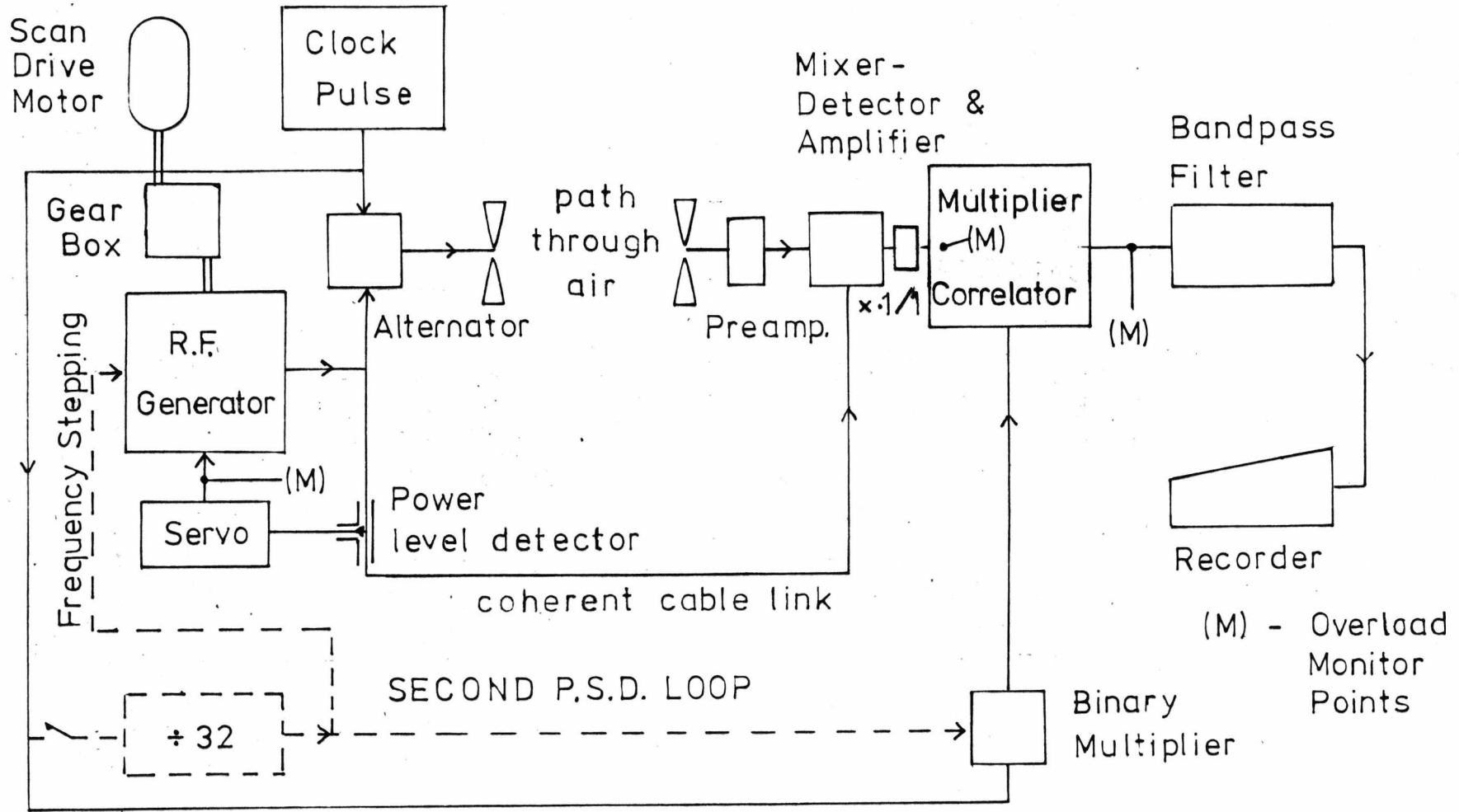
and the rate of change of output in time Δ is approximately the differential of the output with no stepping.

Thus, for example, at a resonance with Q , mid-frequency f_0 and half power bandwidth Δf , the output changes 3 db for a step of frequency:

$$\text{Frequency step}_{3\text{db}} = \frac{1}{2} \Delta f = \frac{f_0}{2Q} \quad \text{E6.7}$$

The final unit of the overall instrumentation was an output filter which fed the signal to the chart recorder. This was a single

The overall system, showing only one of the interferometers.
 Fig 6.8



stage differentiator followed by a single stage integrator both of adjustable time constants. The differentiator (like the frequency stepping considered above) attenuated slowly varying fluctuations below its break frequency, leaving pulses caused by a more rapid change with frequency. The integrator (time constant less than that of the pen recorder) reduced wideband noise, further smoothed the output from the correlator, and reduced the amplitude of the expected signal as considered above.

A perfect system would now give a constant output except at the resonance being looked for. Imperfections give the following which may be considered:

- i. Imperfect balancing of the System and the Reference System (especially a resonance on one side, e.g. an aerial) as the frequency is swept over the range. This gives both quite rapid changes at wideband resonances and slow changes over the band.
- ii. Wideband noise at the input of the first amplifier after the detector, and random noise throughout the system. This noise, including drifts, is reduced by the correlation which picks out only one exact set of harmonic frequencies (c.f. section 4.3(a) and 4.2(b)) If the pulse being looked for is shorter than the clock pulse time, the signal/noise in this band of frequencies is much the same as at the input to the mixer, as the correlation only reduces the noise/signal of lower frequencies.

6.3 The Apparatus

Fig. 6.8 is a simplified representation of the apparatus for each interferometer centred round the air path between the aerials. The details of each main part are considered in separate sections following, including the alternation between the two transmitting

aerials.

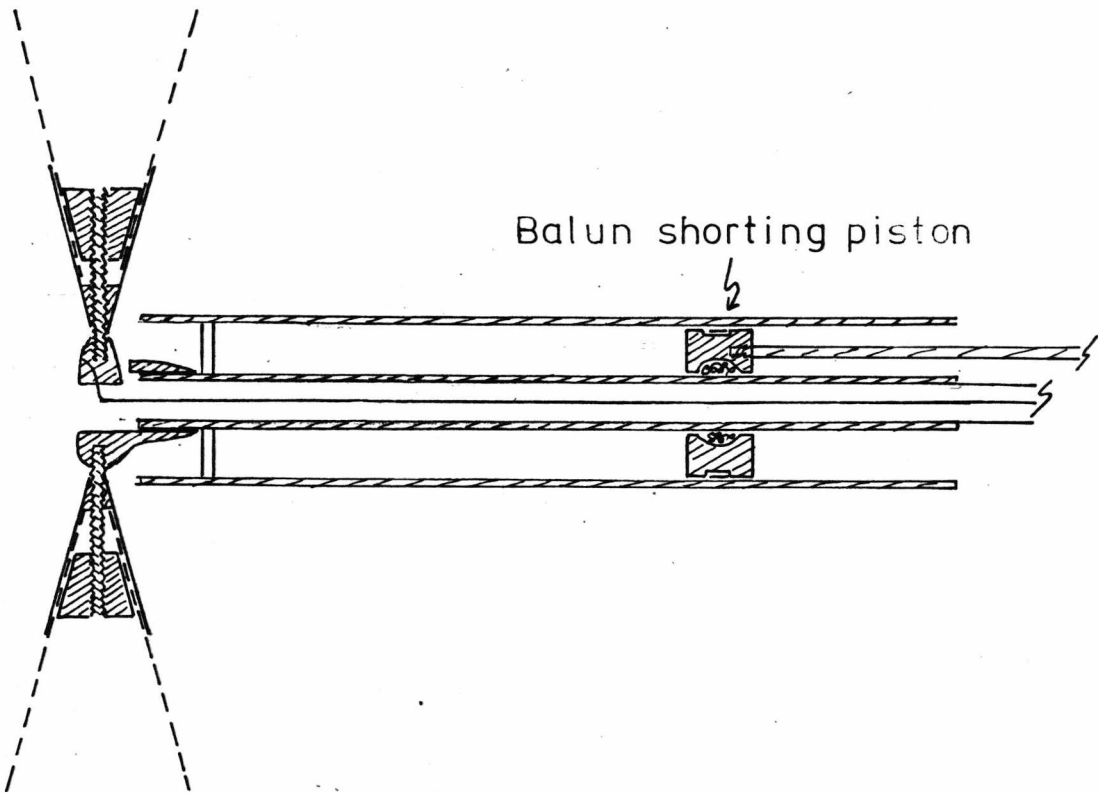
The apparatus was basically a double interferometer. Each interferometer consisting of a reference signal passing along a coaxial cable interfering in the Mixer with a signal transmitted through the space of the room. The signal was switched between the blank side and the measuring side which, for different runs, either had or did not have an electrostatic field, generated by two Van de Graaff generators, across it. The wave frequency was swept through about half an octave in 14 hours for each run and the physical arrangement of all the parts was made as nearly identical as possible as between the two interferometers; so that although each side changed its response considerably with frequency, the difference signal remained small.

The measurement was made both directly, as above, and also with an overall frequency stepping which could be switched in as indicated by the dashed lines in the diagram.

The apparatus was run in a room 30 ft. by 42 ft. by 10.5 ft. high with metal conduits and fluorescent lamps symmetrically above each interferometer. All the electronics except the aerials, preamplifier, and mixer were kept behind the aluminium sheet (9 ft. by 8 ft. high) supporting the transmitting aerials. The cables to the receiving unit were arranged along the floor at the centre between the two interferometers.

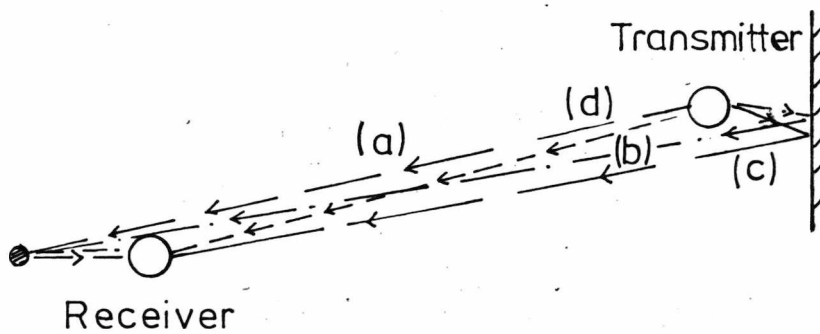
6.4 The Interferometer

The waves were transmitted from two broadband conical dipoles 5 ft. 2 ins. apart. Each aerial was supported horizontally at the end of an adjustable Balun at an adjustable distance which could be set at about quarter wavelength from the plane aluminium sheet. The Balun is an outer co-axial waveguide shorted $\lambda/4$ from the aerial so that



The adjustable biconical aerial and balun.

Fig. 6.9



Four ray paths (a)-(d) between the transmitter and receiver.

Fig. 6.10

the standing wave formed in it prevents any waves travelling back on the outside of the cable. The centre frequency of the aerial resonance could be adjusted by attaching the required size of cone (made of Baco-foil) to the machined brass cups at the boss. This length for a conical aerial is nearer $\lambda/4$ than $\lambda/2$. The Balun was an aluminium tube co-axial with the cable to the dipole, itself encased in a supporting brass tube, with an adjustable piston plunger shorting the outer tube and the cable sheath at the required distance from the end (Fig. 6.9). The cable to the aerial was connected directly to the Polyskop analyser which measures the v.s.w.r. over a range of frequencies and the cone length and distance from the reflector were adjusted to give a broad band resonance at the required frequencies (small v.s.w.r.). The aeriels were matched so that the response of both interferometers was approximately the same.

The receiving aerial was a similar conical dipole supported at the end of a Balun tube. Behind the receiving aerial was a parasitic reflector of adjustable length and distance from the aerial. The aerial was connected to the Polyskop and adjusted to give the required wideband characteristic (it was found that without a reflector behind it, the aerial had a narrower bandwidth. The reflector gave staggered tuning at a different frequency to that of the conical dipole). This aerial was mounted on a wooden mechanical aerial positioner driven in the horizontal plane by two 6 V. reversable motors giving a movement across the beams of 2 ft. and in the direction of the beams of 18 ins. This enabled the receiving aerial to be positioned the same wave distance from each transmitting aerial and to equalize the wave paths in each arm of the interferometer. At a number of spot frequencies over the range being measured, the output signal was reduced to an average minimum by moving the aerial so that the signals in the mixer



Photo 4

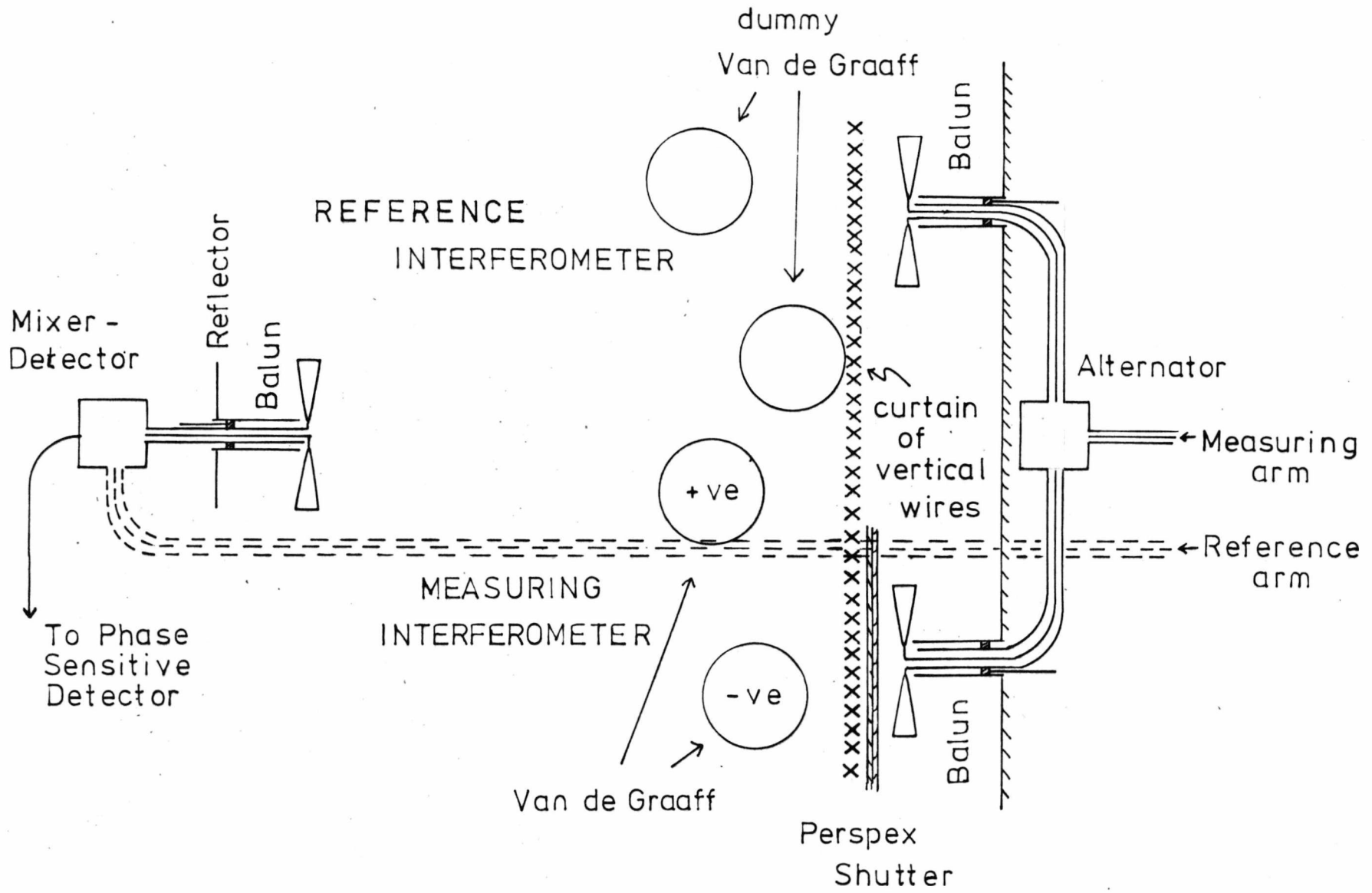


Fig. 6.11

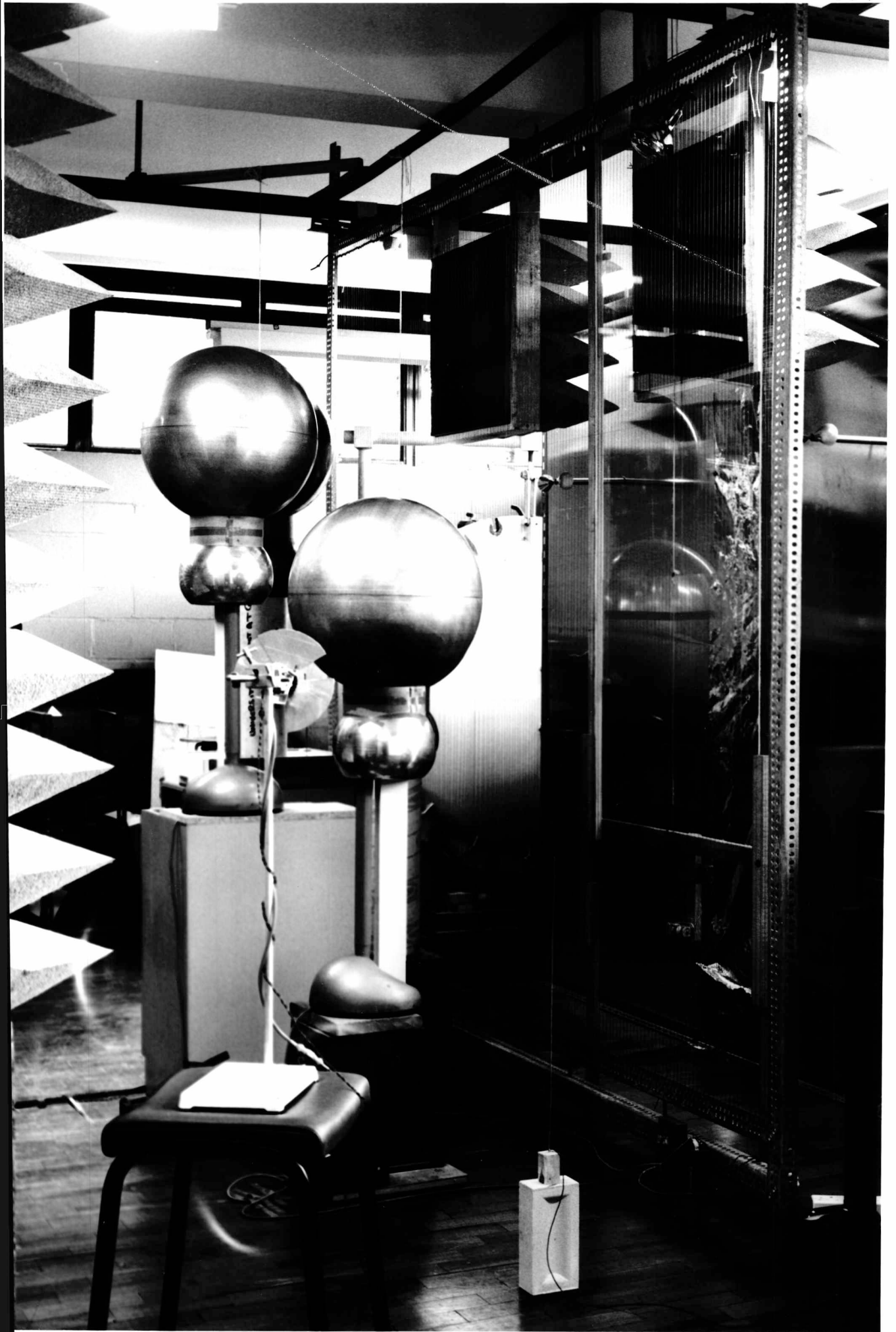


Photo 5

were all in phase. This was only an approximate position over the range because the reflectors behind the aeriols gave wavepaths of different wave distance to that of the main wave (Fig. 6.10).

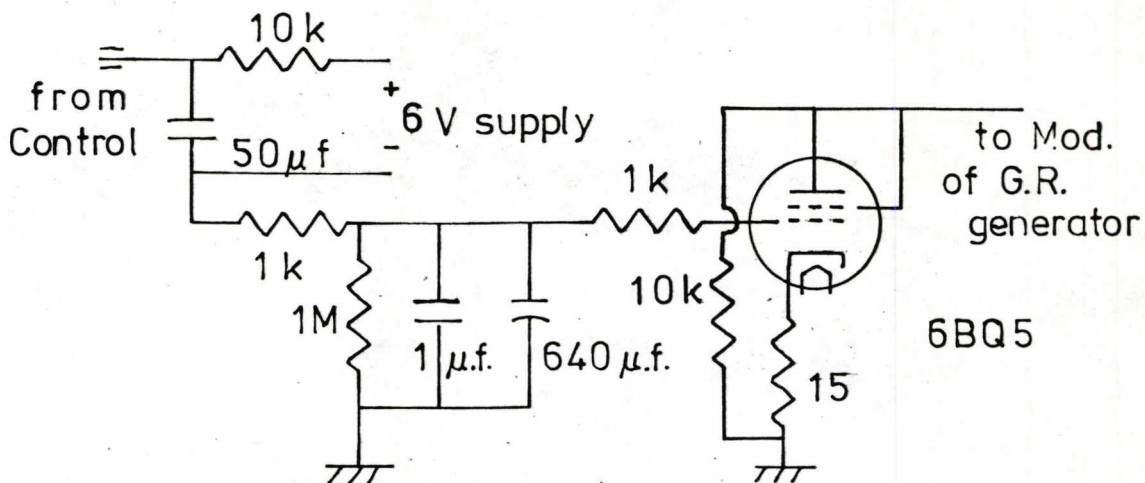
The receiving aerial was surrounded on four sides by 6 ft. by 6 ft. panels of Microsorb material to reduce the waves reflected back from objects in the room which might cause an imbalance between the interferometers (Photo 4). Of importance are the points of specular reflection between transmitter and receiver from the ceiling and this was screened by two squares of Microsorb above and to the front of the transmitting aeriols. The Microsorb is panels of Plessey material type AFP 18 Broad band absorber reflecting less than 1 % incident power over the range 0.4 - 75 G.Hz. A good match to free space is obtained by the use of a tapered profile in the form of pyramids and losses are introduced by carbon loading the low density expanded material.

Between the transmitter and receiver were arranged two Van de Graaff electrostatic generators and on the reference system side a second pair of dummy generators of cardboard tubes and 10 in. diameter metal spheres with 18 in. spheres above them connected by wires to earth (Fig. 6.11).

In front of the transmitter in the measuring interferometer was a Perspex shutter which modulated the r.f. wave passing to the receiver and was used to calibrate the system. (Photo 5).

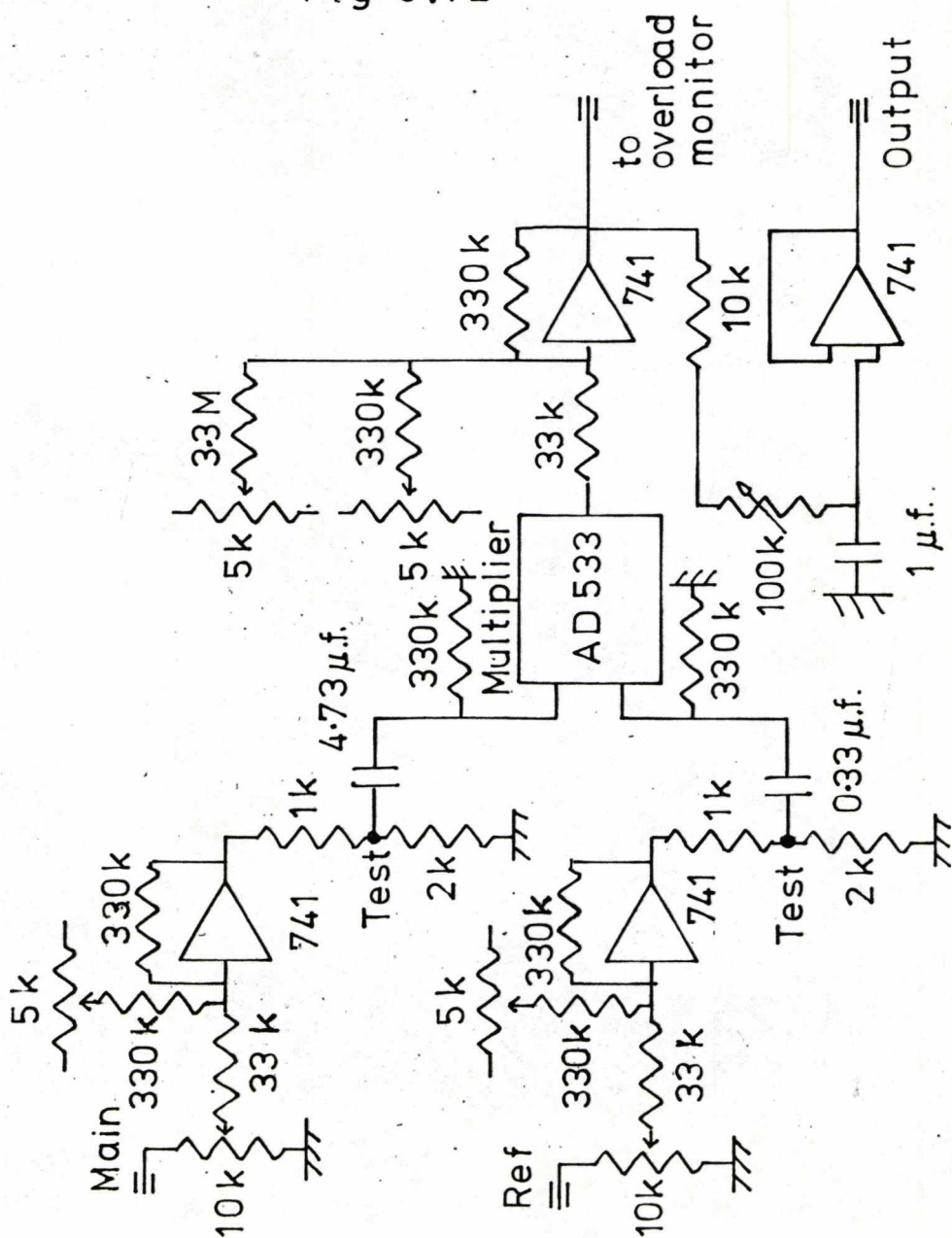
There was a curtain of vertical wires 0.75 ins. apart connected to earth, between the Van de Graaff generators and the transmitting aeriols. This acted as a ground plane to the static field produced by the generators while allowing the cross-polarized r.f. to pass through.

The six Baco-foil cones for each frequency band were made uniformly on a solid conical metal former with slight ring cuts machined at closely spaced intervals along its length in which the



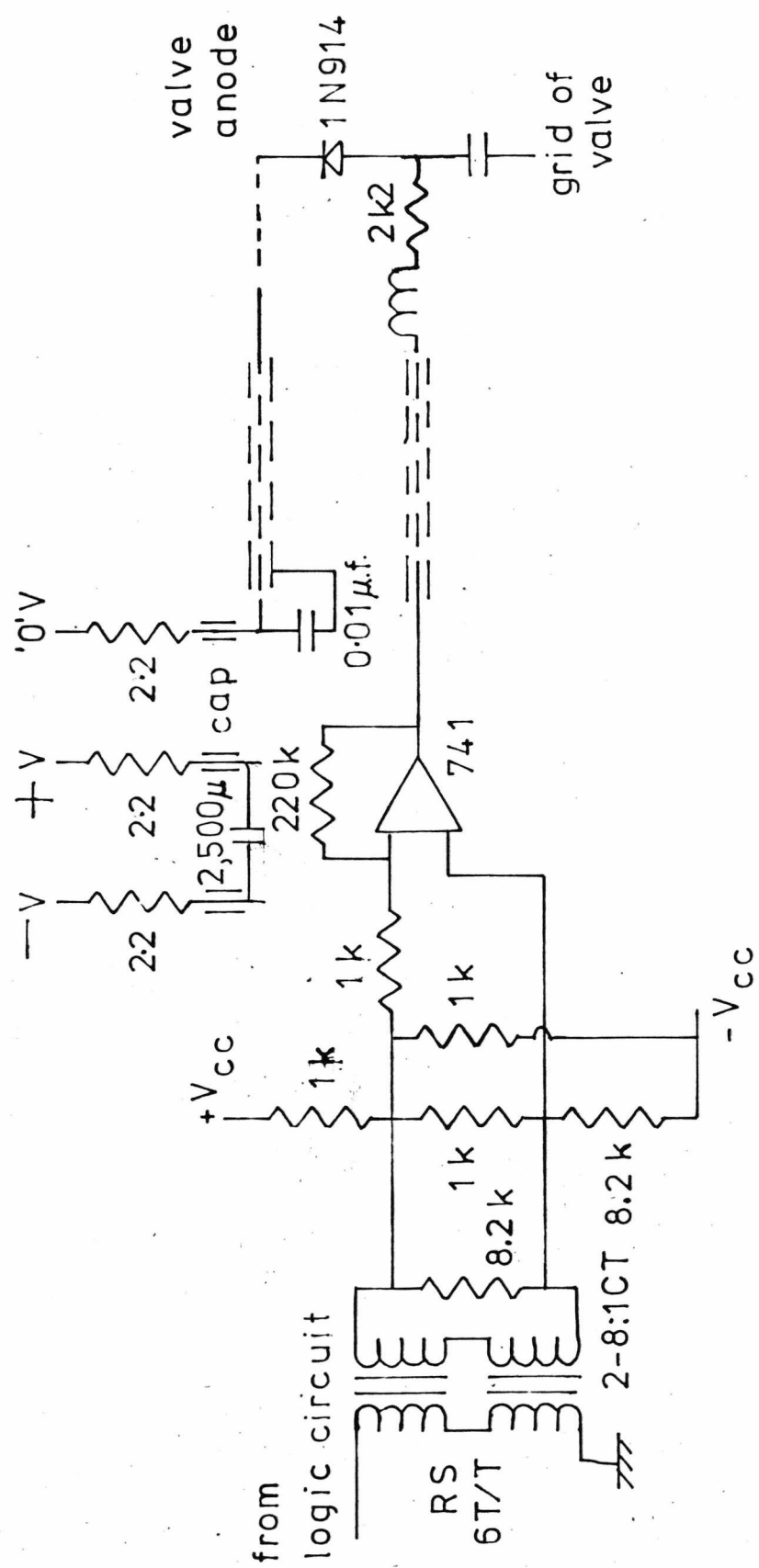
Circuit to modulate the voltage on the anode of the U.H.F. generator valve.

Fig 6.12



The multiplier-correlator circuit.

Fig 6.13



The circuit which stepped the frequency being generated, showing the transformer which isolated the unit.

Fig. 6.14

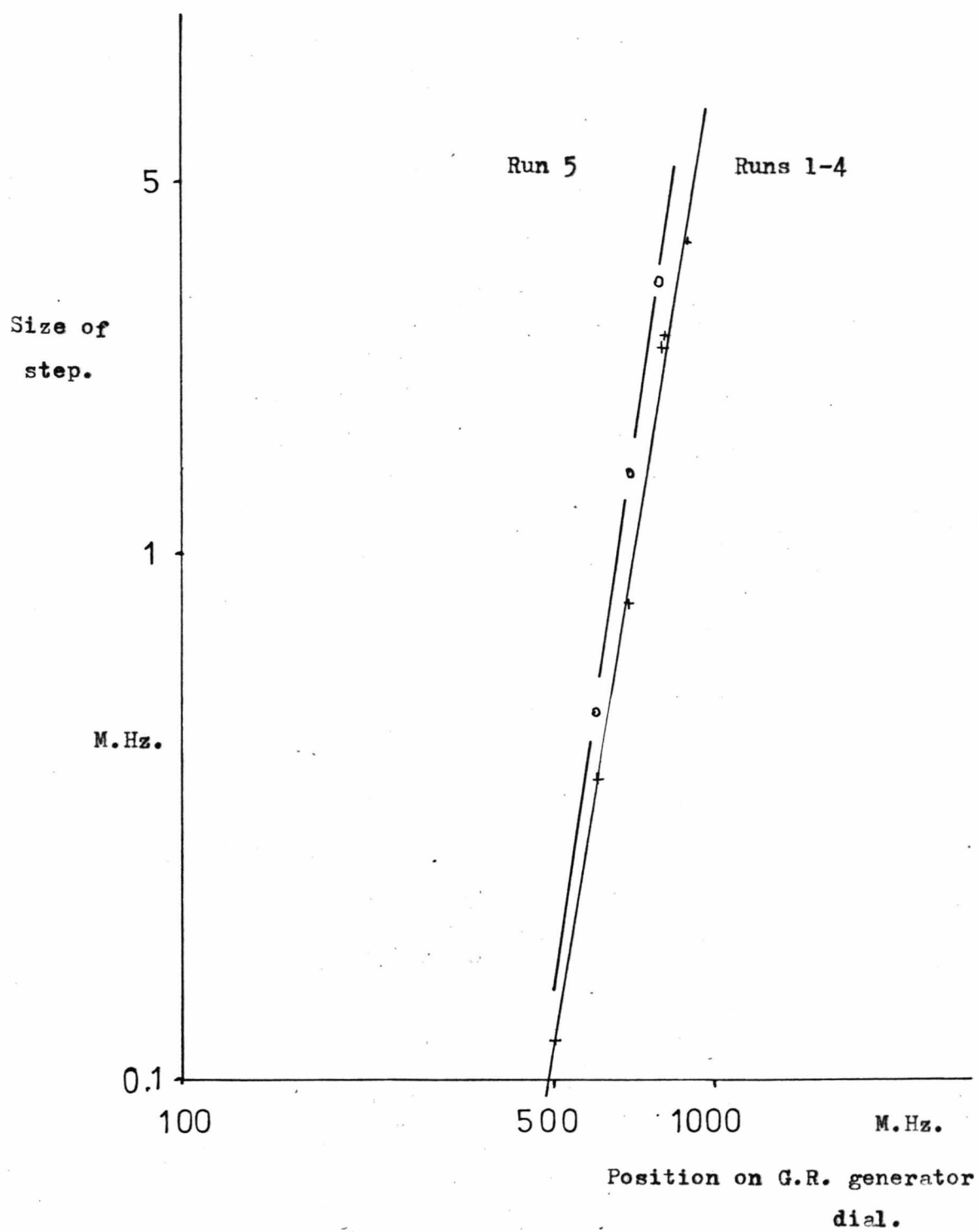
foil was cut to length with a razor.

6.5 The r.f. Generator

The U.H.F. radio waves in the range 250-960 M.Hz. were supplied from a General Radio (G.R.) 1209-C Oscillator powered by a G.R. 1264-A Power supply. This supplies up to 160 m.W. power into a 50 ohm load.

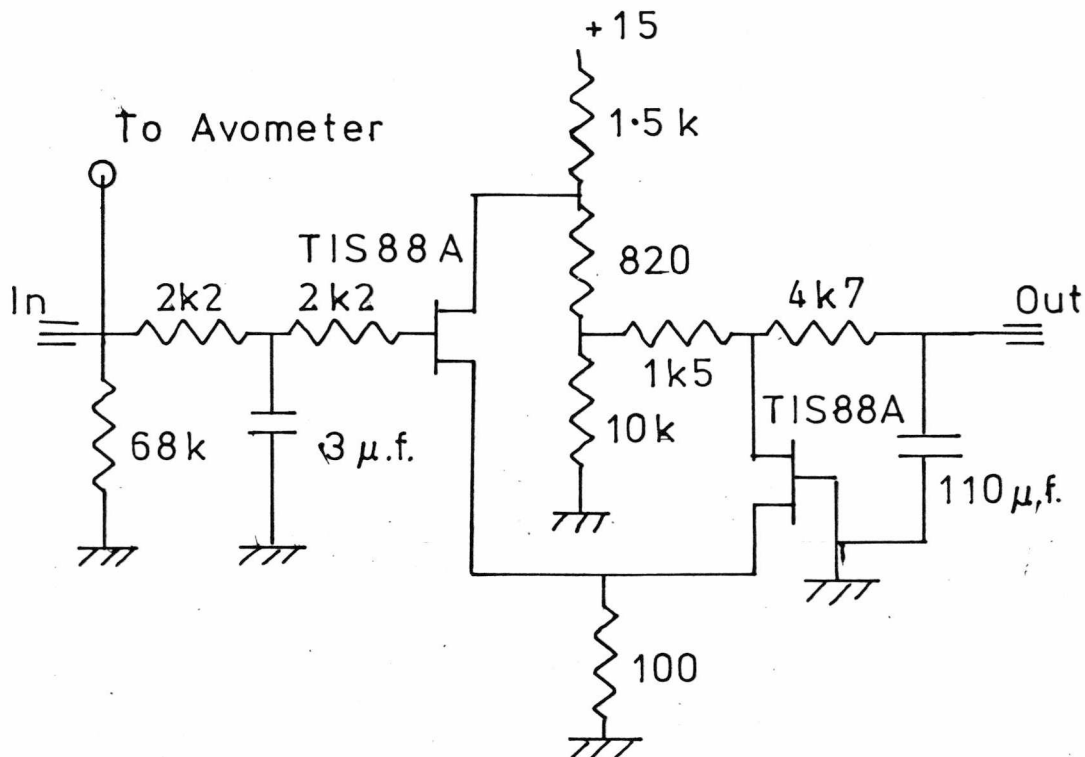
The power from this generator was controlled electronically by a valve control unit (Fig. 6.12) which connected into the Modulator control (J101) of the Oscillator (If the standard G.R. 1263 Power supply had been available it would have performed this function). This controls the voltage to the anode of the GEY 1266 valve by a control signal w.r.t. ground. Also, a 160 μ f. electrolytic capacitor was added across pins 15 and 16 and the filament heated by a separate d.c. supply to reduce mains hum.

Preliminary attempts to step the frequency by a small amount were made by mechanically vibrating (square wave) a plate (2 sq. cm.) near the Butterfly tuning circuit of the Colpitts oscillator in the G.R. generator, driven by the Vibrator transducer of chapter 4. This stepped the frequency, unreliably by too small a step, with a slow ringing change of the mechanical system. The final circuit, which worked well, switched in and out a small additional capacitance by replacing the frequency adjusting tab on the tuning circuit which parallels the Butterfly capacitor, by a similar tag of wire near the valve grid in series with a diode (1N916) which was switched on and off by a current from a 'floating' control amplifier (Fig. 6.14). The circuit had to be d.c. isolated because the oscillator runs at high voltage. It was also r.f. decoupled by lead through capacitors for the wires to this unit. The amount of the frequency step at different points of the scan was measured with the Spectrum Analyser (Hewlett-



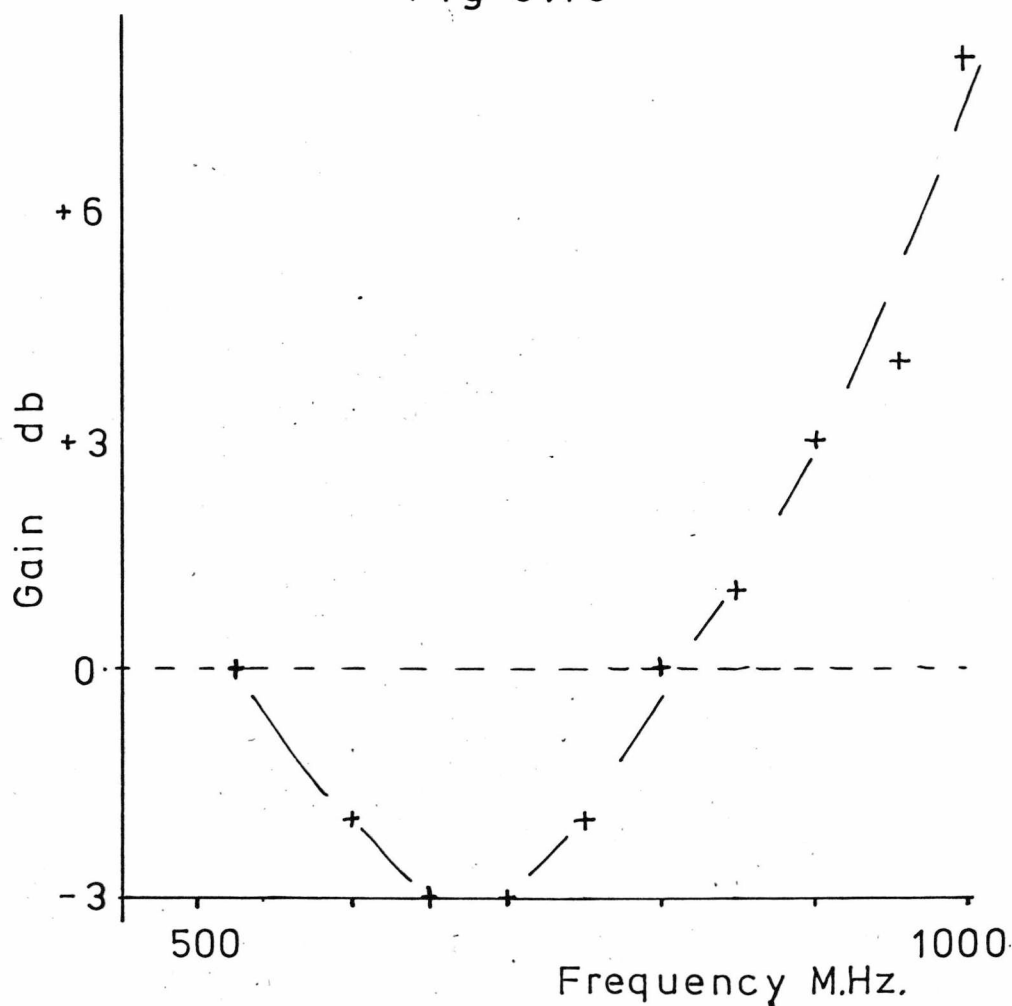
The dependence of the size of the step in frequency on the frequency.

Fig 6.15



Buffer circuit following the diode detector which monitored the power level.

Fig 6.16



The frequency response of the r.f. pre-amplifier.

Fig 6.17

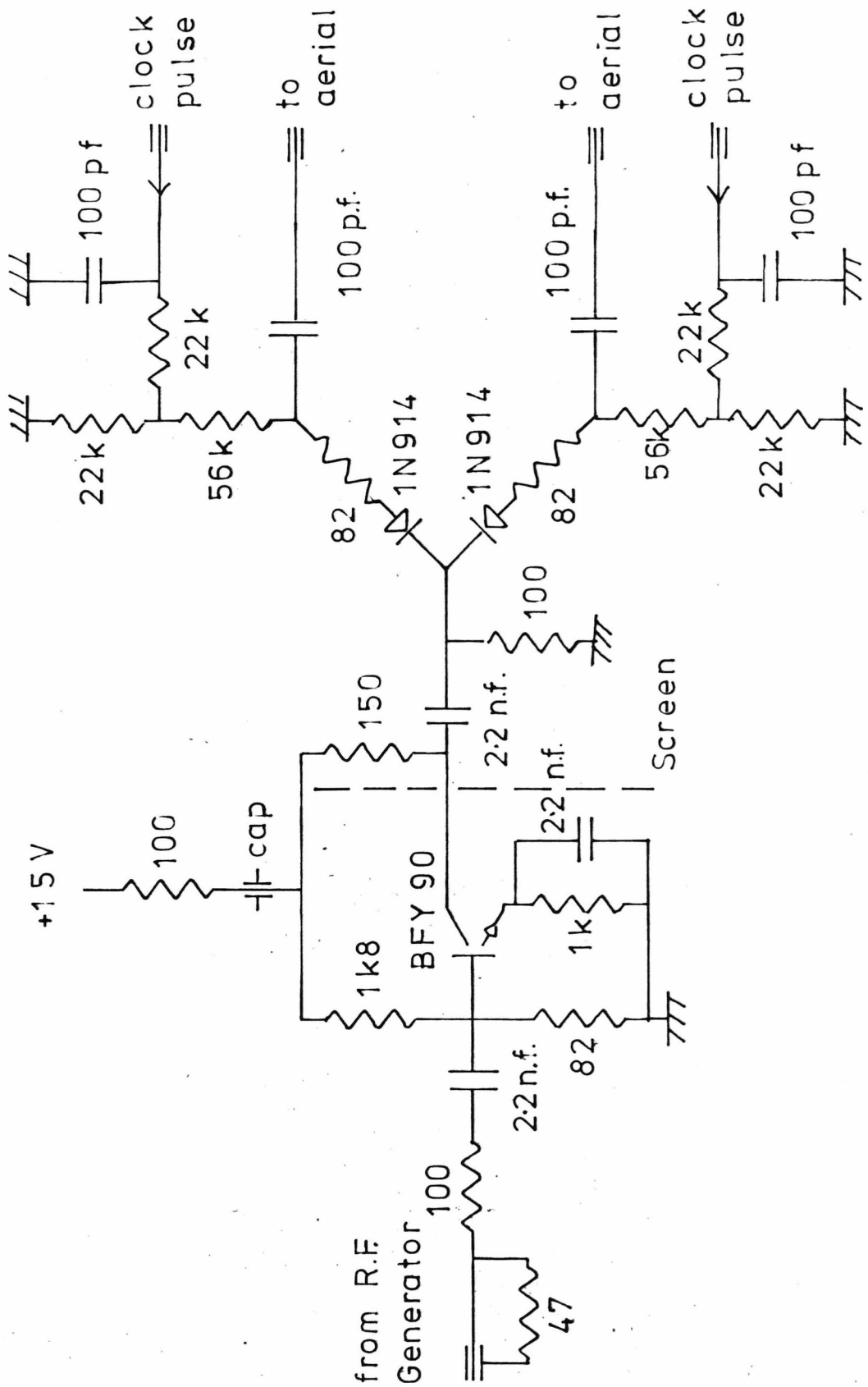
Packard 8551B) and is plotted in Fig. 6.15. The signal to the input of this circuit came from the Switching circuit of section 6.9.

The mechanical dial which is normally used to set the frequency was removed and a drive from a gear train mounted on the front panel, so that a coupling was made to the tuning shaft. The gear train was that supplied with the Monoperm-super-5-Pol 6 V. d.c. motors and a gear box constructed in Meccano, which had adjustable ratios of 4:1, 1:1, 1:2, and 1:3. The gears were driven by a reversible mains powered synchronous motor type RQR of Drayton Controls, Ltd, running at 1.05 rev. per min. The drive from the gear box was through a 2 ft. length of Puch speedometer cable to isolate motor vibrations from the G.R. generator. There was some backlash in the gears but once the gears were turning, there was a smooth turn of the shaft.

6.6 R.f. power control servo

Some of the signal from the G.R. generator was detected by a 874-VQ, T junction incorporating a 1N238 Sylvania diode. This signal went to the buffer circuit of Fig. 6.16 with an FET preventing volts getting back onto the detector diode. An Avometer monitored the detector voltage to indicate the r.m.s. voltage of the signal detected by the diode. The experiment was run with a level of 0.6 V. maintained by the servo. The integrator on the output mainly determined the frequency response of the servo loop.

Then the signal went through the three term controller of chapter 4 followed by an inverter to give negative feedback. Only the k_2 control was adjusted to give maximum gain without introducing oscillation. The frequency dependent terms were not used. The output was monitored by the oscilloscope and by one of the channels of the overload indicator unit.



The circuit which switched the r.f. signal between interferometers.

Fig. 6.18

This signal went to the power control circuit of Fig. 6.12 which has a biasing voltage supplied from a power supply to give a suitable quiescent voltage on the grid. Thus the control loop is completed with negative feedback.

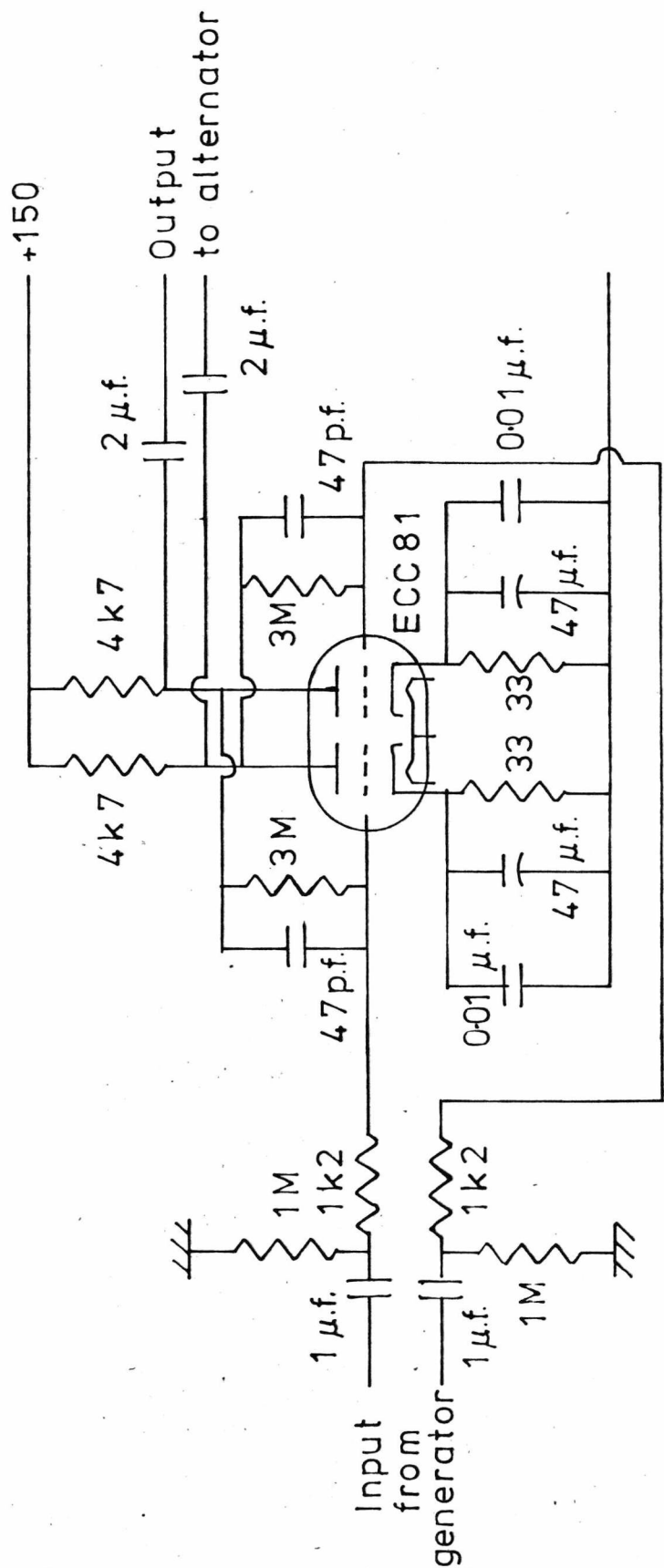
The level at which the power was to be controlled was set by the d.c. bias controls of the controller which compares the signal from the detector with that on the bias control. The additional voltage added by the power supply in the valve circuit was 6 V. which enabled the ± 15 V. from the controller to give the suitable range of bias on the valve. Also the waveguide-below-cutoff piston attenuator on the G.R. generator had to be moved slightly from being fully in, until a suitable range of output power was obtained.

There was a tendency for mains hum due to voltages in the G.R. generator, to be amplified round the control loop. Sufficient integration was added to the output of circuit Fig. 6.16 and input of Fig. 6.12, to reduce control above mains frequency and control slow variations.

6.7 R.f. Circuits

The power from the generator was divided between the Alternator and the reference signal line of the mixer.

The Alternator (Fig. 6.18) led the r.f. power through a buffer circuit with 100 ohm d.c. output load, to a pair of diodes which were switched on alternately by a current from the high impedance source to direct the power into the low impedance cable. The control signals were h.f. decoupled from allowing r.f. back along the wires by decoupling capacitors. The power was led out from the diodes through capacitors to the cables feeding the transmitting aerials. Sufficient signal was required to turn the diode on and reverse bias it off. This was supplied



The amplifier generating large voltage control signals to switch the diodes of Fig. 6.18.

Fig. 6.19

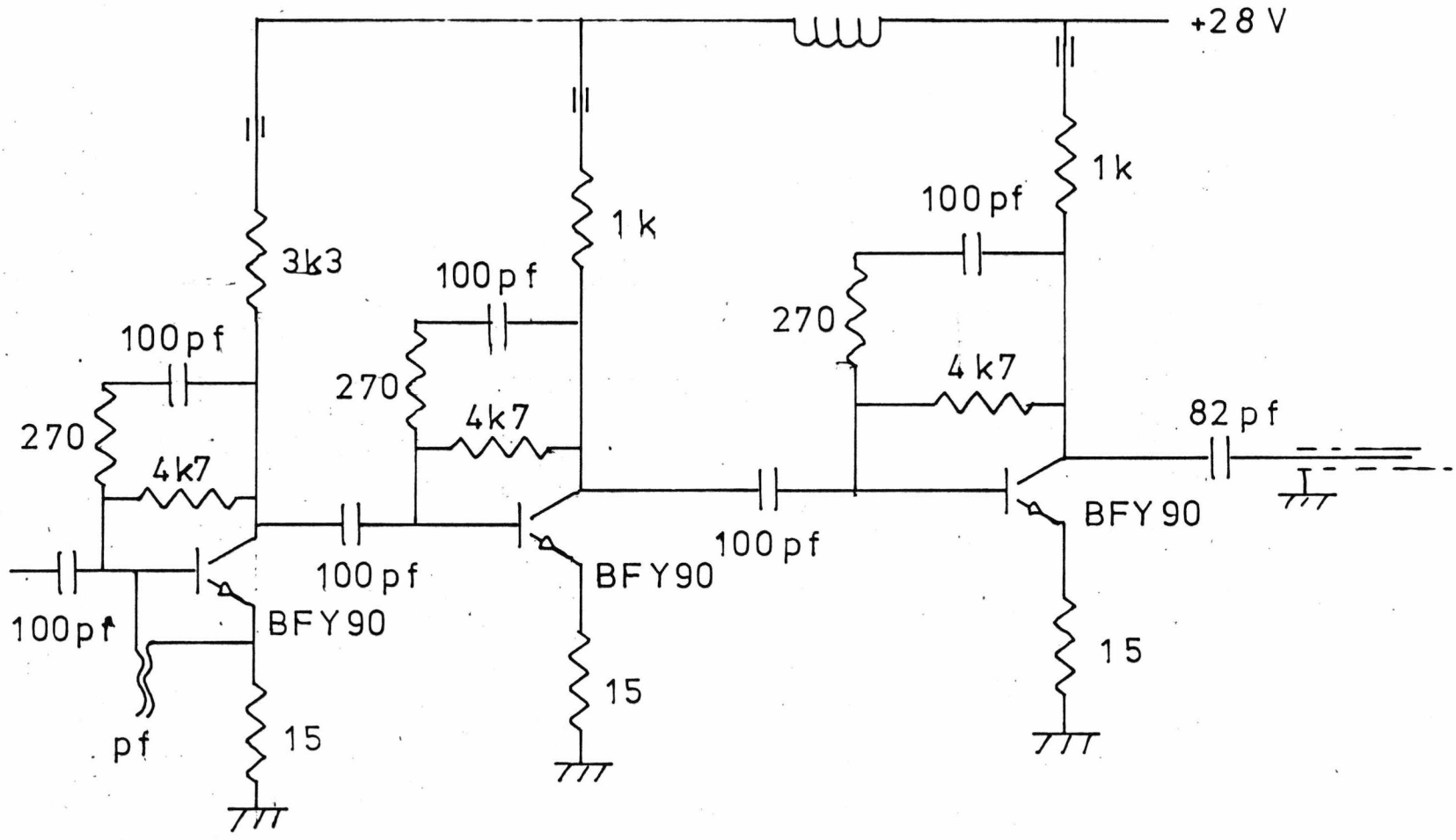
from a valve circuit (Fig. 6.19). The buffer transistor was required to minimise the switching signal to the diodes also going back along the cable to the generator and hence to the reference input of the mixer. The Alternator circuit was switched by large voltage signals from the valve circuit. This was coupled by $2 \mu\text{f}$ capacitors forming a sufficiently long time constant not to distort the 1 k.Hz. square switching waveform. This waveform was improved by the positive feedback on this bistable circuit. The input to this circuit was also r.f. decoupled by lead-through capacitors. The whole of this unit and its power supply were screened with Baco-foil. The Clock pulse generator supplied pulses in phase and anti-phase to the two inputs to this circuit.

The mixer-detector of Fig. 6.20 feeds the received signal to a Germanium diode (GEX 66) which is switched on and off by the reference signal. The reference signal was typically of r.m.s. amplitude 0.5 V. at the diode. Hence the mixing was a modulation of the main signal by the switching of the reference signal. The result is a component twice the original frequency which averages to zero and a component of zero frequency which measures the amplitude of the main signal and compares its phase with that of the reference signal. If the main signal is $A \sin \omega t$ and the reference signal switches the diode on at time θ/ω sec. (phase lag of θ) at the same frequency, the result of multiplying them for a cycle of the reference signal and integrating is:

$$\int_{\theta/\omega}^{\pi+\theta/\omega} A \sin \omega t dt = \frac{2A}{\omega} \cos \theta \quad \text{E6.8}$$

(It was not found practicable to amplify the main signal sufficiently that it could be clipped to have constant amplitude, and give a mixer output depending only on the phase).

The radio frequency pre-amplifier circuit.
Fig. 6.21



Thus the correlation of these functions over a length of time is a measure of the product $A \cos \theta$. The phase of the main signal at the mixer depends on its path through the air gap. If a refractive material of thickness L is inserted the phase change will be (Jenkins⁽⁴²⁾, 1957):

$$\text{Phase change} = \frac{L \omega}{c} (R I - 1) \text{ radians} \quad \text{E6.9}$$

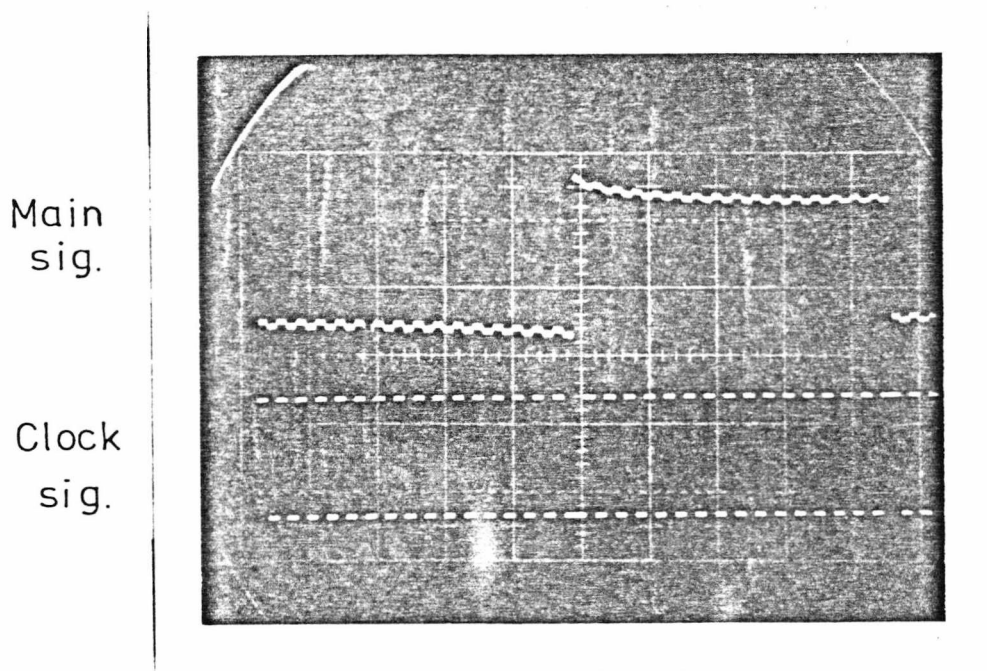
Where:

L is the thickness of material of refractive index $R.I.$ and ω is the frequency of the radiation.

θ could be changed either by inserting a refractive material or by moving the position of the aerial. In general both these operations will also change the amplitude A of the main signal received.

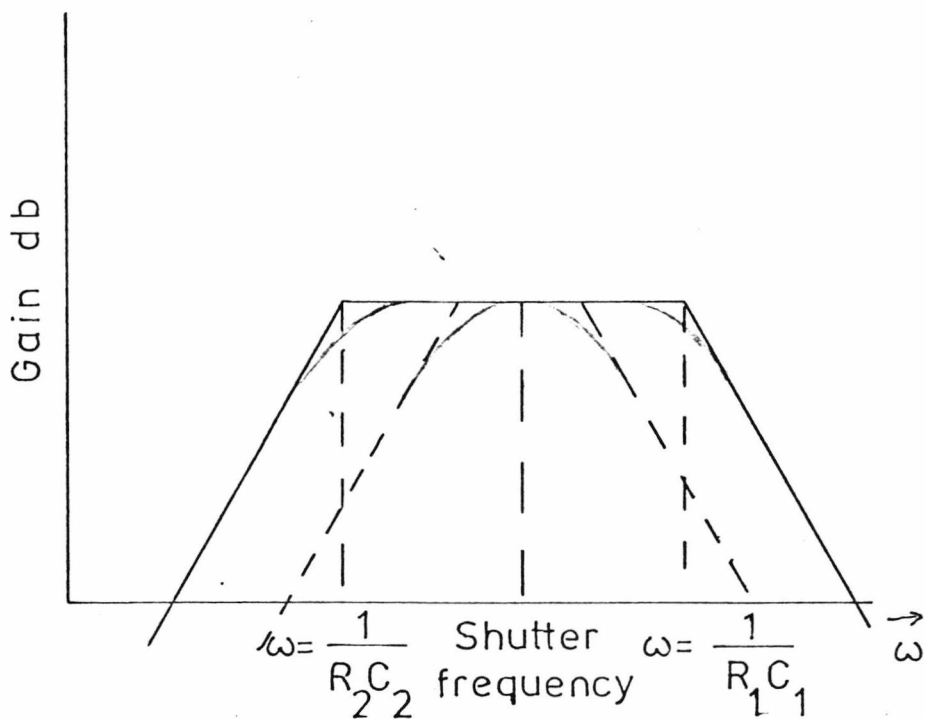
Because of the minimum voltage required to switch on a Germanium diode, a forward biasing current was added. The smoothed output went to a high input impedance, low noise amplifier (TBA 231, which has approximately 10 times less noise than the 741 in this frequency range) of gain 10. Drift was reduced by decoupling the stages. It is at this point that minimum noise should be added to the received signal. The output then went, by a length of cable, to another unit giving gain of 100 just before the Multiplier input. A signal from a signal generator at 2 k.Hz. was fed into the input and increased until it was the same amplitude as the wideband noise monitored on the output of the amplifier. This indicated 0.2 m.V., r.m.s. noise at the amplifier input.

For the runs at the top end of the r.f. range it was found necessary to boost the signal from the receiver aerial with a wideband preamplifier (Fig. 6.21). The frequency response was measured on the Polyskop II (Rohde and Schwarz, type SWOB BN 4245/50) and the exact position of the earthing plate and wire on the output were adjusted to give the flattest response. The final result was not flat and is indicated in Fig. 6.17. The gain at the top of the range was useful,



The signals going to the correlator, showing the stepping due to alternating between interferometers (rapid) and stepping the frequency (slow).

Fig 6.22



Amplitude frequency response of the output filter.

Fig 6.23

and where it drops below unity the rest of the system has rapid increase in signal transfer. The Noise Figure is the Noise Factor expressed in db, where the Noise Factor is the input signal-to-noise power ratio divided by the output signal-to-noise ratio. The Noise Figure was measured for the r.f. amplifier and was 7 db.

The r.f. input impedance of the Alternator, Mixer, and preamplifier were adjusted as near to matching the 50 ohm cables as possible by connecting the input to the Polyskop and adjusting the matching resistors to give a minimum v.s.w.r. Some mismatch remained, giving resonances in a cable of length L_{cab} at a frequency spacing of:

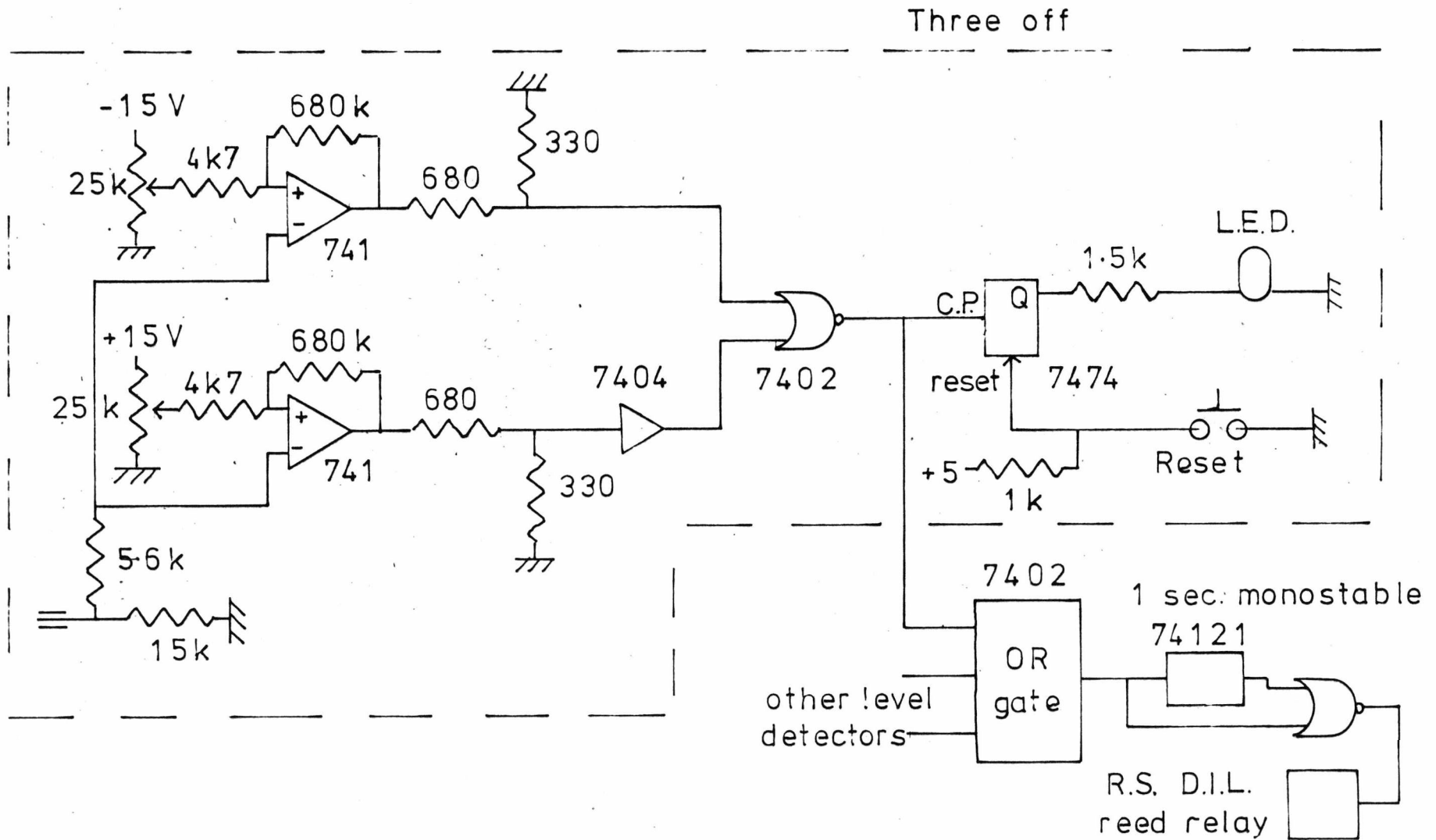
$$\Delta f = \frac{c}{3 L_{cab}} \quad \text{E6.10}$$

For a cable with Velocity Factor of $\frac{2}{3}$. (c.f. Fig. 6.33, $L_{ref.coax} = 5.8 \text{ m.}$)

6.8 A.f. Circuits

The overall system of a.f. amplifiers started at the low noise amplifier on the output of the Mixer. The signal then went to a 100 times amplifier whose output went to a switched attenuator of $\times 1$ or $\times 0.1$ (the lower gain was required when the stepped frequency was running). This signal was fed to the input of the Multiplier with a voltage swing of the order of volts. It consisted of square waves of frequency equal to the Alternator clock frequency and also stepped according to the 31 Hz. frequency stepping (Fig. 6.22 is a typical waveform). The Multiplier (Fig. 6.13) performed a similar function to the correlator of section 4.3. The input signals were adjusted to a suitable bias and gain. The other input to the Multiplier being the Clock pulse reference signal from the switching circuit, amplified by about $6\times$ to give an amplitude $\pm 10 \text{ V.}$ at the test point. The circuit uses an I.C. Multiplier (Analogue Devices AD 533) which contains a

Overload indicator circuit.
Fig. 6.24



transconductance multiplying element. Trimming biases to the Multiplier had been adjusted to give minimum feedthrough of one input with the other zero. The device multiplies in four quadrants. The signals were thus multiplied and integrated with a time constant of 0.1 to 0.01 sec. (the filter following also integrated). There were test points as indicated on the diagram.

This is a correlation as in section 4.3(a) if the square waves are considered as a set of harmonic components, the square waves being in phase. When the frequency stepping was running, the reference signal had already been multiplied by the frequency stepping pulse, so the multiplier correlated both instrumentation loops simultaneously.

The main signal amplitude at the multiplier input test point, and the output from the Multiplier, went to an overload indicator (Fig. 6.24). It has three sets of pairs of 741 comparators which were tripped if the input swung more than the amount set on the potentiometers. The logic then set a flip-flop which lit an indicator light. Once tripped, this light remained on until the reset button was operated. The logic also operated a monostable whose output was OR with the overload signal to operate a relay. The relay was operated either for one second after a transient overload (the monostable) or by a continuous overload. Thus the relay was only operated while the overload was on (and one second after). The relay operated an event recorder on the chart recorder and the indicator light once triggered indicated at the end of the run, which channel had overloaded. It was a useful unit and operated steadily even if the overloads were caused at 30 Hz. The third channel of this unit monitored the output of the controller in the power level servo(section 6.6).

The output filter was two sequential units of RC differentiator and integrator circuits each followed by buffer amplifiers, giving a

combined transfer function:

$$T.F. (s) = \left[\frac{1}{1 + s R_1 C_1} \right] \left[\frac{s R_2 C_2}{1 + s R_2 C_2} \right] \quad E6.11$$

Where:

$R_1 C_1$ is the integration time constant.

$R_2 C_2$ is the differentiation time constant.

Which has the break frequency asymptotes of Fig. 6.23 and is a simple band pass filter. When looking at only one frequency for the calibration with the oscillating Perspex shutter, the time constants were brought nearer together as indicated by the dashed lines on the diagram. When running the search experiment, the frequencies were:

$$R_1 C_1 = 0.05 \text{ sec.} \quad f_{\text{break}} = 3.4 \text{ Hz.}$$

$$R_2 C_2 = 20 \text{ sec.} \quad f_{\text{break}} = 0.008 \text{ Hz.} \quad E6.12$$

The output was monitored on the scope and went to the Chart Recorder (Vitatron, type UR 400/M). The connection was made through a 8.2 k.ohm resistor and 2 μ f. integrating capacitor to reduce voltage spikes from the recorder motor returning to the electronics. There was a switched attenuator giving factors of:

Nominal ' 1 m.V. to 10 m.V.' factor of 1.96

Nominal ' 100 m.V. to 1 V.' factor of 6.50

There was also a $\times 1$ or $\times 5$ potentiometer at the recorder input. These odd values occur because the original recorder (J.J. Instruments Recorder CR 500) was unreliable and replaced by the above unit with the same sensitivities. The recorder is driven by a synchronous motor through a variable gear change including 2 cm./min. and 0.25 cm./min.

The generator of the switching control signals for - 1. Interferometers
 2. Frequency stepping

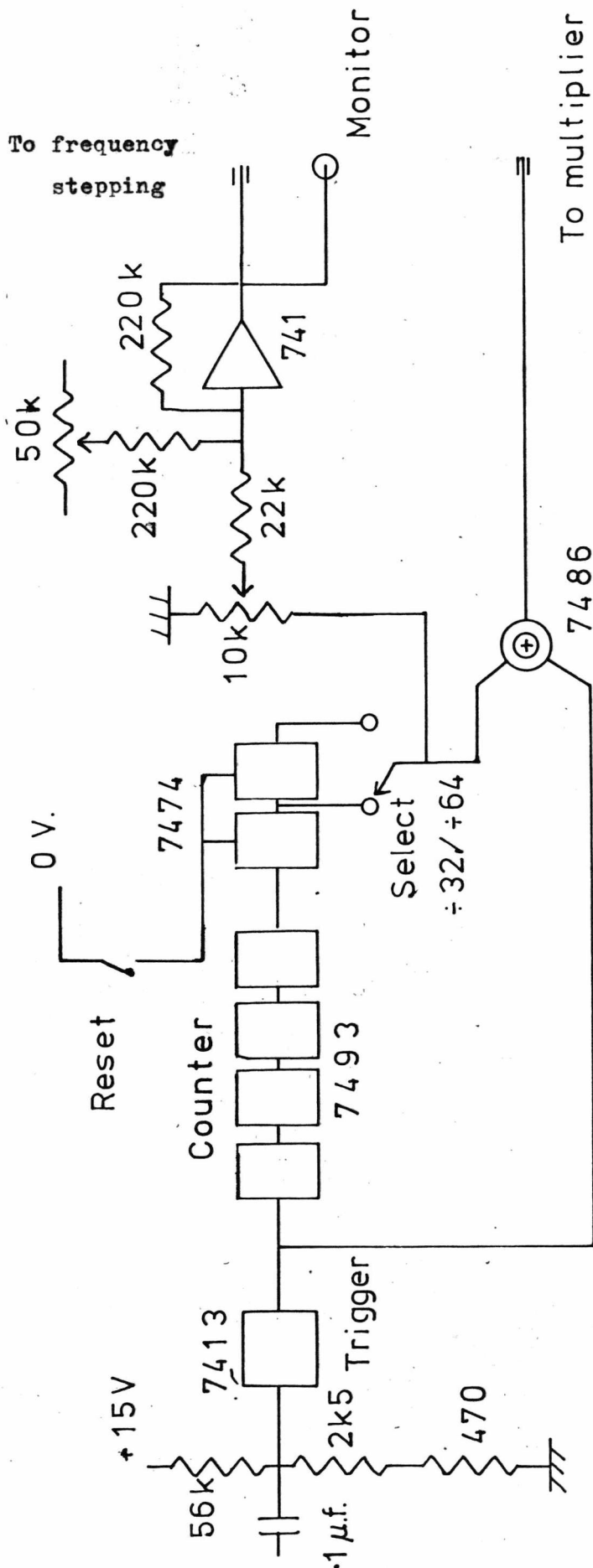


Fig. 6.25

6.9 The switching circuit

The Clock pulse signal to switch the Alternator was supplied by a Feedback Variable Phase Function generator, type TWG 500 running at just over 1 k.Hz. (adjusted to avoid any beats with the mains frequency). The 10 V. square wave (and anti-phase output) went to the Driving circuit (Fig. 6.19) and the 2 V. output (no phase change in the generator) went to the Switching circuit. The mark-space ratio of the signal from the generator was 1:1 and there was no need to divide by two to improve on this.

The input to the Switching circuit (Fig. 6.25) went to a Schmitt trigger circuit (7413) which went to a binary $\div 32$ circuit (7493 & 7474) with an optional further $\div 2$ (not used). Thus the output was a ~ 30 Hz. square wave which went to an Exclusive OR gate (7486) with the original frequency from the trigger, to give an output which was an inversion of the clock pulse every alternation of the 30 Hz. pulse. This signal went to the Multiplier. The 30 Hz. wave also went to an amplifier giving an output for the frequency stepping circuit of Fig. 6.14. There was a test point on this line which could be used to trigger the oscilloscope in synchronisation with the frequency stepping pulse.

If the apparatus was being run in normal mode without the second instrumentation loop, the logic divider circuit could be switched to Reset so that the signal to the Multiplier was the direct clock pulse.

6.10 The Van de Graaff generators

The electrostatic generators were Griffin and George type L81-280 with 17 in. of Perspex insulating column support between upper sphere of 10 in. diameter and lower conductors. The units were modified as follows. As supplied, there was a Perspex lower belt drive and a Polythene upper idler. On one generator the Perspex was run on the

upper position and a Teflon cylinder made to replace the Polythene roller. This gave a positive charge accumulation on the upper sphere for the generator with a Teflon lower roller. The other generator normally collected negative charge on top, although this was somewhat unreliable after the belts had been changed and the weather was warm.

Spun aluminium spheres of 18 ins. diameter were mounted above the original 10 in. spheres to give greater operating area for the static field.

The machines are specified to collect up to 5μ .coulomb of charge, at full speed a current of 20μ .amp. and in ideal, dry, dust free conditions, obtain a 12 cm. spark between the sphere and another sphere. It was thus found necessary to run at a lower field to avoid sparking and this was controlled by adjusting point discharge wires connected to earth and set at suitable distances from the spheres (36 in. and 19 in.)

The first method of operation tried was to set the power to the motors so that, before charging, the motors would run, but when charged the static forces produced enough torque to stop the motor. However, this gave uneven continuity of voltage on the spheres (depending on the amount of charge on the belts) and the method finally used was to run the motors with sufficient power to be always running and move the discharging points.

An infra-red lamp was mounted above the units to direct a warm beam over the volume of the generators and a 100 W. lamp was run beneath to reduce condensation in the air between the generators.

6.11 The Perspex Shutter

Between the main interferometer transmitting aerial and the wire curtain was a shutter of two sheets of Perspex 90 cm. wide by

60 cm. high running vertically in plastic guides and supported by a cord over a pulley the lower end being turned by a 6 V. motor and reversing switch. The shutter oscillated at 0.2 Hz. On the transmitter side of the shutter was a third fixed sheet of sufficient height to always cover the other sheets as they moved, making the first reflecting surface fixed.

The three sheets are close together with 1.5 cm. outer-to-outer surface and thickness of each sheet 0.3 cm. Any wave which is multiply reflected between them will have little effect (compared with the directly transmitted beam) on the phase of the combined wave because it is small in amplitude and extra phase shift.

The combined thickness (0.6 cm.) of the two moving sheets, by equation E6.9, gives a phase change for refractive index approximately 1.5, of:

$$\text{Phase change} = 10^{-11} f \quad \text{E6.13}$$

Where f is the frequency of the radiation.

From Appendix A6.1 it is shown that in theory, if the two sheets are equally spaced with 0.3 cm. air gap, the change in transmitted amplitude when the two further sheets are added, is 0.046. It is surmised that most of the reflected wave was reflected back again by the Aluminium sheet and still reached the receiver. The Perspex absorbs some power which may account for most of the 1/120 amplitude change by the shutter as measured by the radio receiver in section 6.13.

Also there will be some diffraction of waves around the shutter but the amplitude of these is small compared with the main signal.

It may be noted that as the power in the wave is proportional to the square of the field amplitude:

$$P = k A^2$$

The trace on the chart recorder as the aerial was swept in position through the field.

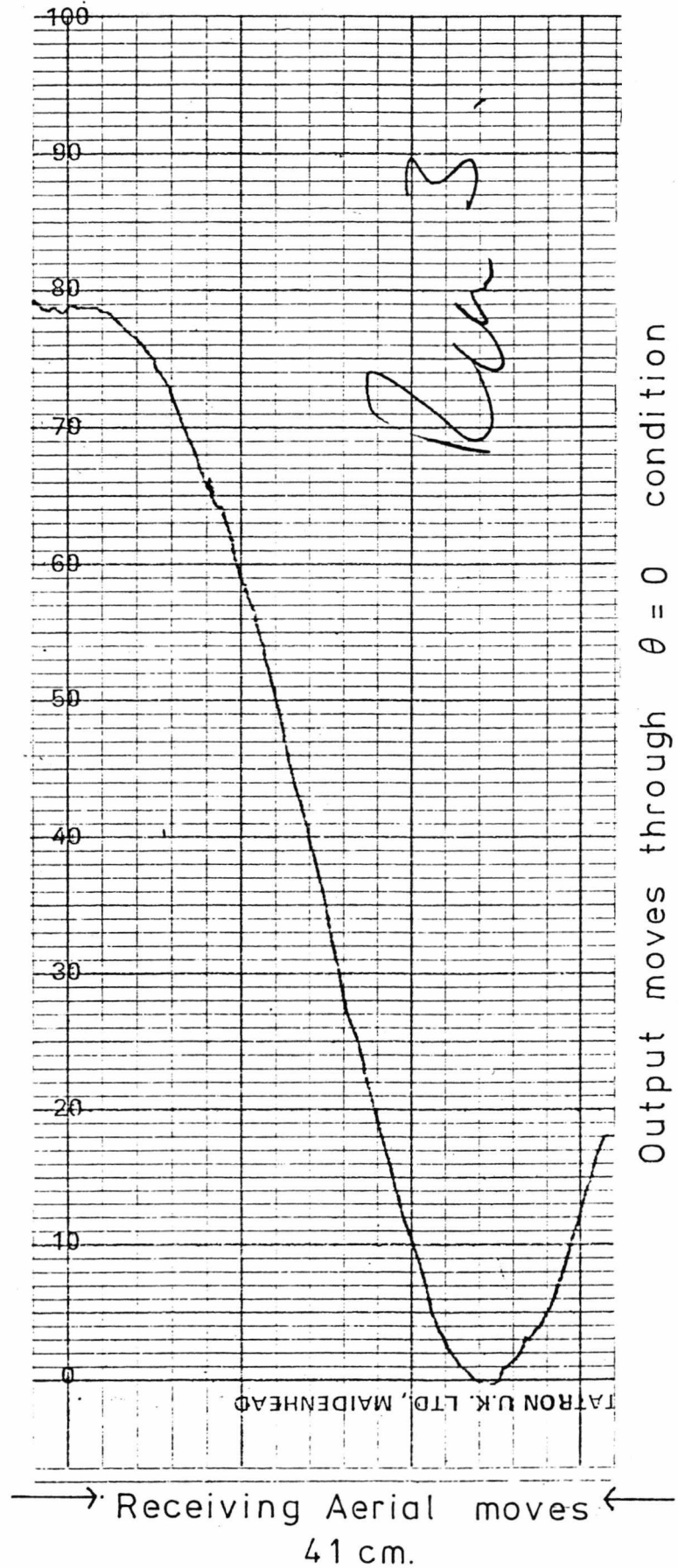


Fig. 6.26

$$dP = 2 k A dA$$

$$\frac{dP}{P} = 2 \frac{dA}{A} \quad \text{E6.14}$$

for small fractional changes in the field.

Thus the combined effect of the shutter at the mixer-detector (from E6.8) is:

$$\frac{\text{Output change}}{A} = \cos \theta - (1 - 0.0083) \cos(\theta - 10^{-11} f) \quad \text{E6.15}$$

This gives a maximum value of output change due to only a phase shift (c.f. E6.20), when θ is:

$$\frac{d(\text{Output})}{d\theta} = A \sin \theta \quad \text{which is maximum if} \quad \text{E6.16}$$

$$\theta = 90^\circ \quad \text{E6.17}$$

6.12 Positioning of the receiving aerial

The receiving aerial was swept in position over a distance of 41 cm. towards the transmitting aeriels. The differentiator was not included in the output filter and a typical result, at 586 M.Hz., is given in Fig. 6.26. Apart from some change in amplitude, the main effect is a variation of phase θ in the equation E6.8. The aerial is swept over the position for which the reference and main signals take the same time, so that $\theta = 0$ and $\cos \theta = 1$. This gives a maximum, and the other extreme is when $\theta = \pi$, giving a maximum of opposite polarity (this can just be seen on Fig. 6.26).

To make the system less susceptible to frequency variation, the aerial was positioned on this maximum where the path times are the same for all frequencies (in practice, an average of this position

over the range of frequencies because of the different ray paths, Fig. 6.10). It may be noted that from equation E6.16, the position of $\theta = 0$ corresponds to the least sensitivity to change of phase. Hence there is a compromise between being frequency insensitive and being phase sensitive.

This measurement is also a measure of the sensitivity of the system as it varies from detecting an average zero of the main r.f. signal to a maximum of a half-wave rectification of the main signal. Thus the amplitude of the Chart recorder sweep corresponds to $2 \times 50\%$ modulation of the r.f. wave.

This measurement was made for each of the final experiment runs. It is a check on the sensitivity measurement made with the Perspex shutter.

6.13 The bandwidth of the aerial

The conical aerial described in section 6.4 set at the end of a Balun, was set at a distance from the reflecting sheet such that it was stagger tuned, to further increase its bandwidth. The Balun is tuned, but, as measurements were made over half an octave at a time, the imbalance at each end was tolerated. The impedance of the conical aerial and Balun at the end of its co-axial cable was measured in a separate experiment, using the slotted line technique, with the grounding plane placed the same distance as was set for one of the final experiments. The measurement was not very accurate as the slotted line had some mechanical variability. The result showed that, at its resonance, the aerial was resistive and matched to the cable. A wide bandwidth was indicated by the plot on the Smith chart of its impedance at different frequencies staying near the centre.

6.14 Method of measuring, approximately, the radio-frequency field

An Eddystone receiver, type S990S, set at one M.Hz. bandwidth, was calibrated at 520 M.Hz. by a signal generator of known (variable) power over a range of input levels from 10^{-5} - 1μ .W. The r.f. and i.f. gains being adjusted each time to give a mid-scale reading. The result was plotted as calibration lines and a check made at 805 M.Hz., using the Spectrum Analyser, which agreed within 4 db.

The field was measured by placing a dipole, attached to a co-axial tuning stub, between the spheres of the Van de Graaff generator, when the length of dipole and stub had been tuned to the measurement frequency. The signal collected was fed to the tuned receiver and measured against the above calibration. The field strength was calculated by the equation:

$$\text{Power} = \frac{1.6 \lambda^2}{4 \pi} \frac{\bar{E}^2}{120 \pi} \quad \text{watt} \quad \text{E6.18}$$

where \bar{E} is the field in Volts/m.

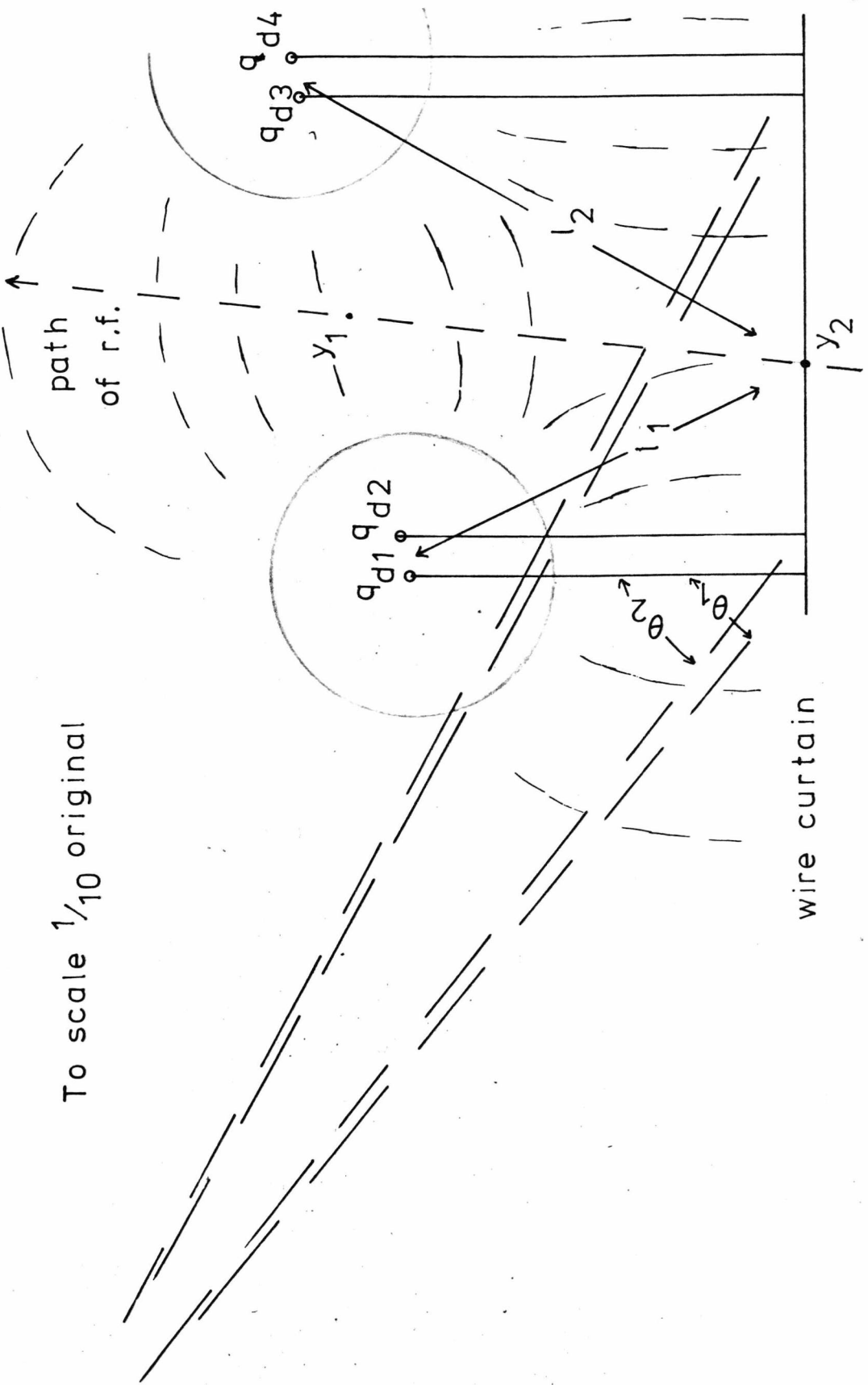
It was determined that the receiver meter reads in proportion to field strength and, with the Perspex shutter running, it was just possible to measure a variation of about 1/120 in field strength caused by the shutter movement.

The 3 db. bandwidth of the signal in the G.R. generator was measured on the Spectrum Analyser and was less than 1 k.Hz. at 500 M. Hz. (the minimum bandwidth measurable by the Analyser).

6.15 Method of measuring the electrostatic field

The voltage on the Van de Graaff generators was measured by a detector consisting of a 16 cm. diameter disc of Aluminium, with alternate quadrants removed, and fixed to a small motor so that it could be spun in front of a fixed single quadrant. This latter was electrically isolated and connected by a co-axial cable to the 1 M.ohm. input at the

+ Y Measure



Scale plan of the relative positions of the field detector and the equivalent charges generating the field of the Van de Graaff generators.

Fig 6.27

oscilloscope. Thus the quadrant picked up a chopped voltage measure of the field. For low signals (below 0.05 V.), the mains hum also picked up had to be compensated for.

The instrument was calibrated by connecting a single Van de Graaff generator to a known voltage supply. With 60 k.V. connected to the sphere, a series of readings was taken over distances from 2 to 5 ft. Plotted on log-log paper of signal versus distance to the centre of the sphere, a straight line of gradient -2 was obtained except for distances less than 2.5 ft. This was extrapolated to 5.75 ft. from where the measurements of the generator under its own power were made.

A detector signal was measured at a fixed distance of 3.25 ft. for a range of values of the sphere voltage of 10-80 k.V., giving a straight line as expected. Hence a calibration graph was obtained for which typically, a signal of 0.16 V. corresponded to 210 k.V.

The theory of the field around the spheres and screening curtain (shown in a scaled diagram in Fig. 6.27) is given in Appendix A6.2. This relates the potential, V , as measured by the detector assuming an inverse square law, to the field between the spheres for the condition that they have equal and opposite voltage, as:

$$E_{\sim \text{Max, between spheres.}} = 8.7 V \quad \text{E6.19}$$

where the detector is at a position to the dipole corresponding to $\theta \sim 50^\circ$, and $r = 5.75$ ft.

In practice the detector was used in this position to measure the field which was mostly determined by the voltage of the sphere on the side nearest to the detector. The detector was also used in an approximately corresponding position on the other side to measure the field that was mostly determined by the voltage on the sphere on that side. These measurements gave an indication of the actual relative voltages on the two spheres (the calculation of Appendix A6.2 assumes

that they are either the same or one sphere is earthed). These measurements were only intended as order-of-magnitude estimates.

At the end of each of the final experiments, this measurement was made of the Van de Graaff voltages.

Chapter 6

Part II - OPERATION OF THE EQUIPMENT AND THE
RESULTS OBTAINED

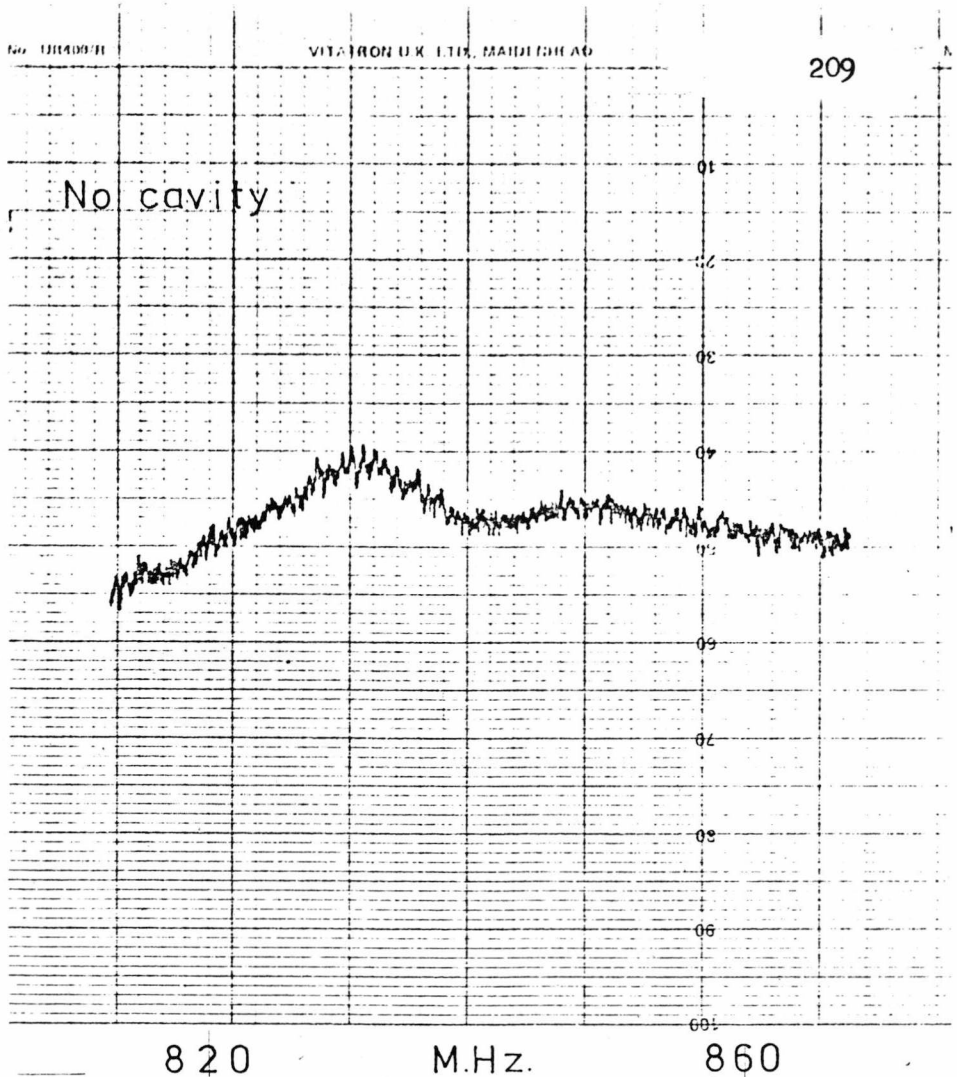
Note

The second part of this chapter has been set under a heading of its own to make clear that the results of the experiment are to be found here. Section 6.16 presents the graphical result of finding a resonance using, however, a metal cavity as an analogue of the resonance looked for in the main experiment. Section 6.17 presents the important results of calibrating the sensitivity of the equipment and so indicating the smallest signal that could be detected in each run. Sections 6.18 and 6.19 tabulate the frequency ranges and field amplitudes occurring in each run and tabulate the final results.

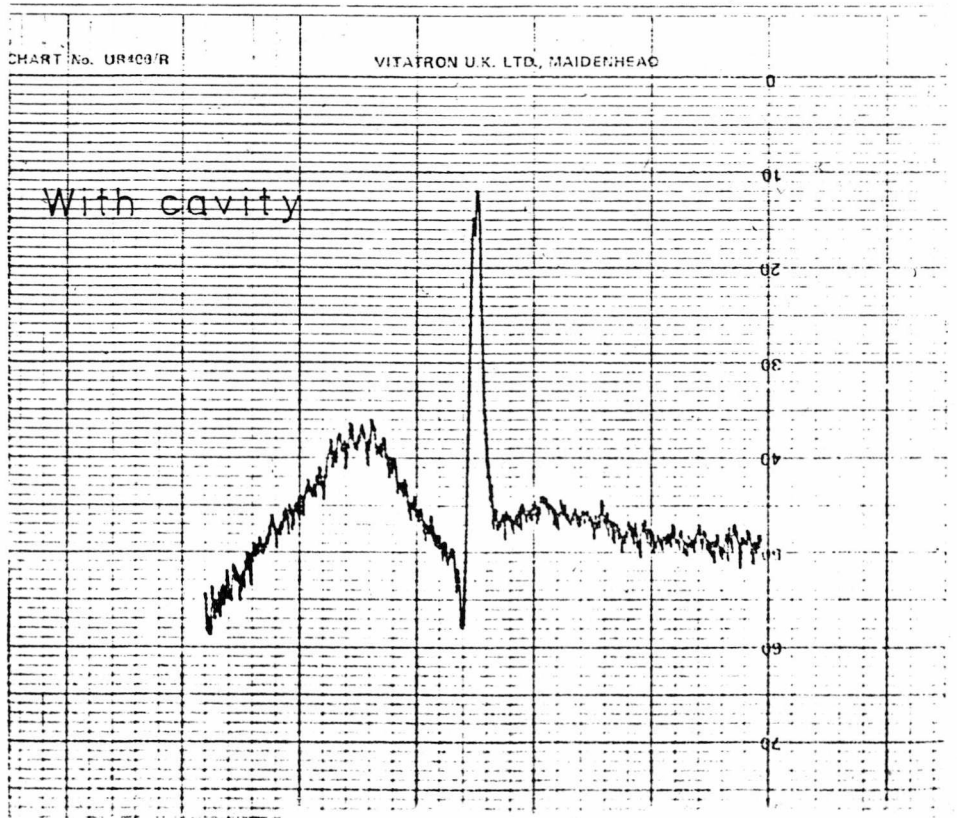
6.16 Experiment to simulate the resonance being looked for

To demonstrate the operation of the instrumentation, the outputs from the Alternator were connected through -20 db. attenuators to a T junction at the input of the Mixer, by cables of the same length as the reference cable, thus replacing the aerial system by direct cables. To simulate the narrow spectral response of the phenomenon being looked for, a brass cylindrical resonant cavity with current loop input and output across one end, was connected in series with one of the cables from the Alternator. The co-axial cavity was 8.5 cm. long by 3 cm. diameter with a 1 cm. diameter adjustable central conductor (it may be said to differ from the rig for Ball lightning in that very little power was transmitted across it except at resonance. However, it simulated a variation at resonance). The transfer function of the cavity was measured on the Polyskop and had a 3 db. bandwidth of about

No cavity

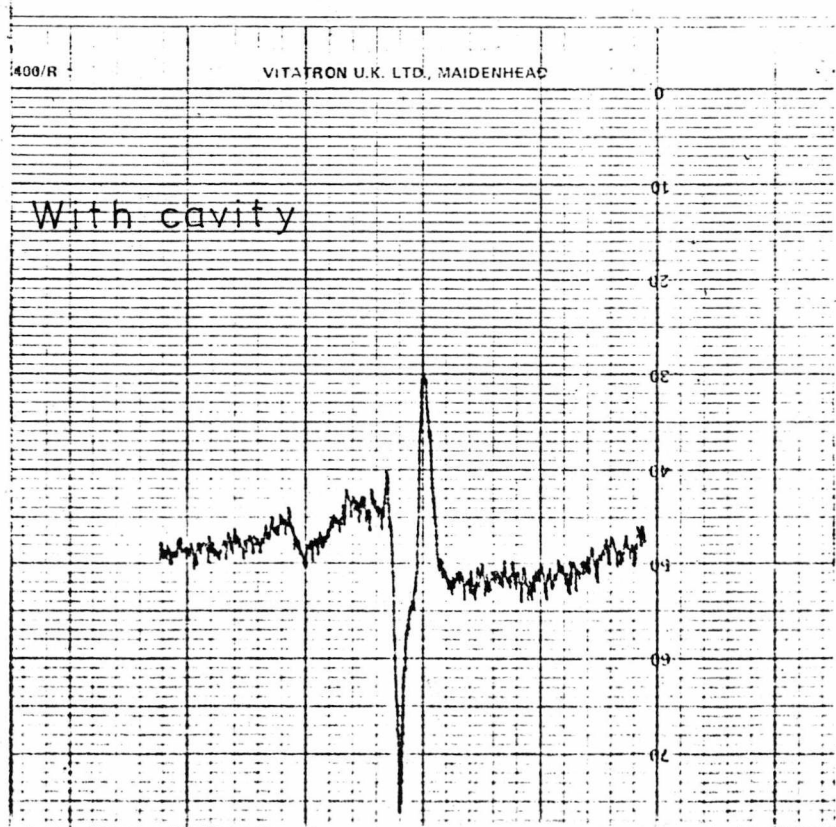
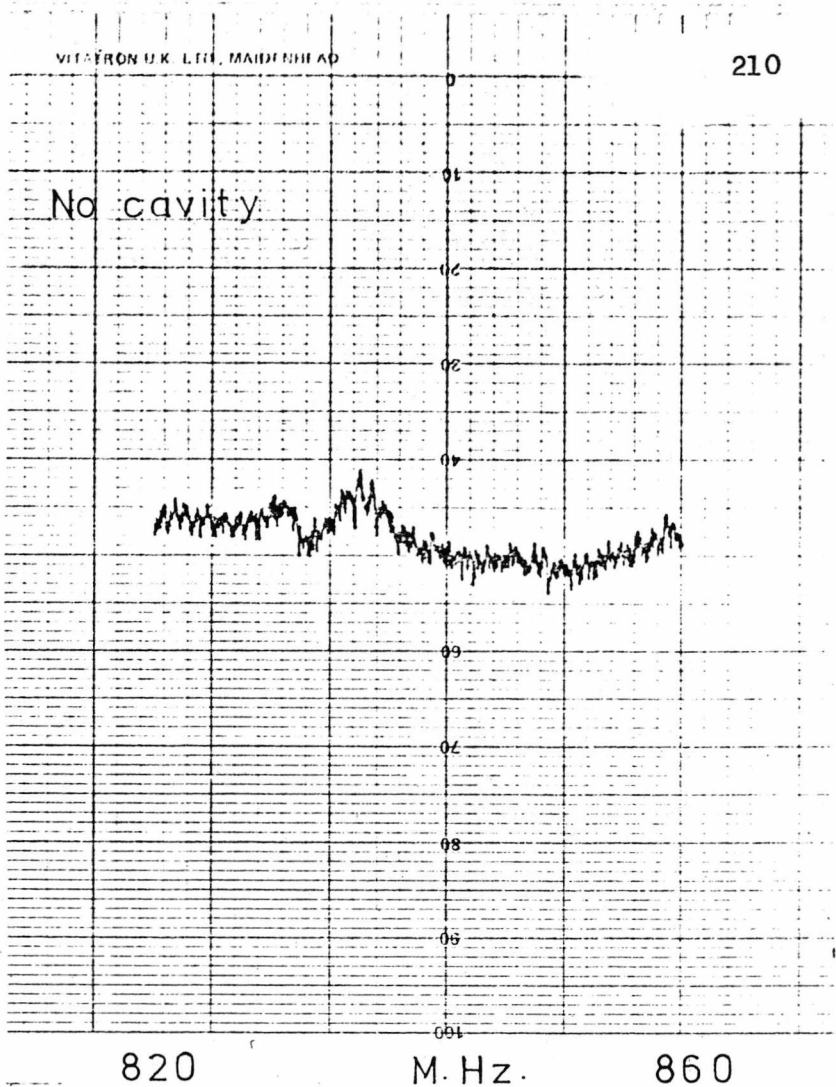


With cavity



Recorder traces obtained in the simulation run with no frequency stepping, showing the resonant peak.

Fig. 6.28



Recorder traces obtained in the simulation run with frequency stepping, showing the double peak as the frequency went through the resonance.

Fig. 6.29

1.5 M.Hz. at 810 M.Hz. giving a $Q \approx 560$. (Hence in E6.7, $\text{step}_{3\text{db}} = 0.75\text{MHz}$)

The instrumentation was run normally over 820-860 M.Hz., with and without the cavity except that the scanning speed was faster at 4:1 gears setting and the recorder speed correspondingly increased to 1 cm./ min. (the Filter differentiator time constant was reduced by 10 times).

Fig. 6.28 gives the result without the second instrumentation loop (no frequency stepping), with and without the cavity. It shows the expected pulse over the resonant frequency.

Fig. 6.29 gives the result with the frequency stepping, with and without the cavity. It shows the characteristic double pulse which has just been resolved into separate pulses with this value of Q and amplitude of the frequency step (2.6 M.Hz.).

The cavity transferred no power out of resonance and -10 db transfer at the peak of resonance.

6.17 Calibration

The sensitivity of the instrumentation could be adjusted at the following points:

- i. A $\times 1$ or $\times 0.1$ attenuator on the main signal input to the Multiplier.
- ii. The gain at the main signal input to the Multiplier.
- iii. At the Chart recorder-
 - a) By one of three switched attenuations (section 6.8).
 - b) By $\times 1$ or $\times 5$ at the recorder input.

The method of calibration was to run the Perspex shutter with the output filter adjusted for the one frequency (Fig. 6.23), and set the above gains to give a suitable amplitude over the frequency band. The scan was made in 100 min. with the gear box stepping up 4:1, and the recorder running at 2 cm./ min.

Overall sensitivity calibration - RUN 1

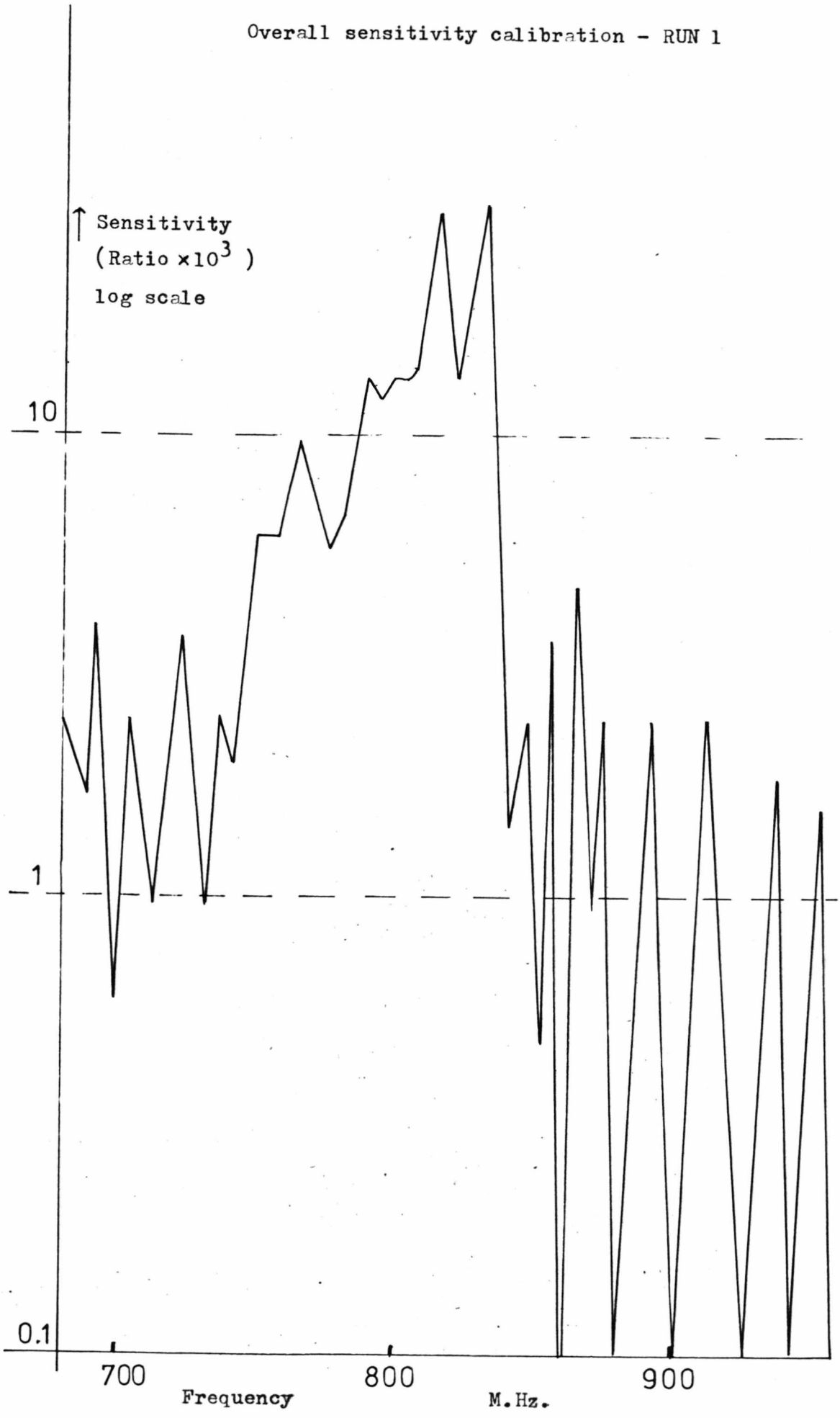


Fig 6.30(a)

Overall sensitivity calibration - RUN 2

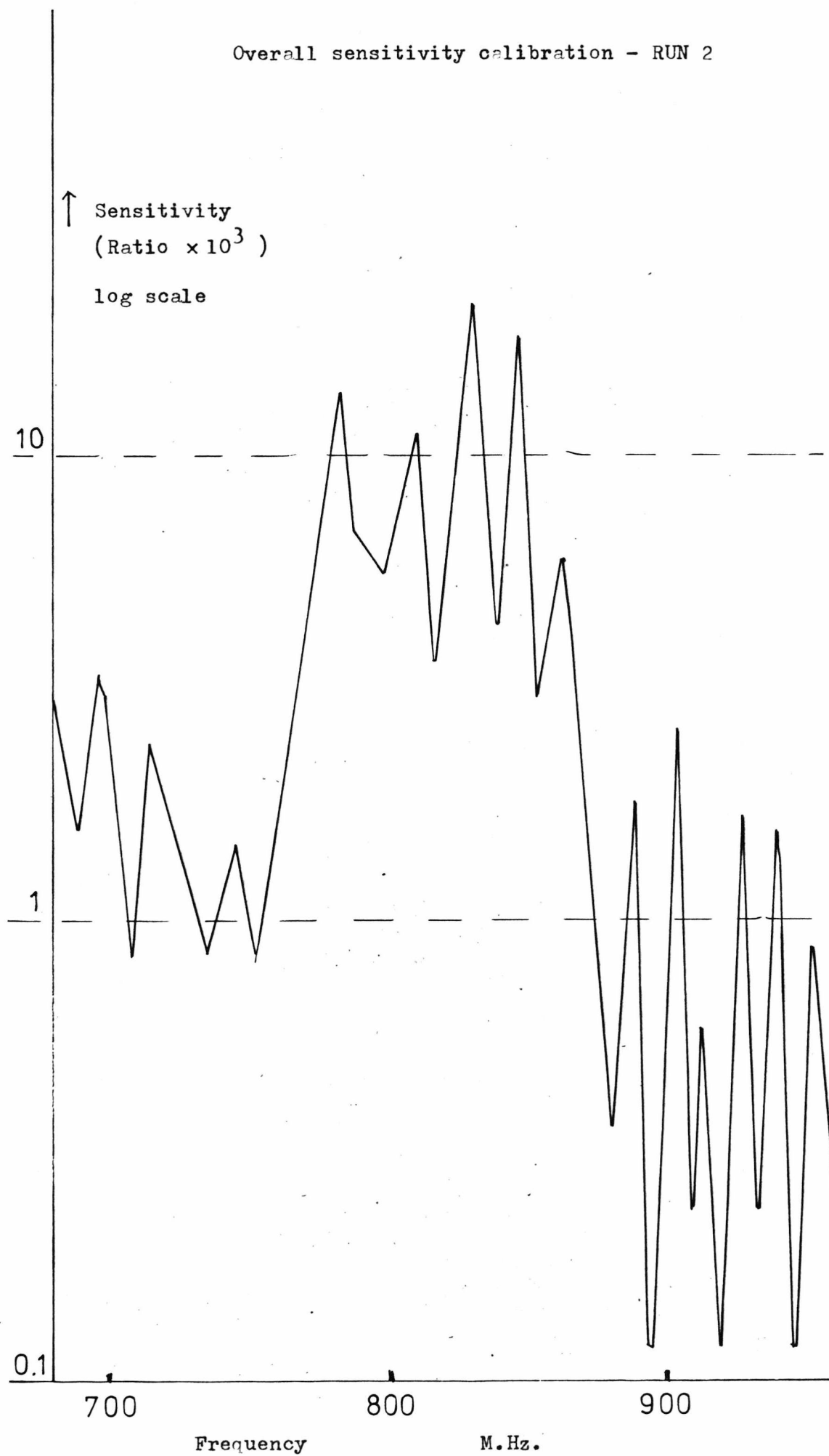


Fig 6.30(b)

Overall sensitivity calibration - RUN 3

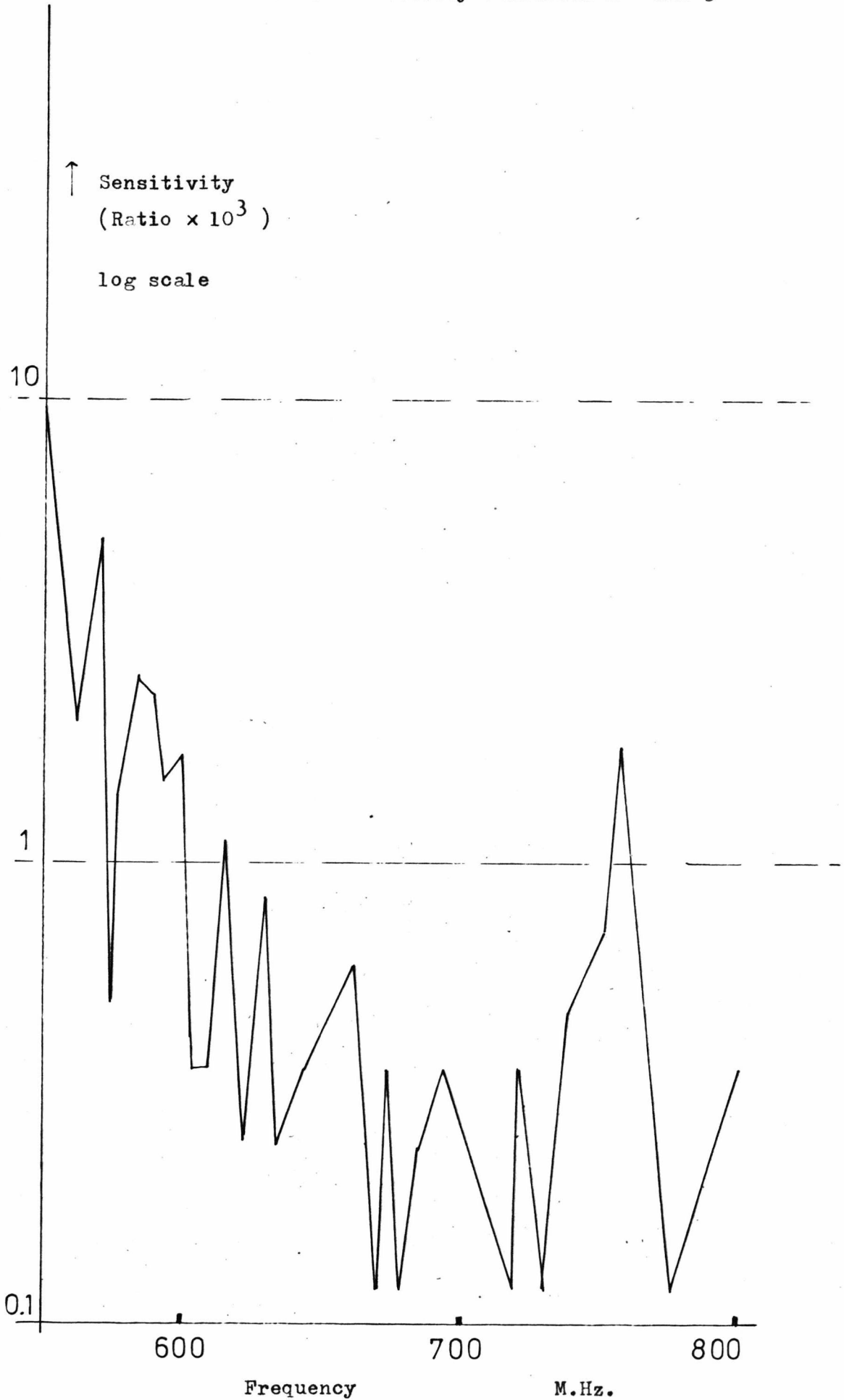


Fig 6.30(c)

Overall sensitivity calibration - RUN 4

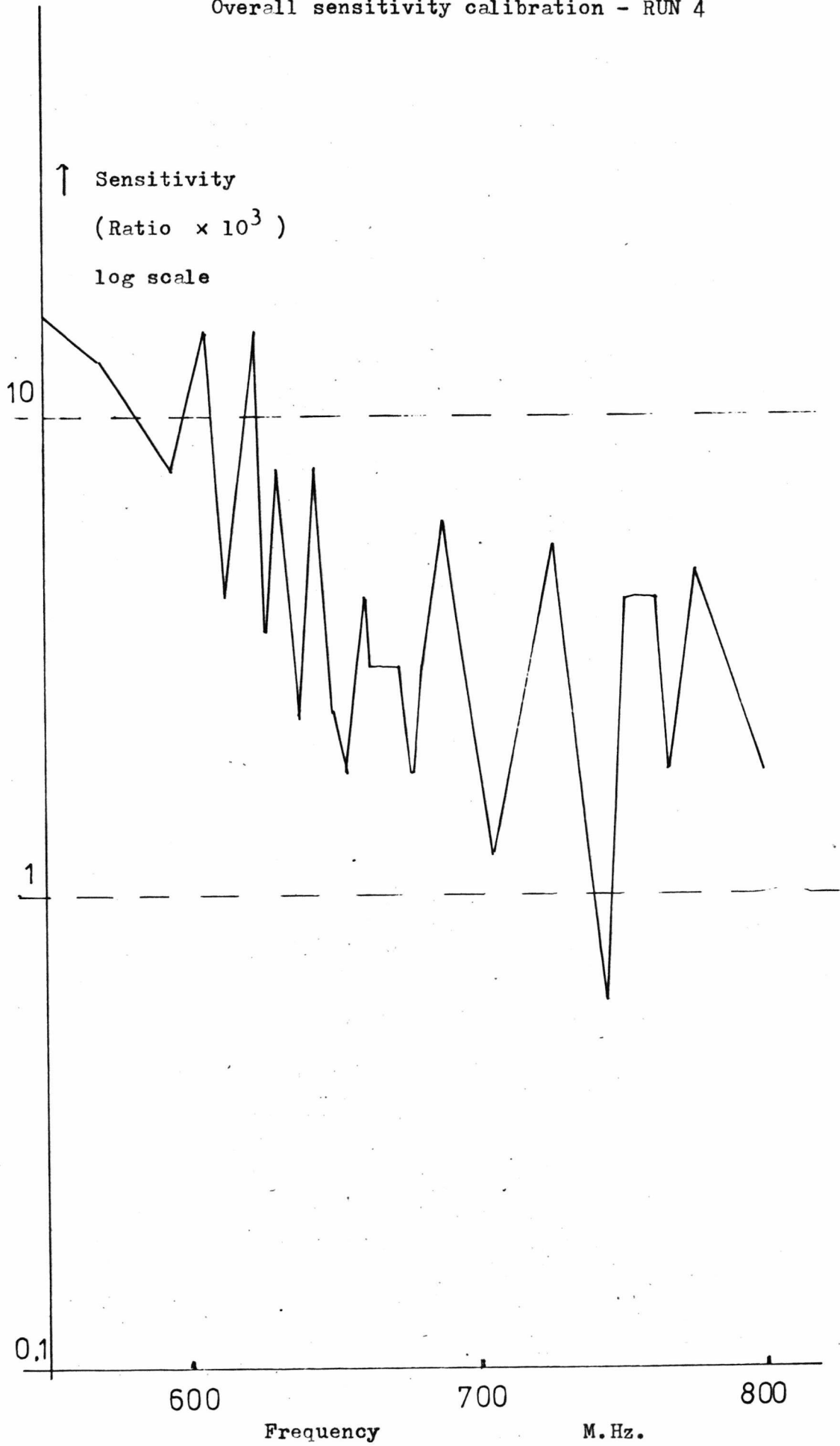


Fig 6.30(d)

Overall sensitivity calibration - RUN 5

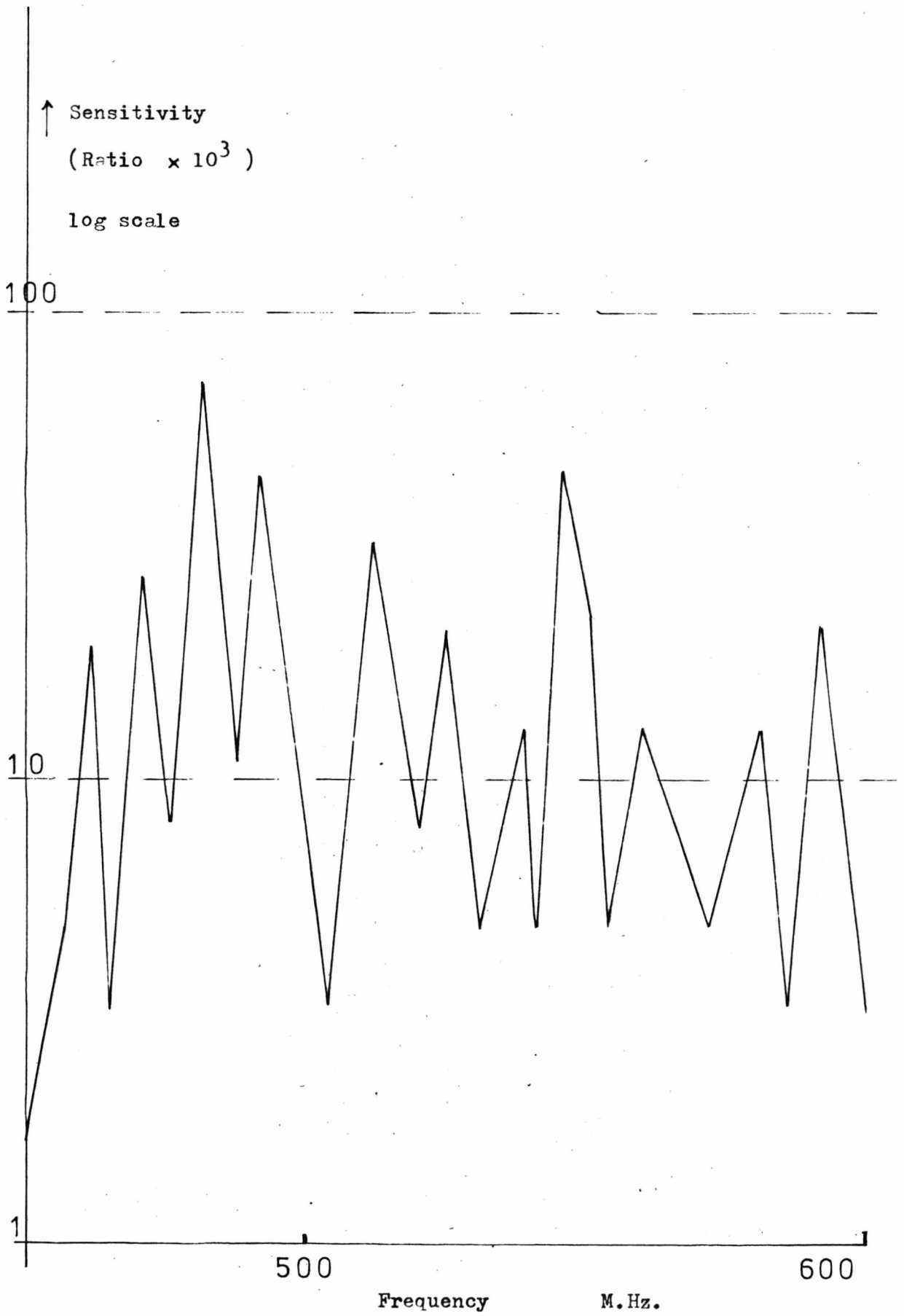


Fig 6.30(e)

The instrument sensitivity was increased a known amount by the above controls. The amplitudes of the recorded calibration trace at a number of frequencies over the record, were measured and multiplied by the above increase in gain for the final measurement. This was multiplied by a further 120 to give the output signal that would be caused by 100 % r.f. amplitude modulation. It was assumed that the major effect of the shutter given by equation E6.15, was a change of amplitude unless θ approaches 90° when the amplitude of the detected signal has become small:

$$\begin{aligned} d(O) &= \frac{\partial(O)}{\partial A} dA + \frac{\partial(O)}{\partial \theta} d\theta \\ &= (\cos \theta) dA + (A \sin \theta) d\theta \end{aligned} \quad \text{E6.20}$$

Where:

$$O = \text{Output} \propto A \cos \theta \quad \text{from E6.8}$$

The result for each Run is plotted in a series of Figs. 6.30, where there is a factor of 10^3 to go with the amplitude scale. The dashed line at 1×10^3 is the level above which a change of $1:10^3$ of the field amplitude could be detected.

It may be assumed that a signal of about 1 cm. could be distinguished above the noise on the final charts for the single instrumentation loop measurements. Hence the reciprocal of the reading on Figs. 6.30 is the fraction of full amplitude modulation which would cause a fluctuation that could just be detected.

Usually the gain for the stepped frequency measurements was reduced by 0.1 but the resulting trace was finer and allowed a smaller fluctuation to be recognised. this gave an effective reduction in sensitivity of about 0.3.

6.18 The Experimental Method

Before the calibration run the aerial distances and Van de Graaff positions had been adjusted to balance the interferometers as far as possible to reduce the amplitude of the main signal stepping at the clock frequency, over the band of frequencies being analysed. The Baluns were checked by earthing each side of the dipole in turn which should give the same effect on the impedance, as measured on the Polyskop.

The gain on the reference signal to the Multiplier was set at maximum. For each experiment, the output filter was set with the time constants given in section 6.8, and after a trial run, the gain at the recorder and Multiplier inputs set to suitable values. The reference signal to the Multiplier was monitored on the oscilloscope while the 'scope was triggered by mains frequency. The Clock pulse generator frequency was adjusted to give lack of synchronisation with mains hum.

The average scanning rate is given in the Run records of Fig.

6.31. and this determines-

- i. For the frequency stepping experiment, to resolve both peaks (assumed very narrow) of the double pulse, the frequency scan in time equal to the recorder settling time (about 0.2 sec.) should be less than the step in frequency.
- ii. If the bandwidth of the signal generator is B k.Hz., and the scan rate M/T_{sc} M.Hz./min., the time to scan the convolution of an impulse with the G.R. spectrum is:

$$\text{Time} = \frac{T_{sc} B 60}{M} \quad \text{m. sec.} \quad \text{E6.21}$$

which is the duration of the pulse being looked for.

- iii. As observed in section 6.2, the frequency step should be greater than the bandwidth of the pulse to be detected if both peaks of the double pulse are to be resolved.

Electrostatic fields -

Run	k.V. on isolated Van de Graaff sphere generating same field at detector as was measured (approx the actual k.V. in experiment)		Case	Total field at		Field normal to r.f. path
	Outer	Inner		y_1	y_2	k.V./m.
1	-150	+120	2	944		905
			(3		161	11)
2	-120	+120	2	840		804
			(3		143	10)
3	-190	+120	2	1084		1039
			(3		185	13)
4	+200	0	1	584		565
5	0	+120	1	350		339

The r.f. fields and detected signals -

Run	From M.Hz.	To M.Hz.	Amp. by Aerial scan. cm.	Gain reduction for F.S.	Av. scan rate Hz./sec.	r.f. pre-amp	Max. r.f. field m.V./m.	Frequency Band
1	680	960	2.5×10^3	0.1	5.6	In	9	} 1
2	680	960	2.5 "	0.069	5.6	In	9	
3	550	800	1.6 "	0.5	5.0	In	10	} 2
4	550	800	0.73 "	0.1	5.0	Out	20	
5	450	600	5.3 "	0.042	3.0	Out	25	3

When going from the N.F.S. measurements to the F.S. measurements, the instrumentation gain was reduced by the factor in the column headed 'Gain reduction for F.S.'.

Tabulation of the results, showing the conditions for each Run.

Fig 6.31

The recorder ran at 0.25 cm./ min. and the gear box stepped down by 1:2. The recorder and scanning motor were set running at the starting frequency on the G.R. generator, in the evening and stopped at the finishing G.R. frequency about 14 hours later the following morning. After each experiment the overload lights were checked and the Van de Graaff voltages measured.

Each Run, for the same setting of the aerials, consisted of:

- i. A calibration measurement.
- ii. A measurement with no frequency stepping and no electrostatic field.
- iii. Three or four measurements with the electrostatic field and no frequency stepping.
- iv. A measurement with frequency stepping and no electrostatic field.
- v. Three or four measurements with frequency stepping and electrostatic field.

A summary of the record sheets for these is given in Fig. 6.31. The resulting traces were numbered and given an indication of frequencies by numbering off from an elastic ruler which had been calibrated from measures on the G.R. dial and stretched to cover the band on the Chart paper.

For the first three Runs, the electrostatic voltage was assumed to be of polarity as recorded in Fig. 6.31 and indeed started this way when measured at the beginning. The fact that occasional sparks crossed between generators tends to confirm this, but later runs after the belts had been changed, make it possible that the polarity changed overnight. For later Runs, only one generator was at voltage. The value of the electrostatic field over the measurements of a Run is only intended as an indication of the approximate value as this unregulated unit was not steady.

Example of traces showing a possible pulse (without the frequency stepping)

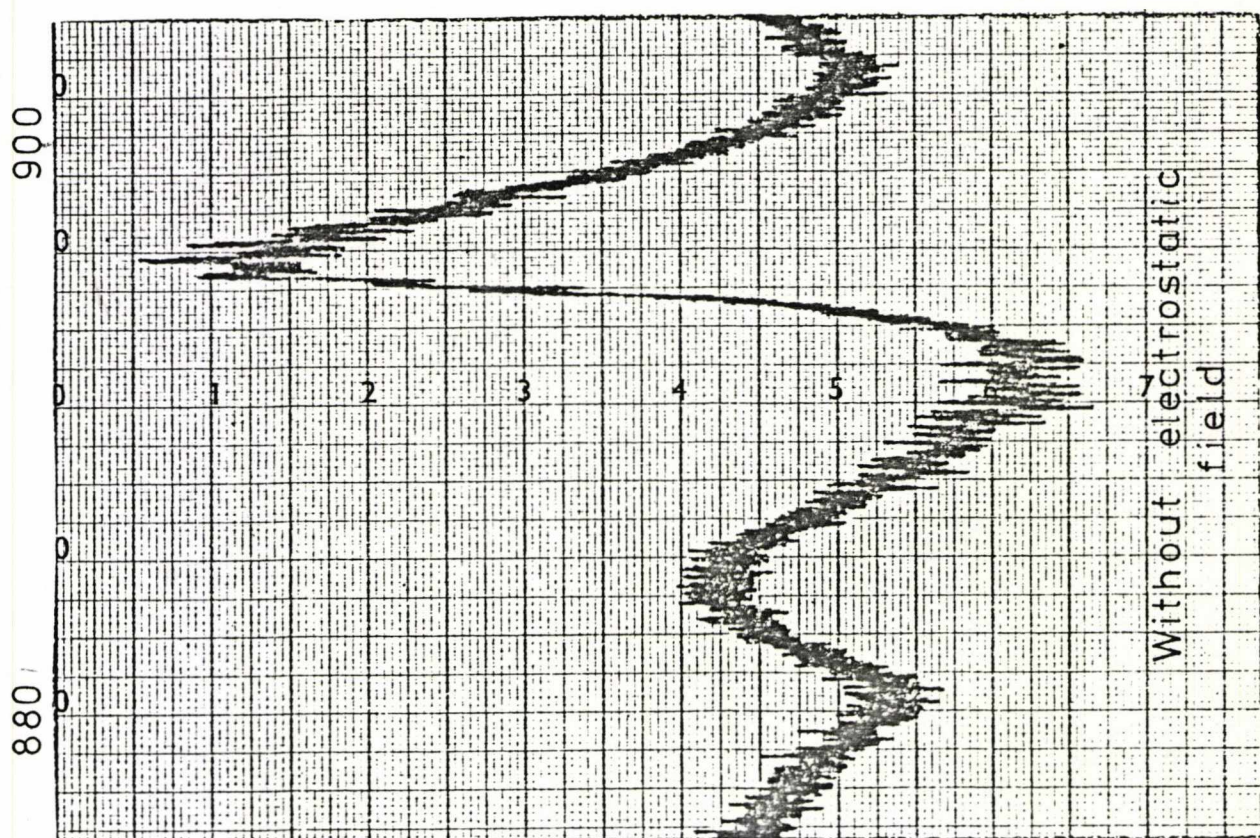
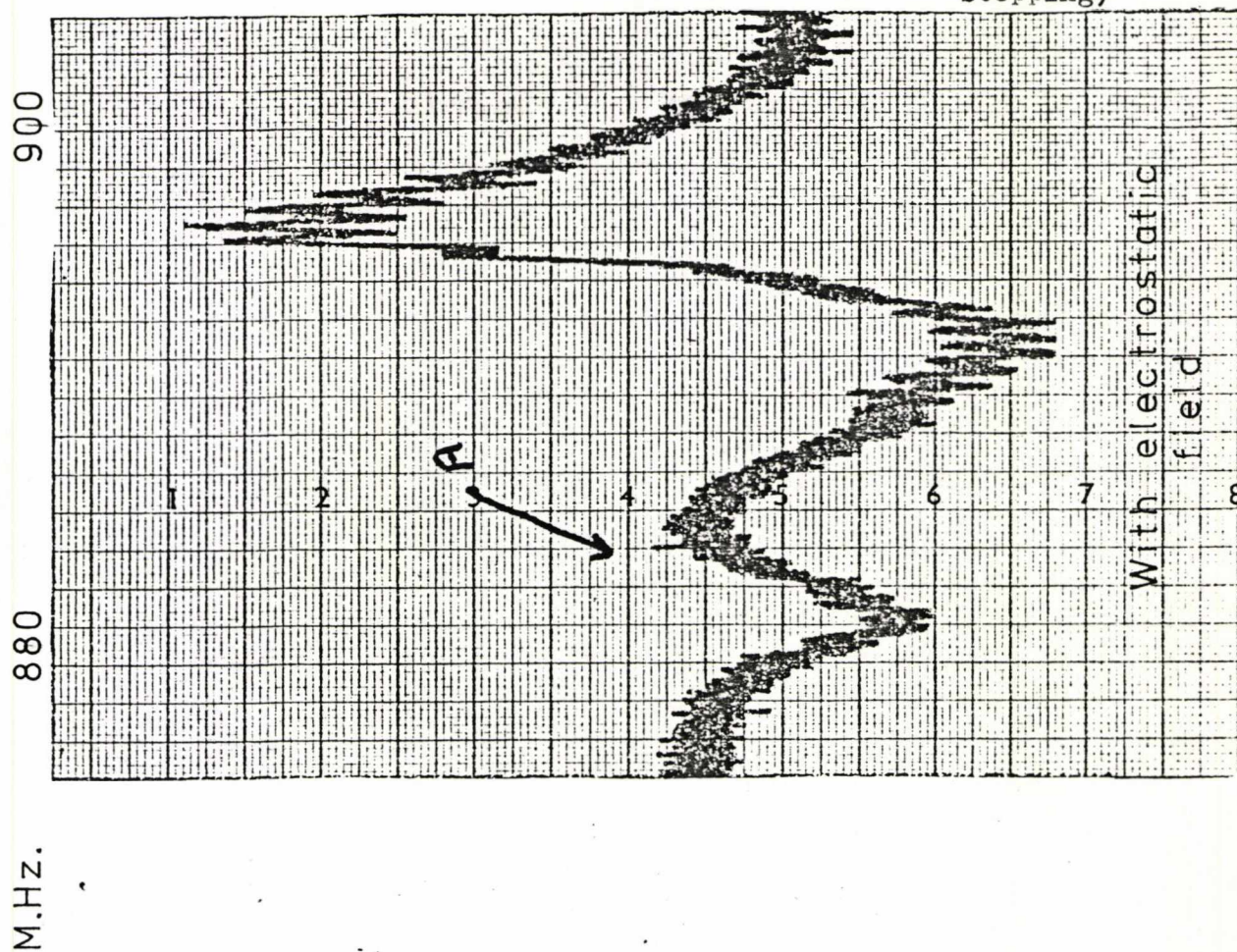
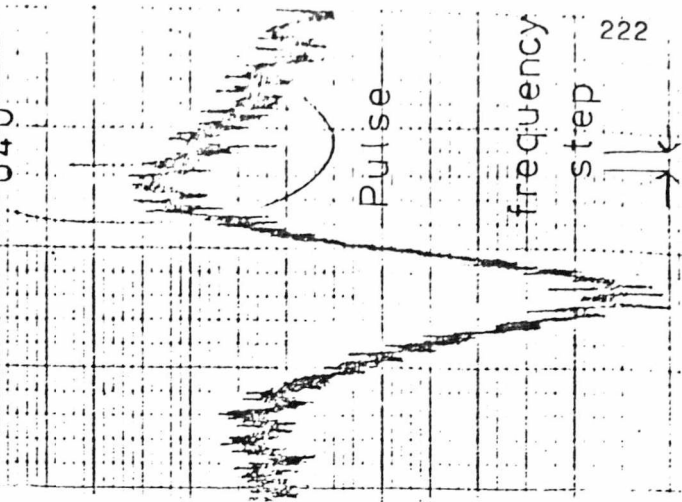
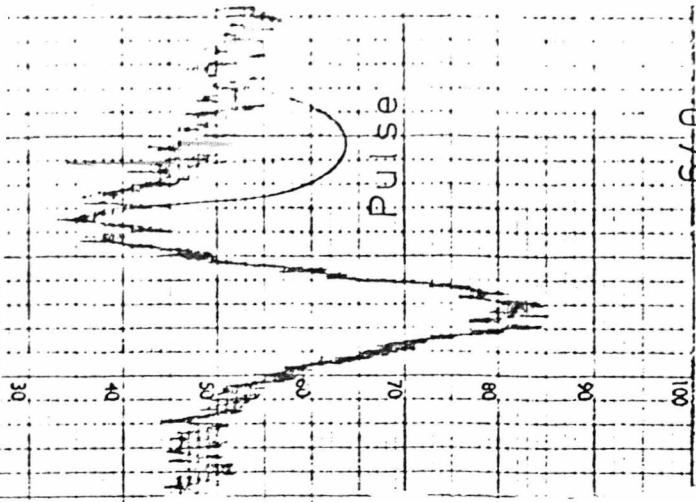


Fig 6.32



Example of traces showing a possible double pulse (with frequency stepping).

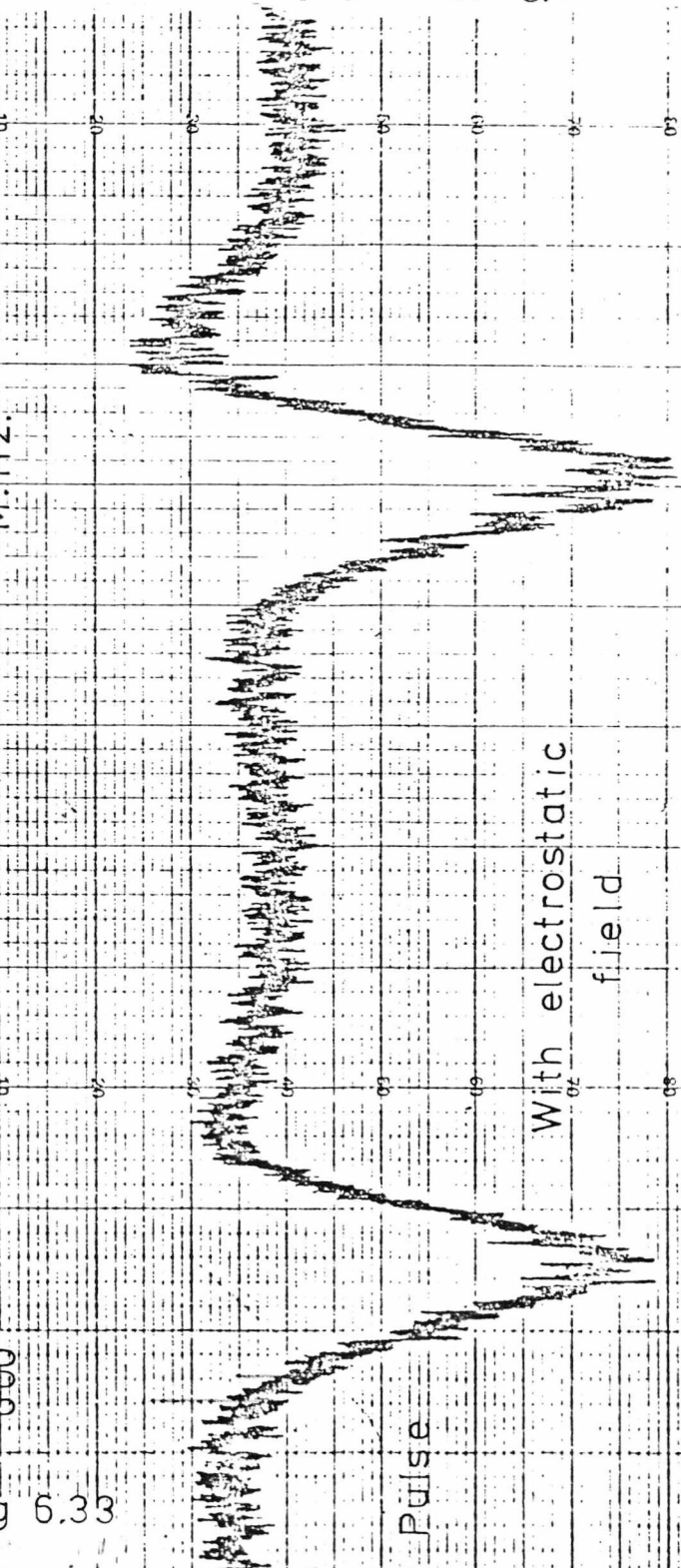
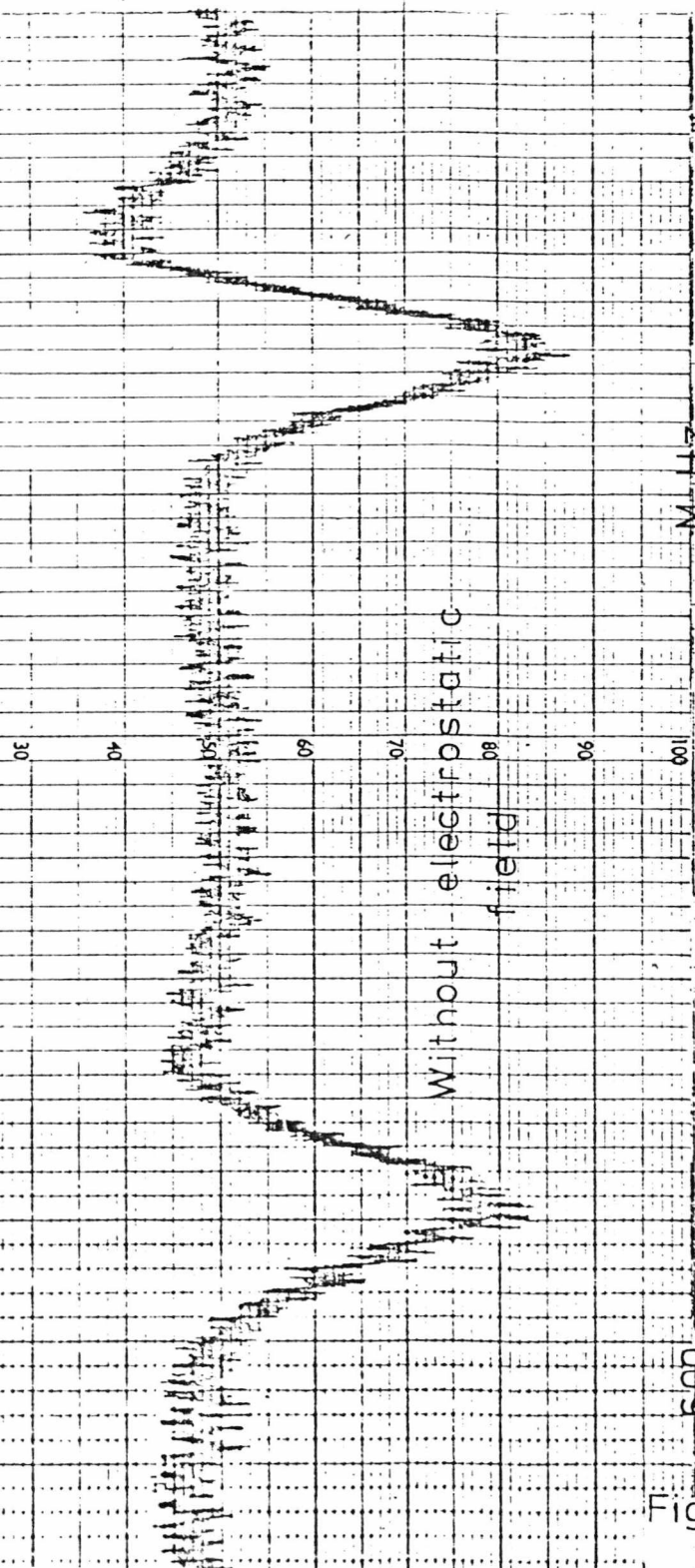


Fig 6.33

<u>RUN 1</u>	M.Hz.	Chart Nos.	
N.F.S.			
	880	6(a),6(b),4	Very small peaks.
F.S.			
	795	8,10(a),10(b)	Suspicion of overloading. blank trace not good.
	940	8,10(a),10(b)	"
 <u>RUN 2</u>			
N.F.S.			
	None		
F.S.			
	818	18,19	A step, not a pulse.
	770	17(a),17(b)	
	850	"	
	880	"	
	905	"	
 <u>RUN 3</u>			
N.F.S.			
	578	26,27,28,29	A good result
F.S.			
	590	39,38,33	Appear to be single pulses
	605	39,33	Double pulses.
	730	33,38,39	Appear to be single pulses.

The results of looking for pulses on the chart recorder traces.

Fig. 6.34(a)

<u>RUN 4</u>	M.Hz.	Chart Nos.	
N.F.S.			
	580	43,50(no e/s)	Noisy
F.S.			
	620	48,49	
	720	49	Suggestion of pulse on No.46(no e/s)
	765	48	Very small double pulse.
<u>RUN 5</u>			
N.F.S.			
	470	54,55,56,65,66,68	Could be from the instrument.
	583	54,55,56,65,66,68	Probably on 67 (no e/s) also.
F.S.			
	495	58,59,61	Not clear that the pulses do not occur on the no e/s trace also.

The results of looking for pulses on the chart recorder traces
(continued).

Fig. 6.34(b)

Comments

Run 1.

This Run still had instrumentation deficiencies. In particular the overload indicator was not used for some of the first measurements of this Run, making the F.S. trace of limited use, and the blank F.S chart poor.

Run 2.

All F.S. pulses appearing on the same two traces (the same paper used twice with different colour of ink).

Run 3.

The N.F.S. pulses are consistent enough to require an explanation but are not confirmed by Run 4, which indeed has a possible pulse on the no electrostatic (e/s) trace.

Run 4.

A higher noise level on the traces.

Run 5.

Noisy traces about the 510 M.Hz. region on N.F.S.

Comments on the chart recorder traces for each Run.

The amplitude by aerial scan, is the size of trace that would by extrapolation have been obtained on the final measurement without frequency stepping trace, when the aerial was scanned in position to give $\theta = 0$ to 180° . It indicates the sensitivity to full modulation of the r.f. wave.

6.19 Results

The abbreviations N.F.S. for 'no frequency stepping' and F.S. for 'frequency stepping' will be used to distinguish the measurements made with only the first instrumentation loop from those with the complete instrumentation.

The charts were accumulated in Run batches and then spread out next each other for similar conditions to compare those with and without the electrostatic field.

Fig. 6.32 is an example of a section of the chart N.F.S. from Run 1. It shows a pulse (labelled A) occurring with the electrostatic field but not without it (the noise level on the charts for later Runs N.F.S, was greater).

Fig. 6.33 is an example of a section of the chart F.S. It shows a pulse (which should be doubled on the alternate side of the trace) occurring with the electrostatic field and not without it. It also shows a double pulse occurring on both traces. This latter happened a number of times during the Runs and is assumed to be either a U.H.F. transmitter or, possibly, mode switching in the G.R. generator.

A summary of each Run is given in Fig. 6.34. which records, in general, for each Run when a pulse occurs on two or more charts at the same approximate frequency, with the electrostatic (e/s) field and none without the e/s field. Comments are given in Fig. 6.35.

It seems strange that a number of pulses occur on F.S. but not

on N.F.S. which has at least ten times more sensitivity. Also the F.S. pulses often lack a double.

6.20 Conclusion

There are a number of causes of random pulses including sparking of the Van de Graeff and mains noise.

The probability of a chance coincidence of pulses on two or more traces may be obtained by considering the traces as issuing from n separate records running in parallel. Given that a pulse occurs on record 1, the probability of a pulse occurring on any of the other records in time ΔT may be obtained by summing the Poisson distribution for the remaining traces (in this case, the same distribution over $n-1$ records). The probability of a pulse on at least one of the $n-1$ records within time ΔT is (Cox and Miller⁽¹⁹⁾, 1965):

$$\text{Prob} = (1 - e^{-\rho \Delta T}) \quad \text{E6.22}$$

Where ρ is the rate occurrence for the combined distribution and is $(n-1)$ times the estimated rate of pulses for each run obtained by counting the pulses on the charts and dividing by the time.

For the case of the N.F.S. charts in Run 3, there were estimated 72 random pulses on 4 charts. Thus the average combined rate of occurrence for 3 charts is:

$$\text{occurrence rate} = \frac{3}{4} \frac{72}{T_{sc}}$$

Where T_{sc} is the time of recording. Then:

$$\rho \Delta T = 78 \frac{\Delta T}{T_{sc}} \quad \text{where} \quad \frac{\Delta T}{T_{sc}} = \frac{1}{120}$$

is the resolution of the recording. From equation E6.22, the probability of coincidence, within ΔT , on two charts is 0.36.

It may be observed that there were pulses on all four traces. The probability of this is the probability of it occurring for each of the (n-1) records simultaneously:

$$\text{Prob}_{\text{coin}} = (0.36)^3 = 0.047 \quad \text{E6.23}$$

Equation E6.21 gives the time duration of the pulse looked for. If this is short compared with the output filter time constant T_f the pulse will be attenuated according to E6.2 by:

$$\frac{T B 60 \times 10^{-3}}{M T_f} \quad \text{E6.24}$$

Which is equivalent to a reduction of sensitivity (Fig. 6.34) by this factor.

A main criticism is the instability of the Van de Graaff generator. These were not as well constructed as could have been obtained (the particle accelerator Van de Graaff units are stable to 1:1000). If the resonant frequency looked for varies with the electrostatic field amplitude, the resonance could be at very different frequencies for each measurement.

The fastest scanning rate (Fig. 6.31) was 5.6 k.Hz./ sec. and assuming the G.R. generator bandwidth was 0.1 of the 1 k.Hz. which was the minimum that could be measured on the analyser, the time for the pulse was, say, 0.018 sec. (the sidebands due to the stepping, E6.5, would give repeated pulses at diminishing amplitudes at 0.18 sec. intervals). The break frequency of the Chart recorder was 2 Hz., corresponding to a time constant of 80 m.sec. Thus the pulse being looked for was attenuated in amplitude according to equations E6.2 and E6.4 (Fig. 6.5) by:

$$\frac{e^{-T/T_f} - e^{-T/2T_f}}{e^{-T/T_f} - 1} \left(\frac{T_p}{T_f} \right) = 0.11 \quad \text{E6.25}$$

Where:

$$T_p = 18 \text{ m.sec.} \quad T_f = 80 \text{ m.sec.} \quad T = 1 \text{ m.sec.}$$

This has been calculated assuming a single break frequency of the output filter. In fact, on going to higher frequencies, there will be more and more breaks added for each component of the system, giving far greater attenuation of pulses composed of higher frequencies.

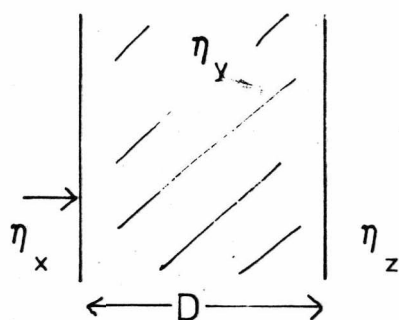
The conclusion to this preliminary experiment is as follows. The investigation was performed over the range of frequencies 450-930 M.Hz., such that a change of amplitude or phase of the received signal, caused by the presence of the electrostatic field, would have been detected if it was such as to constitute a change of at least one part in 10^3 to 10^4 (the more exact values for each frequency are given in the charts of Fig 6.30) in the amplitude or a change of phase of at least 0.045 radians (10^{-3} radians if the phase of the reference signal approaches $\pi/2$ at the extreme end of the scan in frequency). The amplitude of the signal passing through the electrostatic field was of the order 10 m.V./m. (the more exact values are tabulated in Fig. 6.31) and corresponds to a change of field amplitude of about $10 \mu\text{V./m.}$ as giving the minimum detectable signal. The sensitivity to change of phase depended on the phase of the received signal compared with the reference signal. It was arranged that these were in phase about the centre of the band being scanned. The phase change of about 10^{-2} radians caused by the shutter has appreciably less effect than the change of amplitude caused by the shutter, except near the $\theta = \pi/2$ condition. The above figure of 0.045 radians constitutes a maximum when $\theta = 0$. The corresponding figure is less as θ increases. Over the length of the electrostatic field, which was about 50 cm., this change of 0.045 radians corresponds to a change in refractive index (equation E6.4) of 0.0086. Because of this sensitivity to change of phase, the results of moving the position of the aerial (given in Fig.

6.31) is a check that a complete reversal of the phase is the same as reversing the amplitude. These results (within a factor 2) conform that the result of the aerial movement agrees with the result of the sensitivity measurements.

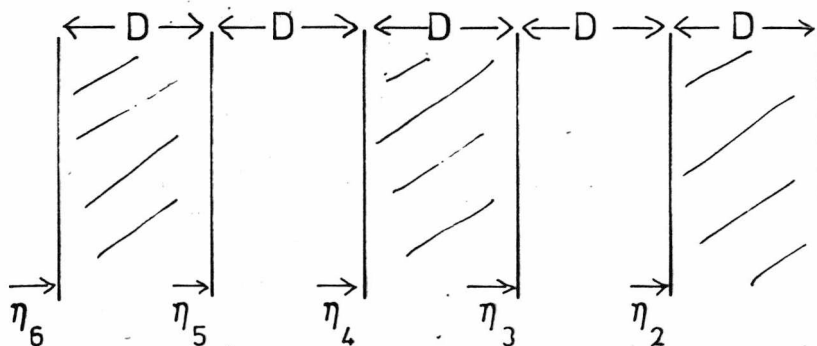
This conclusion, however, assumes that the full effect of any change is not attenuated by the response time of the instruments. There was a lower break frequency of 0.008 Hz. and an upper break frequency of 3.4 Hz. Output pulses are not much attenuated if they are at least 0.1 sec. long. As the scanning rate was about 5 k.Hz./sec. (given more exactly in Fig. 6.31), this requires the bandwidth of the convolution of the effect being looked for with the frequencies generated in the transmitter to be about 0.5 k.Hz. The first side-line of broadening of the continuous wave from the generator (with bandwidth less than one k.Hz.) would be at one k.Hz. spacing, due to the square wave amplitude modulation at 1 K.Hz. Outside this range the output would have been attenuated according to equations E6.24 and E6.25.

The electrostatic field across the beam was of the order of 10 k.V./cm. (given in more detail in Fig. 6.31) but, although the instrument which measured this at the beginning and end of the run was accurate to 20%, the fluctuations during the run were greater than this.

Fig. 6.34 tabulates those charts on which pulses appeared with the electrostatic field present but did not appear when the electrostatic field was not present. The result which appears by both methods of measuring was at about 580 M.Hz. in Run 3 but this did not give clear double pulses in the frequency stepping mode. None of the results were conclusive enough to prompt an immediate follow-up by a more detailed scan over a limited range and time did not permit a general further investigation.



- a) The apparent impedance on moving back a distance D in material of characteristic impedance η_y .



- b) The sequence of alternate layers of Perspex and air.

Fig A 6.1

```

READ(J);
PC=ADD(7);
T[1,1]=READ;
T[2,1]=READ;
T[1,-1]=READ;
T[2,-1]=READ;
YD[1,1]=READ;
YD[2,1]=READ;
YD[1,-1]=READ;
YD[2,-1]=READ;

SS:=1;

'FOR' Q:=1 'STEP' 1 'UNTIL' NL 'DO'
'BEGIN'
T1[1]:=T[1,SS];
T1[2]:=T[2,SS];
Y[1]:=YD[1,SS];
Y[2]:=YD[2,SS];

'IF' Q=2 'THEN' 'GOTO' LL
'ELSE' 'IF' Q=NL 'THEN' 'GOTO' LL
'ELSE' 'GOTO' LP;
LL:'BEGIN'
SUB(X,Y,MA);
ADD(X,Y,NA);
DIV(MA,NA,P);
MA[1]:=P[1];
MA[2]:=-P[2];
MULT(MA,P,NA);
P[1]:=SIGN(MA[1]);
NEWLINE;
PRINTSTRING(<FRACTION_REFLECTED_AT_SURFACE>);
PRINT(Q,2,Q);

NEWLINE;
PRINT(P[1],0,5);
NEWLINE;
'END';
LP:
'IF' Q=NL 'THEN' 'GOTO' LQ;

MULT(Y,J,MA);
MULT(MA,T1,NA);
ADD(Z,NA,MA);
MULT(Z,J,NA);
MULT(NA,T1,P);
ADD(P,Y,NA);
DIV(MA,NA,P);
MULT(P,Y,X);
PRINT(X);
LQ:

Z[1]:=X[1];
Z[2]:=X[2];
SS:=SS*(-1);
'END';

'END';
'END';

```

The programme to compute the impedances to the waves for one layer of Perspex and the sequence of layers of Fig. A6.1(b).

Fig A 6.2

```

'BEGIN'
'INTEGER' NL;
SELECT INPUT(C);
NL:=READ;

'BEGIN'
'INTEGER' Q,SS;
'ARRAY' X,Y,J,P,Z,T1,MA,NA,SC[1:2],T,YD[1:2,-1:1];

'PROCEDURE' ADD(N,M,R);
'VALUE' N,M;
'ARRAY' N,M,R;
'BEGIN'
R[1]:=N[1]+M[1];
R[2]:=N[2]+M[2];
'END' PROCADD;

'PROCEDURE' SUB(N,M,R);
'VALUE' N,M;
'ARRAY' N,M,R;
'BEGIN'
R[1]:=N[1]-M[1];
R[2]:=N[2]-M[2];
'END' PROCSUB;

'PROCEDURE' MULT(N,M,R);
'VALUE' N,M;
'ARRAY' N,M,R;
'BEGIN'
R[1]:= (N[1]*M[1])-(N[2]*M[2]);
R[2]:= (N[1]*M[2])+(M[1]*N[2]);
'END' PROCMULT;

'PROCEDURE' DIV(N,M,R);
'VALUE' N,M;
'ARRAY' N,M,R;
'BEGIN'
'REAL' X,Y;
X:=(N[1]2+M[2]2);
Y:=(N[1]*M[1])+(N[2]*M[2]);
R[1]:=Y/X;

Y:=(N[2]*M[1])-(N[1]*M[2]);
R[2]:=Y/X;
'END' PROCDIV;

'PROCEDURE' READD(B);
'ARRAY' B;
'BEGIN'
B[1]:=READ;
B[2]:=READ;
'END' PROCREADD;

'PROCEDURE' PRINT(C);
'VALUE' C;
'ARRAY' C;
'BEGIN'
NEWLINE;
PRINTSTRING(<REAL_____>);
PRINT(C[1],0,5);
NEWLINES(2);
PRINTSTRING(<IMAGINARY___>);
PRINT(C[2],0,5);
NEWLINE;
'END' PROCPRINT;

```

Fig A 6.2 (continued)

Appendix to chapter 6

A6.1 The Perspex shutter

This was alternate layers of air and material of refractive index approximately 1.5. The fraction of radiation reflected at the boundary depends on the apparent impedance looking into the boundary. Thus, starting with the final surface looking into air from Perspex, the impedance is transformed a known phase angle moving back in the material of known refractive index. This calculation is repeated for each of the three layers of Perspex and the two layers of air, using the general equation for each layer (Fig. A6.1(a)):

$$\eta_x = \eta_y \frac{\eta_z + j\eta_y \tan \beta D}{\eta_y + j\eta_z \tan \beta D} \quad \text{EA 6.1}$$

where:

$\beta = 2\pi/\lambda_d$ and λ_d is the wavelength in the material of thickness D .

η_z is the characteristic impedance of the previous medium.

η_y is the characteristic impedance of the layer being considered.

η_x is the characteristic impedance seen from the next boundary.

For the system being considered, the impedance of air is 377 ohms, for Perspex approximately 251 ohms, and the thickness of all layers is 0.3 cm. $\tan \beta D \approx \beta D$ and is 0.055 for the Perspex and 0.038 for the air at 600 M.Hz.

In general, the fraction of amplitude reflected back into the air at a boundary of impedance η_x , is:

$$\text{Fraction Reflected} = \frac{\eta_x - \eta_{\text{air}}}{\eta_x + \eta_{\text{air}}} \Bigg| \text{Modulus} \quad \text{EA 6.2}$$

The computer program of Fig. A6.2 was written to evaluate

equation EA 6.1 for successive layers as in Fig. A6.1(b), by iterating the calculated η_x back into the equation as η_z for the next layer. The program was written in Algol as it was part of the training for another program on another project (Fortran would normally be used for complex numbers). For the second and sixth boundaries equation EA 6.2 was evaluated to give the fractional reflection for the two conditions of the shutter system as it oscillated. The results were:

```

I*****
 $\eta_2$  { REAL          3.755770  2
      { IMAGINARY   -1.722130  1
      FRACTION REFLECTED AT SURFACE  2
      2.295500 -2
 $\eta_3$  { REAL          3.742830  2
      { IMAGINARY   -1.703480  1
 $\eta_4$  { REAL          3.701570  2
      { IMAGINARY   -3.346300  1
 $\eta_5$  { REAL          3.676950  2
      { IMAGINARY   -3.274530  1
 $\eta_6$  { REAL          3.612590  2
      { IMAGINARY   -4.770480  1
      FRACTION REFLECTED AT SURFACE  6
      6.790530 -2
I*****
I*****
EA 6.3

```

Hence the change of fractional amplitude between one sheet of Perspex and the three of Fig. A6.1 is $0.068 - 0.023 = 0.045$. This is discussed further in section 6.11.

A6.2 The electrostatic field round the two spheres

It is shown in the textbook (Smythe⁽⁹⁰⁾, 1950), that if two spheres of radii a and distance between centres, b are at potentials 1 and 0 (connected to earth) volts, these equipotential surfaces may be formed by replacing the spheres with a set of 'image' charges which are the multiple reflection of the first charge between

The distribution of point charges producing the same field as the charged sphere.

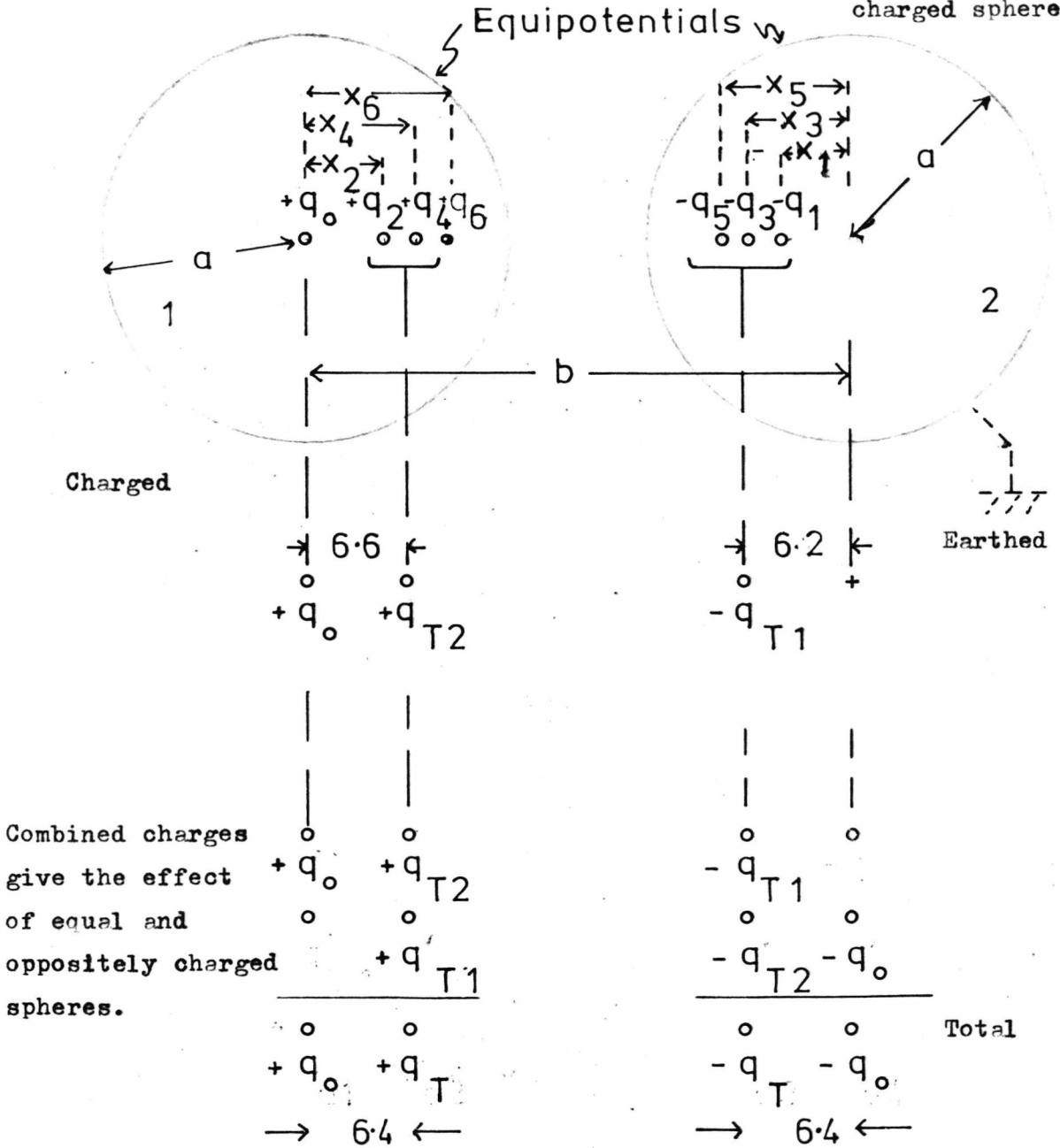


Fig. A 6.3

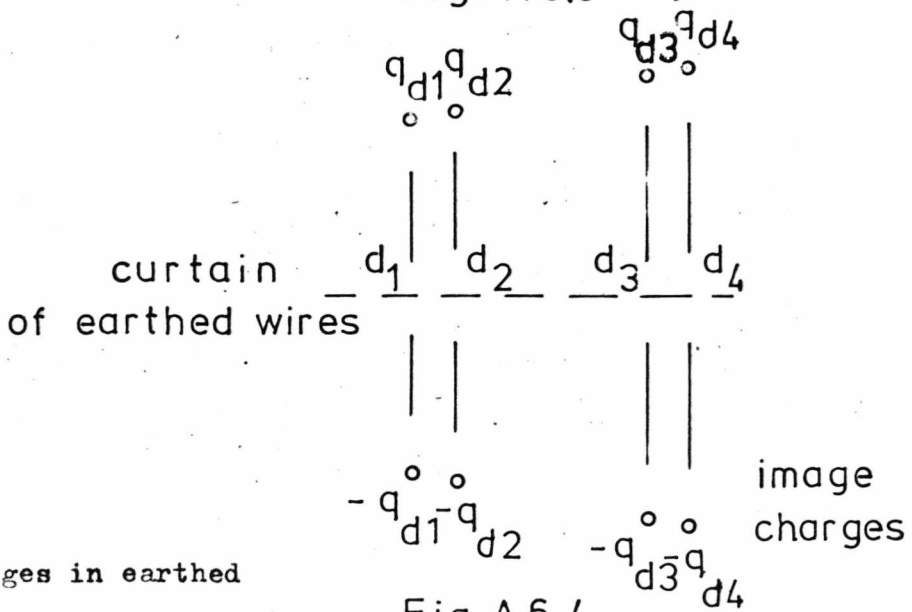


Fig. A 6.4

Image charges in earthed screen

the spheres. Thus Fig. A6.3 indicates the charges and their positions to create a potential of 1 volt on the surface of sphere 1 and of 0 volt on the surface of sphere 2. The magnitudes and positions of successive charges are given by:

$$q_n = \frac{-a}{(b - x_{n-1})} q_{n-1}$$

EA 6.4

$$x_n = \frac{a^2}{(b - x_{n-1})}$$

where the n^{th} image charge, q_n , is a distance x_n from the centre of the sphere in which it is the reflection.

If these are evaluated for the condition $a = 22.9$ cm. and

$b = 85.7$ cm.:

n	x_n (cms.)	q_n
0	0.000	q_0
1	6.119	$- 0.267 q_0$
2	6.590	$+ 0.0769 q_0$
3	6.629	$- 0.0222 q_0$
4	6.632	$+ 0.00644 q_0$
5	6.632	$- 0.00187 q_0$
6	6.632	$+ 0.000542 q_0$
Totals -		$(1 + 0.0839) q_0$ $- 0.291 q_0 = q_{T1}$

EA 6.5

As the image charges form two groups, they are approximated by two charges, $-q_{T1}$ and q_{T2} , as shown in Fig. A 6.3.

For the case in which the second sphere is connected to earth (Case 1), the charge $-q_{T1}$ is brought by induction from ground. Therefore the set of charges to generate the required potentials are q_0 , $-q_{T1}$ and $+q_{T2}$. The field which these charges generate (evaluated by the inverse square law applied to each charge) at a position 177 cm. (the approximate

distance of the detector in the experiment) from the centre of sphere 1 and on the line of the centres of the spheres and to the left, is:

$$\begin{aligned} \tilde{E} &= \left[\frac{q_o}{4\pi\epsilon_o} \right] \left[\frac{1}{177^2} + \frac{0.0839}{185^2} - \frac{0.291}{257^2} \right] \\ &= \left[\frac{q_o}{4\pi\epsilon_o} \right] 3 \times 10^{-5} \quad \text{EA 6.6} \end{aligned}$$

If only the charge q_o at the centre of sphere 1 were present:

$$\tilde{E}' = \left[\frac{q_o}{4\pi\epsilon_o} \right] 3.2 \times 10^{-5} \quad \text{EA 6.7}$$

The fractional difference between E and E' is:

$$\begin{aligned} \text{Fractional Difference} &= \frac{\tilde{E}' - \tilde{E}}{\tilde{E}} = 0.07. \quad \text{EA 6.8} \end{aligned}$$

Thus (as this position of the detector is not much different from that in the experiment), within the approximate estimate which was intended in this measurement, the effect of the combined charges is not much different from that of the single charge on the nearest sphere by itself (this may be used as an approximate check in the results).

If the second sphere has an equal and opposite charge (Case 2) or equal charge of the same polarity (Case 3), the same calculation is made as for equations EA 6.4 for reverse positions of the spheres and subtracted (Case 2) or added (Case 3). This is indicated for case 2 in the lower part of Fig. A 6.3. Again, the charges are grouped together and each group represented approximately by a single charge at each position shown in the figure.

Thus, the approximate distribution of point charges for each case is:

Case 1 -	+ q	+0.0839 q	-0.291 q	
	o	o	o	+

```

'BEGIN'
'INTEGER' NR;
SELECT INPUT(2);
NR:=READ;      -number of positions at which field evaluated

'BEGIN'
'REAL' EX,EY,XP,YP,A,TH;
'INTEGER' N,M;
'ARRAY' X,Y,Q[1:8],XR,YR[1:NR];

PRINTSTRING(<FOR_CHARGES>);
'FOR' N:=1 'STEP' 1 'UNTIL' 8 'DO'
'BEGIN'
X[N]:=READ;
Y[N]:=READ;
Q[N]:=READ;
NEWLINE;
PRINT(X[N],0,4);
SPACES(2);
PRINT(Y[N],0,4);
SPACES(2);
PRINT(Q[N],0,4);
'END';
} positions and magnitudes of charges

'FOR' N:=1 'STEP' 1 'UNTIL' NR 'DO'
'BEGIN'
XR[N]:=READ;
YR[N]:=READ;
'END';
} positions of detectors

'FOR' M:=1 'STEP' 1 'UNTIL' NR 'DO'
'BEGIN'
EX:=0;
EY:=0;
NEWLINES(2);

'FOR' N:=1 'STEP' 1 'UNTIL' 8 'DO'
'BEGIN'
XP:=X[N]-XR[M];
YP:=Y[N]-YR[M];
A:=1/(XP^2+YP^2);
'IF' XP<0 'THEN'
A:=-A;

A:=A*Q[N];
TH:=ARCTAN(YP/XP);
EX:=EX-A*COS(TH);
EY:=EY-A*SIN(TH);
'END';

A:=SQRT(EX^2+EY^2);

NEWLINE;
PRINTSTRING(<AT_POSITION>);
SPACES(2);
PRINT(XR[M],0,4);
SPACES(2);
PRINT(YR[M],0,4);
NEWLINES(2);
PRINTSTRING(<FIELD_IS>);
NEWLINES(2);
PRINT(EX,0,4);
SPACES(2);
PRINT(EY,0,4);
SPACES(2);
PRINT(A,0,4);
'END';

'END';
'END';

```

The programme to compute the electrostatic fields at the detector and between the spheres.

Fig A 6.5

Case 2 -	+ q	+0.375 q	-0.375 q	- q
	o	o	o	o
Case 3 -	+ q	-0.207 q	-0.207 q	+ q

The set of four charges next to the curtain of earthed wires forms a set of image charges as indicated in Fig. A 6.4 (the charges labelled $q_{d1}, q_{d2}, q_{d3}, q_{d4}$, correspond to any one of the sets for each of the cases tabulated above).

The computer programme of Fig. A 6.5 evaluates the total field, at each of a number of positions, formed by the eight charges as in Fig. A 6.4, by applying the inverse square law (q was taken as unity because only the ratio of the field amplitudes at two positions was required).

The programme was run with data corresponding to each of the three cases above to find the field at the position of the detector and positions y_1 and y_2 in the scale diagram of Fig. 6.27. The results for:

Case 1 -	*****				charge	
	FOR CHARGES					
	0.00000	-99	6.42000	0	1.00000	0
	6.00000	-1	6.60000	0	8.39000	-2
	7.68000	0	8.20000	0	-2.91000	-1
	8.32000	0	8.31000	0	0.00000	-99
	0.00000	-99	-6.42000	0	-1.00000	0
	6.00000	-1	-6.60000	0	-8.39000	-2
	7.68000	0	-8.20000	0	2.91000	-1
	8.32000	0	-8.31000	0	0.00000	-99
	x		y			
detector	AT POSITION	-1.62000	1	1.32200	1	
	FIELD IS		x		y	
	-1.89670	-3	1.51490	-4	1.90270	-3
	E_x		E_y		E_{total}	
y_1	AT POSITION	4.15000	0	7.40000	0	
	FIELD IS		x		y	
	7.96370	-2	1.50620	-2	8.10490	-2
	E_x		E_y		E_{total}	
y_2	AT POSITION	3.38000	0	0.00000	-99	
	FIELD IS		x		y	
	-5.42100	-19	-3.06220	-2	3.06220	-2
	E_x		E_y		E_{total}	

EA 6.9

Case 2 (list of charges omitted) -

```

AT POSITION  -1.6200a  1  1.3220a  1
FIELD IS
-1.5089a -3  4.8102a -4  1.5837a -3

AT POSITION  4.1500a  0  7.4000a  0
FIELD IS
 1.5958a -1  3.5641a -2  1.6351a -1

AT POSITION  3.3800a  0  0.0000a-99
FIELD IS
-1.7347a-18 -2.0953a -2  2.0953a -2
I*****

```

EA 6.10

Case 3 (list of charges omitted) -

```

AT POSITION  -1.6200a  1  1.3220a  1
FIELD IS
-2.2849a -3  -1.7803a -4  2.2918a -3

AT POSITION  4.1500a  0  7.4000a  0
FIELD IS
-2.9130a -4  -5.5155a -3  5.5232a -3

AT POSITION  3.3800a  0  0.0000a-99
FIELD IS
 0.0000a-99 -4.0298a -2  4.0298a -2
I*****

```

EA 6.11

The field was evaluated at positions y_1 and y_2 as these give an indication of the magnitude of the field acting on the radio frequency waves passing through the volume between the spheres. In cases 1 and 2 the field at y_1 is greater than at y_2 , and in case 3 the field at y_2 is greater than at y_1 .

This gave the following results for the ratio between the field passed by the r.f. and the field at the detector.:

Case 1 (with sphere 2 earthed)

Field at y_1 : field at detector = 43.

Case 2 (with spheres 1 and 2 charged equally in opposite polarity)

Field at y_1 : field at detector = 103

Case 3 (with spheres 1 and 2 charged equally in the same polarity)

$$\text{Field at } y_2 : \text{field at detector} = 17.6$$

The experiment was performed by measuring the signal at the detector and, from the calibration graph, recording a voltage on the sphere corresponding to that on an isolated sphere at the same distance (as shown above, this is approximately correct). The result is related to the field at the detector according to:

$$\begin{aligned} \tilde{E} &= \frac{C V}{4 \pi \epsilon_0 l^2} & C &= 23 \text{ p.f.} \\ & & l &= 1.75 \text{ m.} \\ &= 0.0679 V \text{ k.V./m.} & \epsilon_0 &= 8.8 \text{ p.f./m.} \end{aligned} \quad \text{EA 6.12}$$

This gives the field at the detector when the voltage V is in k.V.

Hence the field in the r.f. path is (approximately) the product of the field at the detector (evaluated from equation EA 6.12 for the average of the voltages quoted in Fig. 6.31 in cases 2 and 3) times the above factors for each Case. The component of the electrostatic field normal to the path of the r.f. waves may be calculated from the angle (given by the components of the total field in the above table) of the field and the angle of the r.f. path (as measured on Fig. 6.27). The resulting fields are tabulated in Fig. 6.31 of section 6.18.

THE STRUCTURE OF BALL LIGHTNING7.1 Introduction

This chapter considers some of the implications of assuming an entirely electromagnetic structure for Ball lightning. The main properties of Ball lightning have been summarized in section 2.6 of chapter 2 and it is assumed here that the mechanism of storing energy in the lightning ball does not depend on any other agent (for example, the air) than the electromagnetic fields in some form. There have been many attempts to account for the phenomenon of Ball lightning in terms of molecules and ions associated with the lightning strike (in particular, by Kapitza ⁽⁵⁴⁾, 1955 and Edean ⁽²⁷⁾, 1976, as described in section 2.6 of chapter 2), however, Jennison ⁽⁴⁶⁾, 1973, has suggested that the system forming the ball is quite independent of the air. If this is so, it indicates that there is here some basic, novel, electromagnetic mechanism required to account for the self-trapping of the electromagnetic fields. No previous authors have attempted an explanation of Ball lightning along these lines and therefore the only source of theories to explain the mechanism is the suggestions which have been made to account for the analogous phenomenon on the much smaller scale of atomic dimensions.

The theories of previous authors on particle structure have often considered the whole range of atomic particles (the formation of electron-positron pairs from gamma radiation being one example out of this range). Some brief notes on the main line of thought in these theories are given in section 2.7 of chapter 2. A few points from these theories will be considered in this chapter to see if they may assist in accounting for the structure of Ball lightning.

Section 7.2 considers how the mechanism holds together a definite

quantity of energy in a definite volume. The experiment of chapter 6 was looking for a non-linear effect at a specific wavelength. It has been demonstrated in the Trolley experiment of chapter 4 that a fixed wavelength of radiation between reflectors may be used to determine the size of the container. A brief comment is made next on the need for a closed path for the internally trapped waves of the ball. Consideration is made of how the ball is able to lose energy continuously by visible radiation during the life of the ball.

Section 7.3 suggests how the calculations on a one-dimensional etalon in chapters 3 and 4 might be extended to describe some of the properties of rigidity and inertia of a three-dimensional structure of trapped waves.

Section 7.4 is a discussion of the results of the experiment described in chapter 6. In it a rough estimate is made of the field strengths which may occur in the lightning ball. This and the result of the experiment of chapter 6 are compared with what might be expected according to the theory of non-linear electromagnetic fields put forward by Born and Infeld⁽¹⁴⁾, 1934, to account for the formation of electrons.

7.2 A 'quantizing' mechanism

A problem for any closed system which is to represent the above phenomenon is to account for the exact 'quantization' (in the general sense of holding some packet of energy together and not necessarily in specifically Planck's sense) of all similar entities to give them the same size, mass, (and, in the case of charged units, charge). Mention has been made in section 2.7 of the work of authors who have attempted to give a description of atomic particles (in particular, the electron) in terms of a wave structure with poorly defined mechanism to hold it together and of non-linear field theories containing parameters (for

example, a length) which cause coalescence of energy in packets of definite size.

The size of the system might be determined by some fundamental unit of frequency associated with space but there seems to be no further explanation available of this constant. The mechanism of binding the energy into, say, an electron probably involves bringing the electromagnetic wave by some closed path back to the centre and some constant which is experimentally the Compton wavelength. It may be that, although chapter 6 has described the effect in terms of a frequency, it is preferable to think in terms of a fixed unit of energy and an energy density (there seems to be an intimate inter-relation of frequency and energy in the quantization process). The Trolley experiment described in chapter 4 demonstrates how, for a given frequency of internal radiation, the size of the system is determined by the relative positions of the nodes of the standing waves. But this in itself does not determine the total energy, for which a definite quantization is required. Ulmer⁽⁹⁵⁾, 1975, emphasises that previous authors have observed that the constants c and h are not sufficient to define a unified field as it is impossible to form an expression with the dimension of mass with these two constants. A constant of length (or mass) must also be defined. The combined parameters of size and total energy give an average energy density which may be a type of limiting or 'catastrophic' effect' at some field intensity.

A closed system structured around electromagnetism must be held together in some way. To give a description of the structure of the boundary which both contains the internal radiation by reflection while allowing interaction with external fields is difficult. The main property of the enclosing boundary is that it has quantizing parameters so that as a whole it binds itself together but any further energy (waves) incident on it are reflected and not bound into it. It is envisaged

that, however the boundary is formed, it will follow equations similar to E4.15 for the trolley reflectors when the mass of the reflector is negligible.

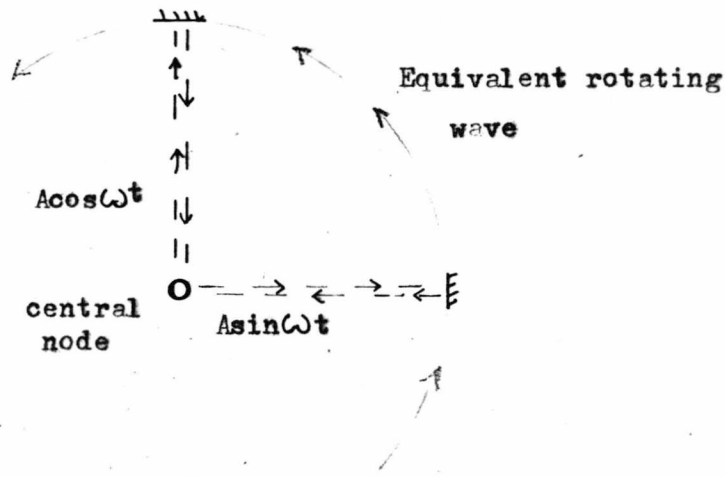
No attempt is made here to present a theory of the mechanism which causes the waves to be trapped in Ball lightning except to suggest that it may be necessary to move away from the previous approaches of other authors, mentioned in chapter 2, to introduce some radical new description in addition to classical electromagnetic field theory. In dealing with such basic concepts there is a philosophical problem that one requires meaningful terms in which these additional properties can be described. Thus previous attempts ranging from Dirac ⁽²³⁾, 1951, (invoking the gauge parameter of classical electromagnetic potentials), to the non-linear fields of Born and Schiff ⁽⁸¹⁾, 1962, (which at large energy density give a nett divergence of the field), to Jennison ⁽⁴³⁾, 1964, (describing in terms of rotation of the fields), present their theories in terms of known physical operations but are probably too limited in themselves to give a complete account of the phenomenon. The foundation premises on which classical electromagnetic theory is based are sometimes thought of as assuming that free space has an effective capacitance and inductance per unit length (analogous to a transmission line) which relate the amount of energy stored per unit volume to the voltage across that volume and the magnetic field in it. Beyond this it is not understood how waves propagate. One might envisage, for the formation of a closed system, that the waves are looped back on themselves along some curved path so that the waves become phase-locked and form a closed system of definite size. This curving of the path is, at least in overall effect, similar to refraction and might be described in terms of a change of the capacitance and/or inductance per unit length of the space.

As the mechanism stabilizing the ball fixes it at a definite 'quantized' size, the binding mechanism cannot lose energy slowly but

only, as in the analogous case of atomic fission, all at once. It is suggested here that the lightning ball emits light, without modifying the energy in its binding mechanism, by a type of corona discharge with the air, caused by an electric field (and its potential energy) associated with the ball. This electric field accelerates electrons in the air near the ball until collision with air molecules gives the molecules metastable states which, on decay, emit light. As electrons from the air at distant points are collected at the surface of the ball, there is a neutralising of the charge of the ball and hence this is the source of the energy illuminating the ball. It may be objected that at least some reports (for example, by Jennison⁽⁴⁶⁾, 1973) suggest that the ball has little nett electric charge. It may be that the charge is distributed in areas of opposite polarities over the surface of the sphere so that there is little overall effect at a distance but there are local effects. It may also be that these local areas alternate in polarity with the oscillations of the internal waves. This oscillation might alternatively be analysed in terms of rotating components.

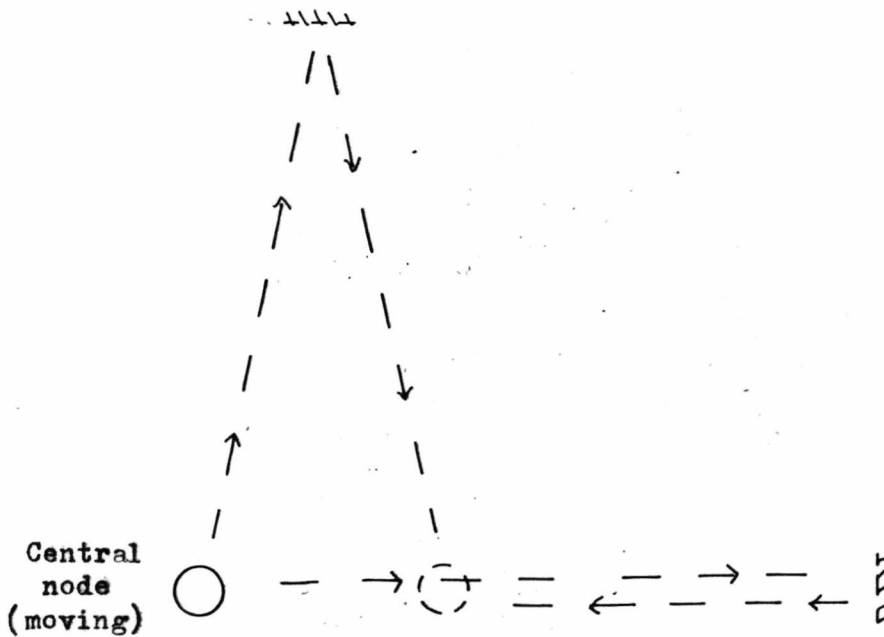
7.3 The implications of the calculations on rigidity and inertia for the lightning ball

The phenomenon of Ball lightning was investigated because it was thought that it might be an example of waves trapped between non-material reflecting boundaries. The etalon described in chapter 3 was shown to have certain properties of rigidity which correspond (in the state of no externally applied forces) to Born's definition of rigidity along a linear bar. Problems arise over extending Born's definition to three dimensions and Synge⁽⁹²⁾, 1960, has mentioned that although the Born criterion of rigidity involves no difficulty when applied to a one dimensional body, difficulties accumulate with increase of dimensionality.



Two component waves in space and time quadrature are equivalent to a rotating wave.

Fig 7.1



The system of reflectors of Fig. 7.1 viewed from a frame moving at constant velocity relative to the system.

Fig 7.2

These inherent difficulties are connected with non-integrability and are avoided when working in an infinitesimal domain. However, at least over sufficiently small regions, the three dimensional system of the lightning ball may be considered in terms of etalon-type systems along each direction. Each of these components corresponds to a quantized and bounded unit, as described in section 7.2, depending on some electromagnetic property of space giving a fundamental resonant frequency involving a time delay and defining a direction in space.

Such an analysis may be compared with the Interferometer experiment of chapter 4, which compares the phase of the returning ray in the controlled arm with that of the returning ray in the reference arm and servoed the reflector so that the phase difference is always the same in the recombined beam. The experiment might have been extended so that the mirror in the reference arm remained at the same distance but the beam-splitter at the centre, photodetector system (and, for appreciably large displacements, the reference arm mirror) were modulated in position along the main beam. The servoed mirror would move as before so that the path lengths in the two arms remained the same. In this arrangement the distance from the centre to the servoed mirror would have properties similar to the etalon analysed in chapter 3 and this may be extended to the conditions envisaged for two orthogonal components of the lightning ball. If the phase comparator at the centre looks for a 90° phase difference between the waves returning in each arm, the combined system of two etalon components in time and space quadrature may be represented (in its proper frame) as in Fig. 7.1 which may be viewed as a rotation of the waves.

If pushed to an inertial frame moving at a constant velocity to the system of Fig. 7.1, Fig. 7.2 indicates the paths of energy flow and, as this is similar to the Michelson interferometer, the Lorentz

transformation of all the properties of each etalon (as calculated in chapter 3) will give a system which is still phase-locked and follows the dynamical motion as calculated for each etalon separately.

This brief analysis suggests that the three-dimensional mechanism of Ball lightning, simplified by considering only two orthogonal components of the complete system, would behave in a similar way to the one-dimensional unit described in chapter 3.

7.4 The field intensity required to give measurable non-linear effects

This section makes a rough estimate of the field strength which may be expected in the lightning ball to compare it with the fields of the experiment of chapter 6. Also, the field strength in the experiment of chapter 6 is inserted in the equations of one of the non-linear field theories to see if it predicts a measurable effect.

It was to investigate the existence of a non-linear term in electromagnetism, which at large energy densities would lead to quantization at a specific resonance frequency, that the experiment of chapter 6 was performed. Previous experiments which attempted to demonstrate non-linear properties of free space electromagnetism are mentioned in chapter 2 section 2.8.

The experiment does not attempt to replicate the energies or energy densities associated with a thunderstorm (section 2.6) but looks for any beginnings of a non-linear effect rather than the formation of the fully trapped wave.

The energy in a typical lightning stroke is 10^{10} Joules. It may be, however, that only a small fraction of the thunderstorm energy is trapped in the ball. The oft-quoted water barrel report (Morris⁽⁷⁰⁾, 1936) giving an estimate of 10^7 Joules may be an over-estimate of the total energy trapped in the ball, due to confusing physical phenomenon which are not

true Ball lightning. One report suggests an estimate, taking the ball to emit light equivalent to 10 watts for 60 sec. and then ending benignly, of as little as 600 joules.

As an approximate order of magnitude calculation, for a uniform density of electromagnetic waves having a total energy equal to 600 Joules in a sphere of the size of the lightning ball (say, 20 cm. diameter) there is a field strength given by:

$$\epsilon_0 \bar{E}^2 \times \frac{4\pi}{3} (0.1)^3 = 600$$

$$\bar{E} = 1.2 \times 10^8 \text{ Volts / m.} \quad \text{E7.1}$$

To compare, the static field strengths set up in the experiment were of the order 10^2 - 10^3 k.V./m. and the energy between the Van de Graaff spheres of the experiment was, for capacitance 20 pf. and, say, 3×10^5 Volts, about one joule. Reports on conditions during thunderstorms (section 2.6) suggest fields of the order 10^4 k.V./m.. The experiment was set up with the intention that the static field between the Van de Graaff generators would occupy a volume at least as large as the lightning ball.

An indication will now be given of how the experimental results compare with that expected from theory. The electrostatic field in the experiment of chapter 6 changed the vector potential over the volume through which the waves passed. The theories mentioned in chapter 2 section 2.7 suggest that there may be a non-linear interaction in terms of the field's vector potential of the electromagnetic field. However, the mechanism being investigated in chapter 6 involves a type of resonance at a specific frequency and it seems likely that this would not be described simply by additional terms to the usual Maxwell equations. Probably a quite different approach to the field equations is required to include this mechanism. Assuming for the moment, however, that the

mechanism may be described by non-linear equations of the type discussed in chapter 2, the following estimate is made.

The case of the Born-Infeld theory will be considered out of the approaches listed in section 2.7 as it is only intended as an indication from a typical theory. This case is the most immediately calculable and does not pre-suppose Dirac quantization. Born and Infeld⁽¹⁴⁾, 1934, (equation 6.4 and 6.15 in this paper) calculate the particular case of an electromagnetic field round a source charge in terms of the (radial) electric field \underline{E} and electric displacement \underline{D} . This gives an effective relative permittivity ($\epsilon_0=1$ in e.s.u., and \underline{E} parallel to \underline{D}) of:

$$\frac{\underline{D}}{\underline{E}} = \frac{r_0^2 (1 + (\frac{r}{r_0})^4)^{1/2}}{r^2} = \epsilon, \quad \text{E7.2}$$

where ϵ is the effective relative permittivity, r is the radial distance from the source and:

$$r_0 = \left(\frac{q}{b} \right)^{1/2}, \quad \text{E7.3}$$

where q is the total central charge and b is a constant of the field strength required by this theory and given as about 10^{16} e.s.u. As the experimental radio frequency was of the order 10 m.V./m., it was a small perturbation on the static field of the order 10^3 k.V./m. and the static field determines the refractive index (equal to $\left[\frac{\epsilon \epsilon_0 \mu \mu_0}{\epsilon_0 \mu_0} \right]^{1/2}$). The field is related to the charge at the centre by the equation:

$$\underline{E} = \frac{q}{r^2} \cdot \quad \text{E7.4}$$

Hence, solving the above equations, the effective relative permittivity is:

$$\epsilon = \left[1 + \left[\frac{\underline{E}}{b} \right]^2 \right]^{1/2}$$

$$= \left[1 + \left[\frac{30}{10^{16}} \right]^2 \right]^{1/2}$$

$$\approx 1 + 0.5 \times 10^{-29}$$

E7.5

for the field strength of 30 e.s.u. in the experiment. Over a distance of about 30 cm., the change of effective refractive index, on switching on the electrostatic field, from unity to the above value would produce a change of phase in the interference pattern which was undetectable within the sensitivity of the experiment.

The above estimate of 600 Joules as the energy content of the lightning ball corresponds to an equivalent mass of 6.7×10^{-15} k.gm.

CONCLUSION8.1 Main results

The basic idea, proposed by Professor Jennison, of analysing a system of monochromatic radiation, trapped between parallel end reflectors one of which is given a step increase in velocity and the other of which moves so as to maintain an integral number of half-wave standing waves between the ends, has proved to be of remarkably continuing interest. In that it propagates perturbations of the inertial motion of one end with the velocity of light to the other end, it is similar to the rod analysed by Hogarth and McCrea⁽³⁹⁾, 1952. But the condition of movement of the free reflector maintaining a balance of binding force and radiation pressure gives a 'locking into' the subsequent motion and properties which in detail differ from the system postulated by McCrea. It was shown that the system may be used to define a rigid rod with mechanical properties determining its exact movement when accelerated. This rod maintains its proper length when moving in a different inertial frame. It is a representation of the theoretical definition of a rigid rod given by Born⁽¹³⁾, 1909. However, like the system of Born's original definition, it is only one dimensional.

Then it has been shown by a theoretical analysis that, to second order accuracy of the relativistic equations, the trapped radiation and its automatically controlled, massless, reflectors behaves dynamically as a massive body which for a change of velocity, V , acquires a:

$$\text{Change of momentum} = m_0 v \left[1 - \frac{v^2}{c^2} \right]^{-1/2} . \quad \text{E8.1}$$

If the 'rest mass' of the system is equated to that of the electron particle, it was shown that the internal frequency is directly related

to that of the gamma ray required for electron-positron pair formation.

The system, although it contains no mass in the conventional sense, follows Newton's laws of motion. The implications of this for Machian-type theories on the physical origin of inertia was discussed. A different approach to the analysis of Sciama and Davidson⁽²⁰⁾, 1957, was presented and indicates that inertial (and gravitational) forces, at least for this structure, are generated locally in the balancing against the internal radiation pressure at the end reflectors of the extended system. It was shown (approximately) that the metric field in non-inertial frames gives null-geodesic paths along which the rays crossing the cavity are affected (when the cavity is held in this frame) so as to generate the inertial forces. Also it was shown (approximately) that true gravitational fields affect the rays crossing the cavity (held in the field) so as to generate the force of gravity.

The experiment with the optical interferometer has demonstrated that a Michelson interferometer may be used to construct a rigid system by comparing the relative positions of two mirrors and hence giving an error-correcting signal to control the position of one mirror (with an error of less than half a wavelength ($0.3 \mu\text{m.}$) of the light used) while the other mirror is moved along the line of the interferometer beam. The maximum controllable closed loop frequency of the apparatus was of the order 30 Hz. for an amplitude of oscillation of 0.5 m.m. This is the same as for the device described by Schede⁽⁸⁰⁾, 1967, and mentioned in section 2.2(a) of chapter 2.

The experiment using microwaves has shown that a type of mutual radar ranging may be used to construct a system of two trolleys which demonstrate inertial movement (the energy in the servo controlling motor reducing the effect of the actual inertia of the trolleys). Each trolley always maintains a rigid distance to the other so that if one

is moving the other follows and they continue to follow each other in an inertial motion. The system behaved as a rod with rigidity modulus 63 k.gm.wt. and breaking force of about 2 k.gm.wt. The response of the system was such that it had to be accelerated slowly (of the order 10 cm.sec.⁻²) if the following trolley was not to lose control. The operation of the loop aerial, so that it detected an antinode of the magnetic field standing wave between the trolleys and ensured that the control circuit maintained a maximum at the boundary of the system, is of interest in considering, for example, the structure of Ball Lightning.

The effect of the time delay for signals to traverse the cavity could only be demonstrated on a time-scaled electronic analogue circuit. It indicated the importance to the behaviour of the cavity of the time delay to propagate effects through the system and demonstrated that this delay causes a series of stepping motions to result from an initial step perturbation.

The experiment on field interactions in free space indicated that the change in refractive index (over a volume about 40 cm. cube) caused by a static electric field of the order of magnitude 5 k.V./cm. was less than 0.009 (± 0.002) under the condition that the apparatus would only have detected the effect of a sharp resonance with a narrow frequency band (of the order 1-400 k.Hz.) in the range 450-960 M.Hz. This sensitivity to change of refractive index is considerably less (by a factor of about 10^9) than the experiments described in section 2.8 of chapter 2. However, the latter were performed at optical frequencies and there were many wavelengths of distance along the path being investigated. This experiment was restricted to wavelengths (suggested by the size of Ball Lightning) for which the path investigated was about one wavelength and hence the change in phase at the receiver would have been the result over only one oscillation. Again, Froome's⁽³²⁾, 1958, experiment with microwaves measured over many wavelengths. This suggests

(from the preliminary experiment) that the mechanism for stabilizing Ball lightning is a 'catastrophic' type of effect at a greater field strength or that it occurs at such energy densities that this experiment was not sensitive enough to detect any departures from linearity.

The discussion of chapter 7 has indicated that a purely electromagnetic structure for Ball lightning requires a mechanism which establishes a definite quantity of energy for the system and a binding mechanism which accounts for the forces containing the energy despite the radiation pressure tending to disperse it.

8.2 Comments

There remains the fundamental problem of the binding mechanism (extended over a region) and its energy.

In the experiments it had been hoped to find a way to represent the effect of the delay time for the waves to traverse the cavity in the Trolley experiment. It takes about 0.1 n.sec. for the waves to move between the trolleys and no appreciable mechanical action would take place in this time. The distance along a delay line would have to have been increased to unmanageable lengths to give a delay time that demonstrated the stepped motion of the trolleys. Also, the setting of the feedback control on the trolley was so critical to obtain no hunting or lack of control that it was difficult to obtain steady, balanced conditions and the motion of the trolleys tended to be underdamped. The friction with the traction studding supplied the main dissipative mechanism and this tended to be variable along the track.

8.3 Suggestions for future work

The experiment of chapter 6 might be extended using more stable conditions of the electrostatic field and extending the range of frequencies investigated, in case the lightning ball involves curved

wavepath convolutions of the wave shape.

The analysis in this thesis raises questions as to the basic nature of the electromagnetic field. In the limit of analysis, wave propagation depends on the nature of spatial extension and the continuum. The fundamental length or resonant frequency associated with particle pair formation may be a function of the electric potential (and indeed, be essentially what the electric field is).

A8.1 Comment on the negligible mass of the reflectors and the 'locking in' process.

The following analysis indicates that the assumption that the mass of each reflector is negligible may be derived as a limiting process which does not give rise to physically unrealistic conditions. This is because the variation in radiation pressure, when the velocity of the reflector varies, gives the equivalent of a damping (or friction) force. It is shown that the velocity of the reflector varies so as to maintain this damping force such that the imbalance of forces acting on either side of the massive reflector tends to an infinitesimal amount as the mass of the reflector becomes infinitesimal.

Here, as in chapter 3, it is assumed that the internal radiation is circularly polarised (as discussed in Appendix A3) so that there is a steady force of radiation pressure against the end reflectors.

Consider a reflector of mass M which is initially stationary with the force from the radiation pressure, F_w , balanced by the binding force, F_b . If an additional steady external force, F , is applied at time $t = 0$, the reflector will immediately start to move into the radiation with increasing velocity, $v(t)$, (before the completion of a circulation round the cavity of the effect of the initial disturbance) because of the imbalance of forces acting on either side of the massive reflector. The resulting equation of motion (from E3.14, E3.16 and E3.20) is, where $M \approx$ Rest mass to first order in v/c ,

$$F_b + F - F_b \frac{1 + \frac{v(t)}{c}}{1 - \frac{v(t)}{c}} = M \frac{dv(t)}{dt}$$

EA8.1

Setting

$$\frac{dv(t)}{dt} \equiv \dot{v} \quad , \quad v(t) \equiv v$$

and putting

$$2 F_b = c B \quad , \quad \text{EA8.2}$$

we have, as $(1 - v/c)^{-1} \approx 1 + v/c + \dots$, to first order in v/c ,

$$M \dot{v} + B v - F = 0 \quad . \quad \text{EA8.3}$$

It may be noted that the second term in this equation gives a force which is proportional to the velocity and directed against the motion. It is therefore a type of damping term.

Equation EA8.3 has the solution

$$v(t) = \frac{F}{B} \left(1 - e^{-\frac{B}{M} t} \right) \quad \text{EA8.4}$$

Thus the time constant M/B of the exponential term becomes infinitesimal as M tends to zero and the velocity reaches its maximum value in an infinitesimal time. In the analysis of chapter 3 it is assumed that the movement of the reflector is determined by the forces of internal radiation pressure, binding force and any additional externally applied force. If the mass of the reflector is negligible, to balance the radiation pressure against the binding force and externally applied force (if any) there must be a step increase in velocity when the step function change of force occurs.

Because the amplitude and frequency of the wave transform according to the same function of velocity (Einstein⁽²⁵⁾, 1905), the condition of the

free reflector moving so as to maintain a constant radiation pressure on its surface is equivalent to maintaining a constant frequency of the wave as received in the frame of the reflector. The control here is derived by comparing the waves travelling in opposite directions to and from the distant reflector and locating the controlled surface where they differ in phase by π radians (thus phase-locking the two waves at the controlled surface). This corresponds to making a radar measure of the distance to the distant reflector and keeping the time for the return journey equal to the time for the wave to change in phase by a fixed amount when it returns to the controlled surface. Under these conditions a lossless reflector may be placed at the node of the electric field, where there is this phase-difference of π radians, to recirculate the wave at the constant frequency required by the above conditions.

As a perfect reflector has been assumed, there must be no resultant component of electric field on the surface of the mirror because this would dissipate energy. Therefore the reflection must occur at the node of the electric field, thus forming a resonant cavity with infinite Q . This boundary condition, together with the fact that the force from the internal radiation pressure must equate to the sum of the binding and externally applied forces, then determines the operation of the system.

The 'locking in' occurs as the wavefront, caused by the application of an external force, returns to the first mirror. If the external force is removed at this instant, the first mirror is a 'free' reflector and moves according to the conditions described above. Thus a complete circulation of the effect of the initial disturbance is required to complete the operation and determine the motion of the boundaries of the cavity. The wavefront from the disturbed first

mirror, arriving at the second mirror, causes it to move at relativistically double the velocity of the initial movement of the first mirror (in order to maintain a balance of forces on the mirror, which corresponds to maintaining the original frequency). As a result of this increase in velocity, when the wavefront returns to the first mirror at a lower frequency (and energy density) than the previous part of the wave-train, the first mirror has to speed-up in order to bring the frequency observed on its surface to the original frequency and give a balancing of the radiation pressure and binding force, assuming that the external force is removed at this instant.

This is the essence of the 'locking in' process. It may be added that at this instant of removal of the external force the velocity of the first mirror changes so that both mirrors are moving at the same velocity (ref. Fig. 3.4) and in the single proper frame of these two reflectors the frequency of the internal radiation is the same as in their proper frame before the external force was applied. The phase-locking is a necessary consequence of the fact that the system is perfectly lossless, it can neither decrease nor increase its internal energy but responds by acquiring kinetic energy (when this 'locking in' is complete) upon the continual application of an external force.

LIST OF REFERENCES

- 1 ACADEMIC PRESS International school of physics 'Enrico Fermi',
Course 20, Academic Press (1962).
- 2 ASHWORTH D.G.
JENNISON R.C. Surveying in rotating systems,
J. Phys. A 2, 35 (1976)
- 3 ATWATER H.A. Introduction to General Relativity,
Pergamon (1974).
- 4 BADEN FULLER A.J. Microwaves,
Pergamon (1969).
- 5 BALYBERDIN V.V. Airplanes and Technical airfleets No. 3,
102 (1965).
- 6 BANWELL C.J.
FARR C.C. Further investigation of the velocity of
propagation of light in vacuo in a transverse
magnetic field,
Proc. Royal Soc. 175, 1 (1940)
- 7 BASRI S.A. Operational foundation of Einstein's General
theory of Relativity,
Rev. Mod. Phys. 37, 288 (1965)
- 8 BASS L.
SCHRODINGER E. Must the photon mass be zero ?
Proc. Royal Soc. 1, 232 (1955).
- 9 BERANEK L.L. Acoustics,
McGraw (1954).
- 10 BERGER J. Laser focus,
p.27 Nov. 1975.
- 11 BIRTWISTLE G. The principles of thermodynamics,
C.U.P. (1927).
- 12 BLANEY T.G.
et al. Measurement of the speed of light,
Proc. Royal Soc. A 355, 61 & 89 (1977).
- 13 BORN M. The theory of rigid electrons in the kinematics
of Relativity theory,
Ann. d. Phys. Vol 4, No.30, 1 (1909).
- 14 BORN M.
INFELD L. Foundations of a new field theory,
Proc. Royal Soc. 144, 425 (1934).
- 15 BRANS C.
DICKE R.H. Mach's principle and the relativistic theory
of gravitation,
Phys. Rev. 124, 925 (1961).
- 16 BURR-BROWN Co. Handbook of Operational Amplifier active RC
networks,
Burr-Brown Research U.S.A. (1966).

- 17 CHIU H-Y (Eds)
HOFFMANN Gravitation and Relativity,
Benjamine NY (1964).
- 18 CLARK R.J.
WATSON W.H. An attempt to detect an electric moment in
a light quantum,
Proc. Cambridge Phil. Soc. 26, 117 (1929).
- 19 COX D.R.
MILLER H.D. The theory of stochastic processes,
Chapman (1965).
- 20 DAVIDSON W. General Relativity and Mach's principle,
Month. Not. Royal Astro. Soc. 117, 212 (1957).
- 21 DICKE R.H.
WHITTKE J.P. Introduction to quantum mechanics,
Addison-Wesley (1960).
- 22 DICKE R.H. The theoretical significance of experimental
Relativity,
Blackie (1964).
- 23 DIRAC P.A.M. A new classical theory of electrons,
Proc. Royal Soc. A 209, 291 (1951).
- 24 EINSTEIN A. The meaning of Relativity,
Methuen (1922).
- 25 EINSTEIN A.
et al. The Principle of Relativity,
Dover, translated 1952.
- 26 ENCYCLOPEDIA
BRITANNICA Items- 'Lightning', 'Thunderstorms'.
- 27 ENDEAN V.G. Ball lightning as electromagnetic energy,
Nature 263, 753 (1976).
- 28 ESSEN L. The velocity of propagation of electromagnetic
waves derived from the resonant frequencies
of a cylindrical cavity,
Proc. Royal Soc. A 204, 260 (1950).
- 29 ESSEN L.
PARRY J.V.L. The Caesium Clock,
Phil. Trans. A 250, 45 (1957).
- 30 EVETT A.A. Relativistic rigid body translations,
Nuovo Cim. 28, 685 (1963).
- 31 FRENCH A.P. Special Relativity,
Nelson (1968).
- 32 FROOME K.D. A new determination of the free-space velocity
of electromagnetic waves,
Proc. Royal Soc. A 213, 123
A 223, 195
A 247, 109 (1958).
- 33 GERHARZ R. A field vector representation of charge and
magnetism,
J. of Electrostatics 2, 133 (1976).

- 34 GOLDE R.H. (Ed.) Lightning Vol.1
Academic (1977).
- 35 GOLDHABER A.S.
NIETO M.M. The mass of the photon,
Scientific American 234, 86 (1976).
- 36 GRAVES J.C. The conceptual foundations of contemporary
Relativity theory,
M.I.T. (1971).
- 37 HASENOHRL F. Zur theorie der Strahlung in bewegten Korpern,
Ann. d. Phys. 16, 589 (1905).
Ann. d. Phys. 15, 344 (1904).
- 38 HAZENFRATZ P.
KUTI J. The Quark bag model,
Physics Reports 40, 75 (1978).
- 39 HOGARTH J.E.
McCREA W.H. The Relativistically rigid rod,
Proc Cambridge Phil. Soc. 48, 616 (1952).
- 40 JAPOLSKI N.S. Rotating electromagnetic waves,
Phil. Mag. 7 th. series 19, 934 (1935).
- 41 JAPOLSKI N.S. On Dr. Podolski's criticism,
Phil. Mag. 7th series 22, 1003 (1936).
- 42 JENKINS F.A.
WHITE H.E. Fundamentals of optics,
McGraw (1957).
- 43 JENNISON R.C. The vanishing electron,
Proc. Institution of Electronics Vol. 7
No.4 p.2-7 (1964).
- 44 JENNISON R.C. Introduction to Radio Astronomy,
Newnes (1966).
- 45 JENNISON R.C. Ball Lightning,
Nature 224, 895 (1969).
Nature 230, 576 (1971).
- 46 JENNISON R.C. Can Ball Lightning exist in a vacuum ?,
Nature 245, 95 (1973).
- 47 JENNISON R.C.
DRINKWATER A.J. An approach to the understanding of inertia
from the physics of the experimental method,
J. Phys. A 10, 167 (1977).
- 48 JENNISON R.C. Relativistic phase-locked cavities as
particle models,
J. Phys. A 11, 1525 (1978).
- 49 JENNISON R.C. Not in print.
(1979).
- 50 JONES R.V. The velocity of light in a transverse
magnetic field,
Proc. Royal Soc. 260 (A), 47 (1961).

- 51 JURY E.I. Sampled data control systems,
Wiley (1958).
- 52 KAMINOW I.P.(Eds.) Laser devices and applications,
SIEGMAN A.E. I.E.E.E. press (1973).
- 53 KANE P.P. Possibility of observation of non-linear
BASAVARAJU G. quantum electrodynamic effects in vacuum,
Rev. Mod. Phys. 39, 52 (1967).
- 54 KAPITZA P.L. On the nature of Ball Lightning,
Collected papers of Kapitza Vol. III
(Ed) Ter Haar D.
translated Pergamon (1967).
- 55 KAPITZA P.L. Free plasma filament in a high frequency
field at high pressure,
Trans. Soviet Phys. J.E.T.P. 30, 973 (1970).
- 56 KENNEDY R.J. A search for an electrostatic analogue to
THORNDIKE E.M. the gravitational red shift,
Proc. Nat. Acad. Sciences (Washington)
17, 620 (1931).
- 57 KINGSLAKE R. (Ed.) Applied optics and optical Engineering,
Vol. IV Academic Press (1967).
- 58 KOSAREV E.L. Results on decimeter radio emissions,
et al. Soviet Phys. - Tech. Phys. 13, 1477 (1969).
- 59 KRAUSE W.H.U. Leibniz and post-Newtonian physics,
Am. J. Phys. 43, 459 (1975).
- 60 LANDAU L.D. The classical theory of fields,
LIFSHITZ translation Pergamon (1951).
- 61 LANDSBERG P.T. A relativistic generalization of thermodynamics,
JOHNS K.A. Nuovo Cim. 52B, 28 (1967).
- 62 LANGILL A.W. Automatic control systems Engineering,
Prentice-Hall (1965).
- 63 LENARD P. Physik Vol. 4,
J.F. Lehmanns Verlag ch. 3 para. 434,
Munich and Berlin 1936.
- 64 LYNDEN-BELL D. On the origin of space-time and inertia,
Mon. Nots. Royal Astro. Soc. 135, 413 (1967).
- 65 MACH E. The science of mechanics,
translation McCormach
La Salle, Ill, Open Court (1908).
- 66 MALAN D.J. Physics of Lightning,
E.U.P. (1963).
- 67 McCREA W.H. The Fitzgerald-Lorentz contraction- some
paradoxes and their resolution,
Proc. Royal Dublin Soc. (N.S.) 26, 27 (1952).

- 68 McCREA W.H. Doubts about Mach's principle,
Nature 230, 95 (1971).
- 69 McVITTIE G.C. The regraduation of clocks in spherically
symmetric space-times of General Relativity,
Proc. Royal Soc. Edinburgh 62, 147 (1945).
- 70 MORRIS W. letter
Daily Mail 5th Nov. 1936.
- 71 NEWBURGH R.G. A practical proposal for the experimental
study of Born rigid motion,
Nuovo Cim. 23B, 365 (1974).
- 72 NIGHTINGALE J.D. Specific physical consequences of Mach's
principle,
American J. Phys. 45, 376 (1977).
- 73 OHANIAN H.C. Gravitation and Space-time,
Norton (1976).
- 74 PAULI W. Theory of Relativity,
translated Pergamon (1958).
- 75 PERGAMON PRESS Recent developments in General Relativity,
Pergamon (1962).
- 76 PODOLSKI B. On interactions of electromagnetic fields,
Phil. Mag. 7th series Vol. 22 No.150, 998(1936).
- 77 RAYLE W.D. Ball Lightning characteristics,
Tech. Notes NASA TN D-3188 (1966).
- 78 REICHENBACH H. The philosophy of Space and Time,
Dover (1958).
- 79 SANDERS J.H. The Fundamental Atomic Constants,
O.U.P. (1965).
- 80 SCHEDE R.W. Interferometers for use as integral parts
of machine tools,
Trans. I.E.E.E. (Ind. & Gen.) Vol. IGA-3
No.4 p.328 (1967).
- 81 SCHIFF H. A classical theory of Bosons,
Proc. Royal Soc. A 269, 277 (1962).
- 82 SCIAMA D.W. On the origin of inertia,
Mon. Nots. Royal Astro. Soc. 113, 34 (1953).
- 83 SCIAMA D.W. Inertia,
Scientific American 196, 99 (1957).
- 84 SCIAMA D.W. The physical foundations of General Relativity,
Anchor (1969).
The unity of the Universe,
Faber (1959).

- 85 SCIAMA D. 'The ether transmogrified,
New Scientist 2 nd. Feb. p.298 (1978).
- 86 SEN D.K. Fields and/or particles,
Academic Press (1968).
- 87 SHAMIR J. Experimental investigation on the behaviour
of light propagating through electromagnetic
fields in air,
Nuovo Cim. 66B, 157 (1970).
- 88 SILBERSTEIN L. The theory of Relativity,
MacMillan (1924).
- 89 SINGER S. The Nature of Ball Lightning,
Plenum (1971).
- 90 SMYTHE W.R. Static and dynamic electricity,
McGraw-Hill (1950).
- 91 STUART E.B. (Eds.) A critical review of thermodynamics,
GAL-OR B. Mono Book (1970).
BRAINARD A.J.
- 92 SYNGE J.L. Relativity: The general theory,
North Holland (1960).
- 93 THIRRING H. Originalmitteilungen
Phys. Zeit. S. 19, 33 (1918).
22, 29(1921).
- 94 THOMPSON J.J. Electronic waves,
Phil. Mag. 7 th. series 27, 1 (1939).
- 95 ULMER W. Spinor fields in the theory of relativity and
a generalization of Heisenberg's non-linear
spinor equation,
Int. J. Theoretical Phys. 13, 51 (1975).
- 96 WOODING E.R. Ball Lightning in Smethwick,
Nature 262, 379 (1976).
- 97 YADAVA K.S. On the stability and genesis of the electron,
Nuovo Cim. 32, 273 (1976).